Nalecz Institute of Biocybernetics and Biomedical Engineering
Polish Academy of Sciences

Institut Européen Des Membranes
University of Montpellier

Doctoral Thesis

Development of new drug delivery systems made with electrostatic and 3D bioprinting techniques

Adam Mirek, M.Sc. Eng.

Supervised by

Dorota Lewińska, Ph.D., D.Sc.
Prof. of Nalecz Institute of Biocybernetics
and Biomedical Engineering
Polish Academy of Sciences

Mikhael Bechelany, Ph.D., D.Sc.
Institut Européen des Membranes
University of Montpellier

Warsaw, 2023

ACKNOWLEDGEMENTS

I would like to express my deepest gratitude to my supervisors, who have been a constant source of support throughout my research, which was invaluable in shaping my ideas, enhancing my skills and contributing to the successful completion of my dissertation.

I am grateful to Prof. Dorota Lewińska for her profound influence on my academic journey. Her mentorship has opened my eyes to the captivating world of professional science and the potential of biomedical engineering. In addition to inspiring my passion for this discipline, her dedication to excellence has also helped me develop a more refined writing style.

I appreciate Dr. Mikhael Bechelany's assistance in my research challenges outside of my home country. Not only has he generously shared with me his vast knowledge of materials science, but he has also imbued in me a spirit of optimism that has been crucial in overcoming the difficulties of scientific research.

I would like to extend my thanks to my colleagues from both Nalecz Institute of Biocybernetics and Biomedical Engineering, Polish Academy of Sciences, and Institut Européen Des Membranes, University of Montpellier, for providing me with a supportive and stimulating research environment, as well as valuable discussions and insights.

Furthermore, I would like to acknowledge Campus France for organizing my joint PhD, and the French Government for financing it. Without the administrative assistance, academic guidance, and financial support provided by them this project would not have been possible.

Lastly, I thank my family and friends, who have supported me with their love, encouragement and understanding throughout my scientific journey. Their belief in me has been a constant source of motivation and the driving force behind my achievements.

Thank you all for helping me to achieve this important milestone in my academic career!

CONTENTS

Acknowledgements · **i**
Contents · **ii**
List of Publications Included in the Thesis · **iii**
Summary · **iv**
Streszczenie · **vii**
Résumé · **x**
List of Abbreviations · **xiii**

1 INTRODUCTION · 1
On the need to use drug delivery systems · **2**
What conditions should a satisfying drug delivery system meet? · **3**
Evolution of drug delivery systems · **8**

2 MAIN GOAL AND RESEARCH THESES · 16

3 EXPERIMENTAL PART · 17
Electrospinning · **17**
3D bioprinting · **20**
Electrostatic microsphere formation · **22**

4 OVERVIEW OF THE RESULTS · 24
Thesis (1) · **24**
Thesis (2) · **29**
Thesis (3) · **33**

5 FINAL CONCLUSIONS · 40

References · **43**
Publications Included in the Doctoral Thesis · **49**

APPENDIX I Declaration of Authors' Contributions
APPENDIX II Other Research Not Included in the Thesis

LIST OF PUBLICATIONS INCLUDED IN THE THESIS

PUBLICATION (1) **Mirek, A.**, Korycka, P., Grzeczkowicz, M., Lewińska, D. Polymer fibers electrospun using pulsed voltage. *Materials and Design*. 183, 108106 (2019). DOI: 10.1016/j.matdes.2019.108106

PUBLICATION (2) **Mirek, A.**, Grzeczkowicz, M., Lamboux, C., Sayegh, S., Bechelany, M., Lewińska, D. Formation of disaggregated polymer microspheres by a novel method combining pulsed voltage electrospray and wet phase inversion techniques. *Colloids and Surfaces A: Physicochemical and Engineering Aspects*. 648, 129246 (2022). DOI: 10.1016/j.colsurfa.2022.129246

PUBLICATION (3) **Mirek, A.**, Grzeczkowicz, M., Belaid, H., Bartkowiak, A., Barranger, F., Abid, M., Wasyłeczko, M., Pogorielov, M., Bechelany, M., Lewińska, D. Electrospun UV-cross-linked polyvinylpyrrolidone fibers modified with polycaprolactone/polyethersulphone microspheres for drug delivery. *Biomaterials Advances**. 147, 213330 (2023). DOI: 10.1016/j.bioadv.2023.213330

PUBLICATION (4) **Mirek, A.**, Belaid, H., Barranger, F., Grzeczkowicz, M., Bouden, Y., Cavailles, V., Lewińska, D., Bechelany, M. Development of a new 3D bioprinted antibiotic delivery system based on a cross-linked gelatin alginate hydrogel. *Journal of Materials Chemistry B.* 10, 8862–8874 (2022). DOI: 10.1039/d2tb01268e

PUBLICATION (5) **Mirek, A.**, Belaid, H., Bartkowiak, A., Barranger, F., Salmeron, F., Kajdan, M., Grzeczkowicz, M., Cavaillès, V., Lewińska, D., Bechelany, M. Gelatin methacrylate hydrogel with drug-loaded polymer microspheres as a new bioink for 3D bioprinting. *Biomaterials Advances**. 150, 213436 (2023). DOI: 10.1016/j.bioadv.2023.213436

$\sum IF_{5\text{-year}} = 18.130$

*** formerly known as Materials Science and Engineering: C**

SUMMARY

Drug delivery systems (DDSs) allow to achieve optimal therapeutic outcomes by enabling the precise transport of the active substance to the desired location in the body during the specified time, while minimizing side effects. They are particularly useful when administration of drugs by conventional methods is ineffective or inconvenient, for example when treatment requires multiple applications, continuous delivery or direct action inside th body. The design of effective DDSs demands a multidisciplinary approach combining materials science and biomedical engineering to ensure the key requirements, such as biocompatibility, precision and stability, are met. Over the years, these systems have undergone significant evolution, moving from the concept stage in the 1950s to the current micro- and nanoscale forms, such as microcapsules, electrospun nanofiber mats, and 3D bioprinted constructs. The most commonly used materials include biodegradable and non-biodegradable synthetic polymers and hydrogels. However, the DDSs developed in this way have two significant disadvantages. The first is the burst effect, which refers to the phenomenon of a rapid release of a large amount (up to 55%) of the immobilized bioactive substance in the initial period of the system operation (during the first hour). The second problem is the small drug capacity of modern DDSs resulting from the limitations posed by their micro- and nanometric building elements.

The aim of my work was to develop a foundation for new controlled drug delivery systems manufactured using electrostatic and 3D bioprinting techniques, which would be characterized by an increased drug capacity and an elimination of the drug burst release effect (occurring in the first stage of action of systems) based on electrospun polymer fibrous mats or 3D bioprinted hydrogel constructs.

My work consists of five thematically related scientific papers that were published between 2019 and 2023 in reputable journals listed in the JCR database and they garnered a total five-year impact factor of 18.130.

I have formulated three main research theses which have been confirmed in my research:

(1) The use of pulsed voltage (PV) with additional controllable electrical parameters, such as the electrical pulse duration and frequency, stabilizes the process of electrospinning and electrostatic droplet formation, enabling the production of synthetic polymer fibers or microspheres of the desired diameter.
(2) Appropriate selection of the cross-linking method and agents used to treat the electrospun or 3D bioprinted constructs leads to obtaining stable, water-insoluble structures of polyvinylpyrrolidone, gelatin and sodium alginate, and in the case of hydrogels, eliminates the burst effect in a 3D bioprinted drug delivery system.

(3) Non-aggregated, drug-loaded synthetic polymer microspheres can be produced and used as an additive to electrospinning suspension or bioink for 3D bioprinting, resulting in an increased drug capacity of the electrospun or 3D bioprinted drug delivery system, and in the case of electrospun fibers, an elimination of the burst effect.

The first part of my work concerned electrostatic techniques. I adopted an innovative approach to the electrospinning process by applying electrical voltage in a pulsed manner. I prepared and analyzed fibrous mats from polyvinylpyrrolidone (PVP) and polylactide (PLA). The research showed that the use of pulsed voltage not only stabilizes the process but also introduces additional parameters (frequency of electric pulses f and their duration τ) which increases the possibilities of modifying the structure of the mats. Subsequently, I developed a new method of obtaining drug-loaded polymer microspheres from biodegradable polycaprolactone (PCL) or non-biodegradable polyethersulfone (PES), combining polymer solution pulsed voltage electrospraying with solidification of the solution droplets by wet phase inversion technique. Single microspheres obtained in this way do not form aggregates, they are characterized by a narrow range of diameters (controlled by manipulating the parameters f and τ) and can be stored in the form of a dried powder. In the next stage of work, I combined the results of the above studies, proposing a new method of obtaining polymer fibrous mats modified with microspheres. Drug-loaded microspheres (of PCL or PES) in the form of powder were dispersed evenly in the polymer solution (PVP) and as a result of electrospinning of such a suspension, I obtained mats with increased drug capacity and eliminated burst effect. In order to make the mats insoluble in water, I subjected them to a cross-linking process using a photoinitiator and ultraviolet light, which, as the tests showed, also affected their transport properties.

In the second part of my research, my focus shifted to the field of 3D bioprinting. I successfully developed two novel bioinks as the basis for hydrogel 3D bioprinting. The first one consisted of gelatin and sodium alginate. I subjected the constructs made of it to the cross-linking process using various agents – calcium ions and glutaraldehyde vapors. As I observed, the dissolution of the investigated substances (rhodamine 640, chlorhexidine acetate) in the bioink allowed to obtain a potential controlled drug delivery system that does not show the burst effect. For the second bioink, I used a suspension of polymer microspheres (PCL or PES) with immobilized active substance (ampicillin) or marker (rhodamine 640) in water solution of gelatin methacrylate and gelatin. I used it to 3D bioprint constructs which were then cross-linked with ultraviolet light (in the presence of a photoinitiator). They were characterized by the expected increased drug capacity and no burst effect.

I tested the developed constructs using numerous techniques, such as: scanning electron microscopy (SEM), Fourier transform infrared spectroscopy (FTIR), X-ray diffraction (XRD), determination of the specific surface using the BET method, differential scanning calorimetry (DSC), thermogravimetric analysis (TGA), spectrophotometric tests of substance marker release, degradation and swelling analysis, mechanical properties tests, antibacterial activity and cytotoxicity tests.

In summary, my work yielded three fundamental (microspheres, polymer fibrous mats, 3D bioprinted constructs) and two hybrid structures that have potential to be a foundation for the controlled drug delivery systems:

- cross-linked, electrospun polyvinylpyrrolidone fibrous mats modified with microspheres (polycaprolactone or polyethersulfone) containing the drug - ampicillin,
- cross-linked, bioprinted hydrogel constructs based on gelatin methacrylate modified with microspheres (PCL or PES) filled with the drug - ampicillin.

The new hybrid systems created in my research possess a high drug capacity and do not exhibit the immobilized substance burst effect during initial period of action. Their transport properties are influenced by factors such as cross-linking time and the type and quantity of microspheres, which enables accurate control over the drug delivery properties of the final product. However, these systems differ in terms of properties and potential applications, and their manufacturing methods require a distinct approach. In the final chapter of my thesis, I provided a comprehensive evaluation of the strengths and weaknesses of electrospinning and 3D bioprinting techniques for producing hybrid drug delivery systems, as well as the benefits and drawbacks of systems based on electrospun fiber mats or 3D bioprinted hydrogel matrices modified with microspheres.

STRESZCZENIE

Systemy kontrolowanego dostarczania leków (DDSs – ang. *drug delivery systems*) pozwalają osiągnąć optymalne efekty terapeutyczne, minimalizując potencjalne skutki uboczne, poprzez uwalnianie określonych ilości substancji aktywnej w konkretnym miejscu w ciele przez odpowiedni czas. Wykazują one szczególną przydatność, kiedy podawanie leków klasycznymi metodami jest nieefektywne lub niewygodne, na przykład gdy leczenie wymaga wielokrotnych aplikacji, ciągłego dostarczania lub działania miejscowego. Projektowanie skutecznych DDSs wymaga multidyscyplinarnego podejścia łączącego inżynierię materiałową i biomedyczną, aby zapewnić spełnienie stawianych im kluczowych wymagań, wśród których można wymienić biokompatybilność, precyzję czy stabilność. Systemy takie znacznie wyewoluowały od momentu powstania konceptu w latach 50. XX wieku. Badane obecnie DDSs projektowane są w mikro- lub nanoskali i mogą przyjąć różne formy – mikrokapsułek, elektroprzędzonych mat nanowłóknistych czy konstruktów wykonanych techniką biodruku 3D. Wśród najczęściej stosowanych materiałów należy wskazać biodegradowalne i niebiodegradowalne polimery syntetyczne i hydrożele. Opracowane tak DDSs mają jednak dwie istotne wady. Pierwszą z nich jest tak zwany efekt wyrzutu (ang. *burst effect*) odnoszący się do zjawiska gwałtownego uwolnienia dużej ilości immobilizowanej substancji leczniczej (wynoszącej nawet 55%) w początkowym okresie działania systemu (podczas pierwszej godziny). Drugi problem stanowi niewielka pojemność nowoczesnych DDSs na lek wynikająca z mikro- i nanometryczne rozmiarów elementów strukturalnych tych systemów.

Celem mojej pracy było zaprojektowanie bazy nowych systemów kontrolowanego dostarczania leków przy użyciu technik elektrostatycznych i biodruku 3D, które charakteryzowałyby się zwiększoną pojemnością na lek i brakiem efektu wyrzutu. Systemy te oparte miałyby być na elektroprzędzonych włókninach polimerowych oraz biodrukowanych modelach hydrożelowych.

Na moją pracę składa się pięć powiązanych tematycznie prac naukowych opublikowanych w latach 2019 – 2023 w czasopismach z listy JCR o całkowitym pięcioletnim współczynniku wpływu IF = 18,130 oraz liczbie punktów MNiSW N = 430.

Sformułowałem trzy główne tezy badawcze, które znalazły potwierdzenie w moich badaniach:

(1) Zastosowanie napięcia pulsacyjnego wraz z dodatkowymi sterowalnymi parametrami elektrycznymi, takimi jak czas trwania i częstotliwość impulsów, stabilizuje proces elektroprzędzenia i elektrostatycznego tworzenia kropli, umożliwiając wytwarzanie syntetycznych włókien polimerowych lub mikrosfer o pożądanej średnicy.

(2) Odpowiedni dobór metody oraz środków użytych do sieciowania systemów elektroprzędzonych lub biodrukowanych prowadzi do uzyskania stabilnych, nierozpuszczalnych w wodzie struktur z poliwinylopirolidonu, żelatyny i alginianu sodu, a w przypadku hydrożeli eliminuje efekt wyrzutu w systemach kontrolowanego dostarczania leków.
(3) Niezagregowane syntetyczne mikrosfery polimerowe z immobilizowanym lekiem są możliwe do wytworzenia i zastosowania jako dodatek do elektroprzędzonej zawiesiny lub biotuszu do biodruku 3D, co skutkuje zwiększoną pojemnością leku w elektroprzędzonym lub biodrukowanym systemie dostarczania leków, a w przypadku włóknin elektroprzędzonych, eliminacją efektu wyrzutu.

Pierwsza część moich prac dotyczyła technik elektrostatycznych. W swoich badaniach zastosowałem nowatorskie podejście do procesu elektroprzędzenia, prowadząc go przy użyciu napięcia elektrycznego podawanego w sposób impulsowy. Wykonałem włókniny z poliwinylopirolidonu (PVP) oraz polilaktydu (PLA). Z przeprowadzonych badań wynika, że użycie napięcia pulsacyjnego stabilizuje proces oraz wprowadza dodatkowe parametry (częstotliwość impulsów elektrycznych f i czas ich trwania τ), co zwiększa możliwości modyfikacji struktury otrzymywanych włóknin. Następnie, opracowałem nową metodę otrzymywania mikrosfer polimerowych z biodegradowalnego polikaprolaktonu (PCL) lub niebiodegradowalnego polieterosulfonu (PES), w których można immobilizować lek, łączącą elektrorozpylanie roztworu polimeru przy użyciu napięcia pulsacyjnego z utwardzaniem kropel roztworu metodą mokrej inwersji faz. Otrzymywane w ten sposób pojedyncze mikrosfery nie tworzą agregatów, charakteryzują się wąskim zakresem średnic (kontrolowanych poprzez odpowiednie zmiany f i τ) oraz mogą być przechowywane w formie wysuszonego proszku. W kolejnym etapie prac, połączyłem wyniki powyższych badań, proponując nową metodę otrzymywania włóknin polimerowych modyfikowanych mikrosferami. Zawierające immobilizowany lek mikrosfery (PCL lub PES) w formie proszku rozproszyłem równomiernie w roztworze polimeru (PVP) i w wyniku elektroprzędzenia takiej zawiesiny otrzymałem włókniny o zwiększonej pojemności na lek i wyeliminowanym efekcie wyrzutu. W celu zabezpieczenia włóknin przed rozpuszczeniem w wodzie, poddawałem je procesowi sieciowania przy użyciu fotoinicjatora i światła ultrafioletowego, co, jak wykazały badania, również miało wpływ na ich właściwości transportowe.

Druga część moich badań skupiona była wokół biodruku 3D. Opracowałem dwa różne biotusze będące podstawą hydrożelowych wydruków. Pierwszy składał się z żelatyny i alginianu sodu, a zbudowane z niego modele poddawałem procesowi sieciowania różnymi metodami – przy użyciu jonów wapniowych oraz oparów glutaraldehydu. Rozpuszczenie substancji aktywnej w biotuszu pozwoliło otrzymać potencjalny system kontrolowanego dostarczania leków niewykazujący efektu wyrzutu. Drugi biotuszu miał formę zawiesiny mikrosfer polimerowych (PCL lub PES) z immobilizowaną substancją aktywną w roztworze wodnym zawierającym syntezowany przeze mnie metakrylan żelatyny oraz żelatynę. Wydrukowane przy jego pomocy modele sieciowane światłem ultrafioletowym (w obecności fotoinicjatora) charakteryzowały się oczekiwaną zwiększoną pojemnością na lek i brakiem efektu wyrzutu.

Opracowane systemy badałem za pomocą licznych technik takich jak: skaningowa mikroskopia elektronowa (SEM), spektroskopia w podczerwieni z transformacją Fouriera (FTIR), dyfrakcja rentgenowska (XRD), wyznaczanie powierzchni właściwej metodą BET, skaningowa kalorymetria różnicowa (DSC), analiza termograwimetryczna (TGA), spektrofotometryczne testy uwalniania markera substancji, analizy degradacji i pęcznienia, badanie właściwości mechanicznych, badanie aktywności antybakteryjnej i testy cytotoksyczności.

Podsumowując, w swojej pracy otrzymałem trzy podstawowe (mikrosfery, włókniny polimerowe, biowydruki 3D) i dwie hybrydowe struktury mogące stanowić bazę do opracowania systemów kontrolowanego dostarczania leków:

- sieciowane, elektroprzędzone włókniny z poliwinylopirolidonu modyfikowane mikrosferami (z polikaprolaktonu lub polieterosulfonu) zawierającymi lek – ampicylinę,
- sieciowane, biodrukowane konstrukty z hydrożelu opartego na metakrylanie żelatyny modyfikowane mikrosferami (PCL lub PES) wypełnionymi lekiem – ampicyliną.

Nowo powstałe hybrydowe systemy charakteryzują się zwiększoną pojemnością na lek i brakiem efekt wyrzutu immobilizowanej substancji w początkowej fazie działania. Na ich właściwości transportowe mają wpływ czas sieciowania oraz rodzaj i ilość mikrosfer, co pozwala na precyzyjną kontrolę cech wytworzonego produktu. Opracowane systemy nie są jednak do końca zbieżne pod względem właściwości i potencjalnych zastosowań, a techniki ich wytwarzania wymagają odrębnego podejścia. W ostatnim rozdziale pracy przedstawiłem przegląd mocnych i słabych stron procesów elektroprzędzenia i biodruku 3D w produkcji hybrydowych systemów dostarczania leków, a także zalety i wady systemów opartych o elektroprzędzone włókniny lub trójwymiarowe biodrukowane modele hydrożelowe modyfikowane za pomocą mikrosfer.

RÉSUMÉ

Les systèmes d'administration contrôlée de médicaments (DDSs, abréviation de « drug delivery systems » en anglais) permettent d'obtenir des résultats thérapeutiques optimaux en transportant la quantité précise de substance active vers l'emplacement spécifique dans le corps pendant la durée spécifiée, tout en minimisant les effets secondaires potentiels. Ces systèmes sont particulièrement avantageux lorsqu'une administration de médicaments par des méthodes conventionnelles est inefficace ou peu pratique, notamment lorsqu'un traitement nécessite des applications multiples, une administration continue ou une action directe à l'intérieur du corps. Pour concevoir un DDS efficace, une approche multidisciplinaire est nécessaire, qui combine la science des matériaux et le génie biomédical afin de s'assurer que les exigences clés, telles que la biocompatibilité, la précision et la stabilité, sont satisfaites. Ces systèmes ont connu une évolution considérable passant du stade de concept dans les années 1950 aux formes actuelles à l'échelle micro et nanométrique, telles que les microcapsules, les nanofibres électrofilés et les constructions bioimprimées en 3D. Les matériaux fréquemment employés incluent des polymères synthétiques, qu'ils soient biodégradables ou non, ainsi que des hydrogels. Toutefois, les DDSs ainsi conçus ont deux inconvénients majeurs. Le premier est l'effet de relargage (« burst effect » en anglais), qui correspond à la libération rapide d'une grande quantité (pouvant atteindre jusqu'à 55%) de la substance bioactive immobilisée au cours de la première heure de fonctionnement du système. Le deuxième problème concerne la faible capacité de ces DDSs modernes pour les médicaments, due aux limitations imposées par leurs éléments de construction micro- et nanométriques.

L'objectif de ma recherche était de développer de nouveaux systèmes d'administration contrôlée de médicaments en utilisant des techniques d'électrofilage et de bioimpression 3D, qui se caractériseraient par leur capacité accrue pour les médicaments et une élimination de l'effet de relargage initiale des systèmes basés sur des fibres polymères électrofilées ou des constructions d'hydrogels bioimprimées en 3D.

Ma thèse est composée de cinq articles scientifiques qui sont liés par leur thématique et qui ont été publiés entre 2019 et 2023 dans des revues réputées répertoriées dans la liste JCR. L'ensemble de ces publications a un facteur d'impact total sur cinq ans de 18,130.

J'ai formulé trois hypothèses principales, qui ont été confirmées dans mes recherches :

(1) L'utilisation de la tension pulsée avec des paramètres électriques contrôlables supplémentaires, tels que la durée et la fréquence des impulsions électriques, stabilise les processus d'électrofilage et de formation électrostatique de gouttelettes, permettant ainsi la production de fibres polymères synthétiques ou de microsphères avec un diamètre contrôlé.

(2) Une sélection appropriée de la méthode et des agents utilisés pour la réticulation des systèmes électrofilés ou bioimprimés conduit à des structures stables et insolubles dans l'eau de polyvinylpyrrolidone, de gélatine et d'alginate de sodium et, dans le cas des hydrogels, élimine l'effet de relargage dans les systèmes d'administration contrôlée de médicaments.
(3) Des microsphères de polymère synthétique non agrégées avec un médicament immobilisé peuvent être produites et utilisées comme additif à une suspension électrofilaire ou à une bioencre pour la bioimpression 3D, ce qui augmente la capacité des systèmes d'administration de médicament électrofilé ou bioimprimé, et dans le cas de fibres électrofilées, permet également le contrôle de relargage.

La première partie de mes recherches s'est focalisée sur les techniques électrostatiques. J'ai adopté une approche novatrice de l'électrofilage en utilisant une tension électrique pulsée. J'ai préparé et analysé des fibres à base de polyvinylpyrrolidone (PVP) et de polylactide (PLA). Les résultats des recherches ont démontré que l'application de la tension électrique pulsée avait deux effets bénéfiques, à savoir la stabilisation du processus d'électrofilage et l'introduction de paramètres supplémentaires tels que la fréquence f et la durée des impulsions électriques τ. Ces paramètres accroissent les possibilités de modification de la structure des fibres. Par la suite, j'ai mis au point une nouvelle méthode permettant de produire des microsphères de polymère chargées en médicament à partir de polycaprolactone biodégradable (PCL) ou de polyéthersulfone non biodégradable (PES). Cette méthode combine l'électronébulisation à tension pulsée de solutions de polymère avec la solidification des gouttelettes de solution par la technique d'inversion de phase. Les microsphères individuelles obtenues grâce à cette méthode ne forment pas d'agrégats, présentent une gamme étroite de diamètres (contrôlées en manipulant les paramètres f et τ) et peuvent être stockées sous forme de poudre séchée. Dans la prochaine étape de mon travail, j'ai combiné les résultats de mes études antérieures pour proposer une nouvelle méthode d'obtention de fibres polymères modifiées avec des microsphères. J'ai uniformément dispersé des microsphères chargées de médicament sous forme de poudre (de PCL ou de PES) dans une solution de polymère (PVP), puis j'ai réalisé l'électrofilage de cette suspension pour obtenir des fibres présentant une capacité de médicament accrue et un effet de relargage contrôlé. Afin de rendre ces fibres insolubles dans l'eau, j'ai effectué un processus de réticulation en utilisant un photoinitiateur et de la lumière ultraviolette, ce qui, comme l'ont montré les tests, a également affecté leurs propriétés de transport.

Dans la seconde partie de mes recherches, j'ai orienté mon intérêt vers le domaine de la bio-impression 3D. J'ai réussi à élaborer deux nouvelles bio-encres pour servir de base à l'impression 3D d'hydrogels. Le premier était composé de gélatine et d'alginate de sodium. J'ai soumis les constructions qui en sont faites au processus de réticulation à l'aide de divers agents - des ions calcium et des vapeurs de glutaraldéhyde. La dissolution de la substance active dans la bioencre a permis d'obtenir un système potentiel d'administration contrôlée de médicaments qui ne présente pas l'effet de relargage. Pour la seconde bio-encre, j'ai préparé une suspension et des microsphères de polymère (PCL ou PES) avec une substance active immobilisée dans une solution aqueuse du méthacrylate de gélatine et de la gélatine. Cette bioencre a été utilisée

pour la bioimpression 3D de structures, qui ont ensuite été réticulées à l'aide de lumière ultraviolette (en présence d'un photoinitiateur). Ces structures ont présenté une augmentation attendue de la capacité et aucun effet de relargage rapide n'a été observé.

J'ai testé les DDSs développés en utilisant de nombreuses techniques, telles que : la microscopie électronique à balayage (SEM), la spectroscopie infrarouge à transformée de Fourier (FTIR), la diffraction des rayons X (XRD), la détermination de la surface spécifique par la méthode BET, la calorimétrie différentielle à balayage (DSC), analyse thermogravimétrique (TGA), des tests spectrophotométriques pour la libération de marqueurs de substance, les analyses de dégradation et de gonflement, les tests de propriétés mécaniques, les tests d'activité antibactérienne et de cytotoxicité.

Pour résumer, mon travail a produit trois structures fondamentales (microsphères, fibres polymères, constructions bioimprimées en 3D) et deux structures hybrides qui ont le potentiel d'être une base pour les systèmes d'administration contrôlée de médicaments :

- des fibres électrofilées réticulées de polyvinylpyrrolidone modifiées avec des microsphères (polycaprolactone ou polyéthersulfone) contenant le médicament ampicilline,
- des constructions d'hydrogel bioimprimé réticulé à base de méthacrylate de gélatine modifié avec des microsphères (PCL ou PES) remplies du médicament ampicilline.

Les nouveaux systèmes hybrides créés dans ma recherche possèdent une capacité accrue et ne présentent pas l'effet de relargage de la substance immobilisée lors de l'action initiale. Leurs propriétés de transport sont influencées par des facteurs tels que le temps de réticulation ainsi que le type et la quantité de microsphères. Cela permet de contrôler avec précision les propriétés du produit final. Néanmoins, ces systèmes présentent des différences en matière de propriétés et d'applications possibles, et leur fabrication requiert une approche spécifique. Le dernier chapitre de ma thèse présente une évaluation complète des forces et faiblesses des techniques d'électrofilage et de bioimpression 3D pour la création de systèmes hybrides d'administration de médicaments, ainsi que des avantages et inconvénients des systèmes basés sur des fibres électrofilées ou des hydrogels bioimprimés en 3D modifiés avec des microsphères.

LIST OF ABBREVIATIONS

BET	analysis technique for the measurement of the specific surface area of materials
BMP-2	bone morphogenic protein 2
BMSCs	bone marrow mesenchymal stem cells
BP	benzophenone
BSA	bovine serum albumin
CA	chlorhexidine acetate
CCD	charge-coupled device
DCV	direct-current voltage
DDS	drug delivery system
DMF	dimethylformamide
DNA	deoxyribonucleic acid
DSC	differential scanning calorimetry
ESR	equilibrium swelling ratio
FTIR	Fourier transform infrared spectroscopy
G-CSF	granulocyte-colony stimulating factor
GelMA	gelatin methacrylate
GTA	glutaraldehyde
HBSS	Hanks′ Balanced Salt Solution
LAP	lithium phenyl-2,4,6-trimethylbenzoylphosphinate
MA	methacrylic anhydride
NMP	N-methylpyrrolidone
PBS	phosphate-buffered saline
PCL	polycaprolactone
PCL/DMF	PCL solution in DMF
PCL/NMP	PCL solution in NMP
PEG	polyethylene glycol
PES	polyethersulphone
PES/DMF	PES solution in DMF
PES/NMP	PES solution in NMP
PLA	polylactic acid
PLGA	poly(lactide-co-glycolide)
PS	polystyrene
PV	pulsed voltage
PVP	polyvinylpyrrolidone
rhBMP-2	recombinant human bone morphogenic protein 2
RNA	ribonucleic acid
SEM	scanning electron microscopy
TGA	thermogravimetric analysis
UV	ultraviolet
XRD	X-ray diffraction analysis

1

INTRODUCTION

A drug delivery system administers a bioactive substance to the human body in a controlled manner. **Its primary goal is to achieve optimal therapeutic outcomes while minimizing any potential side effects by transporting the precise amount of drug to the specific location during the specified time.** Drug delivery systems (DDSs) are developed using biomedical engineering and materials science approaches and they differ remarkably from pharmaceutical products – they are designed to effectively manage the release of the drug for days or even months, whereas pharmaceutics are simply the active substance itself. However, it is important to note that the successful implementation of a DDS in healthcare requires the collaboration of pharmacists and both materials and biomedical engineers. The field of controlled drug delivery is constantly advancing, and researchers are making efforts to overcome the challenges and develop systems that are safe, effective and sustainable.

The use of DDSs is indicated in a number of cases when administering drugs or their mixtures through traditional methods is not sufficient or may be inconvenient:

- daily or multiple daily administrations,
- continuous administration for a long time, e.g. hormones,
- direct administration inside the body, e.g. in the treatment of tumors or postoperative scars of internal organs,
- hard-to-heal wounds, e.g. burns, bedsores, diabetic wounds,
- sensitive and large particles of active substances, e.g. protein biopharmaceuticals (hormones, growth factors, enzymes and antibodies) or nucleic-acid biopharmaceuticals (DNA fragments and RNA),
- drugs considered too toxic for conventional delivery applications.

On the need to use controlled drug delivery systems

Controlled DDSs are designed to address the issues associated with conventional pharmaceutical products such as tablets, capsules, syrups, ointments, injections, etc. [1]. In the case of potent bioactive substances, their handling and proper dosing are very difficult when milligram or microgram doses are required. In addition, some drugs are sensitive to body conditions (humidity, temperature, pH) and require chemical transformation or specific formulation before being used, which may reduce their effectiveness. The use of pure active drug substances is also often associated with a reduction in patient comfort, as they are characterized by unpleasant organoleptic properties (bad smell or taste) [2].

To address the identified shortcomings, excipients can be utilized in the drug formulation process including agents such as dyes, solvents, lubricants, sweeteners, antioxidants [3], and others, e.g. fillers to augment the size of the tablets when the necessary dosage of the drug is too small to administer otherwise [4]. However, the use of excipients does not completely resolve the significant issues of conventional pharmaceutical formulations, namely the abrupt increase in the concentration of the active substance in the body right after drug administration, followed by its rapid metabolism and an exponential decrease in its concentration. Consequently, the duration of the period when the drug concentration falls within the therapeutic window may be insufficient, and attempting to extend it by increasing the dose of the active substance may result in toxicity due to an excessive drug concentration in the blood. **To overcome these issues, controlled drug delivery systems were designed**. Their efficacy in addressing the problems associated with traditional drug administration methods is demonstrated in Fig. 1.

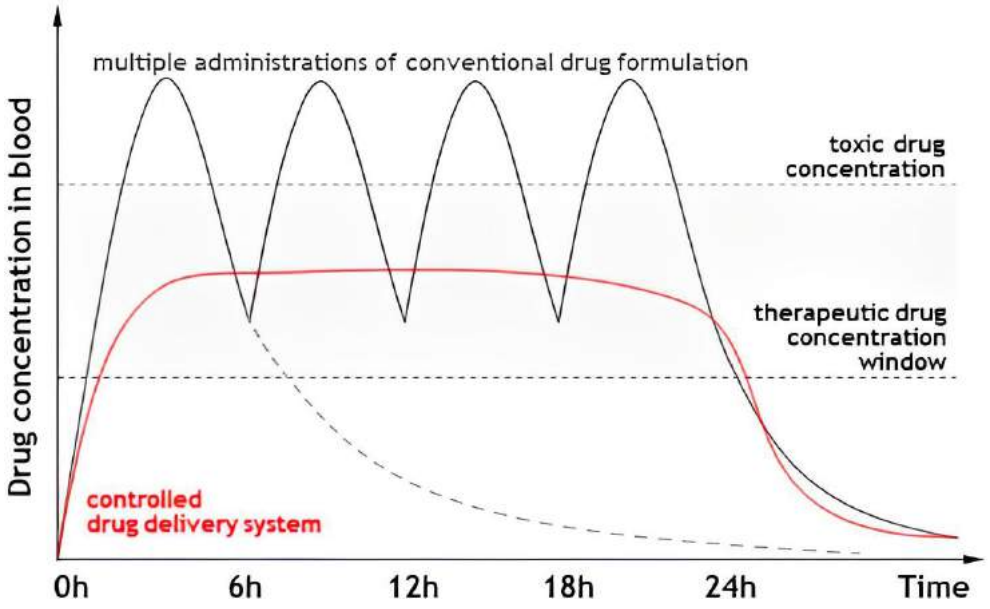

FIGURE 1. Schematic representation of the drug concentration profile in the body administered as multiple doses of a conventional formulation (grey line) and using a controlled DDS (red line). Prepared based on the work by Geraili et al. [5].

The plot shows the changes in drug concentration in the blood after delivery using both approaches. The conventional formulation leads to lower treatment effectiveness and a higher risk of an abrupt increase in blood concentration to toxic levels. Additionally, the drug is rapidly metabolized and cleared from the blood, requiring multiple doses to maintain average therapeutic drug concentrations. However, the drug administration method in question may lead to fluctuations in its concentration in the blood, which may result in its levels falling below the minimum therapeutic range or exceeding the toxic values [6]. Additionally, the need to take multiple doses of the drug per day may impair the patient's comfort and increase the likelihood of dosing errors. A controlled DDS can help prevent these issues by carefully selecting the device, material, manufacturing technique, and initial drug concentration to maintain therapeutic levels of the active substance in the blood with reduced risk of toxicity.

Overall, controlled DDS improve the effectiveness and safety of drug treatments. Traditional pharmaceuticals can sometimes have unpredictable or variable effects, depending on how they are absorbed and metabolized by the body. This can lead to side effects, reduced efficacy, and other problems. Controlled DDS are designed to overcome these limitations by releasing the drug at a specific rate and in a specific location, allowing for more precise control over the drug effects [5, 7]. The use of DDSs protects drugs from degradation and reduction of their potency or formation of toxic by-products [2] [8]. They reduce drug intake frequency and concentration fluctuations in blood, improve patient compliance and comfort, and stabilize their medical condition. Despite this, they must satisfy several requirements to be used effectively and safely.

What conditions should a satisfying drug delivery system meet?

While controlled DDSs unquestionably offer many potential benefits, they also have some challenges to overcome [7]. Some of the key considerations for a safe and efficient DDS are presented in Fig. 2 and described below.

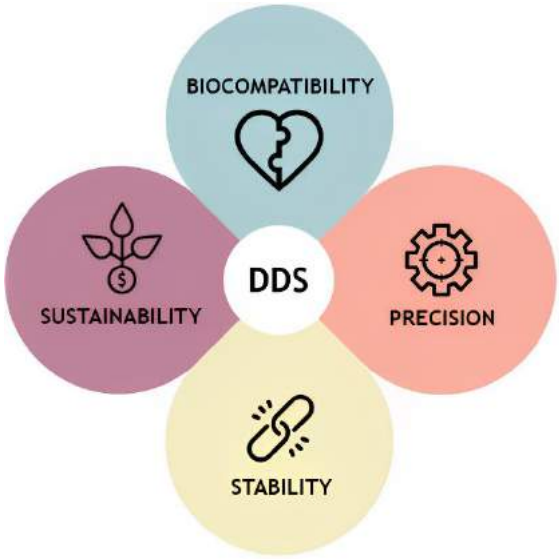

FIGURE 2. Factors to consider when designing a controlled drug delivery system.

Biocompatibility

The biocompatibility of DDSs is a crucial factor in ensuring their safety for use. This means that both the technique and materials used for the manufacture of DDSs must have the ability to be in contact with living systems without causing adverse effects [9]. In practical terms, this requires the non-toxicity, a lack of impact on the immune system, and no induction of hemolysis upon contact with blood. Otherwise, the DDSs may cause irritation or damage to the tissues it comes into contact with, potentially resulting in discomfort, allergic reactions or additional complications. The immune system, recognizing the DDS as a foreign object, attempts to eliminate it from the body, leading to the breakdown or removal of the system before it has had the opportunity to release the drug.

The biocompatibility of a DDS is closely tied to the method and place of administration and strongly dependent on anatomy – it is important to consider the specific tissue where the material will be implanted [2]. There is a variety of biocompatible materials that can be used for DDSs, including polymers (both natural, e.g. polysaccharides, proteins and synthetic, e.g. polyethylene glycol (PEG), polyvinylpyrrolidone (PVP), and polylactic acid (PLA)), ceramics (e.g. hydroxyapatite, alumina) or metals (e.g. gold, silver) [10]. Overall, the choice of material for a DDS will depend on the specific therapeutic requirements of the system and the drug being delivered. The biocompatibility of the DDS can vary depending on its form – microspheres that can stay in the peritoneal cavity for weeks may elicit a different response than nanoparticles that can leave it within days and accumulate in the tissues. Some systems due to their small sizes on the nanometer scale (nanoparticles, nanosuspensions) may interact with living systems upon administration [11, 12]. The size of nanoparticles that determines their biocompatibility varies based on the material, e.g. for silver nanoparticles it is 2 nm, lipid nanoparticles – 50 nm, chitosan/alginate nanoparticles – 20 nm, and silica nanoparticles – 10 nm [13]. The length of time that tissues are exposed to the materials used in a DDS affects their biocompatibility due to DDS corrosion and aging [14]. It should also be remembered that biocompatibility is an ontogenetic concept, and the inflammatory response may vary depending on the organism. In some cases, a risk-benefit analysis must be conducted, weighing the potential risks of slight local irritation against the benefits of controlled drug release [15].

Not only must the material of the DDS itself be biocompatible, but the manufacturing and sterilization methods as well. They should not produce any toxic or harmful by-products that could potentially affect the safety of the system, nor should it introduce any impurities or contaminants that could compromise the biocompatibility of the final product (e.g. residual polymer solvents, cross-linking agents, post-process rinse solutions). It is crucial to ensure that the materials used to manufacture the controlled DDSs as well as all the excipients of the formulation and sterilization methods are non-toxic to the body and do not cause any patient allergic reactions [16].

Precision

The safety of DDS usage can also be impacted by the precision in achieving the desired concentration of the medication during the drug release process. Therefore, it is crucial to have well-engineered systems that can deliver the drug to the target site in the body with accurate dose, rate and duration, ranging from days to months, depending on the needs.

One of the undesirable phenomena that can potentially lead to inefficiency of the DDSs is a burst effect, which refers to the rapid and inefficient release of a large portion of the drug immediately following administration [17]. We observe this effect when the current concentration of the active substance during the initial stage of release from the DDSs (within less than an hour) exceeds the concentration that is eventually reached at equilibrium state, as depicted in Fig. 3. Rapid release of a high amount of the drug in a short time may result in toxicity, especially if the drug is not well tolerated at high doses. The burst effect may also limit the DDS ability to target specific areas of the body because the drug is released too quickly or unevenly. The therapeutic effect of drug may be less than expected.

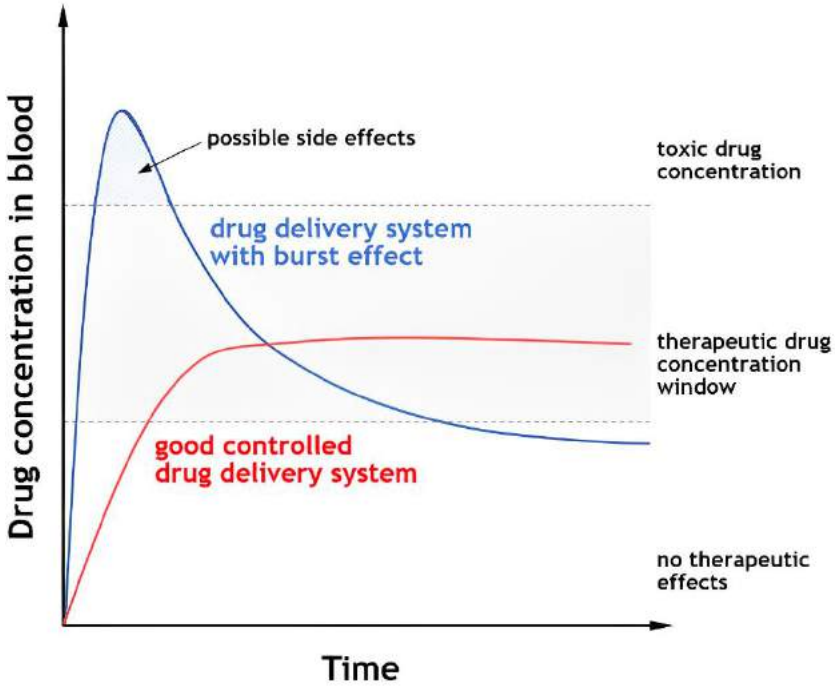

FIGURE 3. Schematic representation of the drug concentration profile from drug delivery systems with burst effect (blue line) and without it (red line).

Another key consideration in the design of a controlled DDS is its capacity for a drug. For instance, drug loading capacity into liposomes and polymeric nanoparticles is typically less than 5%, which limits their effectiveness [18]. Usually, it is advisable to maximize it to enable the delivery of a larger quantity of the drug over an extended duration. Increasing the capacity of the controlled DDS can enhance system efficacy by sustaining consistent drug concentrations in the body. If the delivery system does not release the correct amount of drug at the right time, it may be ineffective in treating the disease or condition. On the other hand, if the DDS releases too much drug at once, it can lead to an overdose, which can be dangerous. In addition,

the precision of controlled DDS may be affected by fluctuations in drug levels, drug interactions if the system releases multiple drugs simultaneously, and simply system failures – these can include mechanical malfunctions, problems with the drug formulation or release mechanism.

By precisely regulating the drug content and tailoring the construction of DDSs, taking into consideration both burst effect [19] and drug capacity [20], it is possible to develop systems that can last for a few hours to several weeks, depending on the needs. To minimize the risk of system failure, it is important to carefully design and test the DDSs.

Stability

The stability and durability of controlled DDSs can significantly affect the release profile of the active ingredient, as well as the overall usability of the system, especially if long-term use (e.g. months) is anticipated. It should be at least as durable and stable as traditional methods of drug administration without the need to be replaced more frequently, with minimal loss of effectiveness over time. An issue that must be considered in the context of DDS stability and durability is its biodegradation as it can be biodegradable or non-biodegradable to suit the intended use.

Biodegradable DDSs are made of materials that can be broken down and eliminated naturally by the body. They are commonly used for short-term drug delivery (less than 24 h) because they can be designed to disintegrate and release the drug over a set period before being fully metabolized and removed from the body. For instance, osmotic pumps consisting of a drug core containing an osmotic agent, surrounded by a semipermeable membrane, e. g. cellulose acetate [21]. The biodegradable DDSs eliminate the need for a retrieval surgery and reduces the potential negative effects associated with the prolonged biomaterial presence in the body. Biodegradation can be controlled and occurs as a result of four effects - hydrolysis, oxidation, photolysis, and proteolysis [2]. Among the mechanisms mentioned, photolysis can be used to design light-sensitive drug delivery systems to photocontrol the release of active substance with high target specificity [22]. Biodegradable materials can be natural (polysaccharide-based such as chitosan, hyaluronic acid, alginate, or protein-based such as gelatin, collagen) and synthetic (mainly polyesters such as polylactic acid, polycaprolactone or polyglycolic acid, but also polyanhydrides and polyamides) [23]. They are frequently used for local drug delivery, such as cancer or inflammation treatment [24], and scaffolds for tissue engineering [25].

Non-biodegradable DDSs are made of materials that are not broken down by the body, including: polymers (acrylics, e.g. polymethacrylate, cellulose derivatives, e.g. cellulose acetate, silicones, and others, e.g. polystyrene), metals (gold, silver, stainless steel, titanium), ceramics and glass [23, 26]. These systems are typically used for long-term drug delivery, as they are designed to release the drug over a prolonged period, e.g. for the treatment of chronic diseases. One of the most well-known non-biodegradable DDS is the drug-eluting stent coated with agents such as antiproliferatives used to prevent re-narrowing of the artery after angioplasty [27]. Another example is a drug-coated balloon inflated inside an artery to deliver a substance at the arterial wall for treating coronary bifurcation lesions [28].

When designing a DDS, it is important to carefully consider material issues to avoid potential problems. In addition to choosing suitable materials for the construction of DDSs, various modifications can also be made to improve their stability. They include surface modification such as coatings to add layers of protection [29, 30]; reinforcements, such as fibers or mesh in the structure of a system [31, 32]; crosslinking of system-building polymer chains [33, 34]; or blending different materials to create a delivery system with improved strength and other desired properties [35, 36]. Aside from upgrading the stability of DDSs, proficient application of these modification techniques also allows for control over their degradation and subsequent release profile or enhance their biocompatibility.

Sustainability

Lastly, the most suitable controlled DDSs should satisfy the sustainability criterion in addition to meeting all the previously listed requirements. The optimal DDS should be financially efficient for both patients and the healthcare system, as well as environmentally sustainable with minimal impact on natural resources [7]. Efforts to improve sustainability in the drug delivery field have usually centered on areas such as device manufacturing, product packaging, and distribution. However, there is a growing focus on incorporating sustainable design principles into the product development process [37]. It should not have any negative effect on the environment through the materials used in its manufacture or the utilization of limited resources, which can lead to resource depletion. Some of DDSs may be costly to produce, potentially rendering them unsustainable in the long term. Logistical issues may also affect the sustainability of these systems. One approach to enhance sustainability is to focus on material substitution and reduction, which can lead to cost savings. When designing DDS, sustainable options include reducing waste through efficient design, utilizing modular packaging, and implementing smart supply chain techniques [38]. Other methods can be similar to those in other industries, such as identifying the environmental impact "hotspots" in the design of the drug delivery systems) and using this information to make changes for sustainability, reducing the number of different devices through consolidation, and exploring new and innovative technologies [37]. Although the sustainability of controlled DDSs may not be the most pressing concern during the scientific research and development phase, it must be taken into account when introducing the system to the market.

Evolution of drug delivery systems

Given the numerous requirements that must be considered, various DDS have been developed, which continues to be an area of ongoing research and interest within the fields of materials and biomedical engineering. The forms that these systems may take are dependent upon their intended use (targeted disease, therapeutic agent, conditions to be met), the materials utilized, and the method of manufacture [2].

The origins of drug delivery systems date back to the early 1950s, with the introduction of pharmaceutical formulations aimed at prolonging drug activity and reducing dosing frequency [39]. These initial efforts focused on macroscale systems, such as macrospheres coated with a mixture of glyceryl monostearate and beeswax of varying thickness to regulate capsule dissolution in the gastrointestinal tract and drug release [40] or drug-loaded capsules made of silicone rubber implanted in the ventricular myocardium [41]. Despite their limitations, these macrosystems laid the foundation for further advancements in drug delivery, leading to the development of more sophisticated methods on a smaller scale.

Nanoparticles and microspheres

The beginnings of the second generation of DDSs can be traced back to the 1980s, marking the first reported use of microparticles, microspheres, and microcapsules of sizes ranging from 1 to 1000 μm [39]. The initial focus was on the development of biodegradable structures made of polyesters, such as poly(lactic acid) and poly(lactic-co-glycolic acid). These particles exhibited first-order release kinetics and represented a great departure from the macroscale systems of the previous era. They were easier to administer in the body and served as a protective shield against degradation of the encapsulated active compound. Additionally, "smart" systems were developed allowing for the release of drugs in response to external stimuli such as pH or temperature [42]. Since their invention, the use of microparticles as DDSs has been a subject of ongoing research and development. A range of techniques, such as microdripping, jet-cutting, vibrating, electrospraying, microfluidics, spray-drying, interfacial polymerization, and coacervation phase separation, have been employed to create microparticles, which can be comprised of a variety of materials, including proteins, waxes, polysaccharides, cellulose derivatives, and synthetic polymers [43, 44]. Recent studies in the field of DDSs have reported e.g. the use of chitosan-BSA multilayered hollow microcapsules loaded with doxorubicin for pulmonary delivery, with a diameter of 5 μm, manufactured based on a $CaCO_3$ template [45]. Another notable example is the use of microcapsules with outer and inner phases composed of polyethylene glycol and dextran, respectively, that are capable of releasing 0.4 μg of a drug over days upon the application of ultrasound [46].

The evolution of DDS research saw a progression towards smaller sizes, eventually reaching the nanoscale in the 1990s. This development opened up opportunities for targeted therapies, particularly in the area of cancer treatment with chemotherapy which does not distinguish between healthy and cancerous cells and can have non-specific mechanisms of action. It is worth noting that only a small percentage (less than 10%) of an anticancer drug reaches

its target tumor tissue [47]. The polymer nanoparticles have been shown to successfully lower the concentration of the therapeutic substance inside the body, potentially decreasing the occurrence of side effects related to the therapy. The selection of an appropriate carrier system is dependent on the specific characteristics of the tissue in question, as well as the drug to be delivered. To date, a lot of clinically useful products based on polymer nanoparticles have been successfully developed and marketed, and the effects of such systems on various forms of cancer, including breast, brain, and liver cancer, have been extensively studied [24]. Scientists aim to improve the functionality of the nanocarriers by incorporating features such as nutrient transporters [48], ligands that target specific receptors in the brain [49], and pH-responsive [50] or enzyme-responsive [51] properties. These modifications are directed towards overcoming limitations related to the blood-brain barrier, infiltration, high heterogeneity of tumor cells, drug resistance, and immune evasion resulting from the tumor microenvironment. The nanomaterial-based DDSs have been shown to not only effectively deliver chemotherapy agents, but they can be used in immunotherapy to enhance the body's anti-tumor immune response to eliminate the malignant cells [52]. Nanoparticles are also useful for pulmonary drug delivery as they are able to bypass the various mechanical, chemical and immunological defense mechanisms the respiratory tract has evolved to prevent inhaled particles from reaching the lungs and inactivate them once deposited [53]. In this case, drug-loaded nanoparticles are administered via inhalers [54]. The size of the nanocarrier determines where the deposition will occur in the respiratory tract, allowing for targeted therapies. Such nanoparticles can be made of a whole spectrum of materials – organic like lipids, polymers, dendrimers, carbon and cyclodextrines, or inorganic like metals (silver, gold), oxides or phosphates [55, 56, 57].

Subsequently, the focus shifted towards devising a carrier that could effectively transport the drug across the blood-brain barrier to treat neurological disorders, and exosomes emerged as a promising solution in 2010s [58]. They are small (30 – 100 nm) extracellular membrane particles found in a variety of tissues, playing an important role in biosignalling by releasing different substances depending on the condition of the cells from which they originated. Because of their extraordinary ability to access difficult-to-reach organs and cross the blood-brain barrier, they are promising candidates for use as substance delivery nanosystems [59]. For example, studies on the immobilization of microRNA in exosomes are currently being conducted [60]. The DDS created in this manner crosses the blood-brain barrier, promoting oligodendrocyte differentiation and controlling the inflammatory response. Furthermore, microRNA increases blood-brain barrier permeability, allowing therapeutic drug concentrations to reach the brain. Among others, exosomes have been proposed for use in Alzheimer's disease [61, 62], autism spectrum disorder [63], and Parkinson's disease [59].

Despite the multitude of the above-mentioned potential applications of micro- and nanoparticles as DSSs, it must be noted that they are not universally applicable. For certain medical conditions, the use of such drug carriers may pose a risk of their displacement in the body, leading to ineffective treatment or adverse effects at unintended locations, particularly in the case of topical wound dressings or transdermal DDSs. In such cases, electrospun fiber-based systems can provide an effective solution.

Electrospun fibrous mats

Although the basics of the electrospinning process were developed at the beginning of the twentieth century, with subsequent materials research and development taking place over the following decades [64], it was not until the 1980s that the first published ideas emerged regarding the use of electrospun fibers in biomedical engineering, with the concept of using electrospun DDSs being introduced only in the early 2000s [65]. Electrospinning is a method of fabricating nano- or microfibers from a polymer solution or melt pressed through a metal nozzle connected to a high voltage. It causes the polymer solution or melt to form the jet which is then solidified into fibers by the evaporation of the solvent or cooling and deposited on a grounded collector. In the context of materials engineering, it is essential to carefully select substances that meet the specific physicochemical and mechanical requirements for electrospinning, thus further enhancing the properties of the resulting DDSs. Electrospun mats can be made of both natural materials and synthetic polymers [66]. The use of natural polymers, such as chitosan, gelatin and silk fibroin, as potential materials for DDSs has gained increased attention, given their remarkable biocompatibility and high cellular affinity [67]. However, these natural polymers often exhibit limited stability under physiological conditions and inferior mechanical properties. The synthetic polymers, such as PEG, PLA, PCL, and poly(lactic-co-glycolic acid) (PLGA), possess improved stability in physiological environments, and can be chemically modified to meet specific physicochemical and mechanical requirements for various targeted applications [68]. Both natural and synthetic electrospun mats have unique physical characteristics, including high surface area per unit mass, exceptional porosity, favorable mechanical properties, remarkable axial strength combined with flexibility, low weight, and cost-effectiveness [64]. These fibers typically exhibit diameters ranging from several nanometers to over 1 μm. By manipulating the key process parameters such as the electric voltage, viscosity of the polymer solution, ambient conditions, and the construction of the system, the resulting fibers can be tuned with respect to their diameter, alignment, porosity, and composition, making electrospinning a highly versatile DDS fabrication technique. The fiber structure plays a crucial role in determining the release profile of the substance incorporated within the fibrous mat. Consequently, any modifications in process conditions enhancing the ability to control this structure are of great importance. For example, electrospinning is typically performed using a continuous application of direct-current voltage (DCV). However, studies have suggested that using pulsed voltage (PV) instead of DCV and incorporating additional electrical process parameters (pulse frequency and duration) may further augment the control over the fiber structure [69]. The main challenge in using electrospun fibers as DDSs is the occurrence of an abovementioned burst release effect and limited drug loading capacity. The amount of burst-released substance might reach up to 55% of the total release [19], which reduces the effective lifetime of the system. Furthermore, the high porosity of the fibers (up to 99.2%) [70] results in limited drug loading, with only small amounts of drugs (typically several mg) being immobilized in the system. To overcome these limitations, various modifications to the electrospinning process have been developed, including the use of coaxial nozzles, the creation of hollow fibers, emulsion electrospinning, and increasing the fiber diameter [64].

The versatility of electrospun fibrous mats, due to their unique characteristics and easy tunability, make them a useful tool for drug delivery in the treatment of a variety of pathologies. Electrospun DDSs have a vital application in the wound healing field, particularly in the case of difficult-to-heal and chronic wounds. In such cases, the avoidance of infection is of utmost importance, making the utilization of fibers loaded with antimicrobial medication an attractive option [71]. Such constructs not only release drugs, but also mimic the extracellular matrix structure, enabling cells to rebuild the damaged skin area [72]. Aside from that, the healing process is complex with the wound surrounding environment rich in enzymes and elevated pH. Thorough understanding of wound physiology is essential in designing a system that addresses the various needs throughout the wound healing stages (hemostasis, inflammation, proliferation, and remodeling) to improve skin regeneration [73]. Multilayer electrospun fibers, have been proposed as a solution for effective wound healing. The outer layer, being responsible for isolation from bacteria and reduction of fluid loss, must be hydrophilic and dense. The inner layer has a crucial role in promoting wound healing process, and must exhibit a high level of porosity, thickness, and fluid absorption capacity. Such fibrous mat mimics the architecture of human skin, enabling more efficient healing than single-layer options [71]. The versatility of electrospun fibers used as DDSs extends far beyond wound dressings. They can be utilized as coatings for orthopedic implants to promote bone regeneration and deter the occurrence of infections [74] or for stents in cardiovascular diseases [75]. They are also useful for cancer therapies through topical chemotherapy [76] and for the treatment of ocular disorders [77].

In addition to the conventional drug delivery applications, there has been a growing interest in using electrospinning to create more sophisticated DDSs that would incorporate living cells capable of producing bioactive substances in situ within the body. The encapsulation of living bacteria within nanofibers has been attempted as early as the 2000s [78]. The immobilization of probiotic bacteria producing antimicrobial agents effective against pathogens in electrospun fibers is possible and leads to improved viability, reaching up to 90 days, and reduction of the detrimental effects on probiotics when ingested orally [79]. Furthermore, the thermal stability of the bacteria is augmented [80]. The successful immobilization of more complex eukaryotic cells, such as model yeast, has been achieved in recent years [81]. The developments in this field hold great promise for the advancement of modern therapies. For instance, the creation of an electrospun DDS incorporating pancreatic islets capable of releasing insulin in response to fluctuations in glucose levels has the potential to offer a sustained and regulated treatment option for diabetes. Also, a DDS incorporating T-cells or natural killer cells capable of delivering anti-tumor agents at the site of disease holds potential in the fight against cancer. However, the encapsulation of living eukaryotic cells within electrospun fibers presents a great challenge due to the unfavourable conditions of the electrospinning process. Providing sufficient oxygen and nutrients to the cells within the fiber matrix is challenging, making it difficult to maintain their viability. The encapsulation process may also result in changes in pH and temperature that can create adverse microenvironments. Furthermore, the mechanical stress imposed on the cells during the electrospinning process can lead to decreased survival rates. The use of toxic solvents is also common, and the possibilities of shaping the resulting

fiber mats are quite limited and this would allow for customization to meet the unique requirements of each patient.

3D bioprinted constructs

The beginning of 21st century presented a promising solution to address the aforementioned challenges – 3D bioprinting. This technology provides the capability to precisely implement pre-designed 3D models utilizing biocompatible materials in mild environments. It has its origins in the 3D printing technique, the first mention of which in the scientific literature appears as early as 1983 and the number of publications on this subject is growing each year, currently reaching several thousand annually [82]. Conventional 3D printing offers an unprecedented flexibility in product design, particularly for medicine. Implants and prostheses of any possible shape can be made by the support of magnetic resonance imaging, computed tomography scan or X-ray and translated into 3D digital models [83]. Moreover, unique dosing forms, personalized drug dosing, complex drug release profile are some of the innovations enabled by using 3D printing [84]. During the 2010s, a significant portion of biomedical and materials engineering focus shifted towards the advancement of abovementioned 3D bioprinting technology as it has the potential to fabricate any type of structure incorporating living cells, making it a versatile tool in the field of DDSs. The ability to create complex structures with precise control over cell placement and organization holds great promise for the development of new therapies. 3D bioprinting is a powerful tool for fabricating biomedical components with a range of applications including advanced tissue engineering, drug delivery and screening, and cancer research [85]. The most common technique employed in 3D bioprinting is extrusion, where controlled volumes of so-called bioink, which may contain bioactive substances (drug particles, nucleic acids, proteins like: enzymes, hormones, growth factors, etc.) and/or living cells, are precisely delivered to predetermined locations, leading to the creation of 3D models.

One of the most challenging stages of 3D bioprinting from the perspective of materials science, is undoubtedly bioink development due to the fact that it must fulfill certain conditions. In addition to having the appropriate biological characteristics (biocompatibility, good cell adhesion, expected biodegradation rate), it must have suitable rheological properties – be sufficiently viscous to be dispensed as a filament. It must provide fast gelation time so the post-printing structural integrity is maintained. The material strength and stiffness is also required later for tissues under mechanical loads [82]. All this imposes many restrictions on the materials and technologies that can be used – all the process parameters must be adapted to reduce bioactive substance degradation and cell mortality [82]. It is advised to 3D bioprint at the temperature between 5°C and 50°C, pH of 6.5 – 7.8 and be aware that high extrusion pressure can cause cell death. In addition, only polymer aqueous solutions are suitable for the bioink preparation due to the toxicity of other solvents. Meeting all requirements, hydrogels seem to be the best bioinks, especially natural ones derived from either mammalian sources such as collagen, gelatin, fibrin, and elastin, or non-mammalian sources such as agarose, alginate, and chitosan [86].

Hydrogels are promising material for wound healing. Thanks to their specific structure, they provide gas exchange as well as fluid balance in the wound – they limit water evaporation, absorb exudates and moisturize the area [87]. Such systems have the potential to support cell growth and immobilize bioactive agents like drugs or growth factors for effective tissue regeneration. The mechanical properties of these materials can be optimized through cross-linking methods, such as using ultraviolet light [88]. The 3D bioprinted structures can be tailored to fit the dimensions of wounds, and loaded with patient-derived cells, reducing the likelihood of immune rejection [89]. The properties of such dressings can be improved through incorporation of living cells – for instance, enclosing living microalga inside the hydrogel to achieve continuous dissolved oxygen generation while exposed to visible light [90]. Moreover, 3D bioprinted models have demonstrated the capability of being utilized in many different applications within the field of tissue engineering and drug delivery. 3D bioprinted hydrogel matrices with immunomodulatory and pro-angiogenic agents can be used as a therapeutic patch for myocardial infarction therapies [91], and hydrogel microspikes containing cardiac stem cells to promote cardiomyocyte proliferation and neovascularization after a heart attack [92]. The bone morphogenetic protein-2 (BMP-2) [93] and mupirocin [94] have been successfully incorporated into the 3D bioprinted constructs for growth factor delivery and antibiotic treatment, respectively. Additionally, the use of 3D bioprinted scaffolds loaded with simvastatin has shown promising results as a controlled release system, exhibiting a drug release duration of 20 days and mechanical properties comparable to healthy human clavicle bones [95]. Furthermore, 3D bioprinted polycaprolactone matrices loaded with levofloxacin have been demonstrated to effectively provide sustained drug release for a period of 4 weeks, displaying potential for the treatment of diabetic foot ulcers [96].

Hybrid systems

In pursuit of the perfect DDS, the integration of different techniques has become a growing area of interest in the field of materials science. By combining the strengths of microspheres, nanoparticles, electrospun fibers and 3D bioprinted constructs, mixed systems with superior properties are being proposed each year. These hybrid systems have the potential to provide a more comprehensive solution to the limitations faced by individual methods of DDS manufacturing.

One way to enhance the properties of 3D bioprinted constructs is by incorporating nanoparticles into the bioink. An example of this hybrid approach can be seen in the study by Deng et al. [97], where a 3D bioprinted scaffold was made from a mixture of PLGA and nano-sized hydroxyapatite and chitosan nanoparticles loaded with recombinant human bone morphogenetic protein 2 (rhBMP-2). It demonstrated successful control of the early burst effect of rhBMP-2, exhibited biocompatibility and effectively repaired an experimental bone defect in rabbit mandibles. The utilization of hybrid 3D bioprinted scaffolds for bone regeneration has also been demonstrated by Lin et al. [98]. They devised a method of 3D bioprinting magnetic chitosan scaffolds with embedded ferric oxide nanoparticles and culturing bone cells on them in the presence of an electromagnetic force. This resulted in enhanced osteoblast proliferation, differentiation and mineralization.

Not only can bioink be loaded with nanoparticles but also with drug-loaded microspheres. Such a hybrid 3D bioprinted system was designed by Johnson et al. who worked on a pectin-Pluronic bioink containing gelatin-pectin-chitosan electrosprayed microcapsules (100 µm diameter) loaded with β-estradiol [99]. The results indicated that microspheres did not adversely affect the bioprinting process. However, biological properties of the system have not been tested. Wen et al. advanced the field with their preparation of a 3D-bioprinted gelatin-alginate scaffold modified with PLGA microspheres loaded with granulate colony-stimulating factor (G-CSF) [100]. This system allowed for spatial control of drug distribution increasing the local concentration of G-CSF. Results showed improved endometrial and vascular regeneration and restored pregnancy function in a rat model with damaged uterine cavity. Such hybrid systems are also being explored for the purpose of promoting bone regrowth. Wei et al. conducted a study focused on 3D bioprinting the PLGA porous scaffold with high levels of hydroxyapatite (similar to that found in natural bone) in the form of microspheres [101]. It had high compressive strength, improved cell adhesion, proliferation, and differentiation, as well as exhibited the osteogenic performance in vivo. Zhuang et al. explored a different method for bone regeneration by first printing a scaffold from PCL and then incorporating core/shell microspheres into its porous structure [102]. The microspheres comprised a heparin-coated PLA core surrounded by an alginate layer, and were loaded with BMP-2. The resulting hybrid system displayed remarkable efficacy in promoting bone regeneration both in vitro and in vivo, as the release of BMP-2 was well-controlled, leading to an improvement in osteogenic performance. Wang et al. aimed to create a stronger bioink for 3D bioprinting by combining gelatin methacrylate (GelMA) with poly(glutamic acid)/hydroxypropyl chitosan microspheres [103]. The composite granular hydrogel showed superior strength and was successfully used as a bioink for bioprinting, with the adipose derived stem cells proliferating well in the material.

Combining the two cutting-edge techniques of 3D printing and electrospinning also provides a powerful platform for fabricating novel hybrid DDS offering a range of advantages over conventional methods, including improved shape control and greater biomimetic properties [104]. Li et al has developed a method for coating 3D bioprinted PCL scaffolds with electrospun PLGA-gelatin-collagen nanofibers, resulting in a fibrous surface structure that promotes adhesion and proliferation of pre-osteoblasts and bone marrow mesenchymal stem cells (BMSCs) [105]. Immobilization of BMP-2 mimicking peptides to the nanofiber-modified scaffolds enhances BMSCs osteogenic differentiation, as indicated by increased microRNA expressions of osteogenic markers. Yoon et al. aimed to address the problem of the fragility of hydrogel-based bioprinted constructs which may limit their practical applications in tissue engineering [106]. They developed a hybrid system that combines 3D bioprinting of sodium alginate bioink with alternating layers of flexible PCL nanofiber mats. This approach resulted in improved shape resolution, reduced shrinkage distortion, enhanced mechanical properties, and the ability to fabricate complex structures with internal channels for improved perfusion and cell growth.

Electrospun fibers can be also modified using nanoparticles, leading to the development of numerous hybrid DDSs [107]. Amini et al. conducted a study to evaluate the potential of electrospun PCL fibers with lignin nanoparticles for nerve regeneration [108]. Such a system had improved water uptake, in vitro degradation, and Young's modulus compared to PCL fibers alone. The study also found that the cell viability and neural differentiation were promoted with increasing lignin content. Jiang et al. integrated curcumin, a potent natural anti-cancer agent, into a hybrid of electrospun PCL-gelatin nanofibers using zeolite Y nanoparticles [109]. In vitro testing showed that this DDS exhibited improved drug release and greater cytotoxicity against glioblastoma cells compared to curcumin-loaded nanoparticles. Ahmady et al. developed a novel alginate nanoparticle-loaded electrospun PCL-chitosan nanofibrous DDS for the controlled release of capsaicin [110]. The results showed that the nanocomposite system effectively prolonged the release of a substance for over 500 hours and inhibited the growth of human breast cancer cells while being non-toxic to human skin cells.

The integration of microspheres into electrospun fibers presents an interesting concept, as the average dimensions of microspheres tend to be larger than those of fibers. This can result in an increased drug capacity of the resultant hybrid DDS. However, research in this area remains limited so far. Gao et al. developed a method to create composite systems by electrospraying PEG microspheres and electrospinning silk fibroin/gelatin nanofibers at the same time [111]. Balzamo et al. presented a novel method for creating composite systems using a combination of electrospinning and vapor-induced phase separation [112]. This approach results in the in-situ creation of polyvinylidene fluoride microparticles within electrospun PCL fibers, having increased Young's modulus and tensile strength while maintaining porosity. Another example of a hybrid DDS is the electrospun polystyrene (PS) nanofibers immobilized with sodium alginate electrosprayed particles loaded with probiotic microorganisms (*Lactobacillus plantarum*) proposed by Grzywaczyk et al. [113]. This system with a "sandwich" layered structure (PS/alginate/PS) has been shown to provide the highest cell activity in comparison with free cells and cells in alginate only.

Despite the vast diversity of DDSs, they all share common characteristics of biocompatibility, precision, stability, and sustainability. The fields of biomedical engineering and materials science have made significant progress in understanding the physiological challenges that can hinder effective drug delivery, as well as in developing new methods of drug delivery that are now used in clinical settings. Researchers are continuously striving to enhance existing drug delivery methods and design novel ones in order to optimize the utility of existing medications.

2

MAIN GOAL AND RESEARCH THESES

The goal of my work was to develop a foundation for new controlled drug delivery systems manufactured using electrostatic and 3D bioprinting techniques, which would be characterized by an increased drug capacity and an elimination of the drug burst release effect in the first stage of action of systems based on electrospun polymer fibrous mats or 3D bioprinted hydrogel constructs.

I have formulated three Theses to accomplish the research objective:

(1) The use of pulsed voltage (PV) with additional controllable electrical parameters, such as the electrical pulse duration and frequency, stabilizes the process of electrospinning and electrostatic droplet formation, enabling the production of synthetic polymer fibers or microspheres of the desired diameter.
(2) Appropriate selection of the cross-linking method and agents used to treat the electrospun or 3D bioprinted constructs leads to obtaining stable, water-insoluble structures of polyvinylpyrrolidone, gelatin and sodium alginate, and in the case of hydrogels, eliminates the burst effect in a 3D bioprinted drug delivery system.
(3) Non-aggregated, drug-loaded synthetic polymer microspheres can be produced and used as an additive to electrospinning suspension or bioink for 3D bioprinting, resulting in an increased drug capacity of the electrospun or 3D bioprinted drug delivery system, and in the case of electrospun fibers, an elimination of the burst effect.

3

EXPERIMENTAL PART

In order to verify the Theses that I had put forth, I implemented a set of three different techniques. Electrospinning and 3D bioprinting served as the foundation for the development of potential drug delivery systems, while the electrostatic manufacturing of polymer microspheres was an innovative method used to modify them. My research was focused on utilizing both natural and synthetic polymeric materials, and I successfully immobilized bioactive substances (antibiotics: chlorhexidine acetate, ampicillin) and their marker (rhodamine 640) within the developed drug carriers. Through a comprehensive set of analyses, I was able to investigate the properties and some potential capabilities of the proposed systems. The details of my experimental work are outlined in this chapter.

Electrospinning

A large part of my research was dedicated to investigating the electrospinning process and electrospun fibrous mats. I examined how various process conditions influence the structure and properties of the resulting mats, and studied methods for modifying the obtained mats to enhance their properties that are crucial in the context of their potential use as DDSs (drug capacity and burst release absence). A comprehensive description of the electrospinning process and my works in this field can be found in the Publications (1) and (3).

Electrospinning with pulsed voltage

In the first stage of my work, I examined the differences in the structure of mats obtained with direct-current (DCV) and pulsed voltage (PV) electrospinning, and I evaluated the impact of modifications of electrical parameters values on the resulting fiber mats.

I used two different polymers – polyvinylpyrrolidone (PVP) with a molecular weight of 1300 kDa and polylactide (PLA) with a molecular weight of 200 kDa. Both of these polymers are commonly employed in the field of biomedical engineering for their potential in the fabrication of DDSs, owing to their biocompatibility and versatility in the formation of various nano-

and microstructures. PVP exhibits water solubility but is not biodegradable, whereas PLA is not water-soluble but demonstrates biodegradability. I prepared solutions of PVP at concentrations of 3.5% and 8.0% using ethanol as solvent, with viscosities of 32 mPa·s and 200 mPa·s (measured at 25°C), respectively. Solutions of PLA at concentrations of 8.0% and 10.0% were prepared with a mixture of chloroform and dimethylformamide as solvents, in a ratio of 9:1, with viscosities of 605 mPa·s and 1310 mPa·s (measured at 20°C), respectively. I performed the electrospinning process using a custom-built setup consisting of a high voltage pulse generator, an infusion pump connected to a steel nozzle (inner diameter of 0.6 mm), and a grounded aluminum collector plate (diameter of 40 mm, thickness of 0.12 mm) placed 150 mm below the nozzle tip. The polymer solution was supplied at a flow rate of 0.9 ml/h. The high voltage values was set as 8 and 15 kV (for both DCV and PV), and in the case of PV, additional parameters were: pulse supply frequency of 20, 50 and 100 Hz and pulse duration of 5 ms. The experiments were performed under ambient conditions of temperature 25°C (20°C) and humidity levels not exceeding 40%.

In the course of the electrospinning process, I examined the geometric shape of the polymer solution as it flowed out of the nozzle under the influence of the applied electric voltage, and subsequently I drew conclusions about the stability of the process based on this observation. Utilizing a monochrome CCD camera, I recorded images of the nozzle outlet. I analyzed the structure of the mats deposited on the collector using scanning electron microscopy (SEM). Next, I quantitatively determined the average diameter of the fibers, as well as the number and size of bead-on-string structures present in the fiber mats. Finally, I performed a statistical analysis of the obtained results to further understand the trends and patterns in the data.

The process setup and research methodology of this part of my thesis are outlined in detail in the Publication (1).

Electrospun fibers modified with microspheres - suspension electrospinning

In the next phase of my research related to electrospinning process, I elaborated a technique of suspension electrospinning that enables the production of fibrous mats modified with drug-loaded microspheres – a potential DDS with enhanced drug capacity and the elimination of the burst release effect. Moreover, I subjected the fibrous mats to cross-linking using photoinitiator and ultraviolet light, thereby introducing additional parameter such as cross-linking time.

In this instance, I chose polyvinylpyrrolidone (PVP) as the fiber-forming polymer due to its biocompatibility and solubility in ethanol – an easily available and relatively safe organic solvent compared to other solvents commonly used in the electrospinning process. Moreover, PVP can be conveniently cross-linked using ultraviolet light in the presence of benzophenone (BP), resulting in a water-insoluble material while also improving control of its properties. I dissolved PVP and BP in ethanol with a concentrations of 18.5% and 3.75%, respectively. Next, I prepared suspensions of polycaprolactone (PCL) or polyethersulphone (PES) microspheres in ethanol with a microsphere content range of 10-65 mg/mL. I fabricated the polymer microspheres before using a novel method developed by me, as detailed in

a subsequent section of this thesis. The average diameters of the microspheres were 14.38 ± 6.28 μm for PCL and 6.20 ± 2.43 μm for PES. Finally, I combined two mixtures using a syringe coupler technique, resulting in a suspension of PCL (or PES) microspheres with final concentrations of 5-30 mg/mL in a 10% PVP ethanolic solution with 2% benzophenone. The suspension was then electrospun. I utilized a custom-built setup with a high voltage pulse generator that provided PV to a steel nozzle of an inner diameter of 0.6 mm. As a collector, I used a rotating grounded aluminum drum with a diameter of 47.5 mm and width of 150 mm placed 150 mm from the nozzle tip. Process parameters were set as: suspension flow rate 0.6 ml/h. voltage 8 kV, pulse frequency 100 Hz, pulse duration 8 ms, drum rotation speed 120 min^{-1}, electrospinning time 6 h. Upon completion of the process, the polymer mats underwent cross-linking having their both sides subjected to UV radiation (365 nm) for 5, 15 and 60 minutes. For the purpose of degradation testing and comparison, I prepared UV-cross-linked fibrous mats without the incorporation of microspheres with a 10% PVP, 2% BP solution in ethanol.

I conducted a thorough examination of the mats, comprising of a range of analyses. Through the use of SEM and digital microscopy, I examined the morphology of the mats. I also analyzed their degradation in a Hanks′ Balanced Salt Solution (HBSS), and compared the diameters of the fibers before and after degradation. I also determined the differences in diameter of the fibers prior to and after incorporating them with microspheres. In addition, the mechanical properties of the mats, such as tensile strength and elongation at break, were evaluated in relation to the cross-linking time and the content and type of microspheres. Utilizing spectrophotometric method, I determined the extent to which modification with marker-loaded (rhodamine) microspheres increased the mat capacity for the active substance, and further characterized the release profiles of the substance from the fibers. The tests were performed within a closed system, the marker substance was released into an aqueous medium, with a sample mass-to-volume ratio of 5.5 mg to 3 mL. I monitored the absorbance of light in the medium at designated intervals, with the wavelength of 574 nm which is absorbed by rhodamine. The measurements were conducted every 2 minutes for the first 2 hours, every 10 minutes for the following hour, every 30 minutes for the subsequent 2 hours, and after 6, 7 and 24 hours. The conversion of absorbance values to rhodamine concentration was achieved by employing the standard curve, established according to the Lambert-Beer law. I mathematically characterized the rhodamine release profiles by fitting a model curve of the transfer between two phases to the experimental data, and subsequently calculated the transport coefficient h [cm/min], which described the release speed of the substance during the first stage. Finally, the antibacterial properties of the ampicillin-loaded mats against *Staphylococcus aureus* (Gram+) and *Escherichia coli* (Gram−) bacteria were assessed.

The research methodology used in this part of my thesis is comprehensively described in the Publication (3).

3D bioprinting

In parallel to my investigations into the electrospinning for manufacturing the new, potential electrospun DDS, I also examined the capabilities of 3D bioprinting for the same purpose. I viewed this technique as a complementary or competitive alternative to electrospinning, offering the ability to design DDSs with distinct properties, tailored for a range of therapeutic applications. The 3D bioprinting process can be conducted under milder conditions and with the use of less toxic materials than electrospinning. This method allows for precise control over the placement of materials, thereby enabling the fabrication of complex three-dimensional structures. Additionally, it allows for the incorporation of living cells into the printed structure, which presents great potential for fields such as tissue engineering. The Publications (4) and (5) provide a description of my research on 3D bioprinting as a potential method for the manufacturing of DDSs using two different bioinks (gelatin-alginate and gelatin methacrylate-gelatin) and further insight into the details of this technique.

3D bioprinted gelatin-alginate hydrogel matrices

In this part of the study, my objective was to combine 3D bioprinting with various cross-linking methods to create a new stable and biodegradable hydrogel matrix composed of natural polymers – gelatin and alginate, with a view towards potential application in drug delivery.

I prepared a bioink by dissolving 0.04 g/mL of sodium alginate and 0.2 g/mL of gelatin in reverse-osmosis water. Some bioink were formulated with the addition of marker (rhodamine 640) at a concentration of 0.1 mg/mL or antibiotic (chlorhexidine acetate, CA) at concentrations of 0.1 mg/mL and 1.0 mg/mL. Using this bioink, I implemented 3D bioprinting to fabricate cubic mesh matrices with dimensions of 20 mm × 20 mm × 12 mm, which were constructed of 6 layers with a grid size of 1.0 mm and a line width of 0.2 mm, all of which I had designed digitally. I experimentally determined the 3D bioprinting parameters through a series of extensive tests. Eventually, I employed the following parameters: a nozzle with an inner diameter of 0.164 mm, a printing speed of 10 mm/s, a temperature of the bioink in the syringe of 37°C, a temperature of the collector Petri dish of 15°C, and a printing pressure of 380 kPa (55 psi). After the 3D bioprinting process, I cured the hydrogel matrices using an ionotropic gelation of sodium alginate with a solution of calcium ions of concentrations of 2% and 5% (for 10 min) and chemical cross-linking of gelatine with glutaraldehyde (GTA) vapors (for 24 h) from water solutions with concentrations of 0.5%, 5% and 25%. By combining the gelation and cross-linking methods in different ways, I generated a total of 12 different samples (including an un-cross-linked one for comparison). Subsequently, I gently rinsed each sample with reverse-osmosis water, I placed the samples for 48 hours in a phosphate-buffered saline solution (PBS) and subsequently for an additional 24 hours in a 20% glycine solution to eliminate and neutralize any remaining GTA residues. I lyophilized the samples for tests requiring anhydrous material.

I evaluated the feasibility of the 3D bioprinting with proposed gelatin-alginate bioink, and I determined the compatibility of the printed model with the digital design. Through the use of SEM, optical and fluorescent microscopy, I examined the structure of the cross-linked hydrogel matrices. Thermal properties of matrices were tested using differential scanning calorimetry (DSC) and thermogravimetric analysis (TGA) to assess the influence of chemical cross-linking and lyophilization on the structure of the matrices. Utilizing a gravimetric method, I established the equilibrium swelling ratio (ESR) of the 3D bioprinted matrices in PBS at 37°C. Furthermore, I investigated the transport properties of the bioprintouts using spectrophotometric method by measuring the concentration of rhodamine in water in which the samples were placed at designated intervals (every 2 minutes for the first 6 hours, every 30 minutes for the next 2 hours, and after 9 hours). This allowed me to determine the release profiles of the substance. I conducted long-term studies to determine the release up to 12th week as well. I mathematically described the experimental data through the fitting of linear and exponential functions. Cytotoxicity of the prints against HaCaT cells was examined as well as the antibacterial properties of the matrices loaded with the CA antibiotic against *Staphylococcus aureus* (Gram+) and *Pseudomonas aeruginosa* (Gram−).

The Publication (4) provides an in-depth description of the research methodology of this part of my thesis.

3D bioprinted microsphere-loaded gelatin methacrylate hydrogel matrices

Due to the difficulties associated with cytotoxicity resulting from the use of glutaraldehyde for cross-linking bioprinted matrices of gelatin-alginate hydrogel and their neutralization, I chose to utilize gelatin methacrylate (GelMA) in my further research. This material can be cross-linked in a non-toxic manner using photoinitiator and ultraviolet light. I also sought to improve the properties, including transport ones and drug capacity, of the hydrogel matrices manufactured in this part of my work by incorporating them with drug-loaded microspheres.

I began with synthesizing GelMA by carrying out the reaction of gelatin with methacrylic anhydride (MA) as described in the established protocols in the literature. The reaction was conducted at 50°C for 3 hours before being stopped by the addition of a large volume of PBS (20°C). Then, I dialyzed the resulting mixture against deionized water for 7 days. Next, I lyophilized the solution and obtained a white solid material – GelMA. I then proceeded to prepare drug-loaded PCL and PES microspheres using a novel method that I had developed for my research, which is further detailed in this chapter. The average microsphere diameters were 14.38 ± 6.28 μm (PCL) and 6.20 ± 2.43 μm (PES). Finally, to prepare the final bioink, I made three initial mixtures: (A) 35% gelatin solution in PBS, (B) 14% GelMA solution in PBS with the addition of 0.7% lithium phenyl-2,4,6-trimethylbenzoylphosphinate photoinitiator (LAP), and (C) suspension of PES or PCL microspheres in PBS in the amount of 15 mg/mL or 30 mg/mL. I used both microspheres without additives and substance-loaded ones with rhodamine for transport studies or ampicillin for antibacterial studies. I blended together the solutions (A), (B) and (C) in the 1.9 : 2.1 : 2 ratio using the syringe coupler method, thus obtaining a bioink composed of microspheres at final concentrations of 5 mg/mL or 10 mg/mL suspended in

11% gelatin and 5% GelMA solutions in PBS, with a 0.25% addition of LAP. Then I executed a 3D bioprinting process of the same model as in the case of gelatin-alginate bioink (a cubic mesh). This time, through experimentation, I chose the following process parameters to print the suspension of microspheres: a nozzle with an inner diameter of 0.164 mm, a printing speed of 10 mm/s, a temperature of the bioink in the heated syringe of 28°C, a temperature of the collector Petri dish of 15°C, and a printing pressure of 345 kPa. After printing the matrices, I cross-linked them using ultraviolet light (wavelength 365 nm) for the periods of 5 minutes and 10 minutes. Overall, I created 10 different samples of matrices that varied in terms of the type and content of immobilized microspheres and cross-linking time. These matrices did not require any further processing such as rinsing or neutralization, and only those intended for tests requiring anhydrous materials were subjected to lyophilization.

I analyzed and characterized the resulting matrices using a variety of techniques to assess their properties and potential as DDSs. First, I assessed the printability of the GelMA-gelatin bioink containing different amounts and types of microspheres and I analyzed the samples that were successfully 3D bioprinted using digital microscopy and SEM. I then used Fourier transform infrared spectroscopy (FTIR) to determine the effect of cross-linking and the addition of microspheres on the chemical structure of the matrices. I also analyzed the effect of bioink modification with microspheres on its thermal properties using DSC and TGA. I examined the swelling of the matrices and determined their ESR in PBS at 37°C using a gravimetric method. I evaluated the transport properties of matrices by spectrophotometric determination of rhodamine concentration in water during its release profile examination. The absorbance measurements were taken at specific intervals – every 2 minutes for the initial 2 hours, every 10 minutes for the subsequent hour, every 30 minutes for the following 2 hours, and then after 6, 7 and 24 hours. I mathematically described these properties with a linear function fitted to the plotted experimental points of the initial one hour of the substance release, which allowed me to determine the transport rate. Cytotoxicity of the bioprinted matrices against HaCaT cells was tested. Lastly, I examined the antibacterial properties of matrices with ampicillin-loaded microspheres against *Staphylococcus aureus* (Gram+) and *Escherichia coli* (Gram–) bacteria.

The full methodology of my study is documented in the Publication (5) for further reference.

Electrostatic microsphere formation

Given the historical origins of controlled drug delivery systems and the fundamental role of microparticles as drug carriers in the development of this field, I drew inspiration from established ideas and I decided to incorporate polymer microspheres into my research. My aim was to utilize them to modify electrospinning and 3D bioprinting processes in such a way that the microspheres are dispersed within the structure of fibers or bioprintouts, serving as drug-loaded microcontainers. To prepare a suspension for electrospinning or bioink for 3D bioprinting, it was essential for the microspheres to have a diameter smaller than the nozzles used in these techniques, be non-aggregated, easily obtainable in powder form, and made of biocompatible polymers, preferably via electrostatic techniques. My thorough literature review

did not uncover any reports of an approach for producing such microspheres. Thus, I elaborated the method myself, drawing on the experience of the Laboratory of Electrostatic Methods of Bioencapsulation and my own. A comprehensive description of the developed method can be found in the Publication (2), with further details on the application of microspheres to modify polymer fibrous mats and 3D bioprintouts provided in the Publications (3) and (5), respectively.

New method for manufacturing the disaggregated polymer microspheres

I prepared a series of polymer solutions, specifically 4-20% PCL in dimethylformamide (DMF), 15% PCL in N-methylpyrrolidone (NMP), 15% polyethersulphone (PES) in DMF, and 15% PES in NMP. Both PCL and PES are biocompatible polymers, however PCL is biodegradable whereas PES is not. I primarily utilized PCL solutions in DMF to elaborate the method and to investigate the impact of process parameters on the structure and size of the microspheres. The other polymer/solvent combinations were used to evaluate the versatility of the method and to determine the effect of the type of polymer/solvent on the final product. The method for producing microspheres is based on electrostatic spraying and subsequent collection of microdroplets in a well-stirred precipitation bath. The spraying part of the experimental setup was similar to that used in electrospinning. The polymer solution was pumped by an infusion pump (at a rate of 0.34 mL/h) through a metal nozzle (inner diameter 0.445 mm) connected to high voltage (DCV or PV) generated by a custom-built generator. The electrical parameters investigated in the study were electrical voltage of 8 kV for DCV and electrical voltage of 8 kV and 11 kV, pulse frequency of 20 – 80 Hz, and pulse duration of 2 – 8 ms for PV. The microspheres were collected in a Petri dish filled with 96% ethanol and then centrifuged and dried to be obtained in the form of powder that was ready for further analysis or application.

During the process, I examined the shape of the meniscus of the polymer solution formed under the influence of electric voltage at the nozzle outlet using a monochrome CCD camera. Through the use of SEM, I analyzed the surface morphology of the microspheres produced. I measured the diameters of the microspheres, calculated their mean values and performed statistical analysis to determine any statistical differences in size between the microspheres produced in different experimental sets. To gain a deeper understanding of the chemical composition of the microspheres, I employed FTIR. Additionally, X-ray diffraction analysis (XRD) was used to determine the crystal structure of the microspheres and their specific surface area was examined through the use of BET nitrogen adsorption-desorption isotherms method. Furthermore, I investigated the potential for active substance immobilization in the microspheres using rhodamine as a marker. Through spectrophotometric analysis, I evaluated the transport properties of the microspheres placed in ethanol by measuring the concentration of rhodamine in solution during the release.

I have documented the specifics of my research methodology concerning microsphere manufacturing in the Publication (2). Using the drug-loaded PCL and PES microspheres manufactured via newly developed method, I modified electrospun fibers and 3D bioprinted matrices, as outlined in previous sections of this chapter as well as in more detail in the Publications (3) and (5).

4

OVERVIEW OF THE RESULTS

The following section provides a thorough overview of the results obtained from the study, organized by the research Theses. The key findings of the study are clearly and concisely described, with a focus on the most important results in relation to the main aim of my doctoral dissertation. The section indicates how the Theses were confirmed and in which Publication the related studies were described. Trends observed in the data are showed, and a summary of the crucial results is provided.

THESIS (1)

The use of pulsed voltage (PV) with additional controllable electrical parameters, such as the electrical pulse duration and frequency, stabilizes the process of electrospinning and electrostatic droplet formation, enabling the production of synthetic polymer fibers or microspheres of the desired diameter.

The Thesis (1) is addressed in the Publications (1) and (2).

During my research, I incorporated the use of pulsed voltage (PV) in two techniques, namely electrospinning and electrostatic droplet formation used in the method for producing microspheres. The PV, in comparison to a direct-current voltage (DCV), was assumed to introduce additional parameters into the process such as pulse duration and frequency, thus potentially elevating the control over the process.

In the electrospinning studies, I demonstrated that the use of PV in this process is possible and can result in better outcomes when compared to the conventional approach of using DCV in certain cases. In Fig. 4, I have presented a highlight of the crucial findings from the Publication (1) that are relevant to the Thesis (1).

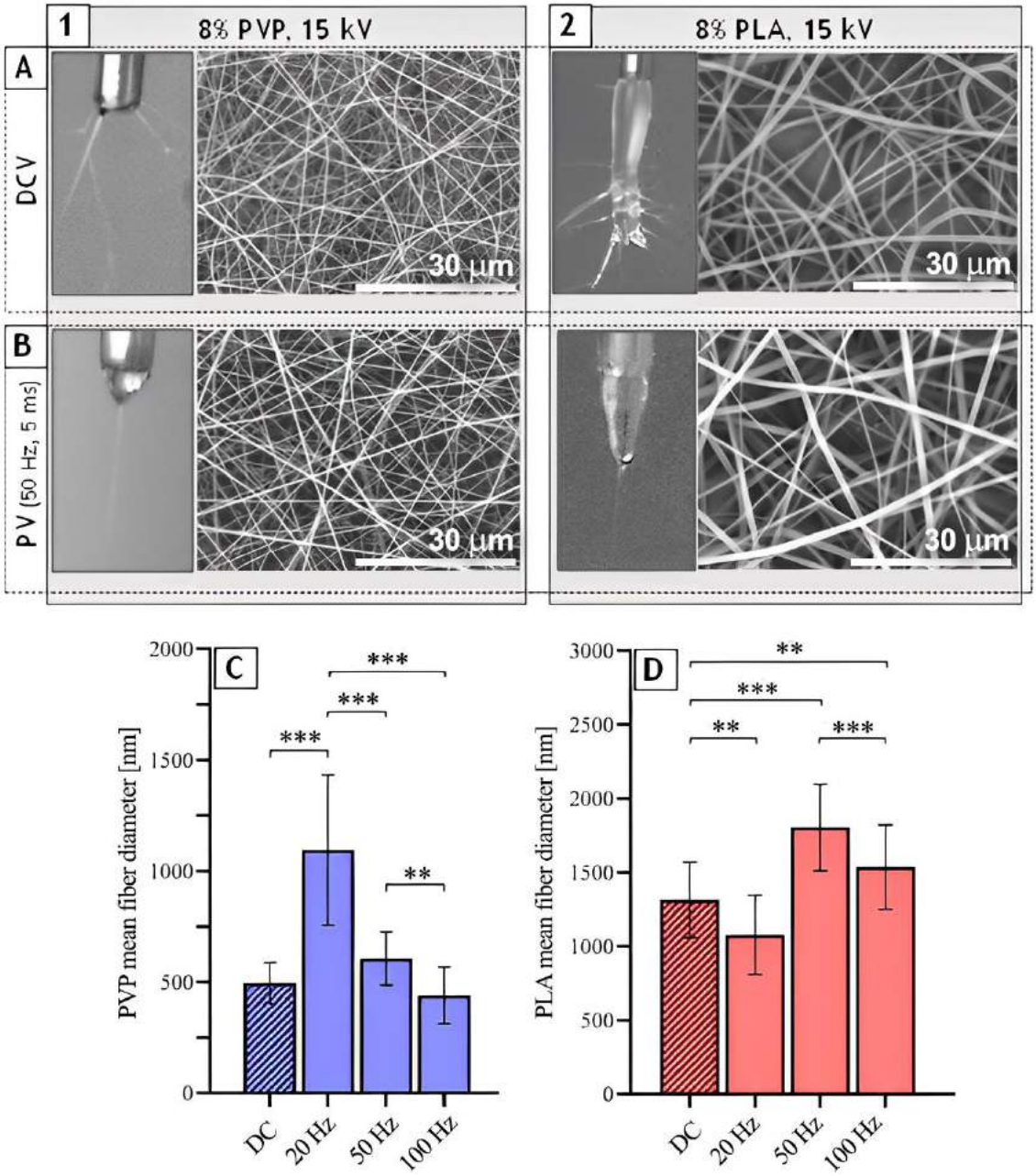

FIGURE 4. Polymer **(1)** PVP and **(2)** PLA solution geometrical shape at the tip of the nozzle during electrospinning under different electrical conditions: **(A)** DCV at 15 kV, and **(B)** PV at 15 kV, 50 Hz, 5 ms. The diameters of fibers obtained with DCV (15 kV) and PV (15 kV, 5 ms) from **(C)** 8% PVP solution and **(D)** 8% PLA solution. The statistical differences between the mean diameters of microspheres obtained in different sets of experiments were determined. The significance level (α) was set at 0.05 and the probability of data was considered statistically significant for p-values < 0.05. The results were marked on charts in the form of asterisks: (*) for $p < 0.05$, (**) for $p < 0.01$ and (***) for $p < 0.001$.

Selected research results from the Publication (1)
Mirek et al., Polymer fibers electrospun using pulsed voltage, *Mater. Des.* 183, 108106 (2019)

I examined the impact of the type of electrical voltage applied to the nozzle on the formation of polymer solution meniscus at the nozzle tip (droplets, cones, and jets) during electrospinning. My findings showed that when an 8% PVP solution was electrospun using DCV (15 kV), the cone formation was disrupted, resulting in the formation of multiple jets (Fig. 4A1), indicating an unstable and uncontrolled process. When the same PVP solution was electrospun using pulsed voltage (15 kV, 50 Hz, and 5 ms pulse length), a stable Taylor cone was formed at the nozzle outlet (Fig. 4B1). Electrospinning of the 8% PLA solution with DCV (15 kV) led to the formation of an elongated liquid shape with multiple side jets (Fig. 4A2), which increased as the process progressed. However, these side jets were inactive (not undergoing electrospinning) and only disturbed the process. Eventually, this resulted in the formation of a polymer plug and clogging of the nozzle. The PLA solution shape was different under the influence of PV (15 kV, 50 Hz, 5 ms), it took a form of a slim bulb, from which a single electrospinning jet was generated (Fig. 4B2). This process was stable and did not cause nozzle clogging. Regardless of the type of polymer solution or applied electrical voltage, smooth fibers were consistently produced (SEM images in Fig. 4). The fibers only varied in terms of mean diameter. For PVP fibers electrospun using DCV the diameter was approximately 500 nm, as indicated on the graph in Fig. 4C. The application of PV electrospinning with a frequency of 20 Hz resulted in a doubling of fiber diameter (1000 nm), while further increasing the frequency to 50 Hz decreased the diameter to 600 nm and to 500 nm at 100 Hz. With regards to electrospun PLA fibers, the average diameter was 1300 nm using DCV (Fig. 4D). The use of PV electrospinning caused a decrease in diameter to 1000 nm at a frequency of 20 Hz, an increase to 1750 nm at 50 Hz, and to 1500 nm at 100 Hz. These differences were statistically significant ($p < 0.01$ and $p < 0.001$) they were attributed only to modifications in the pulse frequency, while retaining a constant pulse duration (5 ms) and electrical voltage (15 kV) values.

The results of this part of my study demonstrate that the incorporation of the electrical pulse frequency as an additional parameter provides enhanced control over the electrospinning process and the fiber diameter, owing to a more precise electrical charge supply. In the Publication (1), I comprehensively analyzed the polymer solution shape at the nozzle outlet across different conditions, including varying concentrations of PVP (3.5% and 8%) and PLA (8% and 10%), and electrical voltage of 8 kV and 15 kV, with pulse frequency of 20 Hz, 50 Hz and 100 Hz. I established correlations between the liquid shape at the nozzle tip and the resultant structure of the electrospun fibrous mats, indicating various possible cases.

I decided to use the pulsed voltage also in the method of producing polymer microspheres in the process of electrohydrodynamic droplet formation using a metal nozzle under high voltage. This was done with the aim of achieving greater process control thanks to more precise delivery of the amount of electric charge to the nozzle, similarly to the advantages observed in the electrospinning process. As a result, I obtained a fraction of microspheres with a small diameter range. The selected results from the Publication (2), which are related to the Thesis (1), have been summarized in a graphical representation in Fig. 5.

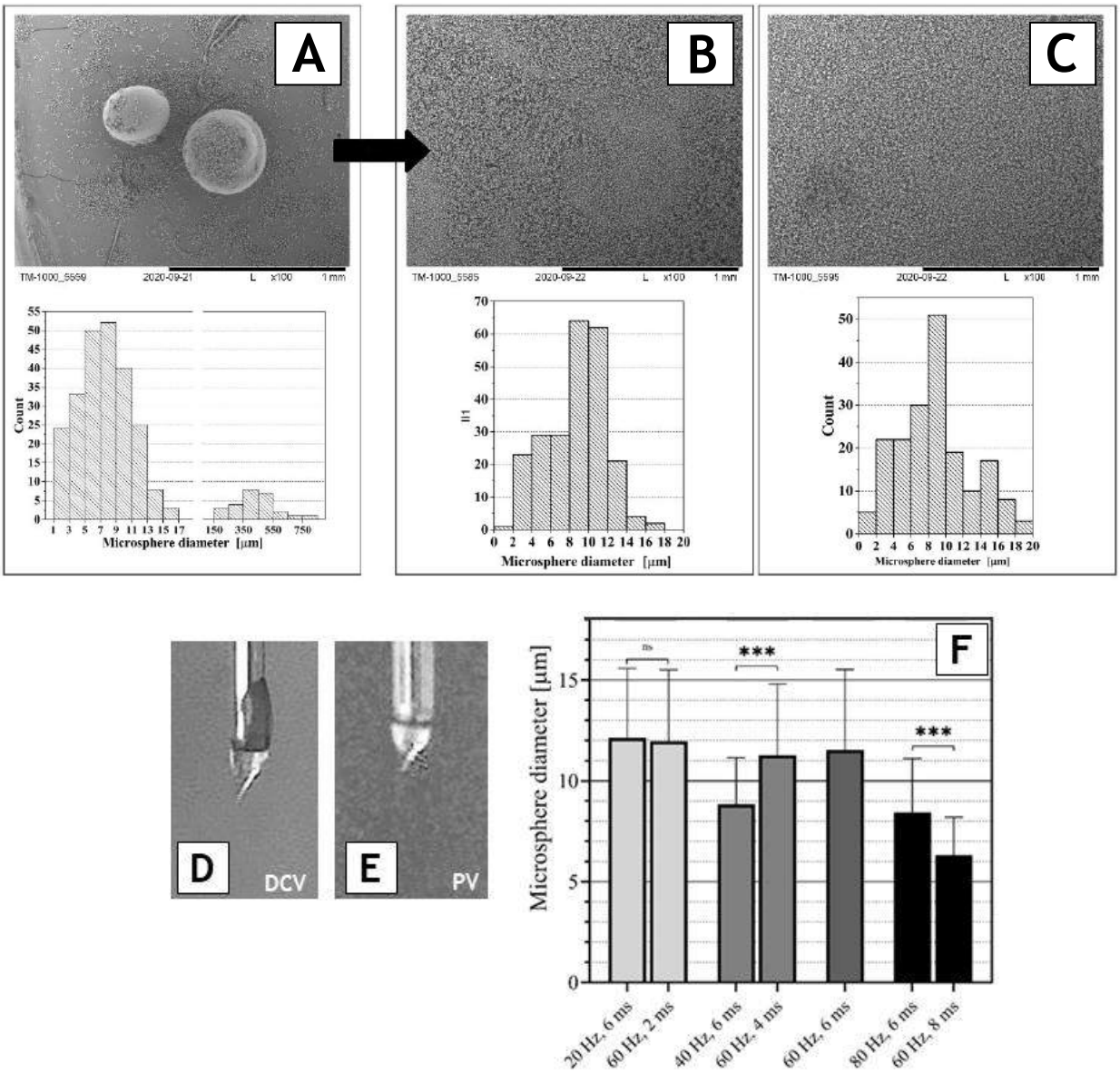

FIGURE 5. (A – C) Scanning electron microscopy pictures of PCL microspheres obtained with 15% PCL/DMF solution under different electrical conditions: **(A)** DCV of 8 kV, **(B)** PV of 8 KV, 70 Hz, 8 ms, **(C)** PV of 8 kV, 50 Hz, 9 ms. Histograms showing the distribution of the measured microsphere diameters for a given sample are located beneath the corresponding photographs. **(D, E)** Frames from process recordings visualizing the geometric shape of outflowing 20% PCL/DMF solution under different electrical conditions: **(D)** DCV of 8 kV, **(E)** PV of 8 kV, 60 Hz, 6 ms. **(F)** The mean diameter of microspheres electrosprayed from the 20% PCL/DMF solution using PV of 11 kV, depending on the value of pulse duration and its application frequency.

Selected research results from the Publication (2)

Mirek et al., Formation of disaggregated polymer microspheres by a novel method combining pulsed voltage electrospray and wet phase inversion techniques, *Colloids Surf. A Physicochem. Eng. Asp.* 648, 129246 (2022)

The SEM images displayed in Fig. 5A-C illustrate PCL microspheres at a magnification of 100× to enable the demonstration of the extra fraction portion of microspheres produced in the process conducted with DCV. As depicted in Fig. 5A, a presence of the supplementary fraction, represented by two large microspheres, can be observed against an abundance of smaller microspheres from the basic fraction. The histogram associated with Fig. 5A illustrates the presence of microspheres ranging in size from 1 to 17 μm, as well as defects in the form of bimodal diameter distribution, ranging from 150 to 850 μm. On the other hand, no supplementary fraction can be observed in the microspheres depicted in Fig. 5B and C, as indicated by the histograms present below the images. The microspheres displayed in Figs. 5B and C were fabricated through the process with PV, with varying parameters, resulting in diameters ranging from 0 to 20 μm. The use of PV in the electrohydrodynamic process has allowed for the elimination of excessively large droplets, commonly produced through the conventional process with DCV (the "satellite fraction"), thus homogenizing the resulting polymer microspheres. The utilization of DCV or PV impacts the geometric shape of the solution at the tip of the nozzle. In the case of the use of DCV, liquid takes a form of a Taylor cone (Fig. 5D). However, the base diameter of this cone exceeds the outer diameter of the nozzle, leading to the upward leakage of the polymer solution along the exterior of the nozzle (as seen in the picture) – this can be considered as a process instability and defect. The application of PV effectively resolves this issue. The cone that is formed at the nozzle outlet (Fig. 5E) is smaller in size, eliminating the need for wiping the nozzle during the process to remove excess polymer solution and reducing the likelihood of nozzle clogging. The bar plot in Fig. 5F demonstrates how the average diameters of microspheres produced from a 20% PCL/DMF solution and the application of a PV of 11 kV depend on both the pulse duration and frequency of the voltage. As evidenced by the graph, the diameters vary from approximately 6 μm for the parameter set of 60 Hz and 8 ms, to approximately 12 μm for 20 Hz, 6 ms or 60 Hz, 2 ms. The statistical significance of these differences is indicated on the graph. The use of DCV leads to a wide microsphere diameter distribution and only one size of microspheres can be achieved for a given voltage value. Implementing PV enhances the ability to control the process by introducing additional parameters. This results in a narrower diameter ranges, and for a given voltage value, various, selectively produced sizes of microspheres can be obtained, depending on the pulse frequency and duration.

The aforementioned study applies only to microspheres composed of 18% or 20% PCL in DMF. The Publication (2) describes more comprehensively an analysis of microspheres fabricated from a broader range of polymer solutions including PCL in DMF (4-15%), PCL in NMP (15%), PES in DMF (15%) and PES in NMP (15%). It provides an in-depth examination of the effect of various process parameters on the size of the microspheres, as well as the influence of PV on the formation of microdroplets at the nozzle outlet.

The postulation put forth as the Thesis (1) has been proved through my findings.

THESIS (2)

Appropriate selection of the cross-linking method and agents used to treat the electrospun or 3D printed constructs leads to obtaining stable, water-insoluble structures of polyvinylpyrrolidone, gelatin and sodium alginate, and in the case of hydrogels, eliminates the burst effect in a 3D bioprinted drug delivery system.

The Thesis (2) is addressed in the Publications (3), (4) and (5).

I cured three different systems via diverse cross-linking techniques. The first system, microsphere-loaded electrospun PVP fibers, was cross-linked using ultraviolet light and benzophenone as the photoinitiator [Publication (3)]. The second system, 3D bioprinted gelatin-alginate hydrogel matrices – by a combination of ionotropic gelation with calcium ions and chemical covalent cross-linking with the glutaraldehyde vapors [Publication (4)]. The third and final system, 3D bioprinted gelatin methacrylate-gelatin hydrogel, was cross-linked through the utilization of ultraviolet light and a LAP photoinitiator [Publication (5)]. I included the detailed descriptions of the mechanisms behind each of the above cross-linking processes in the respective Publications. The methodology of cross-linking for each system was determined experimentally or by referencing literature reports to match the material being used, taking into consideration the cross-linking method, the concentration of cross-linking agents, and the time required for cross-linking. It is important to properly select all cross-linking parameters in order to obtain a desired material.

In the case of electrospun PVP fibers, it was crucial to make the fiber mats water-insoluble, thereby allowing them to function as potential DDSs. Fig. 6 presents results extracted from the Publication (3) that are relevant to the Thesis (2). The SEM images show the successive stages of degradation of PVP fibrous mats in HBBS, while the accompanying graph depicts the change in fiber diameter throughout the degradation process.

The analysis of the results presented in the form of SEM images of the fibrous mats (Fig. 6) highlights that the primary objective of the study was achieved, as they did not dissolve in the aqueous environment of HBSS. Their behaviour in the medium was affected by the cross-linking time. For instance, mats cross-linked for 2×5 min (each side) exhibited the formation of an outer layer, referred to as a "skin", after 6 hours of degradation (Fig. 6B) that persisted after 24 hours (Fig. 6C). A side view of such a structure is presented in Fig. 6G. On the other hand, the degradation of the mats cross-linked for 2×60 minutes resulted in irregular structures slightly fused together (Fig. 6E-F). The mean diameter of the UV-cross-linked PVP fibers was observed to change slightly over time in the medium (Fig. 6H), and this change was dependent on the cross-linking time, with mats cross-linked for 2×5 minutes and 2×15 minutes showing an increase from 0.5 μm to 0.7 μm, whereas mats cross-linked for 2×60 min did not exhibit this phenomenon. This could be attributed to the swelling of PVP, as it is a material widely used for the production of hydrogels. A further analysis of the degradation process of UV-cross-linked PVP fibers can be found in the Publication (3), along with studies on the impact of cross-linking on the mechanical strength and transport properties of the fibrous mats.

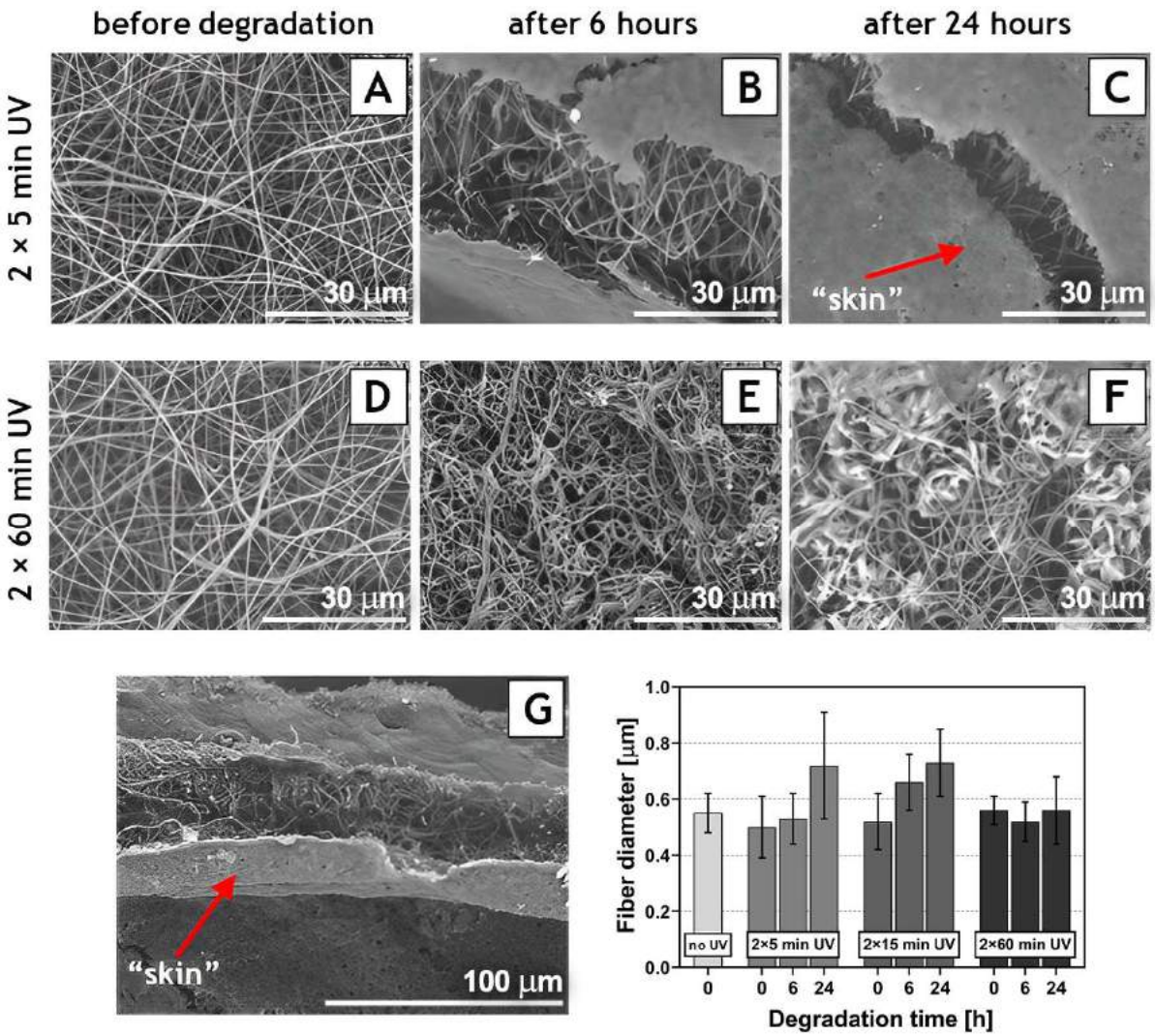

FIGURE 6. **(A-G)** SEM pictures of UV-cross-linked PVP fibers in different stages of degradation in HBSS depending on cross-linking time. **(A-C)** 2×5 minutes: **(A)** before degradation, **(B)** after 6 hours of degradation, **(C)** after 24 hours; **(D-F)** 2×60 minutes: **(D)** before degradation, **(E)** after 6 hours of degradation, **(F)** after 24 hours; **(G)** 2×5 minutes of cross-linking, after 24 hours of degradation, side section. **(H)** The UV-cross-linked PVP fiber mean diameters at different degradation stages. The percentage values of variation coefficients are indicated on each corresponding bar.

Selected research results from the Publication (3)
Mirek et al., Electrospun UV-cross-linked polyvinylpyrrolidone fibers modified with polycaprolactone/ polyethersulphone microspheres for drug delivery, *Biomater. Adv.* 147, 213330 (2023)

The stability of 3D bioprinted hydrogel matrices in an aqueous environment is a crucial factor for their usage as DDSs, similarly to electrospun polymer fibers. I studied the swelling behaviour of hydrogels proposed by me, and the impact of cross-linking on this property for both gelatin-alginate and gelatin methacrylate-gelatin hydrogel matrices. I also investigated the effect of cross-linking on the transport properties of these hydrogels by determining the concentration profiles of the marker (rhodamine) released. Relevant findings from the Publications (4) and (5) in relation to the Thesis (2) are depicted in Fig. 7 and 8, respectively.

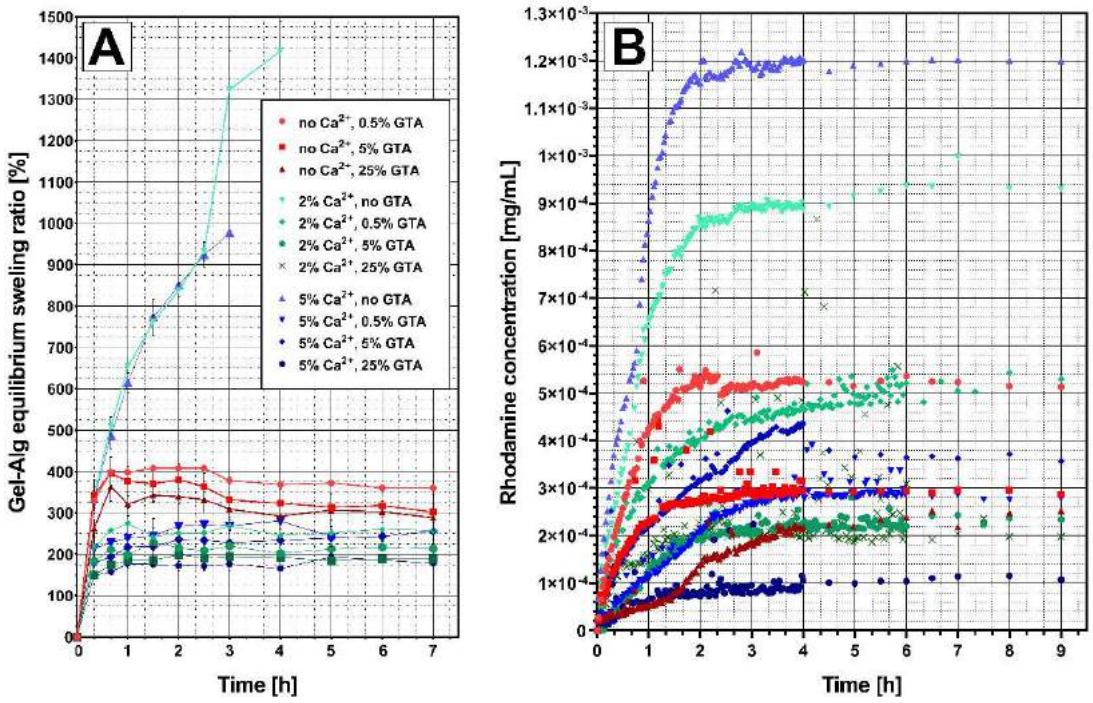

FIGURE 7. (A) Equilibrium swelling ratio of 3D bioprinted gelatin-alginate matrices depending on the cross-linking method and the concentration of cross-linking agent (Ca^{2+} ions and/or GTA vapours). **(B)** Change of the concentration of the rhodamine 640 released from gelatin-alginate matrices cross-linked with different methods.

Selected research results from the Publication (4)
Mirek et al., Development of a new 3D bioprinted antibiotic delivery system based on a cross-linked gelatin-alginate hydrogel, *J. Mater. Chem. B.* 10, 8862–8874 (2022)

The results presented in Fig. 7A demonstrate the stability of the majority of the cross-linked gelatin-alginate hydrogel matrices in an aqueous environment for at least 7 hours, as evidenced by the swelling tests. Without cross-linking the structures composed mainly of gelatin would dissolve under the conditions tested at 37°C. However, it was found that ionotropic gelation alone was insufficient to provide stability as demonstrated by the matrices cross-linked only with calcium ions (light blue and green curves). The matrices cross-linked with 2% Ca^{2+} and 5% Ca^{2+} showed a 980% and 1420% increase in mass and degraded after 3 hours and 4 hours, respectively. The weight of samples cross-linked solely through GTA vapors decreased slightly after 3 hours, which may be also a result of matrix degradation (red curves). Conversely, the remaining matrices achieved an equilibrium swelling ratio after 40-60 minutes, with their degree of hydration ranging from 180% to 400% dependent upon the cross-linking methodology employed. As anticipated, matrices cross-linked with the highest concentrations of both agents (5% Ca^{2+}, 25% GTA) demonstrated the lowest degree of hydration, whereas those cross-linked

with the agents of lowest concentrations (2% Ca^{2+}, 0.5% GTA) absorbed the greatest amount of water. The study on the transport properties of gelatin-alginate hydrogel matrices demonstrates a clear correlation between the method of cross-linking, the concentrations of cross-linking agents and the release profile of the substance. The results show that the release of rhodamine occurs in two distinct stages, and a burst effect was not observed. The release follows zero-order kinetics, with a constant rate determined by time alone. The relationship between the processes of swelling and substance release is indicated by the comparison of their respective curves during the early stage of the sample exposure to aqueous conditions. Further analysis of the swelling process and the release of rhodamine from the matrices, including mathematical modelling, is described in detail in the Publication (4).

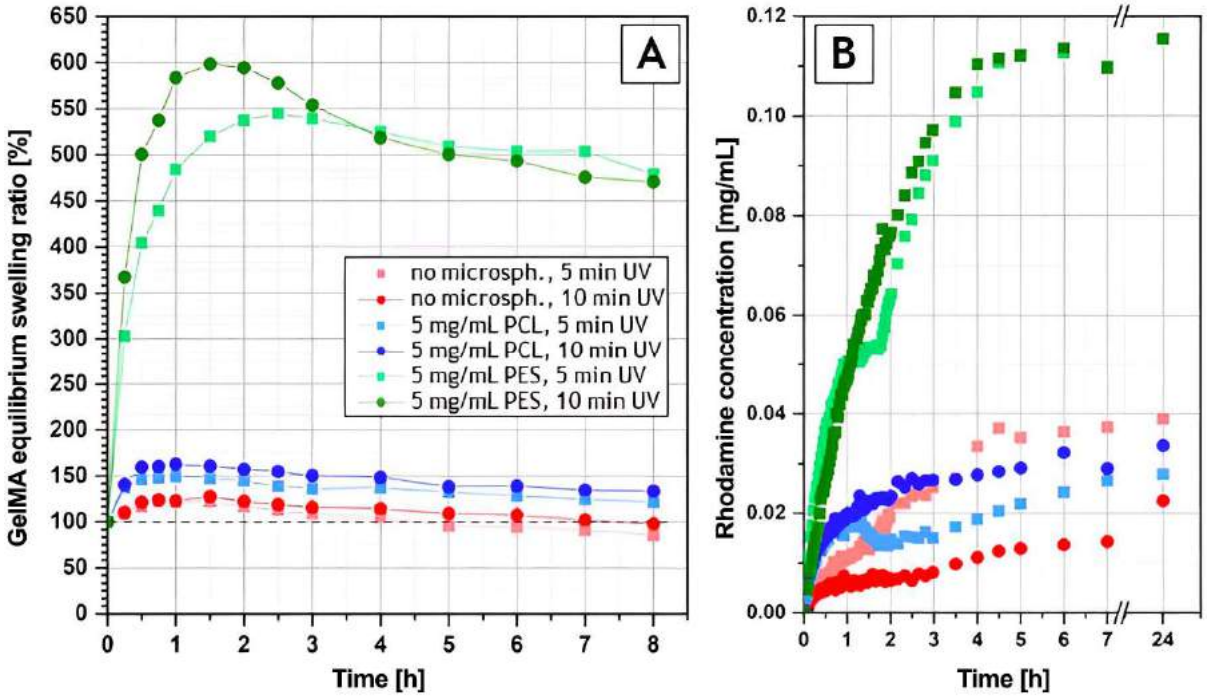

FIGURE 8. Studies on 3D bioprinted GelMA-gelatin hydrogel matrices depending on the cross-linking time and the microsphere content: **(A)** equilibrium swelling ratio and **(B)** rhodamine 640 release profiles.

Selected research results from the Publication (5)
Mirek et al., Gelatin methacrylate hydrogel with drug-loaded polymer microspheres as a new bioink for 3D bioprinting, *Biomater. Adv.* 150, 213436 (2023)

As in the case of 3D bioprinted gelatin-alginate matrices, those built of non-cross-linked gelatin methacrylate-gelatin hydrogel are also soluble in the aqueous environment at the temperature of 37°C, at which I conducted the swelling test. Their rapid degradation would result in the unwanted release of immobilized microspheres. The stability of the cross-linked GelMA-gelatin matrices for at least 8 hours was confirmed by the results of the equilibrium swelling ratio depending on the cross-linking time and the type of microspheres used shown in Fig. 8A. The effect of UV-cross-linking time on swelling is minimal for all materials tested, in contrast to the modification of the system with microspheres. Matrices with PES microspheres (green points) exhibit a much faster swelling than those without microspheres (red points) or with PCL ones (blue points), reaching maximum hydration values of 550 – 600% after 1.5 – 2 hours and experiencing a slight weight loss, while all others reached 120 – 160%.

The rhodamine release curves from cross-liked GelMA-gelatin matrices (Fig. 8B) was found to be similar to those of the previously analyzed gelatin-alginate matrices, with no burst effect being observed in either case. The lack of it can be attributed to the cross-linking of the hydrogel matrix. The curves depicting the rhodamine release from the GelMA-gelatin matrices (Fig. 8B) align with the equilibrium swelling ratio curves (Fig. 8A), as was also seen in the gelatin-alginate matrix study. The release of rhodamine in the initial period of approximately one hour is dependent on swelling, resulting in a release rate that follows zero-order kinetics and can be described mathematically through a linear equation with very good fit with a coefficient of determination (R^2) ranging from 0.9361 to 0.9960, what confirmed the absence of burst release. The slope coefficient *a* was determined and the results showed that the tested samples formed three distinct groups with varying release rates and that the longer the cross-linking time, the slower the release process in each case. Appropriate calculations and a detailed description of the rhodamine release processes from GelMA-gelatin matrices can be found in the Publication (5).

The results of the part of my research described above confirmed the validity of the statement outlined as the Thesis (2).

THESIS (3)

Non-aggregated, drug-loaded synthetic polymer microspheres can be produced and used as an additive to electrospinning suspension or bioink for 3D bioprinting, resulting in an increased drug capacity of the electrospun or 3D bioprinted drug delivery system, and in the case of electrospun fibers, an elimination of the burst effect.

The Thesis (3) is addressed in the Publications (2), (3) and (5).

I employed a combination of pulsed voltage electrospray and wet phase inversion techniques to synthesize non-aggregated PCL and PES microspheres, which were utilized as microcarriers for an active substance. These microspheres were then incorporated into the electrospinning PVP solution forming the suspension to produce modified fibers with increased drug capacity as detailed in the Publication (3) or incorporated into GelMA-gelatin hydrogel to prepare a bioink suspension, which was used to 3D bioprint matrices with increased drug capacity as described in the Publication (5). A comprehensive description of the microsphere production method can be found in the Publication (2).

I performed a successful elaboration of a universal method for formation of disaggregated microspheres with a narrow diameter distribution of 2 – 15 μm which can be loaded with an active substance and serve as drug microcarriers to modify DDSs. The selected results from the Publication (2), evidencing the claims detailed in the Thesis (3), are presented in Fig. 9.

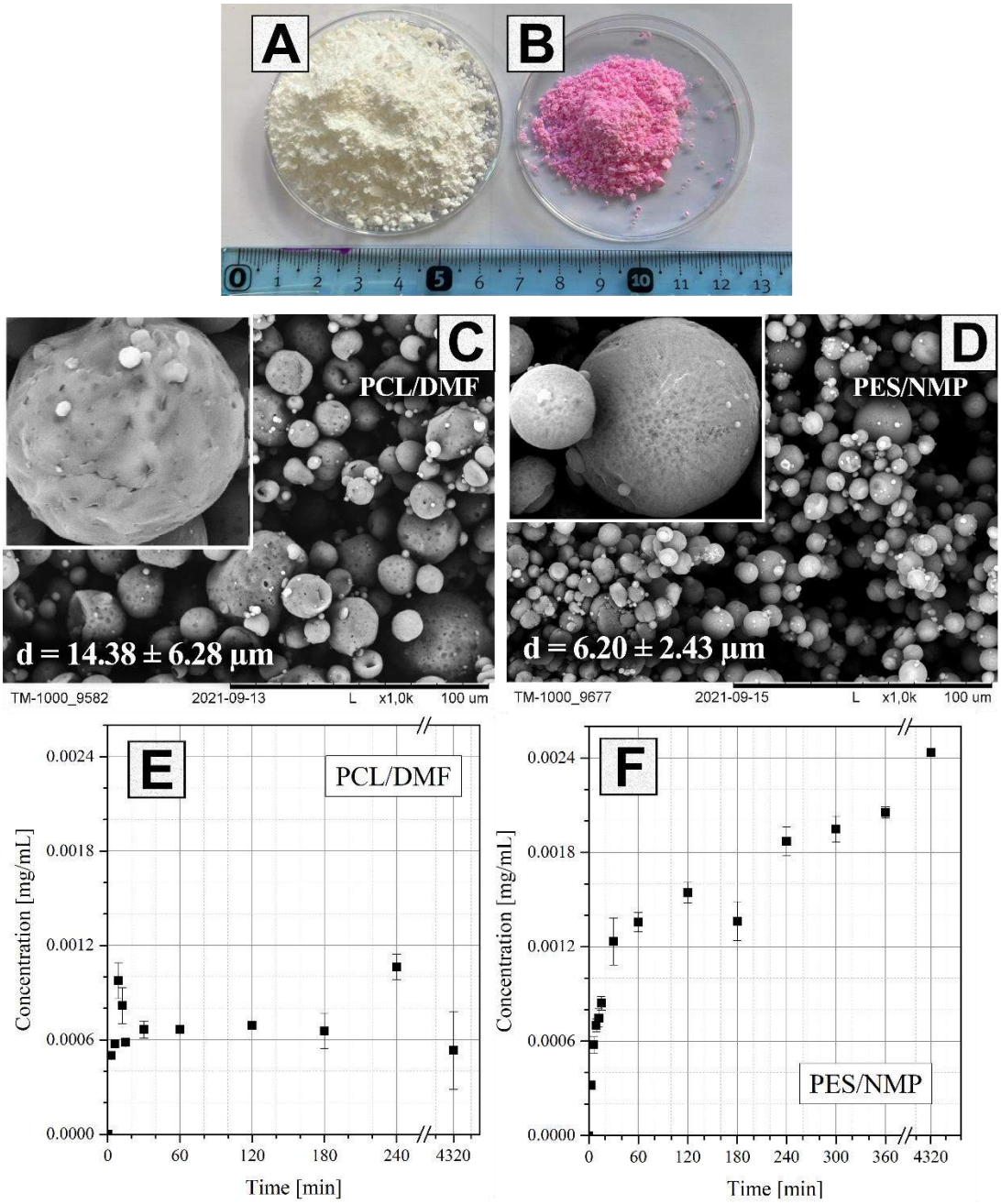

FIGURE 9. **(A)** Powder of dried PCL/DMF microspheres without additions. **(B)** Powder of dried rhodamine-loaded PES/NMP microspheres. **(C, D)** SEM images of microspheres obtained from 15% polymer solution with the microsphere mean diameters *d*: **(C)** PCL/DMF [11 kV, 40 Hz, 4 ms], **(D)** PES/NMP [8 kV, 60 Hz, 6 ms]. **(E, F)** Rhodamine 640 release profiles form the microspheres obtained from 15% polymer solution: **(E)** PCL/DMF [11 kV, 40 Hz, 4 ms], **(F)** PES/NMP [8 kV, 60 Hz, 6 ms].

Selected research results from the Publication (2)
Mirek et al., Formation of disaggregated polymer microspheres by a novel method combining pulsed voltage electrospray and wet phase inversion techniques, *Colloids Surf. A Physicochem. Eng. Asp.* 648, 129246 (2022)

The microsphere production method I proposed is versatile enough to be used to fabricate polymer microspheres from various polymers (PCL and PES), which can be dissolved in different solvents (DMF and NMP). The photograph in Fig. 9A shows PCL/DMF microspheres after drying achieved through evaporation of ethanol at room temperature for several days. The resulting powder is easy to work with and further analysis. Fig. 9B depicts PES/NMP microspheres, which have a pink colour due to an addition of rhodamine to the solution used to electrospray them. After drying, they also take the form of a powder and can be utilized as carriers of active substances. As demonstrated in the SEM images presented in Fig. 9C-D, the method leads to the formation of uniform microspheres. They do not fuse together. I have found that by dispersing the dry microsphere powder in ethanol, a homogeneous suspension can be obtained without the formation of any aggregates. The examination of the SEM images reveals that the choice of polymer and solvent affects the morphological characteristics of the resulting microspheres. The possibility of immobilizing the active substance in the microspheres produced by the developed method is confirmed by the results presented in Fig. 9E-F. They depict the release profiles of the rhodamine from the PCL/DMF and PES/NMP microspheres over 4 h and 6 h, respectively. The final point on the graph displays the rhodamine concentration after 72 h (4320 min). The data highlights that the transport properties of the microspheres are influenced by the type of polymer and solvent used. The PCL/DMF microspheres exhibit a rapid release of the active substance, with an initial burst effect and an equilibrium state reached within 30 min. The total amount of rhodamine released after 72 h was 0.043 ± 0.014 mg of rhodamine per gram of PCL. The PES/NMP microspheres displayed a slower release profile, with no observable burst effect, and did not reach an equilibrium even after 72 h, with a total release of 0.171 ± 0.014 mg of rhodamine per gram of PES.

The transport properties of microspheres are further explored in the Publication (2), where I analyzed four different types of microspheres: PCL/DMF, PES/NMP, PCL/NMP, and PES/DMF. The analysis includes their surface area (BET), chemical structure (FTIR), and crystal structure (XRD). The Publication (2) discusses the challenges associated with polymer microsphere manufacturing and highlights the advantages of the proposed method. These benefits include the formation of non-aggregated microspheres through the use of electrohydrodynamic microdripping and wet phase inversion technique, a narrow distribution of microsphere diameters and greater control over the product diameter and size homogeneity through the use of pulsed voltage, the universality of the method and the use of common reagents such as ethanol, as well as its high level of reproducibility.

In a next phase of my research, I used the manufactured PCL and PES microspheres to modify electrospun PVP fibers. The feasibility of this approach, as well as the influence of the microspheres on the fibrous mat transport properties, which is a part of the Thesis (3), are confirmed by selected results from the Publication (3) as depicted in Fig. 10.

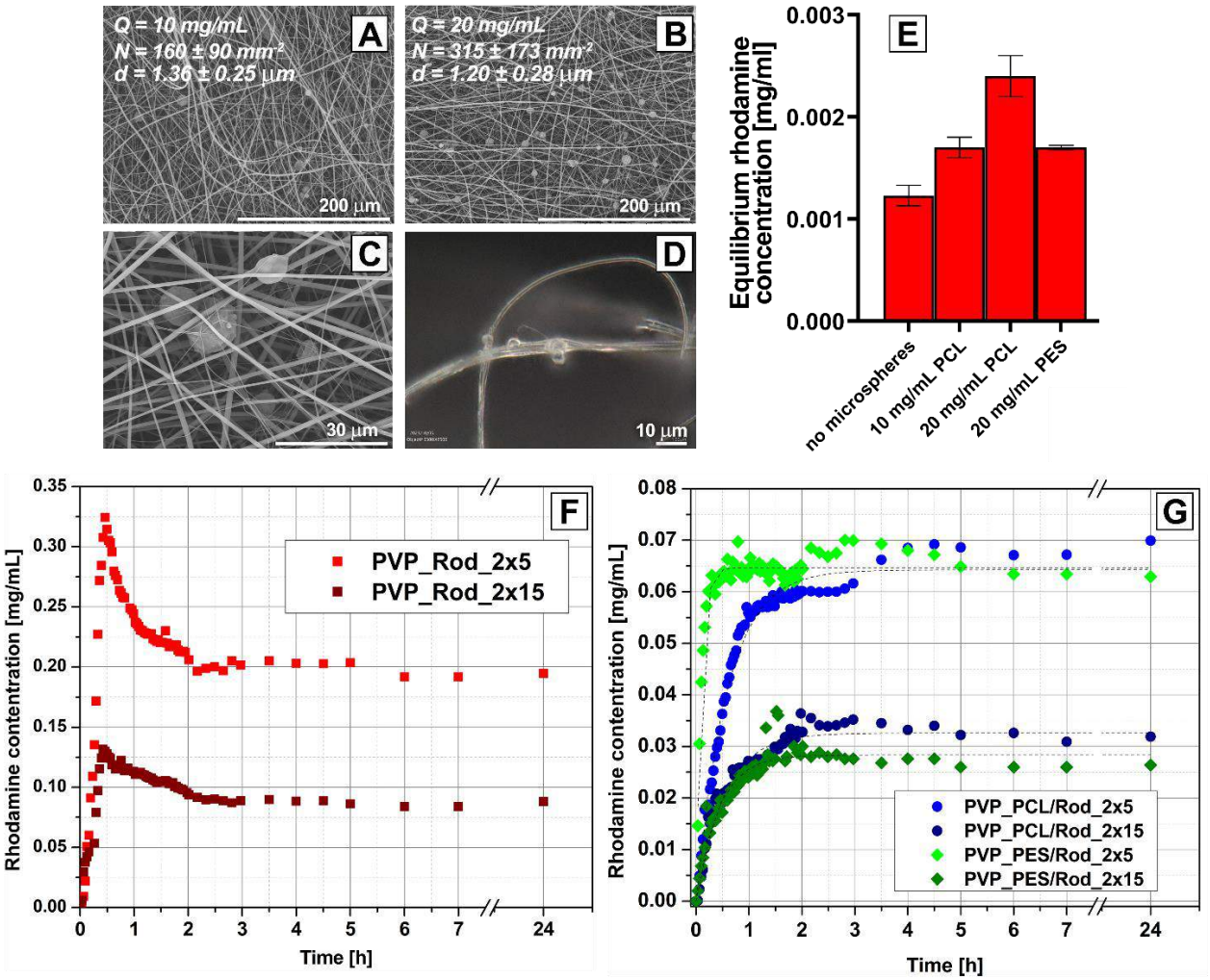

FIGURE 10. (A-C) SEM images of PCL microsphere-loaded PVP fibers depending on the content of microspheres in the suspension *Q* [mg/mL]: **(A)** 10 mg/mL, mag. 500×, **(B)** 20 mg/mL, mag. 500×, **(C)** 10 mg/mL, mag. 2500× with the estimated content of microspheres in the mats *N* [mm^{-2}] and fiber mean diameter *d* [µm]. **(D)** Optical microscope picture of PCL microsphere-loaded PVP fibers, mag. 2500×. **(E)** The equilibrium concentration of rhodamine after a 4-hour release from UV-cross-linked PVP fibers, with the addition of microspheres loaded with the substance, depending on the type and quantity of microspheres used and the cross-linking time. **(F, G)** Rhodamine release profiles from UV-cross-linked PVP fibrous mats: **(F)** fibers without microspheres (PVP_Rod) with rhodamine incorporated directly in the fibers, **(G)** fibers with the addition of rhodamine-loaded PCL (PVP_PCL/Rod) or PES (PVP_PES/Rod) microspheres.

Selected research results from the Publication (3)
Mirek et al., Electrospun UV-cross-linked polyvinylpyrrolidone fibers modified with polycaprolactone/ polyethersulphone microspheres for drug delivery, *Biomater. Adv.* 147, 213330 (2023)

After incorporating the microspheres into the polymer solution and electrospinning it with PV, I successfully obtained modified fibrous mats, as demonstrated by SEM images in Fig. 10A-C. The process of suspension electrospinning is indeed feasible, but there is a limit to the content of microspheres that can be used. The nozzle used for the suspension electrospinning has an inner diameter of 0.6 mm, while the maximum diameter of the microspheres is around 15 – 20 µm, which presents a risk of clogging when the concentration of microspheres is too high. In my research, I determined that the threshold content of PCL/DMF microspheres was 20 mg/mL. Electrospinning was stable for its levels of 10 mg/mL and 20 mg/mL, as shown in the SEM images in Fig. 10A and B, respectively. The microspheres are entangled in the polymer fiber network, or become incorporated into the fiber structure and covered with a fiber-forming polymer outer layer (Fig. 10C), as confirmed by optical microscope images (Fig. 10D). The addition of the microspheres does not affect the fiber diameter (1.20 – 1.36 µm), which is even 10 times smaller than the diameter of the microspheres (6.20 – 14.38 µm). Including such large objects in the fiber structure increases the drug capacity of the entire system. It was confirmed in the study of the rhodamine release after 24 hours from various cross-linked fiber mats, the results of which are shown in Fig. 10E. The addition of PCL and PES microspheres led to an increase in the amount of rhodamine immobilized, as indicated by the increase in its equilibrium concentration from approximately 0.0012 mg/mL (for fibers without microspheres) to 0.0024 mg/mL (for fibers electrospun with 20 mg/mL of PCL microspheres). The modification of the fiber mats with the microspheres also eliminated the undesirable burst effect that occurs in fiber systems without them (Fig. 10F). For example, for a 2×5 min cross-linked mat, the concentration of rhodamine reached 0.33 mg/mL after 30 min, but dropped to an equilibrium state of 0.20 mg/mL after 2 h. The burst effect was not observed for mats with microspheres (Fig. 10G), probably due to the presence of an abovementioned polymer outer layer around the microspheres that slows down the marker diffusion. The concentration profiles in this case were smoother, and equilibrium was reached after 2 – 3 h. Due to the absence of burst effect, the rhodamine release curves could be described using an exponential function model, and the speed of the release process was assessed using transport coefficients h. The results of the study demonstrate a relationship between the type of immobilized microspheres and the speed of substance release, with the slowest release observed for mats cross-linked for 2×5 minutes modified with PCL microspheres ($h = 2.32\times10^{-6}$ cm/min ± 17%) and the fastest for the ones cross-linked for 2×5 min with PES microspheres ($h = 26.58\times10^{-6}$ cm/min ± 11%). All of the calculations and an extensive analysis of the results and discussion concerning electrospun UV-cross-linked PVP fibers modified with PCL/PES microspheres have been summarized in the Publication (3).

Another issue of my study was to explore the potential of incorporating PCL/PES microspheres into 3D bioprinted constructs, made from a suspension bioink with the base of GelMA-gelatin hydrogel, in a manner similar to the modification of electrospun mats. Through my investigation, I confirmed the feasibility of this approach and determined its impact on the drug capacity of the systems. The results extracted from the Publication (5) presented in Fig. 11 provide evidence in support of the Thesis (3).

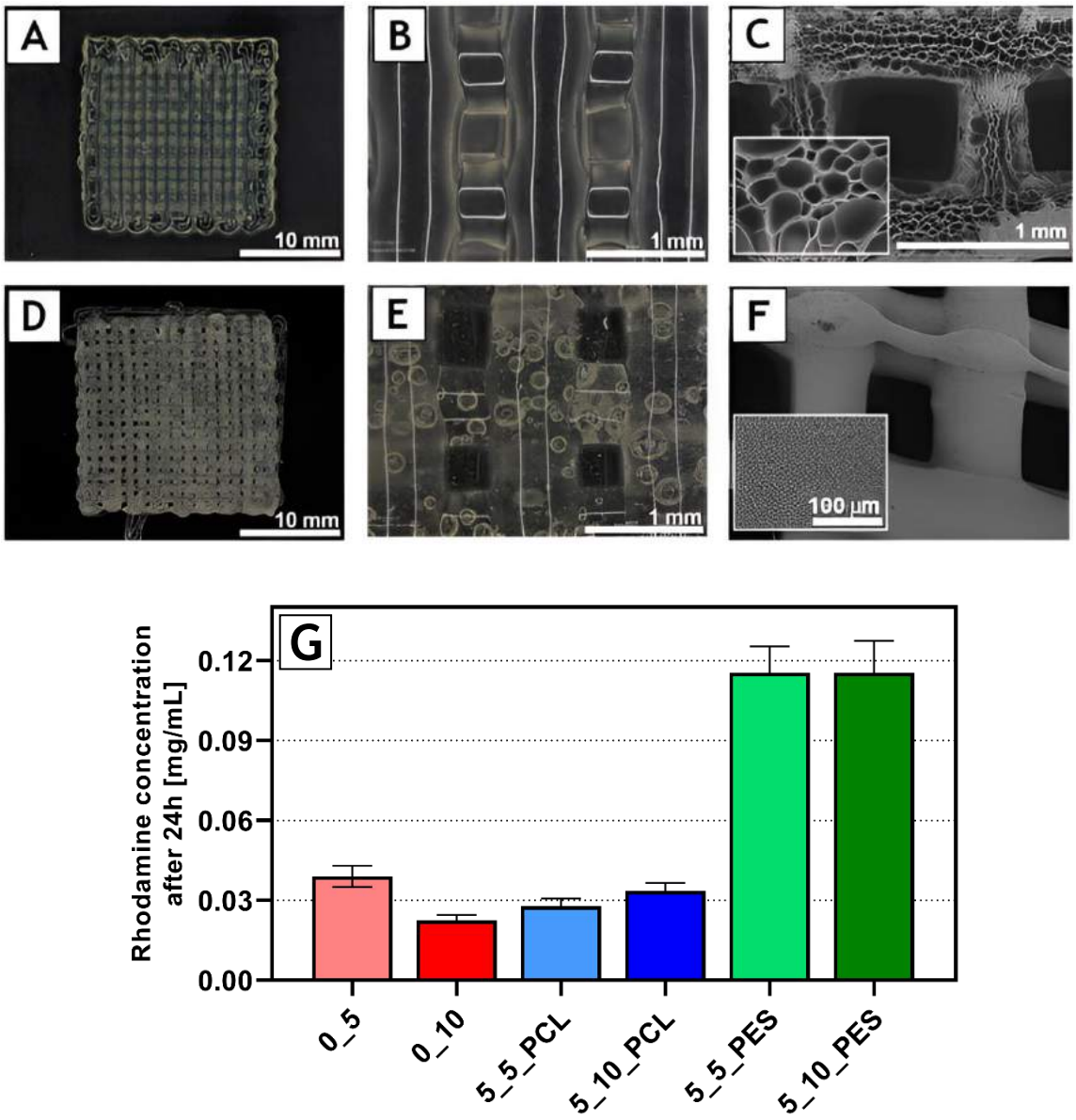

FIGURE 11. (A, B, D, E) Digital microscope pictures of 3D bioprinted GelMA/gelatin hydrogel matrices before lyophilization. **(A, B)** Matrix without additives, no cross-linking, magnification **(A)** 20× and **(B)** 100×. **(D-E)** Matrix with 5 mg/mL PCL microspheres, UV-cross-linked for 10 minutes, magnification **(D)** 20×, **(E)** 100×. **(C, F)** SEM images of lyophilized GelMA/gelatin matrices: **(C)** no microspheres, no UV-cross-linking, **(F)** 5 mg/mL PCL microspheres, no UV-cross-linking. **(G)** The concentration of rhodamine released after 24 hours from UV-cross-linked GelMA/gelatin matrices modified with substance-loaded microspheres.

Selected research results from the Publication (5)
Mirek et al., Gelatin methacrylate hydrogel with drug-loaded polymer microspheres as a new bioink for 3D bioprinting, *Biomater. Adv.* 150, 213436 (2023)

The successfully 3D bioprinted hydrogel matrices are presented in the optical microscope photos shown in Fig. 11A - matrix without microspheres, and Fig. 11D – matrix with the addition of PCL microspheres. These photos confirm the printability of bioink in the form of a suspension of polymer microspheres in a GelMA-gelatin hydrogel. The structure of the printouts is consistent with the previously prepared digital matrix model [Publication (5)]. It is important to note once again that the extrusion-based techniques such as bioprinting and electrospinning require that the microspheres in the bioink do not clog the nozzle. The nozzle I used for the 3D bioprinting of the described matrices had an internal diameter of 0.164 mm, smaller than that used in the electrospinning process. As a result, the concentration of microspheres allowing for unobstructed 3D bioprinting was lower in this case and limited to 5 mg/mL. Fig. 11B and E show the matrices described above at a higher magnification, revealing that the addition of PCL/DMF microfibers maintains the overall structure of the matrix. The microspheres can be observed dispersed within the printed structure in Fig. 11E. The SEM images presented in Fig. 11C and Fig. 11F demonstrate the impact of the presence or absence of microspheres on the morphology of the freeze-dried matrices. The samples without microspheres exhibit a wrinkled and porous structure, however, the PCL-loaded matrices present a more compact and uniform morphology. This differences can be attributed to the microspheres acting as fillers, causing the hydrogel to cling to them during drying and thereby avoiding the formation of wrinkles. The data presented in Fig. 11G indicates that the incorporation of PCL microspheres into the 3D bioprinted matrices does not lead to a remarkable increase in the amount of released rhodamine compared to unmodified matrices. On the other hand, the use of PES microspheres results in a four-fold increase in the concentration of rhodamine released after 24 hours (0.12 mg/mL), with value of 0.03 mg/mL for unmodified matrices. It is worth adding that the unmodified matrices and those modified with PCL microspheres did not reach an equilibrium state even after 24 h, whereas matrices modified with PES microspheres reached it after approximately 5 h, as illustrated in Fig. 8B. An in-depth analysis of bioprinted matrices from GelMA-gelatin hydrogel with the addition of PCL or PES microspheres, including a set of tests of their structure (FTIR) and thermal properties (DSC, TGA) along with a discussion of the results, is included in the Publication (5).

All above data collected in this part of my study provides evidence in support of the Thesis (3).

5

FINAL CONCLUSIONS

The aim of my research was accomplished as I developed new potential controlled drug delivery systems manufactured using electrostatic and 3D bioprinting techniques. Employing pulse voltage contributed to the stabilization of the electrostatic processes and introduced supplementary process parameters, ultimately enhancing control over the structure of the final product. Some systems underwent cross-linking via diverse methods, which modified their mechanical and transport properties. Various constructs were formulated as a result:

- non-aggregated, drug-loaded microspheres (made of PCL or PES) produced with a method combining pulsed voltage electrospray and wet phase inversion techniques developed by me,
- drug-loaded UV-crosslinked electrospun PVP fibers,
- drug-loaded 3D bioprinted gelatin-alginate hydrogel matrices cross-linked with GTA or Ca^{2+}.

Based on the constructs mentioned above, I developed two new potential hybrid DDSs that would incorporate the strengths of each system while mitigating their respective limitations:

- UV-cross-linked electrospun PVP fibrous mats modified with drug-loaded microspheres (of PCL or PES) incorporated within the fibers,
- UV-cross-linked 3D bioprinted gelatin methacrylate-gelatin hydrogel constructs modified with drug-loaded microspheres (of PCL or PES) incorporated within the bioink.

The newly created hybrid DDSs exhibit an increased drug capacity and eliminate the drug burst release effect during the initial stage of action. The transport properties of such DDSs are affected by the cross-linking time, type, and amount of microspheres, allowing for precise control over the manufacturing process to achieve the desired product. However, these systems are not entirely convergent in terms of their properties and potential applications, and their production processes require a distinct approach. Table 1 provides an overview of the strengths and weaknesses of electrospinning and 3D bioprinting processes in manufacturing of hybrid DDSs, while Table 2 outlines the benefits and drawbacks of using electrospun fibrous mats or 3D bioprinted hydrogel constructs modified with drug-loaded microspheres as controlled DDSs.

TABLE 1.

Comparison of strengths and weaknesses of electrospinning and 3D bioprinting processes as hybrid drug delivery system manufacturing techniques.

	ELECTROSPINNING	3D BIOPRINTING
STRENGTHS	The relatively large inner diameter of the nozzle. It does not affect the diameter of the fibers, which is determined by the jet at the tip of the Taylor cone. The possibility of electrospinning of suspensions of large microspheres with higher concentrations, increasing the drug capacity of the system. Room temperature. The preparation procedure is facile, involving a simple arrangement and mixing of components, followed by a prolonged processing time with minimal required activity of the operator. At the laboratory scale, the required equipment is affordable, scaling up can be achieved by multiplying the nozzles. The wide availability of synthetic polymers and the potential for their modification. The numerous process parameters (electrical, ambient, and physicochemical related to the solution) allow for accurate design of the desired mat.	The fabrication of a single printout can be achieved within a few minutes, depending on the size. The process is not affected by ambient humidity conditions as there is no solvent evaporation occurring. The use of water and biocompatible natural polymers as materials for bioink preparation. Precise control over the 3D structure of the final product. High reproducibility and accuracy in terms of producing the same product multiple times. The capability to prepare 3D bioprinted constructs directly in the operating room during surgery.
WEAKNESSES	The process is time-consuming as it may take several hours to electrospin a mat with the desired thickness. Due to the reliance on solvent evaporation, the process is highly sensitive to fluctuations in humidity, necessitating the control and stability of this parameter. The process involves the use of synthetic polymers dissolved in potentially toxic organic solvents. Maintaining constant values of multiple process parameters can be challenging. Production of a larger waste amount (such as excess mat).	The size of the nozzle must be minimized to ensure the desired size of basic structural element (a print line). This may be challenging when bioprinting suspension bioink (nozzle clogging). To ensure the appropriate conditions for thermal gelation of the hydrogel, the temperature difference between the heated nozzle and the cooled collector must be appropriately maintained. Personnel with appropriate qualifications are required for both the design of a digital 3D model and the preparation of bioink. Continuous monitoring of the process and frequent nozzle changes are necessary when bioprinting a series of constructs due to the relatively short print time. Specialized and high-cost equipment difficult to operate, maintain, and repair.

TABLE 2.

Benefits and drawbacks of using electrospun fibrous mats or 3D bioprinted constructs modified with drug-loaded microspheres as controlled drug delivery systems.

	ELECTROSPUN FIBROUS MATS	3D BIOPRINTED CONSTRUCTS
BENEFITS	Polymer mats have greater mechanical strength and flexibility than hydrogels. High surface area to volume ratio. The size of the basic structural element (a fiber) can be modified in the range from nanometers to micrometers. The mats can be stored with low storage requirements, at room temperature with reduced humidity. The mats have potential applications as coatings, e.g. for implants or medical equipment.	The drug capacity is increased as a result of the greater total volume of the system and can be adjusted to the needs of a specific patient. The 3D structure can be freely controlled, allowing for the creation of complex geometries and internal architectures. Possibility to immobilize living eukaryotic cells, microorganisms and biomolecules. Potential to create patient-specific DDS for personalized medicine. Possibility to print customized DDS based on the patient's anatomy or disease state, which can improve the treatment outcomes. Swelling properties enable the absorption of wound exudate, demonstrating its potential as a promising wound healing material, also within the patient’s body.
DRAWBACKS	The two-dimensional structure of limited thickness. The immobilization of living eukaryotic cells, microorganisms and biomolecules (e.g. hormones, enzymes, nucleic acids) poses significant challenges.	The mechanical strength and elasticity are lower than those of polymer fibers. The size of the basic structural element (a print line) is limited by the inner diameter of the nozzle and equals typically several hundred micrometers. It is necessary to store the material in a dry state, preferably under refrigeration, to prevent decay or spoilage.

REFERENCES

[1] S. Adepu, S. Ramakrishna, „Controlled Drug Delivery Systems: Current Status and Future Directions," *Molecules,* 26, p. 5905, 2021.

[2] D. S. W. Benoit, C. T. Overby, K. R. Sims Jr., M. A. Ackun-farmmer, „2.5.12 - Drug Delivery Systems," w *Biomaterials Science (Fourth Edition) - An Introduction to Materials in Medicine*, Academic Press, 2020, pp. 1237-1266.

[3] S. P. Chaudhairi, P. S. Patil, „Pharmaceutical Excipients: A review," *International Journal of Advanced in Pharmacy, Biology and Chemistry,* 1, 1, pp. 21-34, 2012.

[4] H. J. Patel, V. Shah, U. Upadhyay, „New pharmaceutical excipients in solid dosage forms – A review," *International Journal of Pharmacy & Life Sciences,* 2, 8, pp. 1006-1019, 2011.

[5] A. Geraili, M. Xing, K. Mequanint, „Design and fabrication of drug-delivery systems toward adjustable release profiles for personalized treatment," *VIEW,* 2, 5, p. 20200126, 2021.

[6] S. Habet, „Narrow Therapeutic Index drugs: clinical pharmacology perspective," *Journal of Pharmacy and Pharmacology,* 73, 10, pp. 1285-1291, 2021.

[7] K. K. Jain, „An Overview of Drug Delivery Systems," w *Drug Delivery Systems*, 2059, Methods in Molecular Biology book series, 2019, pp. 1-54.

[8] E. J. Silva, L. G. Souza, L. A. D. Silva, S. F. Taveira, R. C. Guilger, L. M. Liao, L. H. K. Queiroz Junior, M. J. Santana, R. N. Marreto, „A Novel Polymer-Lipid Hybrid Nanoparticle for the Improvement of Topotecan Hydrochloride Physicochemical Properties.," *Current Drug Deliery,* 15, 7, pp. 979-986, 2018.

[9] M. Vert, Y. Doi, K.-H. Hellwich, M. Hess, P. Hodge, P. Kubisa, M. Rinaudo, F. Schué, „Terminology for biorelated polymers and applications (IUPAC Recommendations 2012)," *Pure and Applied Chemistry,* 84, 2, pp. 377-410, 2012.

[10] S. O. Adeosun, M. O. Ilomuanya, O. P. Gbenebor, M. O. Dada, C. C. Odili, „Biomaterials for Drug Delivery: Sources, Classification, Synthesis, Processing, and Applications.," w *Advanced Functional Materials*, London, IntechOpen, 2020.

[11] K. Jain, N. K. Mehra, N. K. Jain, „Nanotechnology in Drug Delivery: Safety and Toxicity Issues," *Current pharmaceutical design,* 21, 29, pp. 4252-4261, 2015.

[12] Y. A. Tereshkina, T. I. Torkhovskaya, E. G. Tikhonova, L. V. Kostryukova, M. A. Sanzhakov, E. I. Korotkevich, Y. Y. Khudoklinova, N. A. Orlova, E. F. Kolesanova, „Nanoliposomes as drug delivery systems: safety concerns," *Journal of drug targeting,* 30, 3, p. 313–325, 2022.

[13] M. M. A. N. Ranjha, B. Shafique, A. Rehman, A. Mehmood, A. Ali, S. M. Zahra, U. Roobab, A. Singh, S. A. Ibrahim, S. A. Siddiqui, „Biocompatible Nanomaterials in Food Science, Technology, and Nutrient Drug Delivery: Recent Developments and Applications," *Frontiers in nutrition,* 8, p. 778155, 2022.

[14] D. S. Kohane, J. Y. Tse, Y. Yeo, R. Padera, M. Shubina, R. Langer, „Biodegradable polymeric microspheres and nanospheres for drug delivery in the peritoneum," *Journal of Biomedical Materials Research. Part A,* 77, 2, pp. 351-361, 2006.

[15] D. S. Kohane, R. Langer, „Biocompatibility and drug delivery systems," *Chemical Science,* 1, 4, pp. 441-446, 2010.

[16] L. Wang, J. Du, Y. Zhou, Y. Wang, „Safety of nanosuspensions in drug delivery," *Nanomedicine: Nanotechnology, Biology and Medicine,* 13, 2, pp. 455-469, 2017.

[17] S. Bhattacharjee, „Understanding the burst release phenomenon: toward designing effective nanoparticulate drug-delivery systems," *Therapeutic delivery,* 12, 1, pp. 21-36, 2021.

[18] Z. Huang, S. N. Kłodzińska, F. Wan, H. M. Nielsen, „Nanoparticle-mediated pulmonary drug delivery: state of the art towards efficient treatment of recalcitrant respiratory tract bacterial infections," *Drug Delivery and Translational Research,* 11, pp. 1634-1654, 2021.

[19] J. Yoo, Y.-Y. Won, „Phenomenology of the Initial Burst Release of Drugs from PLGA Microparticles," *ACS Biomaterials Science & Engineering,* 6, pp. 6053-6062, 2020.

[20] Z. Huang, T. Zhou, Y. Yuan, S. N. Kłodzińska, T. Zheng, C. Sternberg, F. Wan, „Synthesis of carbon quantum dot-poly lactic-co-glycolic acid hybrid nanoparticles for chemo-photothermal therapy against bacterial biofilms," *Journal of Colloid and Interface Science,* 577, pp. 66-74, 2020.

[21] M. L. Laracuente, M. H. Yu, K. J. McHugh, „Zero-order drug delivery: State of the art and future prospects," *Journal of Controlled Release,* 327, pp. 834-856, 2020.

[22] K. Watanabe, T. Ohtsuki, „Photocontrolled Intracellular RNA Delivery Using Nanoparticles or Carrier-Photosensitizer Conjugates," *Progress in Molecular Biology and Translational Science,* 139, pp. 101-119, 2016.

[23] S. K. Prajapati, A. Jain, A. Jain, S. Jain, „Biodegradable polymers and constructs: A novel approach in drug delivery," *European Polymer Journal,* 120, p. 109191, 2019.

[24] N. Salari, F. Faraji, F. M. Torghabeh, F. Faraji, K. Mansouri, F. Abam, S. Shohaimi, H. Akbari, M. Mohammadi, „Polymer-based drug delivery systems for anticancer drugs: A systematic review," *Cancer Treatment and Research Communications,* 32, p. 100605, 2022.

[25] F. Zhang, M. W. King, „Biodegradable Polymers as the Pivotal Player in the Design of Tissue Engineering Scaffolds," *Advanced Healthcare Materials,* p. 1901358, 2020.

[26] H. Idrees, S. Zaidi, A. Sabir, R. Khan, X. Zhang, S.-U. Hassan, „A Review of Biodegradable Natural Polymer-Based Nanoparticles for Drug Delivery Applications," *Nanomaterials,* 10, p. 1970, 2020.

[27] J. C. K. Ng, D. W. Y. Toong, V. Ow, S. Y. Chaw, H. Toh, P. E. H. Wong, S. Venkatraman, T. T. Chong, L. Tan, Y. Y. Huang, H. Y. Ang, „Progress in drug-delivery systems in cardiovascular applications: stents, balloons and nanoencapsulation.," *Nanomedicine (Lond),* 17, 5, pp. 325-347, 2022.

[28] D. Dash, R. Mody, N. Ahmed, S. R. Malan, B. Mody, „Drug-coated balloon in the treatment of coronary bifurcation lesions: A hope or hype?," *Indian Heart Journal,* 74, 6, pp. 450-457, 2022.

[29] C. Pan, Z. Zhou, X. Yu, „Coatings as the useful drug delivery system for the prevention of implant-related infections," *Journal of Orthopaedic Surgery and Research,* 13, p. 2020, 2018.

[30] A. I. Visan, G. Popescu-Pelin, G. Socol, „Degradation Behavior of Polymers Used as Coating Materials for Drug Delivery-A Basic Review.," *Polymers,* 13, 8, p. 1272, 2021.

[31] V. Petrova, V. Elokhovskiy, S. Raik, D. Poshina, D. Romanov, Y. Skorik, „Alginate Gel Reinforcement with Chitin Nanowhiskers Modulates Rheological Properties and Drug Release Profile," *Biomolecules,* 9, 7, p. 291, 2019.

[32] Y. Huang, N. Dan, W. Dan, W. Zhao, „Reinforcement of Polycaprolactone/Chitosan with Nanoclay and Controlled Release of Curcumin for Wound Dressing," *2019,* 4, 27, pp. 22292-22301, 2019.

[33] A. W. Martinez, J. M. Caves, S. Ravi, W. Li, E. L. Chaikof, „Effects of crosslinking on the mechanical properties, drug release and cytocompatibility of protein polymers," *Acta Biomaterialia,* 10, 1, pp. 26-33, 2014.

[34] L. Aguero, S. Alpdagtas, E. Ilhan, D. Zaldivar-Silva, O. Gunduz, „Functional role of crosslinking in alginate scaffold for drug delivery and tissue engineering: A review," *European Polymer Journal,* 160, p. 110807, 2021.

[35] F. G. Prezotti, I. Siedle, F. I. Boni, M. Chorilli, I. Müller, B. S. F. Cury, „Mucoadhesive films based on gellan gum/pectin blends as potential platform for buccal drug delivery," *Pharmaceutical Development and Technology,* 25, 2, pp. 159-167, 2020.

[36] P. Ghasemiyeh, S. Mohammadi-Samani, „Polymers Blending as Release Modulating Tool in Drug Delivery," *Frontiers in Materials,* 8, p. 762813, 2021.

[37] S. Malorni, G. Bostock, „Rethinking Drug Delivery Devices for Sustainability and Innovation"," *ONdrugDelivery,* 112, pp. 34-37, 2020.

[38] E. Sheridan, M. Patel, „Sustainability in drug delivery: a green future without compromising safety and efficacy," *Chemistry Today,* 39, 1, 2021.

[39] K. Park, „Controlled drug delivery systems: past forward and future back," *Journal of controlled release : official journal of the Controlled Release Society,* 28, 190, pp. 3-8, 2014.

[40] R. H. Blythe, „Sympathomimetic Preparation". USA Patent 2738303, 13 March 1956.

[41] J. Folkman, D. M. Long, „The use of silicone rubber as a carrier for prolonged drug therapy," *The Journal of surgical research,* 4, pp. 139-142, 1964.

[42] S. Binauld, M. H. Stenzel, „Acid-degradable polymers for drug delivery: a decade of innovation," *Chemical communications (Cambridge, England),* 49, 21, pp. 2082-2102, 2013.

[43] M. Lengyel, N. Kállai-Szabó, V. Antal, A. J. Laki, I. Antal, „Microparticles, Microspheres, and Microcapsules for Advanced Drug Delivery," *Scientia Pharmaceutica,* 87, 3, p. 20, 2019.

[44] M. N. Singh, K. S. Hemant, M. Ram, H. G. Shivakumar, „Microencapsulation: A promising technique for controlled drug delivery," *Research in pharmaceutical sciences,* 5, 2, pp. 65-77, 2010.

[45] S. Heidari, M. Akhlaghi, M. Sadeghi, A. Mokhtari Kheirabadi, D. Beiki, A. Emami Ardekani, A. Rouhollah, P. Saeidzadeh, R. Soleyman, „Development of 64Cu-DOX/DOX-loaded chitosan-BSA multilayered hollow microcapsules for selective lung drug delivery," *Journal of Drug Delivery Science and Technology,* 73, p. 103477, 2022.

[46] R. D. Field, M. A. Jakus, X. Chen, K. Human, X. Zhao, P. V. Chitnis, S. K. Sia, „Ultrasound-Responsive Aqueous Two-Phase Microcapsules for On-Demand Drug Release," *Angewandte Chemie,* 134, 20, p. e202116515, 2022.

[47] V. Gyanani, J. C. Haley, R. Goswami, „Challenges of Current Anticancer Treatment Approaches with Focus on Liposomal Drug Delivery Systems," *Pharmaceuticals,* 14, 9, p. 835, 2021.

[48] Y. Zhao, Z. Zhao, Y. Cui, „Redox-responsive glycosylated combretastatin A-4 derivative as novel tubulin polymerization inhibitor for glioma and drug delivery," *Drug Development Research,* 82, 7, pp. 1063-1072, 2021.

[49] Q. Y. Fu, Y. Zhao, Z. Z. Yang, „Liposomes actively recognizing the glucose transporter GLUT1 and integrin αv β3 for dual-targeting of glioma," *Archiv der Pharmazie,* 352, 2, p. e1800219, 2019.

[50] S. Zhaoqing, L. Qianqian, L. M. , „pH-Sensitive nanoscale materials as robust drug delivery systems for cancer therapy," *Chinese Chemical Letters,* 31, 6, pp. 1345-1356, 2020.

[51] H. Park, G. Saravanakumar, J. Kim, „Tumor microenvironment sensitive nanocarriers for bioimaging and therapeutics," *Advanced Healthcare Materials,* 10, 5, p. e2000834, 2021.

[52] Z. Jiang, W. Zhang, J. Zhang, T. Liu, J. Xing, H. Zhang, D. Tang, „Nanomaterial-based drug delivery systems: a new weapon for cancer immunotherapy," *International Journal of Nanomedicine,* 17, pp. 4677-4696, 2022.

[53] S. P. Newman, „Drug delivery to the lungs: challenges and opportunities," *Therapeutic Delivery,* 8, 8, pp. 647-661, 2017.

[54] J. G. Weers, J. Bell, H.-K. Chan, D. Cipolla, C. Dunbar, A. J. Hickey, I. J. Smith, „Pulmonary formulations: what remains to be done?," *Journal of Aerosol Medicine and Pulmonary Drug Delivery,* 23, 2, pp. S5-S23, 2010.

[55] B. R. C. De Menezes, K. F. Rodrigues, V. M. Schatkoski, R. M. Pereira, R. G. Ribas, T. L. d. A. Montanheiro, G. P. Thim, „Current advances in drug delivery of nanoparticles for respiratory disease treatment.," *Journal of Materials Chemistry B,* 9, 7, pp. 1745-1761, 2021.

[56] M.-X. Luo, S. Hua, Q.-Y. Shang, „Application of nanotechnology in drug delivery systems for respiratory diseases," *Molecular Medicine Reports,* 23, 5, p. 325, 2021.

[57] A. Sharma, D. Kumar, K. Dahiya, S. Hawthorne, S. K. Jha, N. K. Jha, P. Nand, S. Girgis, S. Raj, R. Srivastava, V. K. Goswami, Y. Gregoriou, S. A. El-Zahaby, S. Ojha, H. Dureja, G. Gupta, S. Singh, D. Chellappan, K. Dua, „Advances in pulmonary drug delivery targeting microbial biofilms in respiratory diseases," *Nanomedicine (Lond),* 16, 21, pp. 1905-1923, 2021.

[58] H. Chen, L. Wang, X. Zeng, H. Schwarz, H. S. Nanda, X. Peng, Y. Zhou, „Exosomes, a New Star for Targeted Delivery," *Frontiers in Cell and Developmental Biology,* 9, p. 751079, 2021.

[59] R. Mittal, N. Bencie, J. Langlie, J. Mittal, A. A. Eshraghi, „Exosomes as drug delivery vehicles and biomarkers for neurological and auditory systems," *Journal of Cellular Physiology,* 236, pp. 8035-8049, 2021.

[60] X. Xia, Y. Wang, Y. Huang, H. Zhang, H. Lu, J. C. Zheng, „Exosomal miRNAs in central nervous system diseases: biomarkers, pathological mediators, protective factors and therapeutic agents," *Progress in Neurobiology,* 183, p. 101694, 2019.

[61] S. Srivastava, R. Ahmad, S. K. Khare, „Alzheimer's disease and its treatment by different approaches: A review," *European Journal of Medicinal Chemistry,* 216, p. 113320, 2021.

[62] Q. Ouyang, Y. Meng, W. Zhou, J. Tong, Z. Cheng, Q. Zhu, „New advances in brain-targeting nano-drug delivery systems for Alzheimer's disease," *Journal of Drug Targeting,* 30, 1, pp. 61-68, 2022.

[63] N. Alessio, A. L. Brigida, G. Peluso, N. Antonucci, U. S. D. Galderisi, „Stem cell-derived exosomes in autism spectrum disorder," *International Journal of Environmental Research and Public Health,* 17, 3, 2020.

[64] M. B. A. S. H. M. Ahmed Barhoum, Handbook of Nanofibers, Springer Cham, 2019.

[65] T. J. Sill, H. A. v. Recum., „Electrospinning: Applications in drug delivery and tissue engineering," *Biomaterials,* 29, 13, pp. 1989-2006, 2008.

[66] J. Xue, T. Wu, Y. Dai, Y. Xia, „Electrospinning and Electrospun Nanofibers: Methods, Materials, and Applications. , 119(8), 5298–5415.," *Chemical Reviews,* 119, 8, pp. 5298-5415, 2019.

[67] T. C. Yadav, A. K. Srivastava, P. Mishra, D. Singh, N. Raghuwanshi, N. K. Singh, A. K. Singh, S. K. Tiwari, R. Prasad, V. Pruthi, „Electrospinning: An Efficient Biopolymer-Based Micro- and Nanofibers Fabrication Technique," *ACS Symposium Series,* 1329, 10, pp. 209-241, 2019.

[68] S. Agarwal, J. H. Wendorff, A. Greiner, „Use of electrospinning technique for biomedical applications," *Polymer,* 49, 26, pp. 5603-5621, 2008.

[69] K. Li, Y. Wang, G. Xie, J. Kang, H. He, K. L. Y. Wang, „Solution electrospinning with a pulsed electric field," *Journal of Applied Polymer Science,* 135, 15, p. 46130, 2017.

[70] X. Huang, C. S. Brazel, „On the importance and mechanisms of burst release in matrix-controlled drug delivery systems," *Journal of controlled release : official journal of the Controlled Release Society,* 73, 2-3, pp. 121-136, 2001.

[71] Y. Liu, T. Li, Y. Han, F. Li, Y. Liu, „Recent development of electrospun wound dressing," *Current Opinion in Biomedical Engineering,* 17, p. 100247, 2021.

[72] A. R. Chandrasekaran, J. Venugopal, S. Sundarrajan, S. Ramakrishna, „Fabrication of a nanofibrous scaffold with improved bioactivity for culture of human dermal fibroblasts for skin regeneration," *Biomedical Materials,* 1, 015001, p. 6, 2011.

[73] S. Saghazadeh, C. Rinoldi, M. Schot, S. S. Kashaf, F. Sharifi, E. Jalilian, A. Khademhosseini, „Drug delivery systems and materials for wound healing applications," *Advanced Drug Delivery Reviews,* 127, pp. 138-166, 2018.

[74] F. Liu, X. Wang, T. Chen, N. Zhang, Q. Wei, J. Tian, Y. Wang, C. Ma, Y. Lu, „Hydroxyapatite/silver electrospun fibers for anti-infection and osteoinduction," *Journal of Advanced Research,* 21, pp. 91-102, 2020.

[75] D. Kersani, J. Mougin, M. Lopez, S. Degoutin, N. Tabary, F. Cazaux, L. Janus, M. Maton, F. Chai, J. Sobocinski, N. Blanchemain, B. Martel, „Stent coating by electrospinning with chitosan/poly-cyclodextrin based nanofibers loaded with simvastatin for restenosis prevention," *European Journal of Pharmaceutics and Biopharmaceutics,* 150, pp. 156-167, 2020.

[76] J. Zhao, W. Cui, „Functional Electrospun Fibers for Local Therapy of Cancer," *Advanced Fiber Materials,* 2, pp. 229-245, 2020.

[77] N. Forouzideh, S. Nadri, A. Fattahi, E. Dalir Abdolahinia, M. Habibizadeh, K. Rostamizadeh, A. Baradaran-Rafii, H. Bakhshandeh, „Epigallocatechin gallate loaded electrospun silk fibroin scaffold with anti-angiogenic properties for corneal tissue engineering," *Journal of Drug Delivery Science and Technology,* 56, Part A, p. 101498, 2020.

[78] W. Salalha, J. Kuhn, Y. Dror, E. Zussman, „Encapsulation of bacteria and viruses in electrospun nanofibres," *Nanotechnology,* 17, p. 4675, 2006.

[79] T. D. J. Heunis, M. Botes, L. M. T. Dicks, „Encapsulation of Lactobacillus plantarum 423 and its Bacteriocin in Nanofibers," *Probiotics and Antimicrobial Proteins volume,* 2, pp. 46-51, 2010.

[80] S. Stojanov, A. Berlec, „Electrospun Nanofibers as Carriers of Microorganisms, Stem Cells, Proteins, and Nucleic Acids in Therapeutic and Other Applications," *Frontiers in Bioengineering and Biotechnology,* 8, 130, 2020.

[81] Y. Fan, X. Tian, L. Zheng, X. Jin, Q. Zhang, S. Xu, P. Liu, N. Yang, H. Bai, H. Wang, „Yeast encapsulation in nanofiber via electrospinning: Shape transformation, cell activity and immobilized efficiency," *Materials Science and Engineering: C,* 120, p. 111747, 2021.

[82] L. Valot, J. Martinez, A. Mehdi, G. Subra, „Chemical insights into bioinks for 3D printing," *Chemical Society Reviews,* 48, pp. 4049-4086, 2019.

[83] G. T. Klein, M. Y. Wang, „3D printing and neurosurgery - ready for prime time?," *World Neurosurgery News,* 80, 3, pp. 133-235, 2013.

[84] A. Ali, U. Ahmad, J. Akhtar, „3D Printing in Pharmaceutical Sector: An Overview," *Pharmaceutical Formulation Design - Recent Practices,* pp. 1-13, 2020.

[85] M. C. Teixeira, N. S. Lameirinhas, J. P. F. Carvalho, A. J. D. Silvestre, C. Vilela, C. S. R. Freire, „A Guide to Polysaccharide-Based Hydrogel Bioinks for 3D Bioprinting Applications," *International Journal of Molecular Sciences,* 23, 12, p. 6564, 2022.

[86] G. Poologasundarampillai, A. Nommeots-Nomm, „Materials for 3D printing in medicine: Metals, polymers, ceramics, hydrogels," *3D Printing in Medicin,* pp. 43-71, 2017.

[87] M. Farokhi, F. Mottaghitalab, M. Babaluei, Y. Mojarab, S. C. Kundu, „Advanced Multifunctional Wound Dressing Hydrogels as Drug Carriers," *Macromolecular Bioscience,* 22, p. 2200111, 2022.

[88] Y. Shi, T. L. Xing, H. B. Zhang, R. X. Yin, S. M. Yang, J. Wei, W. J. Zhang, „Tyrosinase-doped bioink for 3D bioprinting of living skin constructs," *Biomedical Materials,* 13, p. 035008, 2018.

[89] H. Si, T. Xing, Y. Ding, H. Zhang, R. Yin, W. Zhang, „3D Bioprinting of the Sustained Drug Release Wound Dressing with Double-Crosslinked Hyaluronic-Acid-Based Hydrogels," *Polymers,* 11, 10, p. 1584, 2019.

[90] C. H., C. Y., T. J., Y. P., Z. X., C. Y., H. Y., W. J., „Dissolved oxygen from microalgae-gel patch promotes chronic wound healing in diabetes," *Science Advances,* 6, 20, p. 6.

[91] T. Wu, W. Liu, „Functional hydrogels for the treatment of myocardial infarction," *NPG Asia Materials,* 14, 9, 2022.

[92] T. Su, K. Huang, M. Daniele, M. Hensley, A. Young, J. Tang, T. Allen, A. Vandergriff, P. Erb, F. Ligler, „Cardiac stem cell patch integrated with microengineered blood vessels promotes cardiomyocyte proliferation and neovascularization after acute myocardial infarction.," *ACS Applied Materials & Interfaces,* 10, 39, pp. 33088-33096, 2018.

[93] N. M. Ergul, S. Unal, I. Kartal, C. Kalkandelen, N. Ekren, O. Kilic, L. Chi-Chang, O. Gunduz, „3D printing of chitosan/ poly(vinyl alcohol) hydrogel containing synthesized hydroxyapatite scaffolds for hard-tissue engineering," *Polymer Testing,* 79, p. 106006, 2019.

[94] E. Naseri, C. Cartmell, M. Saab, R. Kerr, A. Ahmadi, „Development of N,O-Carboxymethyl Chitosan-Starch Biomaterial Inks for 3D Printed Wound Dressing Applications," *Macromolecular Bioscience,* 21, 12, p. 2100368, 2021.

[95] P. J. Kondiah, P. P. D. Kondiah, Y. E. Choonara, T. Marimuthu, V. Pillay, „A 3D Bioprinted Pseudo-Bone Drug Delivery Scaffold for Bone Tissue Engineering," *Pharmaceutics,* 12, 2, p. 166, 2020.

[96] K. Glover, E. Mathew, G. Pitzanti, E. Magee, D. A. Lamprou, „3D bioprinted scaffolds for diabetic wound-healing applications," *Drug Delivery and Translational Research,* 2022.

[97] N. Deng, J. Sun, Y. Li, L. Chen, C. Chen, Y. Wu, Z. Wang, L. Li, „Experimental study of rhBMP-2 chitosan nano-sustained release carrier-loaded PLGA/nHA scaffolds to construct mandibular tissue-engineered bone," *Archives of Oral Biology,* 102, pp. 16-25, 2019.

[98] H.-Y. Lin, H.-Y. Huang, S.-J. Shiue, J.-K. Cheng, „Osteogenic effects of inductive coupling magnetism from magnetic 3D printed hydrogel scaffold," *Journal of Magnetism and Magnetic Materials,* 504, p. 166680, 2020.

[99] D. L. Johnson, R. M. Ziemba, J. H. Shebesta, J. C. Lipscomb, Y. Wang, Y. Wu, „Design of pectin-based bioink containing bioacive agent-loaded microspheres for bioprinting," *Biomedical Physics & Engineering Express,* 5, 6, p. 067004, 2019.

[100] J. Wen, B. Hou, W. Lin, F. Guo, M. Cheng, J. Zheng, P. He, W. Ji, „3D-printed hydrogel scaffold-loaded granulocyte colony-stimulating factor sustained-release microspheres and their effect on endometrial regeneration," *Biomaterials Science,* 10, pp. 3346-3358, 2022.

[101] J. Wei, Y. Yan, J. Gao, Y. Li, Q. Zou, Y. Zuo, J. Li, J. Wang, R. Wang, M. Zhu, „3D-printed hydroxyapatite microspheres reinforced PLGA scaffolds for bone regeneration," *Biomaterials Advances,* 133, p. 112618, 2022.

[102] W. Zhuang, G. Ye, J. Wu, L. Wang, G. Fang, Z. Ye, G. Lai, X. Qiu, H. Sang, „A 3D-printed bioactive polycaprolactone scaffold assembled with core/shell microspheres as a sustained BMP2-releasing system for bone repair," *Biomaterials Advances,* 133, p. 2022, 2022112619.

[103] W. Wang, X. Chen, L. Liu, „Multi-network granular hydrogel with enhanced strength for 3D bioprinting," *Journal of Biomaterials Applications,* 36, 10, 2022.

[104] D.-L. Yang, F. Faraz, J.-X. Wang, N. Radacsi, „Combination of 3D Printing and Electrospinning Techniques for Biofabrication," *Advanced Materials Technologies,* 7, 7, p. 2101309, 2022.

[105] R. Li, A. McCarthy, Y. Zhang, J. Xie, „Decorating 3D Printed Scaffolds with Electrospun Nanofiber Segments for Tissue Engineering," *Advanced Biosystems,* 3, 12, p. 1900137, 2019.

[106] Y. Yoon, C. H. Kim, J. E. Lee, J. Yoon, N. K. Lee, T. H. Kim, S.-H. Park, „3D bioprinted complex constructs reinforced by hybrid multilayers of electrospun nanofiber sheets," *Biofabrication,* 11, p. 025015, 2019.

[107] H. Y. Vargas-Molinero, A. Serrano-Medina, K. Palomino-Vizcaino, E. A. López-Maldonado, L. J. Villarreal-Gómez, G. L. Pérez-González, J. M. Cornejo-Bravo, „Hybrid Systems of Nanofibers and Polymeric Nanoparticles for Biological Application and Delivery Systems," *Micromachines,* 14, 1, p. 208, 2023.

[108] S. Amini, A. Saudi, N. Amirpour, M. Jahromi, S. S. Najafabadi, M. Kazemi, M. Rafienia, H. Salehi, „Application of electrospun polycaprolactone fibers embedding lignin nanoparticle for peripheral nerve regeneration: In vitro and in vivo study.," *International journal of biological macromolecules,* 159, pp. 154-173, 2020.

[109] B. Jiang, Z. Yang, H. Shi, A. T. Jalil, M. M. Saleh, W. Mi, „Potentiation of Curcumin-loaded zeolite Y nanoparticles/PCL-gelatin electrospun nanofibers for postsurgical glioblasa treatment," *Journal of Drug Delivery Science and Technology,* 80, p. 104105, 2023.

[110] A. R. Ahmady, A. Solouk, S. Saber-Samandari, S. Akbari, H. Ghanbari, B. E. Brycki, „Capsaicin-loaded alginate nanoparticles embedded polycaprolactone-chitosan nanofibers as a controlled drug delivery nanoplatform for anticancer activity," *Journal of Colloid and Interface Science,* 638, pp. 616-628, 2023.

[111] J. Gao, J. Zhu, J. Luo, J. Xiong, „Investigation of microporous composite scaffolds fabricated by embedding sacrificial polyethylene glycol microspheres in nanofibrous membrane," *Composites Part A: Applied Science and Manufacturing,* 91, Part 1, pp. 20-29, 2016.

[112] G. Balzamo, X. Zhang, W. A. Bosbach, E. Mele, „In-situ formation of polyvinylidene fluoride microspheres within polycaprolactone electrospun mats," *Polymer,* 186, p. 122087, 2020.

[113] A. Grzywaczyk, A. Zdarta, K. Jankowska, A. Biadasz, J. Zdarta, T. Jesionowski, E. Kaczorek, W. Smułek, „New Biocomposite Electrospun Fiber/Alginate Hydrogel for Probiotic Bacteria Immobilization," *Materials (Basel, Switzerland),* 14, 14, p. 3861, 2021.

PUBLICATIONS INCLUDED IN THE DOCTORAL THESIS

PUBLICATION 1

Polymer fibers electrospun using pulsed voltage

Mirek, A., Korycka, P., Grzeczkowicz, M., Lewińska, D.
Materials and Design. 183, 108106 (2019).
DOI: 10.1016/j.matdes.2019.108106

Materials and Design 183 (2019) 108106

Contents lists available at ScienceDirect

Materials and Design

journal homepage: www.elsevier.com/locate/matdes

Polymer fibers electrospun using pulsed voltage

Adam Mirek*, Paulina Korycka, Marcin Grzeczkowicz, Dorota Lewińska

Nalecz Institute of Biocybernetics and Biomedical Engineering, Polish Academy of Sciences, Warsaw, Poland

HIGHLIGHTS

- Fibrous mats obtained in the electrospinning process with direct-current (DCV) and pulsed (PV) voltages are compared.
- The solution shapes at the nozzle tip were observed and linked to the structures of the polymer mats.
- The average fiber diameter, the bead size (in the bead-on-string type structure) and their concentration were determined.
- Electrospinning with PV is possible and, in some cases, may result in more favorable effects than with DCV.
- Preliminary predictions in the structure of electrospun products can be made by observing the meniscus at the nozzle tip.

GRAPHICAL ABSTRACT

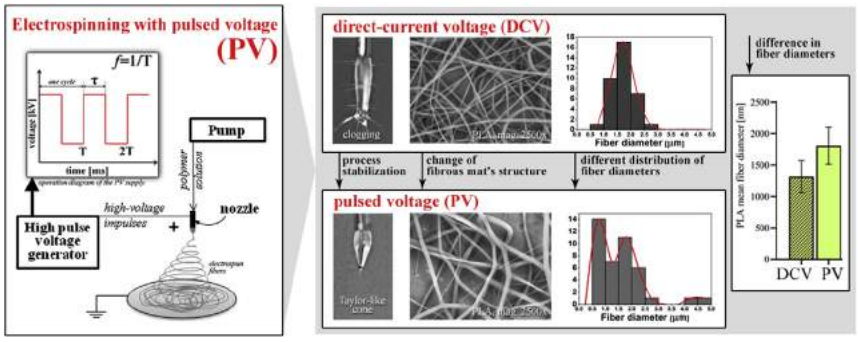

ARTICLE INFO

Article history:
Received 26 June 2019
Received in revised form
6 August 2019
Accepted 7 August 2019
Available online 7 August 2019

Keywords:
Electrospinning
Pulsed voltage
Polymer fibers
Meniscus
Droplet shape
Electrospinning jet

ABSTRACT

Electrospinning processes are commonly conducted with direct-current voltage (DCV) but the fibers can also be electrospun using a pulsed voltage (PV). Although this method has been used in other electrostatic processes, there is little research on its application in nanofibers production. In this work, the voltage was supplied to the polymer solution in pulses with a given amplitude, frequency, and duration. Experiments were performed with two polymers (polyvinylpyrrolidone and polylactide) using both DCV and PV. The shape of the liquid jet formed at the nozzle tip was observed and linked to the structure of the polymer mats, including the diameters of the electrospun fibers and the sizes and the concentrations of spherical elements. Some differences in products electrospun using DCV and PV were observed both for polyvinylpyrrolidone and polylactide. The parameter that most strongly influenced the examined properties of the polymer mats was the pulse frequency. Moreover, for polylactide the PV method eliminates polymer clogging, providing greater stability of the electrospinning and changes the distribution of fiber diameters into a bimodal one. In general, PV gives better control over fiber diameters and bead sizes because of the possibility of more precise electric charge delivery due to a lower effective voltage.

1. Introduction

Since the electrospinning process began gaining popularity in the early 20th century, scientists from around the world have been

* Corresponding author at: Nalecz Institute of Biocybernetics and Biomedical Engineering, Polish Academy of Sciences, Ks. Trojdena 4 st., 02-109 Warsaw, Poland.
E-mail address: amirek@ibib.waw.pl (A. Mirek).

https://doi.org/10.1016/j.matdes.2019.108106

improving it and looking into new areas for further applications. Using this low-complexity method, polymeric fibers with diameters from nano- to micrometers can be obtained. These fibers can be applied in areas such as optoelectronic devices, adsorption filters, and materials for biomedical applications (tissue engineering, enzyme immobilization, drug release, and wound dressing) [1–5].

A typical electrospinning setup is comprised of only a few components: a high voltage supply, a polymer (melt or solution) dosing system, a metal nozzle, and a grounded collector. A high voltage is applied to the nozzle from which the polymer solution (or melt) extrudes. Next, the shape of the fluid meniscus at the nozzle tip changes and a charged polymer solution jet is formed and deposited on the grounded collector [1]. Although the experimental setup is relatively simple, it is possible to modify any individual step of the process to obtain fibrous mats with different properties made of different sized fibers and structures [6].

One of the physicochemical parameters of the polymer solution that influences the characteristics of the obtained electrospun product is its viscosity, which depends primarily on the polymer structure, its molecular weight, and the solvent and solution concentrations [7–13]. Lowering the molecular weight of the polymer results in bead formation rather than the smooth fibers that appear at higher molecular weights to ultimately take the form of microribbons [7], even at low concentrations [8]. As the concentration increases, different types of structures obtained for different viscosities can be distinguished [9]: electrosprayed micro- or nanoparticles [10], mixed bead-on-string type structures and fibers [11,12], uniform smooth fibers [11,12], and helix-shaped microribbons [13]. The appearance of beads in the fibrous mats or the fabrication of smooth fibers can be controlled using various solvents or their mixtures [13,14]. Other physicochemical properties of polymer solutions that can affect electrospun products are the surface tension [13] and conductivity [15,16], which depend largely on the composition of the solutions (concentration, solvent mixtures, additives like salts, etc.).

Fibers with different structures can be obtained by choosing the appropriate ambient conditions, such as the process's humidity or temperature. The relationship between the temperature and the viscosity of the solution is inversely proportional, giving thinner fibers at higher temperatures [17]. Changes in the ambient humidity affects the evaporation rate of the solvent and the equilibrium vapor pressure, which results in changes in the structure of the fibrous mats (e.g., fused fibers and film-like morphologies for humidities over 70%) [14,18,19]. A similar effect can be achieved by adjusting the polymer solution's flow rate. A lower value of this parameter is more advantageous as it can provide the solvent more time to evaporate. The residues of the solvent in the fibrous mat can fuse the fibers together and change its structure [20,21].

The structure of the electrospun product can be also controlled by changing the construction and design of the electrospinning system. Thus, different types of spinnerets are currently extensively investigated in order to modify the fiber structure: single [5,7,10,14,19,20], coaxial [22,23], multiaxial [24,25] or side-by-side [26] nozzles. These innovations allow the preparation of monolithic, core/shell or Janus fibers. Also, the distance between the tip of the nozzle and the collector can be a factor that influences the fiber diameter and its morphology, e.g., increasing the working distance produces thinner fibers [20,27]. A parameter of great importance is the collector, including its shape, type, orientation, size, and speed if it is mobile (e.g. rotary) [4].

It has been shown that the process parameter with the greatest influence on the diameter of the fibers is the voltage [21,28]. This is a crucial factor that affects the geometric shape of the liquid at the tip of the nozzle, meaning it determines whether the electrospinning process occurs or not [10]. There is a minimum voltage threshold at which a charged polymer solution jet is ejected from the Taylor's cone with stable and repeatable conditions [29,30]. The voltage value changes the height and angle of the Taylor cone as well as the length of the solution jet [31]. The influence of this factor on the fiber diameter may vary depending on the values of the other parameters, ambient conditions, and the selection of the polymer and its solvent [20,32–34].

Most researchers [20,21,28,29,32–34] have used direct current voltage (DCV) in the electrospinning process, which means that a constant voltage is supplied continuously to the end of the nozzle. However, there are some studies where the pulsed voltage (PV) is used in electrohydrodynamic processes such as hydrogel microbead production [35,36]. In this case, the voltage is supplied to the polymer solution in pulses of a given frequency and duration (duty cycle). It was shown [35] that all these parameters strongly influenced the diameter and the size uniformity of microbeads. As a result, improved control over the electric charge delivered to the polymer solution is possible. The same conclusion has been drawn by Kessick and co-workers [37].

In recent years, the application of PV for electrospinning has also been reported. [30,37–41]. The work of Li et al. [37] showed the impact of the PV parameters (voltage, frequency, and duty cycle) and the flow rate of the polymer solution on the diameter of fibers made of polyvinylpyrrolidone (PVP) using a factorial design approach. They also proved that electrical factors affect the fiber diameter in the following order: duty cycle, flow rate, voltage, and frequency. The authors compared the fiber diameters obtained using DCV and PV, leading to the conclusion that fibers with smaller diameters were formed using PV. Xie et al. [38] studied the influence of the duty cycle and the frequency of the pulsed electric field on the diameter and morphology of fibers electrospun from a poly-L-lactide (PLLA) melt. It was shown that the use of PV with an increasing frequency caused a decrease in the fiber diameter. Some researchers showed that PV can change not only the diameter but also the length of the produced fibers. Baba et al. [30] noted that it is possible to obtain chopped fibers using PV due to its periodic nature, as there are periods when a high voltage is supplied to the nozzle (the electrospinning process occurs) and when the voltage supply is interrupted (the process is interrupted as well), no fiber is spun.

While the influence of PV on the electrospun fiber size (length and diameter) has been previously investigated, there has not been a discussion on the general structure of fibrous mats e.g. beaded or beadless. These previous works were focused on obtaining short fibers or those with diameters smaller than in the case of using DCV. To the authors' knowledge, none of the researchers studied the impact of pulse frequency on the liquid jet shape at the nozzle tip. Furthermore, no attempts have been made to link the liquid shape to the electrospun product when using PV.

The aim of this work was to examine the differences between the structure of fibrous mats obtained in the electrospinning process with both DCV and PV. There is emphasis on the observations of the geometric shape of the liquid at the nozzle tip, linking it to the structure of the polymer mats, including the diameters of the electrospun fibers and the size and concentration of bead-like structures formed in some of the mats obtained. The experiments were performed using solutions of two biodegradable polymers: polyvinylpyrrolidone (PVP) and polylactide (PLA), of significantly different viscosities.

2. Method

2.1. Materials

Poly(vinyl pyrrolidone) (PVP, $M_w = 1300$ kDa) was purchased from Acros Organics and polylactide (PLA, $M_w = 200$ kDa) was from

Table 1
The properties of the prepared polymer solutions.

Polymer	Solvent	Concentration C (w/w)	Viscosity μ [mPa·s]
PVP	C_2H_5OH	3.5%	32 (25 °C)
		8.0%	200 (25 °C)
PLA	$CHCl_3$/DMF (9:1)	8.0%	605 (20 °C)
		10.0%	1310 (20 °C)

Sigma Aldrich. Ethanol (purchased from Polmos, Poland) was used as a solvent for the PVP. The mixture of chloroform (POCH, Poland) and dimethylformamide (Chempur, Poland) in a ratio of 9:1 was used as the PLA solvent. The concentrations and viscosities of the prepared solutions are given in Table 1.

2.2. Electrospinning setup

The electrospinning process was performed using a custom-built setup (Fig. 1), which includes a high voltage pulse generator, an infusion pump connected by a drain with a steel nozzle (external diameter of 0.9 mm), and a grounded, aluminum, flat, round plate collector with a diameter of 40 mm and a thickness of 0.12 mm as placed 15 cm below the nozzle tip. The generator supplied a high, rectangular wave voltage to the nozzle with frequency f, duration τ, and amplitude U. All these parameters were variables in the experiments. The time domain waveform signal of the PV supply is schematically presented in the Fig. 1.

The polymer solution was delivered at a flow rate of 0.9 ml/h to the nozzle where high voltage pulses of 8 or 15 kV were applied. A voltage of 8 kV was used only for the PVP solutions because attempts to electrospin the PLA solution at 8 kV did not produce an electrospinning jet at the nozzle tip nor were fibers deposited on the collector; only droplets were formed. Electrical pulses were supplied with frequencies of 20, 50 and 100 Hz, and duration of 5 ms. The resulting product was deposited on the collector plate for a specified time so the same amount of solution was used in each experiment. The electrospinning of the investigated solutions was also performed using DCV as a comparison (8 kV or 15 kV; 0.9 ml/h) with the same setup. All experiments with the PVP (PLA) were carried out at a temperature of 25 °C (20 °C). The humidity did not exceed 40% in any case. Fig. 2 shows a scheme for the experiments.

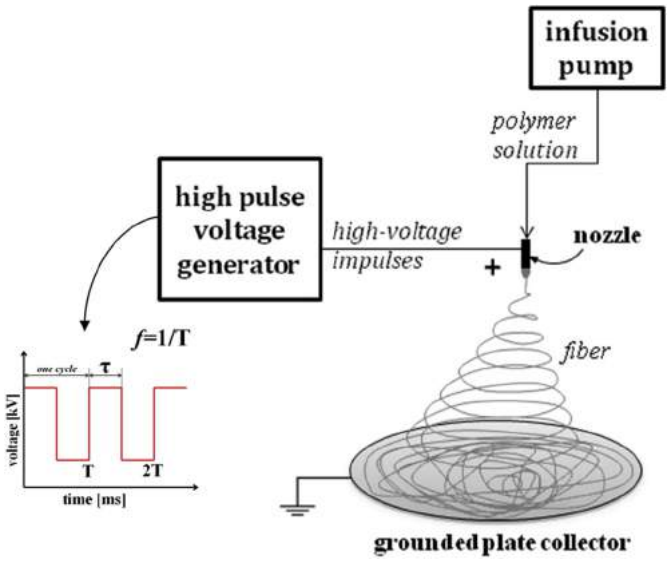

Fig. 1. Scheme of the electrospinning process setup with an operation diagram of the PV supply (red line).

2.3. Mat structure

The geometric shapes of the polymer solution at the end of the nozzle were recorded using a monochrome CCD camera. The morphology of the polymer fibers was examined using scanning electron microscopy (SEM, Hitachi TM-1000). The samples were coated with thin layer (10 nm) of gold to prevent charging. The diameters of thirty randomly selected (from one image) fibers or beads were measured using the software provided with the microscope and their average values were calculated (d for fibers and d_b for beads). The size of the beads was determined in an analogous manner to the method described by Korycka et al. [12] (Fig. 3). A structure where the widest point (s) was at least three times greater than the diameter of the fiber (d_f) was defined as a bead. The size of a bead (d_B) is the distance between the points where the fiber begins to expand to form a bead (Fig. 3). Based on the SEM images, the beads in the mats were counted and their concentration was determined as the number of beads per surface unit [beads/mm^2]. Microsoft Excel and the Statistica software were used to perform the calculations. The column graphs were made using the GraphPad Prism software.

2.4. Statistical analysis

The statistical differences between the mean diameters of fibers obtained applying the DCV and PV (for different pulse frequencies) were determined using a one-way analysis of variance (ANOVA) followed by Scheffe and RIR Tukey's test (post-hoc) with the help of the Statistica software. The significance level (α) was set at 0.05 and the probability of the data was considered statistically significant for p-values < 0.05. The results were marked on the charts (Figs. 7, 9) in the form of asterisks ((*) for $p < 0.05$, (**) for $p < 0.01$ and (***) for $p < 0.001$).

3. Results and discussion

3.1. Droplets, cones, and jet formation

The effects of an electrical voltage applied to the nozzle on the droplet, cone, and jet formation for the polymer solution were investigated by comparing short films recorded during the electrospinning process under the various conditions. A frame was cut from each film one minute after the experiment began, as shown in Fig. 4.

When the PVP solution with a concentration of 3.5% was electrospun, the DCV at 8 kV did not allow the creation of a cone (Fig. 4A1); however, one thread was spun from the slowly expanding droplets. For this solution, a voltage of 15 kV caused the cone to split and create several jets, called the multi-jet mode (Fig. 4A2). The Taylor cone was obtained for an 8% solution and a DCV of 8 kV (Fig. 4A3), while the 15 kV voltage had a similar effect on the liquid as for the 3.5% solution (Fig. 4A4).

The influence of the PV on the shape of the liquid at the nozzle tip can be observed by analyzing the images presented in Fig. 4B–D. For the 3.5% solution and a voltage of 8 kV, the jet was created only for $f = 100$ Hz (Fig. 4D1). At 20 (Fig. 4B1) and 50 Hz (Fig. 4C1), dripping occurred more often creating smaller droplets than observed for the DCV, and there were no fibers obtained for these cases (Fig. 5). The use of PV at 15 kV for a 3.5% solution resulted in a reduced number of jets compared with DCV. Furthermore, this prevented the formation of any cone as the electrospinning jets were formed just at the tip of the nozzle without the creation of the fluid cone for each frequency (Fig. 4(B-D)2). For the 8% PVP solution at 8 kV, neither the Taylor cone nor jet were formed at 20 Hz (Fig. 4B3) and there were no fibers obtained (dripping mode). However, the jet appeared at 50 Hz (Fig. 4C3), and at the frequency

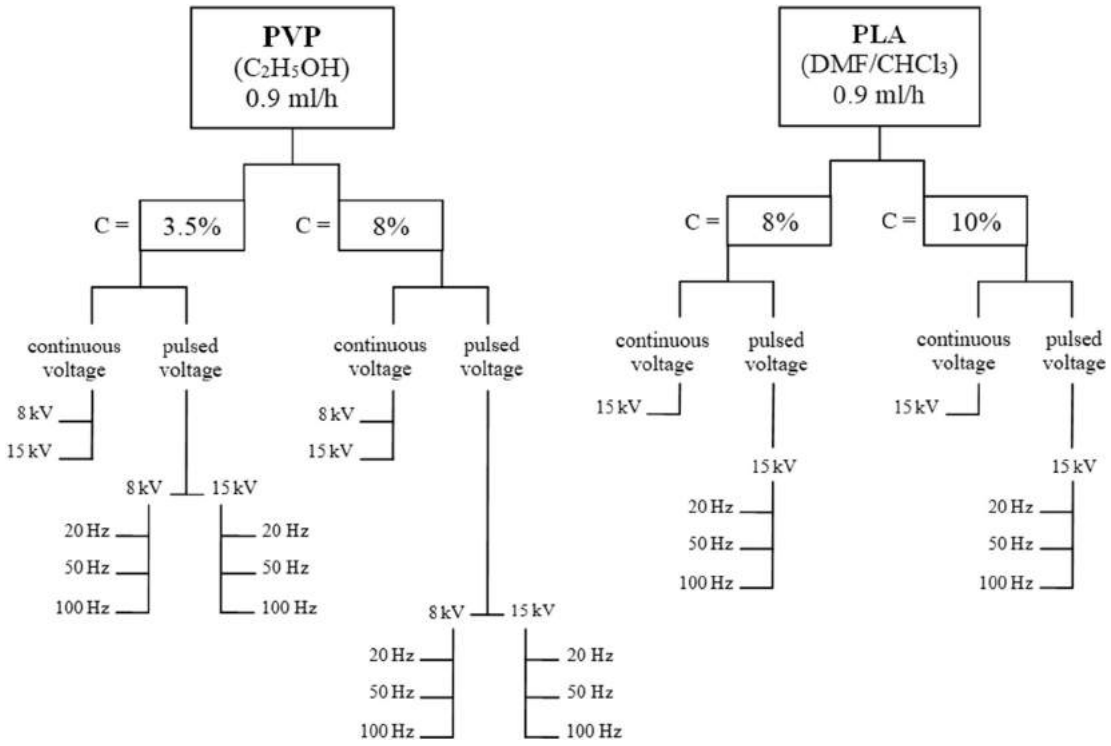

Fig. 2. Scheme of the experiments conducted.

of 100 Hz the liquid formed a shape similar to that for DCV, but with an additional side jet (Fig. 4D3). The use of 15 kV PV for the 8% solution resulted in a reduced number of jets compared with DCV, but fluid cones were obtained in each case (Fig. 4(B–D)4) while a Taylor cone was formed at 50 Hz (Fig. 4C4).

The experiments with the PLA solution in a mixture of DMF and $CHCl_3$ illustrated different liquid behaviors at the nozzle tip than for the PVP solutions. There is the evident effect of the polymer structure as well as the solvent and solution properties on the fluid jet shape [13,14]. For all the analyzed conditions with PLA (Fig. 4(A–D)5 and (A–D)6), the shape of the polymer solution at the nozzle tip was more or less extended, and the quick evaporation of the solvent (faster for chloroform [boiling point of 61.2 °C] than ethanol [boiling point of 78.37 °C]) caused the formation of a big polymer clot (nozzle clogging) in the case of DCV (Fig. 4A5, A6). The ends of the clots had a small cones consisting of threads spun from the tip. A similar phenomenon was observed by Liu et al. [42] and Wang et al. [43].

When the voltage was set at 8 kV, only droplets were formed at the nozzle tip without any electrospinning jet. For higher voltages (15 kV) when DCV was used (Fig. 4A5 and A6), the formation of a very elongated fluid shape and many additional side jets was seen, while the number of jets increased during the process. However, this is a different phenomenon than the typical multi-jet (e.g. Fig. 4A4) where the side threads were passive (no electrospinning). This described anomaly appears for both the 8% and 10% PLA solutions. The PV at 20 Hz caused vibrations in the extending fluid shape and formation of a nearly imperceptible jet. At 50 and 100 Hz, the solution took the shape of a slim bulb. In all the PV experiments performed for the PLA solutions electrospinning process was stable with a single jet, and fibers were obtained on the collector for all parameters (no dripping mode was observed).

These experiments showed the occurrence of the following shapes of the liquid at the nozzle tip (depending on the processing

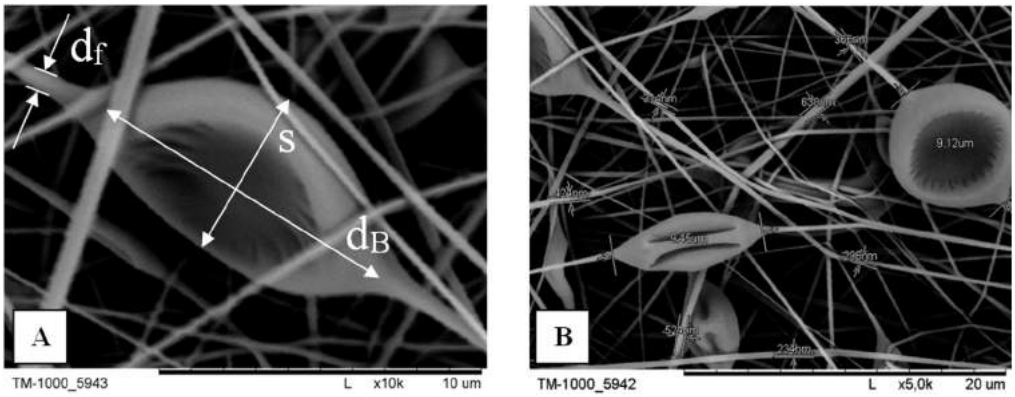

Fig. 3. (A) The method to measure the average fiber diameter d_f and the bead size d_B ($s \geq 3\ d_f$). (B) Beaded PVP fibrous mat with example fiber diameters and bead sizes marked.

conditions and the viscosity of the polymer solution):

- large droplets (dripping mode) (e.g. Fig. 4A1 and B3),
- very elongated solution shape with additional passive side jets (e.g. Fig. 4A5),
- elongated solution shape with a single electrospinning jet (e.g. Fig. 4D1, and C5),
- Taylor cone (e.g. Fig. 4A3 and C4) or Taylor-like cone with additional jets (e.g. Fig. 4D3),
- very small cone (almost imperceptible), from which a few jets spin (multi-jet mode) (e.g. Fig. 4A4 and C2).

Based on past experience, the absence of an electrical potential causes the liquid to flow in the form of single drops as opposed to a stream [44]. The droplet grows to a certain size before detaching from the nozzle. The droplets are maintained by the forces of the liquid surface tension and break off when the weight of the droplet exceeds these forces. In processes that include an electric voltage, additional forces associated with the electrostatic interactions appear, which produces a new force balance. In electrospinning process, there is an electrical potential difference between the grounded collector and the nozzle connected to the high voltage supply source. The high intensity of the field around the formed droplets creates a high surface charge density. The electrostatic force is created along the electric field lines, and the resultant force acting on the drops is the vector sum of gravity and the electrostatic forces. This leads to a significant elongation and eventually burst of the drops. A Taylor cone is formed at the end of the nozzle for high-viscosity solutions containing long-chain polymers, causing the drop to become a jet.

The value and type of electric voltage applied to the nozzle has a large influence on the outflowing liquid shape. There is a range of voltages for which the Taylor cone is obtained and the electrospinning process is stable, which depends on the properties of the solution or polymer (type, molecular mass, concentration, etc.) and the environmental conditions. For instance, the Taylor cone occurred for the 8% PVP solution electrospun with a DCV of 8 kV but was not formed for the lower polymer concentration (3.5%). Below the voltage threshold, dripping occurs (e.g., voltages below 8 kV for the PLA solution), while above this threshold there were two or more vertices from which the fibers were electrospun (multi-jet mode), such as in the case of the PVP solution electrospun with a

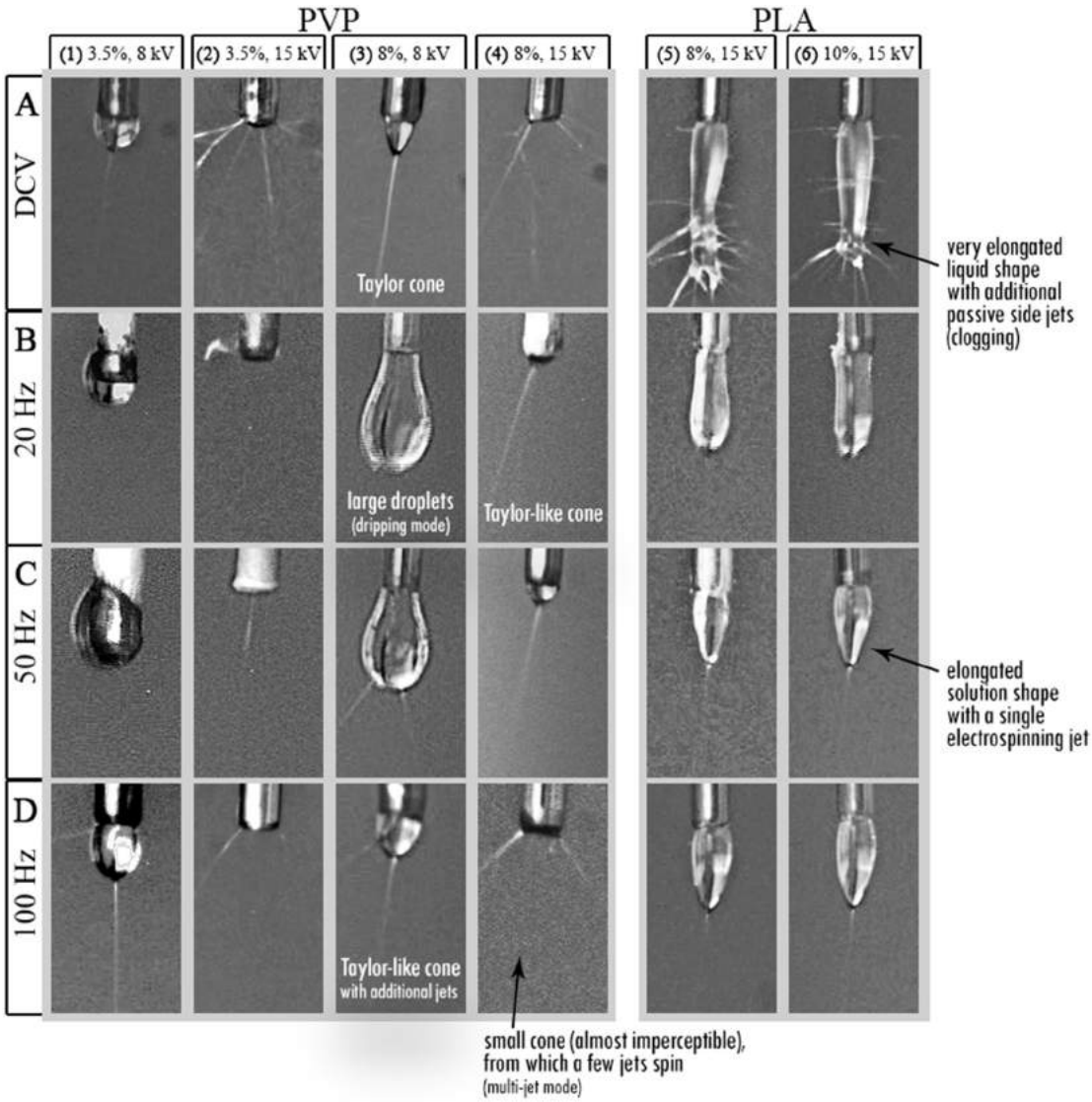

Fig. 4. Polymer (PVP and PLA) solution droplet, cone, jet, and multi-jet formation at the tip of the nozzle during electrospinning under different electrical conditions: (A) DCV, and PV at (B) 20 Hz, (C) 50 Hz, and (D) 100 Hz.

DCV of 15 kV. These dependencies were described by Baba et al. [30].

One of the problems occurring during the electrospinning of high-viscosity solutions is nozzle clogging (Fig. 4A5 and A6) which disturbs the process. A way to stabilize the electrospinning process and eliminate the clogging is to use a coaxial nozzle with an additional shell solvent [42,43]. Wang et al. used ethanol as a shell fluid to control the formation of fibers more precisely. However, this method is labor-intensive, as it requires an interference in the process setup (changing a single nozzle into a coaxial one, adding a second pump) and additional experiments and time to take control of a more complicated two-liquid system (to optimize the value of electrospinning parameters like the flow rate of both core and shell fluids). Therefore, the use of PV seems to be a much simpler and easier solution. An explanation of the stabilizing effect of PV on the electrospinning process requires additional, detailed research considering a wide range of changes to all the PV parameters (including pulse duration). This is probably due to supplying the nozzle with a smaller total amount of electric charge. The effective voltage U_{eff} for a PV of amplitude U, duration τ and a period of one cycle T (see the operational diagram in Fig. 1) is specified by the Eq. (1):

$$U_{eff} = \sqrt{\tau/T} \cdot U \tag{1}$$

Thus it is always lower than the voltage U used in the case of DCV.

The next stage of the work was to examine the polymeric mat structures and link them to the geometric shape of the liquid at the nozzle tip.

3.2. Structure of electrospun mats

Figs. 5 and 6 show SEM images of the electrospun fibrous mats manufactured from all the experiments. These images illustrate that the process parameters have a great impact on the obtained product, causing the formation of several different electrospun structures even for solutions of the same polymer, concentration, and properties.

The analysis of photos for the mats obtained from the PVP suggests that there is a certain limiting value of the supplied electric charge, below which electrospinning does not occur and fibers are not produced (Fig. 5(B–C)1 and B3). When the high voltage supply was switched into the pulsed mode, fibers were not obtained for 20 Hz (3.5% and 8% concentration) or 50 Hz (3.5% concentration) – dripping mode was observed.

At 8 kV, when the voltage was supplied continuously (DCV), the PVP solution was electrospun for both the 3.5% and 8% concentrations. At 15 kV, the amount of supplied electric charge was sufficient to obtain fibers regardless of the generator working in the continuous or pulsed mode (even for 20 Hz).

Fibrous mats obtained from the 3.5% PVP solution are characterized by the presence of a bead-on-string type structure for either applied voltage scheme (Fig. 5A1, D1, and (A–D)2). Such structures are known to be present when a polymer solution concentration is low [29]. Baba et al. [30] and Aliyev et al. [40] obtained similar

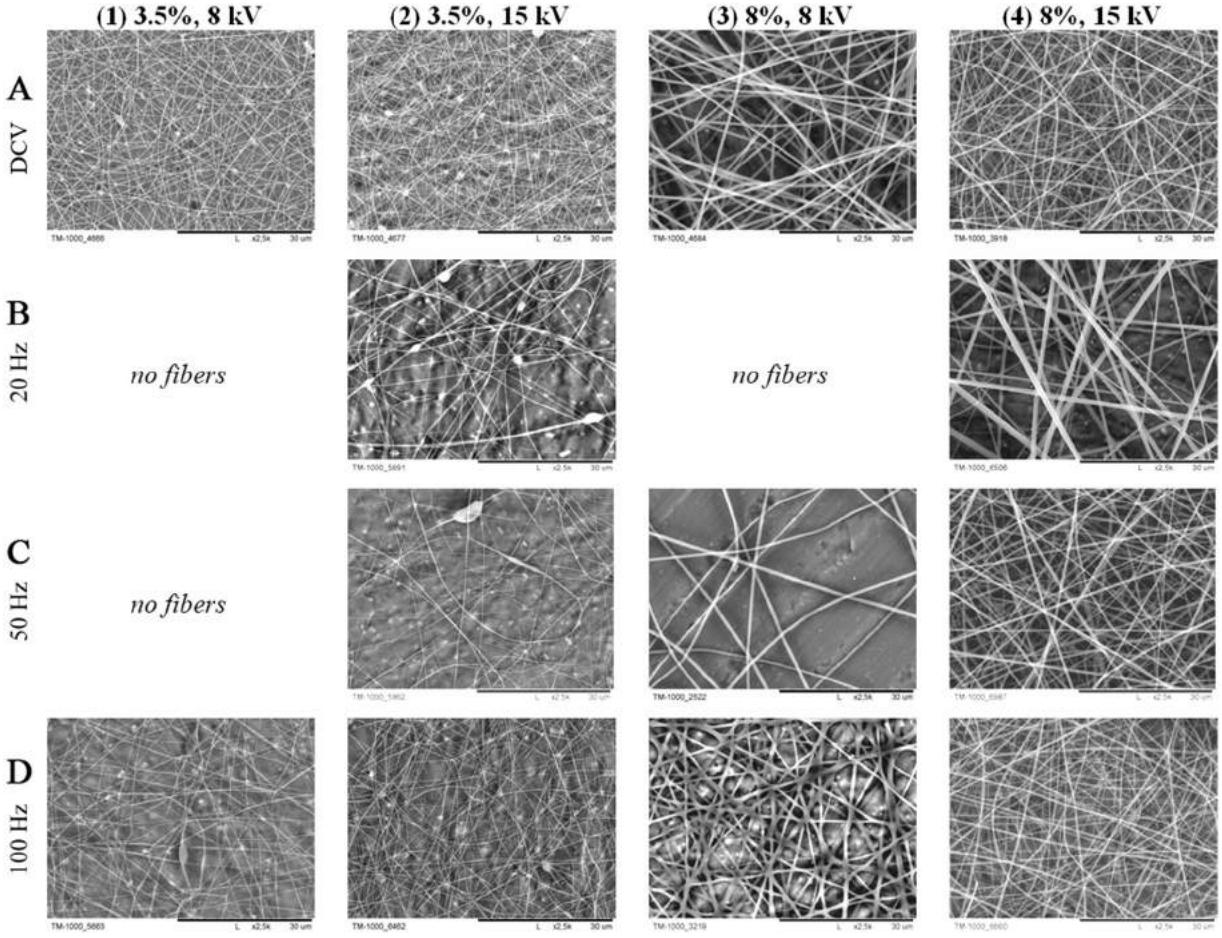

Fig. 5. Scanning electron microscope images of the PVP mats obtained from the electrospinning process under different electrical conditions: (A) DCV, and PV at (B) 20 Hz, (C) 50 Hz, and (D) 100 Hz under a magnification of 2500×.

beaded mats, but their fibers were chopped instead of being continuous. Interestingly, the use of PV results in lower density mats – the lowest fiber densities were obtained at 20 Hz (e.g. Fig. 5B2) and 50 Hz (e.g. Fig. 5C3) depending on the polymer concentration and voltage. The only structurally distinctive mat is the one obtained for 8 kV and 100 Hz with the 8% solution where its fibers appeared melted to each other (Fig. 5D3).

The PLA fibers were obtained in each experiment regardless of the concentration of the solution or value and type of the supplied voltage (Fig. 6). All fibers were smooth and without beads, where the only differences were in their diameters. In all cases the distribution of fiber diameters is bimodal with clearly observed thinner and thicker fibers. The density of the mats is comparable, except for the variant 15 kV and 20 Hz (Fig. 6B2), where the fibers are visibly less numerous. Comparing Figs. 4 and 6 confirms the relationship between the shape of the solution at the nozzle tip and the electrospun product. In all the experiments where the electrospinning jet occurred, fibers were formed on the collector as a

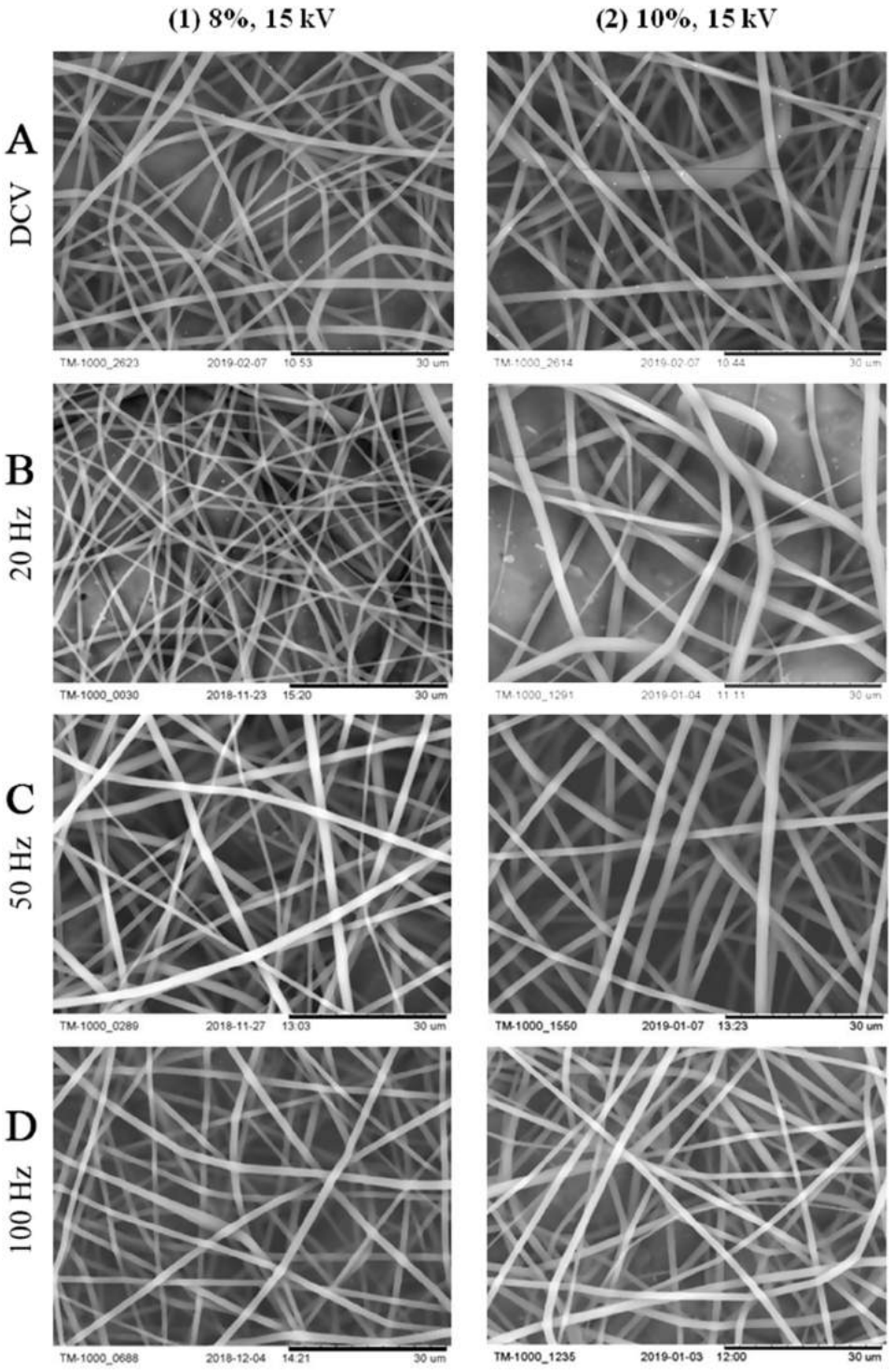

Fig. 6. Scanning electron microscope images of the PLA mats obtained in the electrospinning process under different electrical conditions: (A) DCV, and PV at (B) 20 Hz, (C) 50 Hz, (D) 100 Hz with a magnification of 2500×.

direct result.

This research showed the occurrence of the following polymeric fibrous electrospun mat structures depending on the process conditions and viscosity of the solution (especially the solvent and polymer selection):

- fibers with a bead-on-string type structure (e.g., PVP – Fig. 5A1 and B2),
- uniform fibers forming a sparse mat (e.g., PVP – Fig. 5C3), or a dense one (e.g., PVP - Fig. 5A3 and PLA - Fig. 6D2),
- mats made of fused fibers (e.g., PVP - Fig. 5D3),
- mats made of fibers having diameters with a bimodal distribution (e.g., PLA –Fig. 6B2 and C1).
- no fibers (e.g., PVP – Fig. 4B1).

There was no case in which chopped fibers were obtained as described in the works by Baba et al. [30] and Aliyev et al. [40]. This difference may be due to the fact that Ref [30] used PV with a pulse duration that was 10–100 times greater than this work. They also used a different polymer (polyethylene oxide) and solvents (water). Aliyev et al. used an electrospinning setup with a much greater distance between the nozzle tip and collector (23.5 cm). Hence, there are differences between the type of product obtained in their and this work. As is well-known, changes of the working distance has a significant impact on the structure of manufactured electrospun products [20,21].

Comparing Figs. 4 and 5 indicates that the polymer solution shape at the nozzle tip is associated with the product obtained in a respective electrospinning process. For instance, when only the dripping of the solution was observed (Fig. 4(B–C)1 and B3), fibers were not produced (Fig. 5(B–C)1 and B3). In any case, when the jetting occurs, the electrospinning process resulted in the manufacture of fibers with varying diameters, structures and number (such as in Fig. 5C3). It is noted that the resulting mat is clearly thinner there than for the other pictures. Comparing this case with the corresponding Fig. 4C3 picture supports this observation, where a dripping mode together with an electrospinning jet can be seen. It can therefore be concluded that a part of the polymer was deposited on the collector not in the form of fibers, but together with falling droplets sufficiently large to remain unseen in the small

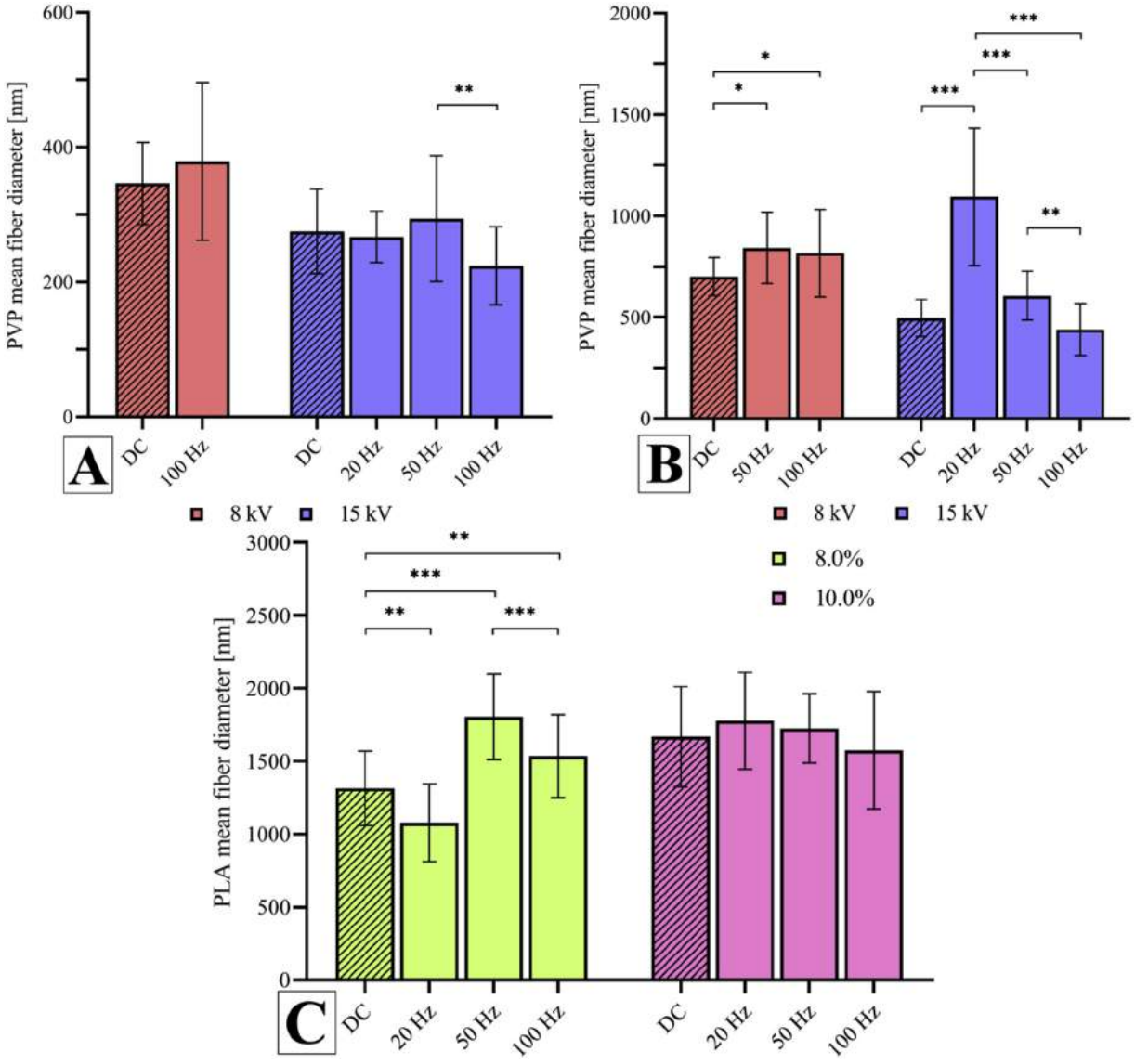

Fig. 7. The diameters of the fibers obtained from (A) the 3.5% PVP solution, (B) the 8.0% PVP solution with DCV and PV (8 kV and 15 kV, $\tau = 5$ ms), (C) the 8% and 10% PLA solutions with DCV and PV (15 kV, $\tau = 5$ ms).

sample of mat structure examined under SEM.

3.3. Fiber diameter

Fig. 7 shows the calculations and statistical analysis from the visual inspections of the mean fiber diameters. Each group of data compares the average diameters of the fibers obtained using DCV and PV.

For a PVP concentration of 3.5% (Fig. 7A), the resulting fibers had diameters between 300 and 400 nm for the 8 kV (red columns) and between 200 and 300 nm for the 15 kV (blue columns). There are no statistically significant differences between the fiber average diameters as obtained for the DCV and PV except for one case ($p < 0.01$). The thinnest fibers were obtained at 15 kV and 100 Hz, which differ statistically from those obtained at 15 kV and 50 Hz.

For more concentrated PVP solution (Fig. 7B), the differences between the diameters of the fibers obtained using DCV and PV are more explicit. At the 8 kV voltage (red columns), fibers with diameters in the 700–800 nm range were obtained. The PV case resulted in the formation of thicker fibers compared with the DCV (around 100 nm difference). When the DCV value was set at 15 kV (blue columns), fibers with average diameter around 500 nm were produced. The use of PV at 20 Hz resulted in more than a twofold increase in the fiber diameters, which was also observed in the SEM images (Fig. 5B4). Increases in the frequency caused a decrease in the fiber diameter – approximately 600 nm for 50 Hz and 500 nm for 100 Hz (the same as DCV). All statistically significant differences are shown in the plots. Li et al. [37] noticed similar dependencies, but their work was carried out at much higher frequencies (above 1 kHz).

The effect of the solution concentration on the fiber diameter is clearly visible (Fig. 7C) for the PLA mats. The fibers obtained from the 8% solution (green columns) have average diameters in the range of 1000–1800 nm. The thickest fibers were obtained at 50 Hz with the thinnest ones at 20 Hz. The differences in this group are statistically significant ($p < 0.01$ or $p < 0.001$). Electrospinning the 10% solution (pink columns) resulted in the production of fibers with diameters in the range of 1500–1750 nm regardless of the operating mode of the generator or the values of the electrical parameters. There are no statistically significant differences between the fiber diameters in these experiments.

The PLA fibers were much thinner than those obtained by Xie et al. [38] despite the use of PV as well as the same polymer in both cases. This is likely due to the fact that in the work by Xie et al., a polymer melt was used instead of a solution and the impulse frequencies were higher than 1 kHz (100 times greater than in this work).

The bimodal distribution of the PLA fiber diameters can be indirectly confirmed by comparing the diagrams for the diameters of the PVP (Fig. 7A and B) and the PLA fibers (Fig. 7C). The standard deviation from the average fiber diameter for the PVP is around 100–200 nm but is much higher for the PLA at around 500–600 nm. This suggests that the diameters of the PVP fibers are more uniform than the PLA ones. The histograms (Fig. 8) directly confirm the bimodal distribution of the PLA fiber diameters.

3.4. Bead size and concentration

The graphs presented in Fig. 9 show the results for the bead-on-string type structure with the 3.5% PVP solution in terms of their size and concentration in the mats. In each group, the data obtained from the electrospinning process using DCV were compared with those obtained using PV.

For both 8 and 15 kV voltages, beads 2–3 times larger were

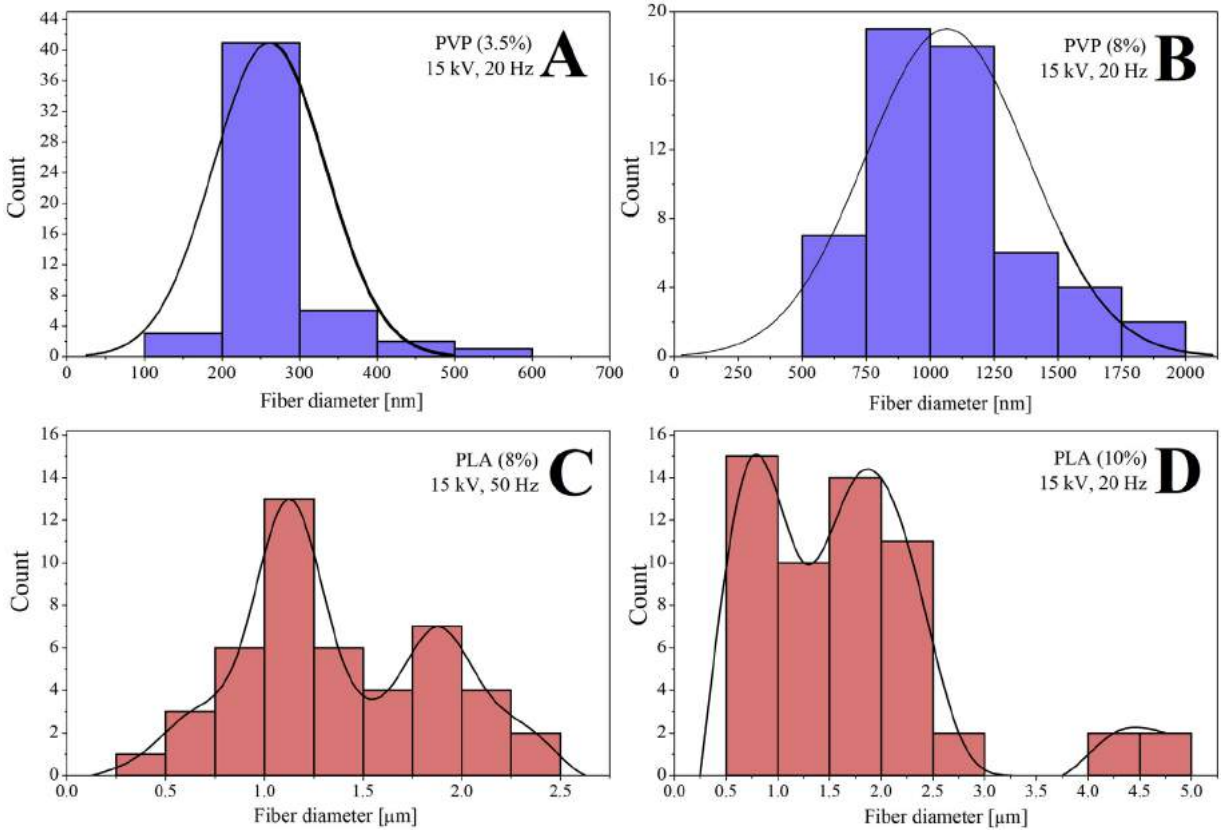

Fig. 8. The distribution of the (A, B) PVP and (C, D) PLA fiber diameters.

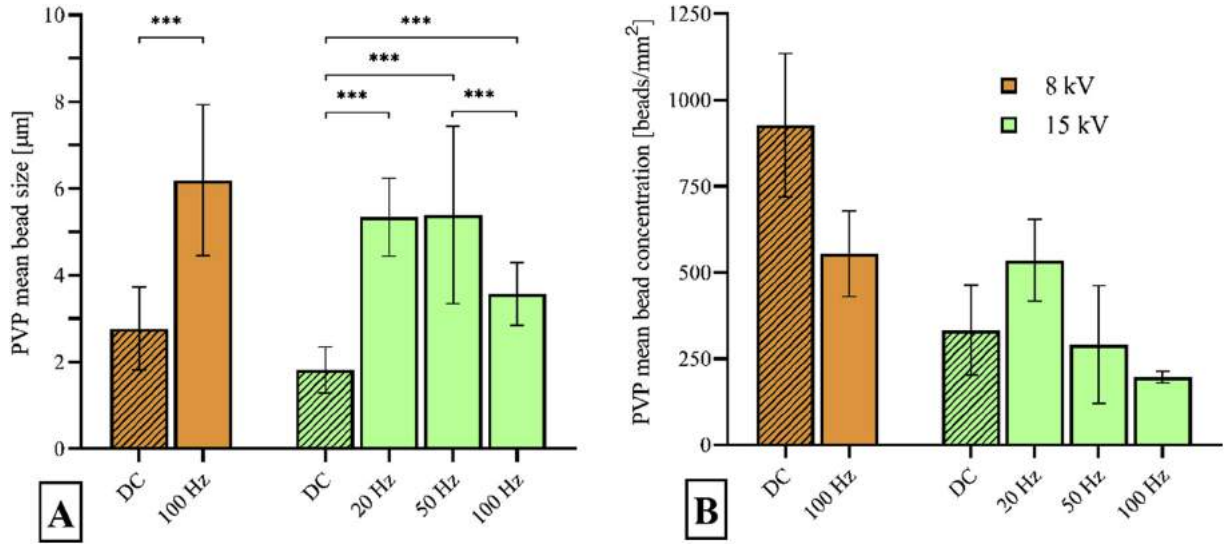

Fig. 9. The (A) size and (B) concentration of beads obtained from the 3.5% PVP solution for DCV and PV.

obtained using PV (Fig. 9A). The bead sizes for DCV were in the range of 2−3 μm and were 4 to 6 μm for PV. In general, larger beads are produced at lower voltages, as previously confirmed in Ref. [29].

It is concluded that at the 8 kV voltage (Fig. 9B), the use of PV causes a twofold decrease in the number of beads per square mm. Comparing Fig. 9A and B suggests that when the voltage is 8 kV, smaller beads are obtained for the DCV than for the PV, but they are more numerous. At 15 kV, this relationship is not observed, and there are in general fewer beads than at 8 kV (as seen in the SEM images from Fig. 5). PV increases the concentration of beads only at a frequency of 20 Hz.

When describing the concentration of the beads, it is impossible to determine the statistical significance of the differences due to an insufficient number of samples.

4. Conclusion

This study examined the differences between the electrospinning process performed with either a direct-current or pulsed electrical voltage supply. The following aspects of the process were considered: the shape of liquid and jet formed at the nozzle tip, the structure of the electrospun fibrous mats in terms of the average fiber diameter, as well as the average bead size (in the bead-on-string type structure) and their concentration.

It was observed that the electric charge delivery (DCV or PV) and the values of the electrical parameters, such as the electric voltage, pulse frequency, and pulse duration, affect whether the electrospinning process is induced. The pulse frequency has a direct impact on the shape of the liquid formed at the outlet of the nozzle and, consequently, on the structure of the obtained product. It is possible to link this shape with the electrospun product to initially predict its structure based on simple observations of the nozzle tip.

Moreover, the use of PV stabilizes the liquid jet shape at the nozzle tip during the process, especially at higher voltage values and low or middle frequency due to a reduction in the number of jets formed at the tip of the outflowing liquid. In several examined cases, the polymer solution turned into a single electrospinning jet while no multi-jets or side passive jets were observed. The fibrous mats obtained in these process variants were homogeneous with smooth fibers, regardless of the type of applied voltage (DCV or PV). The exception is mats obtained for low concentrations of PVP solution which are characterized by a bead-on-string type structure (for both DCV and PV). This confirms that appropriate selections of the electrical process parameters can control the fiber structure, which leads to more desired products (for example, uniform fibers), as neither dripping nor multi-jetting occurs. This study also indicates that depending on the solution concentration and the type of polymer, switching the operating mode of the voltage generator from DCV to PV significantly affects the diameters of the obtained fibers. In addition, a strong effect is seen for the size and number of beads per square millimeter for the lower concentrated solutions.

Based on the experiments conducted, it was found out that electrospinning with PV is possible and, in some cases, may result in more favorable effects than with DCV − process stabilization, better control over fiber diameters and bead sizes, lower power consumption, etc. Providing the exact cause of this phenomenon would require additional, detailed research considering a wide range of changes of all PV parameters (including pulse duration).

Acknowledgements

This project was supported by European Social Fund [POWR.03.02.00-00-1028/17-00] as well as by Nalecz Institute of Biocybernetics and Biomedical Engineering, Polish Academy of Sciences via project number St/1823.

Data availability

The raw and processed data required to reproduce these results are available by contacting the authors.

Authorship statement

All persons who meet authorship criteria are listed as authors, and all authors certify that they have participated sufficiently in the work to take public responsibility for the content, including participation in the concept, design, analysis, writing, or revision of the manuscript. Furthermore, each author certifies that this material or similar material has not been and will not be submitted to or published in any other publication before its appearance in “Materials & Design”.

References

[1] S. Agarwal, J.H. Wendorff, A. Greiner, Use of electrospinning technique for biomedical applications, Polymer 49 (26) (2008) 5603−5621, https://doi.org/

10.1016/j.polymer.2008.09.014.
[2] T.D. Brown, P.D. Dalton, D.W. Hutmacher, Progress in polymer science melt electrospinning today: an opportune time for an emerging polymer process, Prog. Polym. Sci. 56 (2016) 116–166, https://doi.org/10.1016/j.progpolymsci.2016.01.001.
[3] X. Lu, C. Wang, Y. Wei, One-dimensional composite nanomaterials: synthesis by electrospinning and their applications, Small (21) (2009) 2349–2370, https://doi.org/10.1002/smll.200900445.
[4] W.E. Teo, S. Ramakrishna, A review on electrospinning design and nanofibre assemblies, Nanotechnology 17 (2006) R89–R106, https://doi.org/10.1088/0957-4484/17/14/R01.
[5] A. Greiner, J.H. Wendorff, Electrospinning: a fascinating method for the preparation of ultrathin fibers, Angew. Chem. 46 (30) (2007) 5670–5703, https://doi.org/10.1002/anie.200604646.
[6] B.D. Li, Y. Xia, Electrospinning of nanofibers: reinventing the wheel? Adv. Mater. (14) (2004) 1151–1170, https://doi.org/10.1002/adma.200400719.
[7] A. Koski, K. Yim, S. Shivkumar, Effect of molecular weight on fibrous PVA produced by electrospinning, Mater. Lett. 58 (3–4) (2004) 493–497, https://doi.org/10.1016/S0167-577X(03)00532-9.
[8] Y.Y. Zhao, Q.B. Yang, X.F. Lu, C. Wang, Y. Wei, Study on correlation of morphology of electrospun products of polyacrylamide with ultrahigh molecular weight, J. Polym. Sci. B Polym. Phys. 43 (16) (2005) 2190–2195, https://doi.org/10.1002/polb.20506.
[9] J. Zheng, H. Zhang, Z. Zhao, C.C. Han, Construction of hierarchical structures by electrospinning or electrospraying, Polymer 53 (2) (2012) 546–554, https://doi.org/10.1016/j.polymer.2011.12.018.
[10] J. Deitzel, J. Kleinmeyer, D. Harris, N. Beck Tan, The effect of processing variables on the morphology of electrospun nanofibers and textiles, Polymer 42 (1) (2001) 261–272, https://doi.org/10.1016/S0032-3861(00)00250-0.
[11] G. Eda, S. Shivkumar, Bead-to-fiber transition in electrospun polystyrene, J. Appl. Polym. Sci. 106 (1) (2007) 475–487, https://doi.org/10.1002/app.25907.
[12] H. Fong, I. Chun, D.H. Reneker, Beaded nanofibers formed during electrospinning, Polymer 40 (1999) 4585–4592, https://doi.org/10.1016/s0032-3861(99)00068-3.
[13] Q. Yang, Z. Li, Y. Hong, Y. Zhao, S. Qiu, C.E. Wang, Y.E.N. Wei, Influence of solvents on the formation of ultrathin uniform poly (vinyl pyrrolidone) nanofibers, J. Polym. Sci. B Polym. Phys. 42 (20) (2004) 3721–3726, https://doi.org/10.1002/polb.20222.
[14] N. Yuya, I. Kim, W. Kai, K. Byoung-Suhk, Morphology controlled electrospun poly (vinyl pyrrolidone) fibers: effects of organic solvent and relative humidity, Journal of Materials Science and Engineering with Advanced Technology 2 (1) (2010) 97–112.
[15] C. Huang, S. Chen, C. Lai, D.H. Reneker, H. Qiu, Y. Ye, H. Hou, Electrospun polymer nanofibres with small diameters, Nanotechnology 17 (6) (2006) 1558–1563, https://doi.org/10.1088/0957-4484/17/6/004.
[16] T. Isık, M. Demir, Medical waste treatment via waste electrospinning of PS, Fibers and Polymers 19 (4) (2018) 767–774, https://doi.org/10.1007/s12221-018-1037-0.
[17] C. Mit-uppatham, M. Nithitanakul, P. Supaphol, Ultrafine electrospun polyamide-6 fibers: effect of solution conditions on morphology and average fiber diameter, Macromol. Chem. Phys. 205 (17) (2004) 2327–2338, https://doi.org/10.1002/macp.200400225.
[18] C.L. Casper, J.S. Stephens, N.G. Tassi, D.B. Chase, J.F. Rabolt, Controlling surface morphology of electrospun polystyrene fibers: effect of humidity and molecular weight in the electrospinning process, Macromolecules 37 (2) (2004) 573–578, https://doi.org/10.1021/ma0351975.
[19] S. Tripatanasuwan, Z. Zhong, D.H. Reneker, Effect of evaporation and solidification of the charged jet in electrospinning of poly(ethylene oxide) aqueous solution, Polymer 48 (19) (2007) 5742–5746, https://doi.org/10.1016/j.polymer.2007.07.045.
[20] X. Yuan, Y. Zhang, C. Dong, J. Sheng, Morphology of ultrafine polysulfone fibers prepared by electrospinning, Polym. Int. 53 (11) (2004) 1704–1710, https://doi.org/10.1002/pi.1538.
[21] Y. Yang, Z. Jia, Q. Li, Z. Guan, Experimental investigation of the governing parameters in the electrospinning of polyethylene oxide solution, IEEE Trans. Dielectr. Electr. Insul. 13 (3) (2006) 580–584, https://doi.org/10.1109/TDEI.2006.1657971.
[22] M. Jin, D.-G. Yu, X. Wang, C.F. Geraldes, G.R. Williams, S.W. Bligh, Electrospun contrast-agent-loaded fibers for colon-targeted MRI, Advanced Healthcare Materials 5 (8) (2016) 977–985, https://doi.org/10.1002/adhm.201500872.
[23] H.-F. Wen, C. Yang, D.-G. Yu, X.-Y. Li, D.-F. Zhang, Electrospun zein nanoribbons for treatment of lead-contained wastewater, Chem. Eng. J. 290 (2016) 263–272, https://doi.org/10.1016/j.cej.2016.01.055.
[24] A. Khalf, S.V. Madihally, Modeling the permeability of multiaxial electrospun poly(ε-caprolactone)-gelatin hybrid fibers for controlled doxycycline release, Mater. Sci. Eng. C 76 (2017) 161–170, https://doi.org/10.1016/j.msec.2017.03.093.
[25] A. Khalf, S.V. Madihally, Recent advances in multiaxial electrospinning for drug delivery, Eur. J. Pharm. Biopharm. 112 (2017) 1–17, https://doi.org/10.1016/j.ejpb.2016.11.010.
[26] D.-G. Yu, C. Yang, M. Jin, G.R. Williams, H. Zou, X. Wang, S.W. Annie Bligh, Medicated Janus fibers fabricated using a Teflon-coated side-by-side spinneret, Colloids Surf. B: Biointerfaces 138 (2016) 110–116, https://doi.org/10.1016/j.colsurfb.2015.11.055.
[27] C.S. Ki, D.H. Baek, K.D. Gang, K.H. Lee, I.C. Um, Y.H. Park, Characterization of gelatin nanofiber prepared from gelatin–formic acid solution, Polymer 46 (14) (2005) 5094–5102, https://doi.org/10.1016/j.polymer.2005.04.040.
[28] M. Demir, I. Yilgor, E. Yilgor, B. Erman, Electrospinning of polyurethane fibers, Polymer 43 (11) (2002) 3303–3309, https://doi.org/10.1016/S0032-3861(02)00136-2.
[29] P. Korycka, A. Mirek, K. Kramek-Romanowska, M. Grzeczkowicz, D. Lewińska, Effect of electrospinning process variables on the size of polymer fibers and bead-on-string structures established with a 2^3 factorial design, Beilstein Journal of Nanotechnology 9 (2018) 2466–2478, https://doi.org/10.3762/bjnano.9.231.
[30] R. Baba, C.J. Angammana, S.H. Jayaram, L.T. Lim, Electrospinning of alginate and poly-ethylene oxide blends using pulsed electric fields to fabricate chopped nanofibres, in: Proc. ESA Annual Meeting on Electrostatics 2010, 2010 (Paper H2).
[31] Shi Zhou, Fang Wan, Chen Yu, Liu, The relationships between process parameters and polymeric nanofibers fabricated using a modified coaxial electrospinning, Nanomaterials 9 (6) (2019) 843, https://doi.org/10.3390/nano9060843.
[32] D.H. Reneker, I. Chun, Nanometre diameter fibres of polymer, produced by electrospinning, Nanotechnology 7 (3) (1996) 216–223, https://doi.org/10.1088/0957-4484/7/3/009.
[33] X. Zong, K. Kim, D. Fang, S. Ran, B.S. Hsiao, B. Chu, Structure and process relationship of electrospun bioabsorbable nanofiber membranes, Polymer 43 (16) (2002) 4403–4412, https://doi.org/10.1016/S0032-3861(02)00275-6.
[34] O.S. Yördem, M. Papila, Y.Z. Menceloğlu, Effects of electrospinning parameters on polyacrylonitrile nanofiber diameter: an investigation by response surface methodology, Mater. Des. 29 (1) (2008) 34–44, https://doi.org/10.1016/j.matdes.2006.12.013.
[35] D. Lewińska, S. Rosiński, A. Weryński, Influence of process conditions during impulsed electrostatic droplet formation on size distribution of hydrogel beads, Artificial Cells, Blood Substitutes, and Biotechnology 32 (1) (2004) 41–53, https://doi.org/10.1081/bio-120028667.
[36] U. Prüsse, L. Bilancetti, M. Bučko, B. Bugarski, J. Bukowski, P. Gemeiner, D. Lewińska, …, K.-D. Vorlop, Comparison of different technologies for alginate beads production, Chem. Pap. 62 (4) (2008), https://doi.org/10.2478/s11696-008-0035-x.
[37] K. Li, Y. Wang, G. Xie, J. Kang, H. He, K. Wang, Y. Liu, Solution electrospinning with a pulsed electric field, J. Appl. Polym. Sci. 135 (15) (2017), 46130, https://doi.org/10.1002/app.46130.
[38] G. Xie, Y. Wang, X. Han, Y. Gong, J. Wang, J. Zhang, Y. Liu, Pulsed electric fields on poly-L-(lactic acid) melt electrospun fibers, Ind. Eng. Chem. Res. 55 (26) (2016) 7116–7123, https://doi.org/10.1021/acs.iecr.6b00958.
[39] R. Kessick, J. Fenn, G. Tepper, The use of AC potentials in electrospraying and electrospinning processes, Polymer 45 (9) (2004) 2981–2984, https://doi.org/10.1016/j.polymer.2004.02.056.
[40] Y.T. Aliyev, B.M. Dabynov, D.U. Bodykov, U.S. Musabekov, Z.A. Mansurov, Development and use of a modified pulse electrospinning setup for producing short fibers, J. Eng. Phys. Thermophys. 89 (1) (2016) 265–271, https://doi.org/10.1007/s10891-016-1374-z.
[41] J. Torfifard, E. Norian, R. Ahmadi, M.T. Ahmadi, Polymer concentration effect on nanofiber growth using pulsed electrospinning, iMedPub Journals 4 (2:14) (2018) 1–7, https://doi.org/10.4172/2471-9935.100041.
[42] Z.-P. Liu, Y.-Y. Zhang, D.-G. Yu, D. Wu, H.-L. Li, Fabrication of sustained-release zein nanoparticles via modified coaxial electrospraying, Chem. Eng. J. 334 (2018) 807–816, https://doi.org/10.1016/j.cej.2017.10.098.
[43] Q. Wang, D.-G. Yu, L.-L. Zhang, X.-K. Liu, Y.-C. Deng, M. Zhao, Electrospun hypromellose-based hydrophilic composites for rapid dissolution of poorly water-soluble drug, Carbohydr. Polym. 174 (2017) 617–625, https://doi.org/10.1016/j.carbpol.2017.06.075.
[44] D. Poncelet, R.J. Neufeld, M.F.A. Goosen, B. Burgarski, V. Babak, Formation of microgel beads by electric dispersion of polymer solutions, AICHE J. 45 (9) (1999) 2018–2023, https://doi.org/10.1002/aic.690450918.

PUBLICATION 2

Formation of disaggregated polymer microspheres by a novel method combining pulsed voltage electrospray and wet phase inversion techniques

Mirek, A., Grzeczkowicz, M., Lamboux, C., Sayegh, S., Bechelany, M., Lewińska, D.
Colloids and Surfaces A: Physicochemical and Engineering Aspects. 648, 129246 (2022).
DOI: 10.1016/j.colsurfa.2022.129246

Colloids and Surfaces A: Physicochemical and Engineering Aspects 648 (2022) 129246

Contents lists available at ScienceDirect

Colloids and Surfaces A: Physicochemical and Engineering Aspects

journal homepage: www.elsevier.com/locate/colsurfa

Formation of disaggregated polymer microspheres by a novel method combining pulsed voltage electrospray and wet phase inversion techniques

Adam Mirek [a,b,*], Marcin Grzeczkowicz [a], Cassandre Lamboux [b], Syreina Sayegh [b], Mikhael Bechelany [b], Dorota Lewińska [a]

[a] Nalecz Institute of Biocybernetics and Biomedical Engineering, Polish Academy of Sciences, 02–109 Warsaw, Poland
[b] Institut Européen des Membranes, IEM, UMR-5635, University of Montpellier, CNRS, ENSCM, 34095 Montpellier CEDEX 5, France

GRAPHICAL ABSTRACT

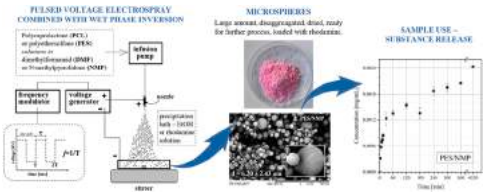

ARTICLE INFO

Keywords:
Microspheres
Electrospray
Pulsed voltage
Wet phase inversion
Polymer

ABSTRACT

Polymer microspheres with controlled sizes have attracted interest due to their potential use in medical field. Therefore it is of great importance to be able to produce a large number of disaggregated microspheres with a narrow diameter distribution. This work describes the successful elaboration of the method combining electrospray and wet phase inversion for the manufacturing of such polymer microspheres with mean diameters of 2 – 15 μm. Their recovery and drying are easy and they can be directly applied afterwards. The method is universal enough to produce microspheres from various polymers (polycaprolactone, polyethersulfone) and different solvents (dimethylformamide, N-methylpyrrolidone). It was noticed on the basis of microscopic images and using the nitrogen adsorption–desorption method that the specific surface of the microspheres differs depending on the polymer and solvent used. The work introduces additional parameters resulting from the use of pulsed voltage in the electrospray (pulse frequency f and duration τ) which results in better process control. As an example of the use of microspheres as drug carriers, they were loaded with rhodamine and its release was tested. Such microspheres could be dispersed in polymer solution and used in extrusion-based techniques (electrospinning, 3D printing) to form novel complex drug delivery systems.

1. Introduction

Due to their spherical shape and small size, polymer microspheres are characterized by a large specific surface and as a consequence they have a number of unique properties, for example adsorption, dispersion, mass transfer, permeability, and adhesion behaviors [1–3]. The size, shape and porosity of the polymer microspheres can be easily controlled by appropriate selection of process for their production and its conditions. The sphericity of such particles reduces their tendency to aggregate compared to non-spherical particles [4]. The use of polymers as the

* Corresponding author at: Nalecz Institute of Biocybernetics and Biomedical Engineering, Polish Academy of Sciences, 02–109 Warsaw, Poland.
E-mail address: amirek@ibib.waw.pl (A. Mirek).

https://doi.org/10.1016/j.colsurfa.2022.129246
Received 21 March 2022; Received in revised form 12 May 2022; Accepted 13 May 2022
Available online 21 May 2022

material for microspheres makes it possible to control their physico-chemical properties and to modify their surface.

The unique features of polymer microspheres compared to other polymer materials with a different geometry results in a large field of their applications. They are used in various areas: adsorption [1,5], catalysis [6,7], separation [8,9], microreactors [10,11], and temperature monitoring [12]. They are particularly common in medicine and pharmacy as tissue regeneration scaffolds [13], biosensors [14], vaccines [15], and the most common – controlled drug delivery systems [16]. Research in this area has been carried out for several years, still yielding many interesting results [16,17]. Various substances can be delivered in this way such as anti-cancer drugs [18], antibiotics [19], growth factors [20], imaging markers [21], anti-inflammatory drugs [22], and others [23,24]. Sometimes, combinations of different therapeutic scopes can be used in one system [25,26].

In the case of polymer microspheres used as drug delivery systems, the most important parameters that determine their potential use are their diameters, monodispersity and enhanced specific surface. For example, microspheres with a diameter of 1 – 5 μm can be used to target specific cells, porous ones with a diameter of 5 – 20 μm are effective as drug delivery vehicles for lungs, those with a diameter of 10 – 20 μm can be targeted at tumor tissue by chemoembolization and microspheres of 10 – 100 μm in diameter are small enough to be injected with a syringe and large enough to avoid removal by phagocytic cells, so they can serve as intramuscular or subcutaneous small-scale drug containers [27]. Microspheres have many properties that can be controlled by the method of their preparation and the respective process conditions.

In recent years, a lot of ideas have arisen on how such microspheres can be obtained. All methods share the same general principle – the polymer solution has to be dispersed into microdroplets and then the polymer droplets have to be solidified to obtain microspheres. The dispersion of the microsphere-forming solution may be based on emulsification, extrusion or microfluidics [28]. The final formation of microspheres can take place by polycondensation, polymerization, coacervation, ionotropic gelation [16], and phase inversion by solvent evaporation or precipitation [29]. The classic methods commonly used today are shown schematically in Fig. 1.

Among the mentioned methods of microdroplets formation, one of the most interesting is the extrusion-based electrohydrodynamic technique. This method was developed by Poncelet et al. [30], it is easy to apply and gives satisfying results. This process involves pressing the polymer solution through a metal nozzle to which the electric voltage is applied. As soon as the electrostatic charge repulsion on the surface of the meniscus overcomes the forces of the surface tension, the jet of liquid is interrupted and the droplet breaks off and falls. Eventually, the microspheres can be formed using various solidification techniques. Shang et al. [31] prepared ionically crosslinked drug-loaded chitin microspheres of diameter of 400–500 μm. They used the aqueous Fe^{3+} solution to solidify microspheres and direct current voltage (DCV) to form microdroplets. However, the use of pulsed voltage (PV), developed by our team, enables precise control of the size of the generated droplets, which is its advantage over DCV [32]. The electrohydrodynamic droplet formation with PV was also used to form alginate microspheres that were solidified in a calcium ion bath in the work of Prüsse et al. [33]. This method was compared to others and it was found to perform best with regard to the size distribution and the shape of the microspheres. The use of PV also makes it possible to avoid too large (or too small) droplets that may appear in the conventional process, apart from the droplets of the desired size (the so-called satellite fraction). Sometimes falling of such large droplets (800 ± 100 μm) into the gelation bath can cause flattening and deformation of the microspheres [34].

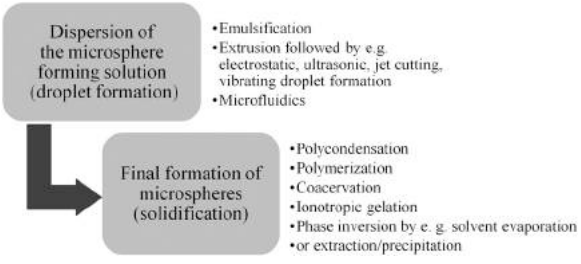

Fig. 1. Methods of producing polymer microspheres and microcapsules.

Another method for the manufacturing of smaller microspheres is the combination of extrusion-based solution dispersion in the form of electrospray followed by the solvent evaporation to finally form the solid particles [35]. Electrospray is formed when a much higher voltage is applied in an electrohydrodynamic droplet formation system. Then, electrostatic atomization of the liquid stream flowing from the nozzle occurs, resulting in formation of uniform droplets of sizes between tens of nanometers to tens of micrometers which are deposited on a grounded collector (usually aluminum plate) [36]. Due to this, the method is widely used on a laboratory scale, as well as due to good particle size control, low cost, easy and adaptable methodology, low residue generation, and high substance encapsulation efficiency. For example, Tang et al. used the electrospray method to successfully obtain poly (lactic-co-glycolic acid) (PLGA) microspheres with magnetic response and controlled release of vincristine and doxorubicin. The obtained particles had a two layer structure and diameter distribution of 0.03–1.81 μm. Under the action of external magnetic field they showed a long term sustained release of drugs in the osteosarcoma area [37]. Similarly, the method of polymer solution electrospraying on a grounded collector in the form of aluminum foil was used by Yao et al. who manufactured the microspheres from an emulsion of PLGA in chloroform and Congo red/albumin in water. The result of their studies was microspheres with a size of 6 – 10 μm which showed the properties of substance release through the degradation of the polymer matrix [38].

Unfortunately, in most cases of electrohydrodynamic methods, the collector for microsphere solidification takes the form of a flat aluminum foil. As a result, the microspheres are collected in layers, they form aggregates of different sizes and adhere to the collector surface. It makes them impossible to be used for example as additives for various complex drug delivery systems manufactured via extrusion-based techniques – microencapsulation, electrospinning or 3D printing). Such microsphere aggregates cannot be dispersed in polymer solution and then pressed through a narrow nozzle in these methods due to their size. Moreover, the process efficiency in the case described above is very low because the process time is limited by the available collector area. The solution to this problem could be to use a different collector – a well-stirred bath filled with a non-solvent (A) of the polymer (B). The used bath filling must be miscible with the solvent (C) used to prepare the microsphere forming polymer solution. Then, when the microdroplet of the solution (B+C) falls into the bath, according to the Gibbs phase rule, there is a transition from the three-component single-phase system to the two-phase system. The solvent (C) is washed away due to the mixing with non-solvent (A), the polymer (B) is precipitated, and solidified microspheres are formed. The mechanism of the wet phase inversion process is shown schematically in the ternary plot in Fig. 2.

Solidification of microspheres from synthetic polymers by this method allows to obtain a porous structure on their surface. The quantity and size of pores can be controlled by appropriate selection of the polymer concentration, composition of the precipitation bath, but also by adding pore precursors to the polymer solution [39]. It is important that the bath is very well mixed as it prevents the droplets from aggregating until they harden completely. The wet phase inversion technique makes it possible to obtain larger amounts of microspheres ready for further use, which is the starting point for the research presented in this article.

Hence, the aim of the work was to develop a method of combined electrospray and wet phase inversion techniques for manufacturing disaggregated polymer microspheres with a narrow size range (5 – 15

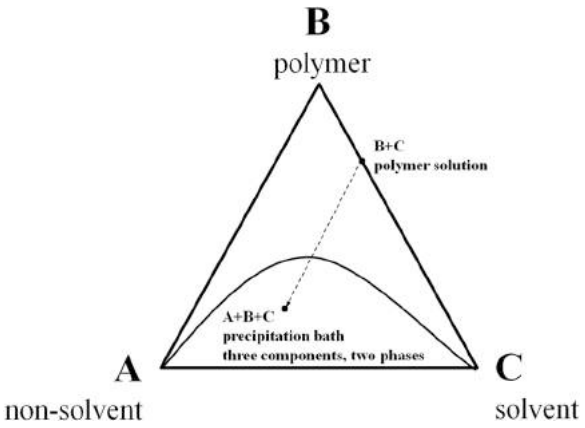

Fig. 2. General exemplary Gibbs triangle showing the mechanism of solidification of microspheres by wet phase inversion in a non-solvent bath.

micrometers). Such microspheres would be small enough to be easily pressed through a narrow nozzle (usually several tens of micrometers in diameter) as a dispersion in polymer solution in extrusion-based techniques such as microencapsulation, electrospinning, 3D (bio)printing. These complex structures would be a promising material to be used as novel drug delivery systems. The additional assumption in our work was that the elaborated method was universal enough to be able to produce microspheres from various polymers of different physicochemical properties (including chemical affinity). Therefore, two polymers were selected for the study – biodegradable polycaprolactone (PCL) and non-biodegradable polyethersulfone (PES). Two types of solvents were used – dimethylformamide (DMF) and N-methylpyrrolidone (NMP). Ethanol was used as filling in the precipitation bath. Investigations were carried out with the use of two types of electric voltage – the one with the electric charge supplied continuously (direct current voltage) and another with the charge in the form of pulses of a specific frequency f and duration τ (pulsed voltage). The influence of different process parameters (the electrical parameters, the concentration of the polymer, the type of polymer and solvent) on the structure of the obtained microspheres was determined. The influence of the applied polymer/solvent solution composition (PCL/DMF, PCL/NMP, PES/DMF, PES/NMP) on the size of the specific surface area of the microspheres was investigated. Additionally, all types of microspheres were loaded with rhodamine (marker) and the release of the marker was investigated in dependence on the polymer/solvent composition.

2. Materials & methods

2.1. Materials

Polycaprolactone (PCL, M_w = 70 kDa, CAS Number: 24980–41–4) was purchased from Scientific Polymer Products, USA and polyethersulfone (PES, M_w = 42 kDa, Ultrason E2020) from BASF, Germany. Dimethylformamide (99%, DMF, Chempur, Poland, CAS Number: 68–12–2) and N-methyl-2-pyrrolidone (98%, NMP, Chempur, Poland, CAS Number: 872–50–4) were used as solvents for the polymers. Ethanol (95%, EtOH, Polmos, Poland) was used as a non-solvent to induce phase separation in a bath. Rhodamine 640 perchlorate (M_w = 591.05 Da, Exciton, USA, CAS Number: 72102–91–1) was used as a marker.

2.2. Experimental setup

The microspheres were manufactured using both direct-current voltage (DCV) and pulsed voltage (PV) and the results were compared. The process was carried out using the setup shown schematically in Fig. 3. Polymer solution was placed in a syringe and pressed through a drain to a stainless steel nozzle (inner diameter 0.445 mm) using an

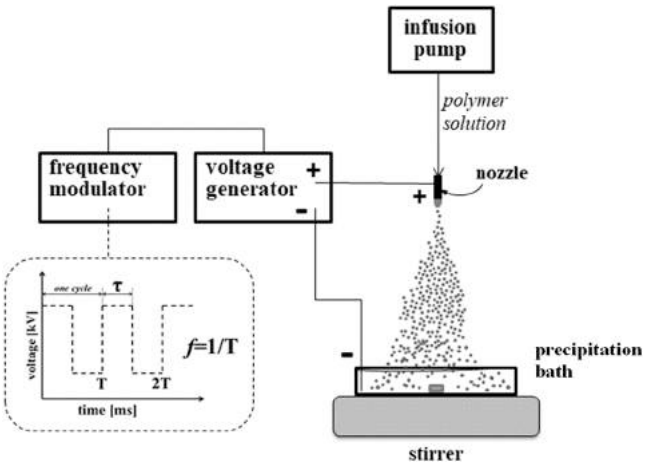

Fig. 3. Scheme of the process setup with an operation diagram of the PV supply (dotted line on the graph).

infusion pump (Alaris Asena GH). The nozzle was connected to a custom-built high voltage generator of direct-current voltage complemented by a frequency modulator providing voltage impulses. Droplets were formed at the nozzle tip, detach and fall to the grounded precipitation bath below. A Petri dish with a diameter of 7 cm and a height of 1.5 cm fully filled with ethanol was used as the bath. The distance between the nozzle tip and the surface of the bath liquid was set as 5 cm.

Working in a PV mode the generator can supply a high, rectangular wave voltage to the nozzle with the applied voltage value U (in the range 0 – 25 kV, stepwise), frequency of impulse application f (in the range 1 – 100 Hz, stepwise), and duration time of the voltage impulse τ (in the range 1 – 9 ms, stepwise). The time domain waveform signal of the PV supply is schematically presented in Fig. 3. The same set-up was used for DC voltage operation (without using a frequency modulator).

2.3. Preparation of microspheres

The following polymer solutions were used to form microspheres:

- 4, 6, 10, 15, 18, 20% PCL in DMF,
- 15% PCL in NMP,
- 15% PES in DMF,
- 15% PES in NMP.

The values of the electrical parameters investigated in the study were U = 8 kV for DCV and U = 8 kV and 11 kV, f = 20 – 80 Hz, τ= 2 – 8 ms for PV. The polymer solution was delivered to the nozzle at a flow rate of 0.34 mL/h. The resulting product was collected in the stirred ethanol bath for around 90 min. After the precipitation process the bath content was transferred to a falcon and centrifuged. Excess ethanol was poured off above the sedimented microspheres. The microspheres were dried at room temperature for several days. All experiments were carried out at a temperature of 25 °C and a humidity not exceeding 40%.

2.4. Characterization of the microspheres

The meniscus of the polymer solution formed at the nozzle tip during the process was recorded using a monochrome CCD camera. A frame was cut from each film ten minutes after the experiment began.

The morphology of the microsphere surfaces was examined on the basis of pictures received by scanning electron microscopy (SEM, Hitachi TM-1000). To prepare the sample for SEM, 100 microliters of microsphere suspension in ethanol were placed directly on the carbon tape on the SEM support. After the ethanol had completely evaporated,

the samples were coated with a thin layer (10 nm) of gold and subjected to SEM. The diameters of 200–300 randomly selected microspheres (from several images of one sample) were measured and their mean values and standard deviation were calculated using Statistica software. In order to check the repeatability of the method, several batches of microspheres were made at the same conditions and microsphere diameters were measured. All the graphs were made using GraphPad Prism software.

Fourier transform infrared spectroscopy (FTIR) was used to determine the chemical structure of the microspheres. The FTIR spectra of each sample was recorded using the NEXUS instrument equipped with an attenuated total reflection (ATR) accessory in the frequency range of 600–4000 cm^{-1} with an average of 64 scans at 2 cm^{-1} resolution. The crystalline phase of the materials was analyzed by X-ray diffraction (XRD), using a PANAlytical Xpert-PRO diffractometer equipped with an X′celerator detector using Ni-filtered Cu-radiation (l = 1.54 A). The scan step size was fixed to 0.0167°/step and the time per step was 55.25 s/step. The specific surface area of the microspheres was determined from BET nitrogen adsorption–desorption isotherms at liquid nitrogen temperature using Micromeritics ASAP 2010 equipment (degassing conditions: room temperature – 24 h).

2.5. Immobilization of rhodamine in microspheres

The possibility of using microspheres as carriers of biologically active substances, in this case the marker – rhodamine, was investigated. The marker-loaded microspheres were prepared directly from a polymer solution with the addition of rhodamine. For this purpose, the method of producing microspheres described above with minor modifications was used. At the stage of preparation of the polymer solutions (concentration 15%), rhodamine was also added to them, so that its concentration was 0.1 mg/mL (resulting microspheres: PCL/DMF+Rod, PCL/NMP+Rod, PES/DMF+Rod and PES/NMP+Rod). To avoid the diffusion of rhodamine from the microsphere-forming solution to the precipitation bath, a 0.1 mg/mL solution of rhodamine in ethanol was used as a bath instead of pure ethanol. Then the electrospray/wet phase inversion process was carried out. The resulting suspensions were centrifuged, the supernate was collected, and the microspheres were dried.

2.6. Rhodamine release tests

For the rhodamine release tests, 70 mg of each type of marker-loaded microspheres (PCL/DMF+Rod, PCL/NMP+Rod, PES/DMF+Rod and PES/NMP+Rod) were weighed, placed in test tubes which were then filled with 5 mL of pure ethanol each. The suspensions were stirred to remove excess rhodamine from the outer surface of the materials and centrifuged after 2 min. The washed microspheres were then suspended in 3.5 mL fresh pure ethanol each. The suspensions in the test tubes were mixed, and at specified time intervals, they were centrifuged and the absorbance of the rhodamine solution was measured spectrophotometrically (light wavelength: 574 nm). The experiment results are presented in the graphs showing the change of the released rhodamine concentration profile over time.

2.7. Statistical analysis

The normality of the distribution of the measured diameters of microspheres in all samples was tested using the graphical method of the normality plots complemented by the Shapiro-Wilk test. Due to the high sample sizes, the mean diameter and median for individual samples had almost the same value, therefore the mean diameter was used as a parameter characterizing the microspheres. Since in most cases the distributions were not normal, the statistical differences between the mean diameters of microspheres obtained in different sets of experiments were determined using the non-parametric Kruskal-Wallis one-way analysis of variance test on ranks (instead of the parametric ANOVA test) followed by post-hoc test for multiple comparisons. The significance level (α) was set at 0.05 and the probability of data was considered statistically significant for p-values < 0.05. The results were marked on charts in the form of asterisks: (*) for $p < 0.05$, (**) for $p < 0.01$ and (***) for $p < 0.001$ or (ns) when the differences were non-significant. All the calculations were performed with Statistica software.

3. Results & discussion

The most important result of the described research was a successful elaboration of an electrostatic method for manufacturing microspheres in the form of a powder in every case (PCL/DMF, PCL/NMP, PES/DMF, PES/NMP). Fig. 4A shows a macroscopic image of dried PCL/DMF microspheres ready for further use and characterization. Moreover, it was shown that such microspheres can be used, for example, as substance carriers. Fig. 4B shows dried rhodamine-loaded microspheres. The elaborated method was proven reproducible – the diameters of the microspheres formed at the same conditions in different batches (freshly prepared solution, another day) have similar values which do not differ statistically significantly (Table 1.).

3.1. Direct-current voltage electrospray

The influence of the concentration of the PCL solution (4 – 20%) on the geometric shape of the liquid at the nozzle tip as well as on the shape and diameter of the microspheres obtained in the electrospray process using DCV with a precipitation bath was investigated.

Recordings showing the solution shape at the nozzle tip during the process were compared to determine the above-mentioned effect. Frames from the films are shown in Fig. 5. In all cases, it can be seen that the solution takes an elongated spike-like shape. During the process, the liquid at the nozzle tip vibrated vertically, causing the polymer droplets to break up in the form of a spray of the tip of the jet. The liquid vibrations are visible in the photos in the form of striped blur. For more concentrated solutions (15% and 20%) it can be seen that the liquid drips up on the outside of the nozzle (Fig. 5D and E).

Fig. 5 also features the SEM images of the electrosprayed microspheres manufactured from all the experiments with DCV. These images illustrate that the solution concentration has a great impact on the obtained product. For example the polymer non-spherical artifacts can be formed and their quantity is reduced as the polymer concentration increases. Moreover, the higher the concentration of the polymer, the more spheroidal the microparticle shape. Additionally, it is evident that the increase in polymer concentration causes an increase in the diameter of the microspheres, which is also confirmed by the measurements presented in the plot in Fig. 6 below.

The plot in Fig. 6 shows the average diameters of the obtained microspheres depending on the polymer concentration. The lower curve (square points) shows the basic fraction of microspheres obtained in

Fig. 4. (A) dried PCL/DMF microspheres in the form of a powder without any addition, **(B)** dried rhodamine-loaded PES/NMP microsphere powder.

Table 1
The microsphere average diameter and standard deviation obtained in different batched from 15% polymer solution: PCL/DMF [11 kV, 40 Hz, 4 ms], PCL/NMP [11 kV, 40 Hz, 4 ms], PES/DMF [8 kV, 60 Hz, 6 ms], PES/NMP [8 kV, 60 Hz, 6 ms].

	Average diameter ± standard deviation [μm]			
	PCL/DMF	PCL/NMP	PES/DMF	PES/NMP
Batch 1	14.08 ± 5.15	13.54 ± 5.47	8.39 ± 3.68	6.75 ± 3.52
Batch 2	14.61 ± 5.81	12.83 ± 4.25	8.30 ± 2.79	5.34 ± 1.81
Batch 3	13.89 ± 7.38	14.35 ± 3.42	8.51 ± 2.70	6.89 ± 2.75
Batch 4	13.63 ± 4.89	–	9.33 ± 2.73	5.88 ± 1.67

each case. It confirms the increase in the diameter of the microspheres with the increase of the polymer concentration. The average diameter of the microspheres in the basic fraction is less than 20 micrometers. However, in some cases (for concentrations of 5%, 10% and 15%), an additional fraction (triangular points) of much larger microspheres is also obtained, with sizes even exceeding 500 micrometers. The SEM images showing these fractions are presented in Fig. 6. The extra fraction in the case of the 6% solution has irregularly shaped particles, which cannot be considered as spheres. With increasing polymer concentration, the spheroidicity of the particles increases, at 15% they take the shape of slightly flattened spheres.

3.2. *Use of pulsed voltage to eliminate the extra fraction of large microspheres*

The SEM photos in Fig. 7A-C show that the use of pulsed voltage can eliminate the formation of an extra fraction of large microspheres for the solutions of the polymer concentration less than 20%. Such solutions were selected for the study, because their use in the case of DCV led to obtaining two fractions of microspheres – small (1 – 17 μm) and large (150 – 850 μm). Histograms presenting the distribution of the measured diameters of the microspheres in the samples were placed under the photos (Fig. 7).

Fig. 7 A shows a sphere of the extra fraction surrounded by multiple microspheres of the basic fraction as well as the histogram that confirms the distribution of microsphere diameters is bimodal in this sample – the basic fraction is within 1 – 17 μm, the extra fraction is an order of magnitude larger, its range is 150 – 850 μm. Among the microspheres shown in the photos in Fig. 7B and C, no large microspheres of the additional fraction are observed. This is also confirmed by the

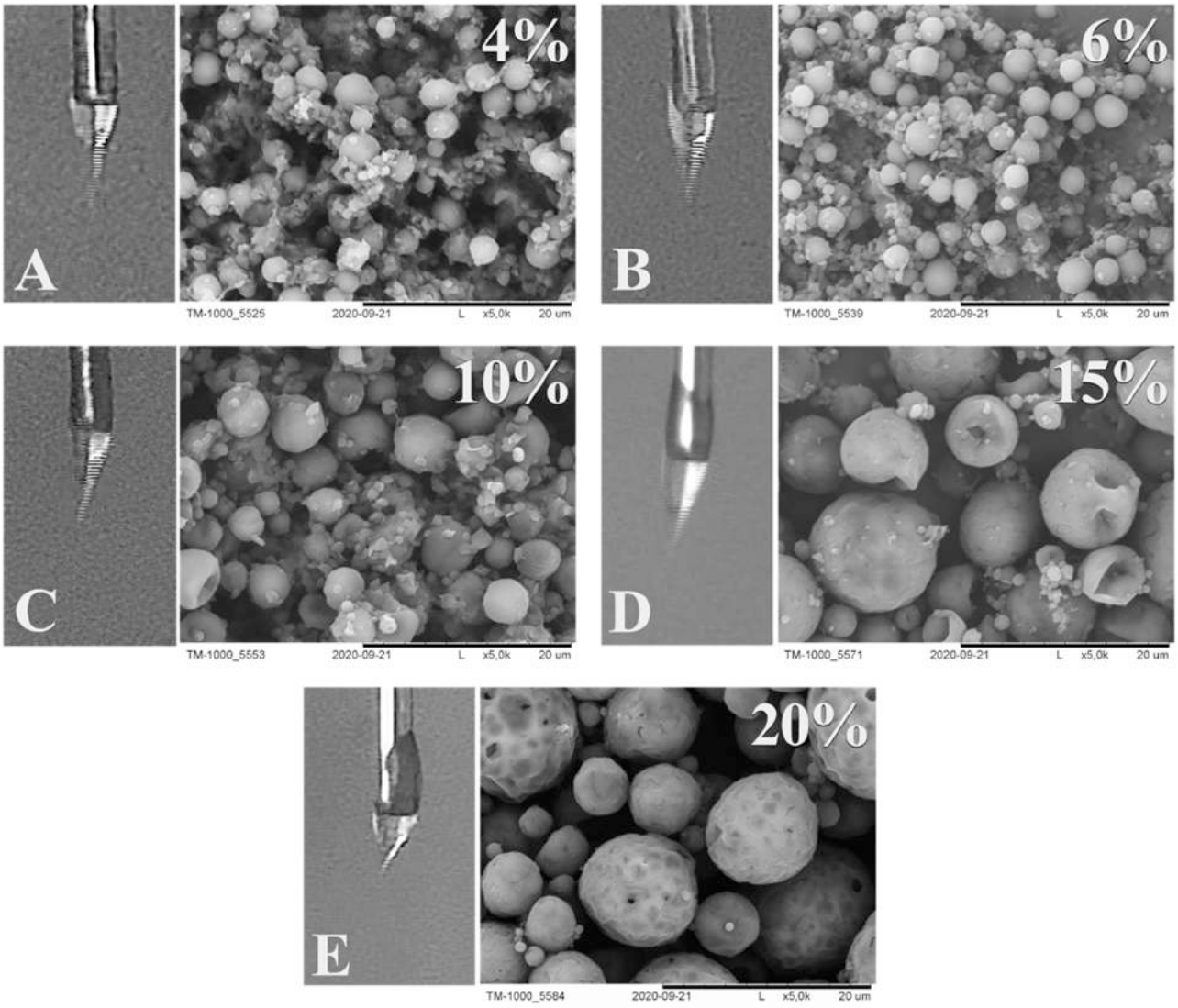

Fig. 5. Liquid cone and microdroplet jet formation at the tip of the nozzle during electrospray process under DCV of 8 kV with the PCL solutions of different concentrations: **(A)** 4%, **(B)** 6%, **(C)** 10%, **(D)** 15%, and **(E)** 20%. Scanning electron microscope images of the PCL microspheres obtained from the process with the mentioned solutions.

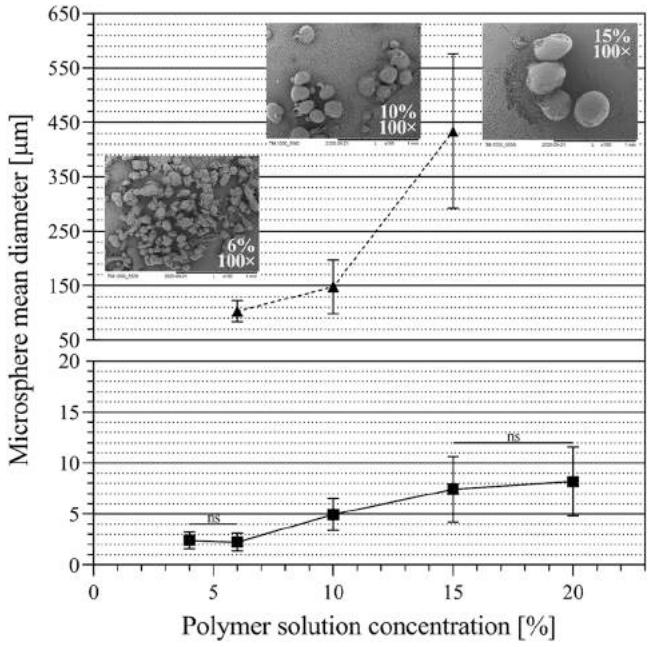

Fig. 6. The relationship between the concentration of the PCL solution and the diameter of the microspheres obtained in the electrospray process (squares). In some cases, two microsphere fractions (marked with a triangle) are visible. The SEM pictures show these fractions.

histograms showing the unimodal distribution of the diameters of the measured microspheres, and in both cases their range is 0–20 µm. These pictures show microspheres obtained using PV (Fig. 7E and F).

On the basis of the graphs presented in Fig. 8A, which shows the mean diameters of the microspheres for the above-described conditions for the polymer solution concentration of 15%, it can be seen that properly selected PV conditions (U, f, τ) do not significantly change the diameter of the microspheres. In the case of DCV, the microbead mean diameter was 7.44 ± 3.22 µm, which is smaller than the mean diameter obtained for PV (8.72 ± 3.10 µm for 70 Hz, 8 ms and 8.73 ± 4.12 µm for 50 Hz, 9 ms), but only in the first of these cases the difference is significant statistically, but yet at a low confidence level.

In the previous paragraph it was mentioned that the PV conditions must be properly selected. The crucial parameter that characterizes the PV is the effective voltage U_{eff}. For a PV of amplitude U, impulse frequency f, duration τ and a period of one cycle T (see the operational diagram in (Fig. 3) U_{eff} is specified by the Eq. (1):

$$U_{eff} = \sqrt{\tau/T} \quad \bullet \quad U = \sqrt{\tau \bullet f} \bullet U \tag{1}$$

Thus, effective voltage is always lower than the voltage U used in the case of DCV so a smaller total amount of electric charge is supplied to the nozzle.

The above remark explains why Fig. 7D shows a sphere belonging to the extra fraction of large spheres even though the sample was made with PV. This photo presents microspheres electrosprayed with the voltage value of 8 kV, frequency of 60 Hz, and pulse time of 6 ms from the 18% PCL solution. The photo is complimented by a histogram showing the bimodal distribution of the measured microsphere dimeters. The basic fraction is in the range 0 – 24 µm and the extra fraction 40 – 840 µm. Increasing the voltage during the process to 11 kV while maintaining the same values of parameters f and τ, eliminates the additional fraction (Fig. 7E) and the diameter distribution becomes unimodal in the range of 0 – 11 µm. Fig. 7F shows a sample obtained from the 18% PCL solution while maintaining the voltage value of 8 kV, but with changed values of parameters f and τ, respectively 80 Hz and 5 ms. There is only the basic fraction with a unimodal diameter distribution in the range of 0 – 18 µm. In both mentioned cases (Fig. 7E and F) the effective voltage value is increased in relation to the initial case (Fig. 7D), which results in the elimination of the extra fraction of large microspheres.

The change in the mean diameter of the microspheres in the above-mentioned variants of the experiment is shown in the graph in Fig. 8B. The average diameter of the microspheres in the initial case (8 kV, 60 Hz, 6 ms) is 10.50 ± 4.92 µm and is slightly larger than the diameter of the microspheres in the case with changed f and τ values (8 kV, 80 Hz, 5 ms) – 8.45 ± 3.22 µm, however, this difference is statistically insignificant. In the case with increased voltage (11 kV, 60 Hz, 6 ms), the diameter of the microspheres is significantly smaller – 5.45 ± 1.99 µm, which confirms that with increasing voltage, the diameter of the microspheres in the electrospray process decreases [32].

3.3. Influence of impulse duration τ and frequency f on microsphere size

The previous section presents examples of such selection of PV parameters for which the diameters of microspheres obtained in the electrospray process with the precipitation bath do not differ significantly. More detailed research was carried out to see if this is the case under all conditions.

The analysis of the SEM images shown in Fig. 9 leads to the observation that the PCL microspheres obtained with a 20% polymer solution in DMF for the voltage value of 11 kV and various parameters f and τ show no differences in structure. They all have regular spherical shapes, some of them with small pores. These microspheres resemble those obtained from the same solution for DC voltage (Fig. 5E). The difference can be seen at the outlet of the nozzle, where for the PV a much smaller meniscus with a shorter tip is observed in comparison to the one formed with DCV (Fig. 5). For the PV, the nozzle does not clog and the polymer solution does not leak upward on its outer side as in the case of the use of DCV (Fig. 5D–E).

The plot in Fig. 10A shows the change in the diameter of the microspheres obtained in the electrospray process using 20% PCL solution for a voltage of 11 kV and a pulse duration of 6 ms for various values of the pulse frequency from 20 to 80 Hz. The diameters of the obtained microspheres differ significantly in each case except for two pairs [20 Hz and 60 Hz] and [40 Hz and 80 Hz]. The diagram has a specific sawtooth shape but based on the results, the relation between the diameter of the microspheres and the pulse frequency cannot be explicitly determined although the tendency may appear to be slightly declining.

The graph in Fig. 10B shows the change in the diameter of the microspheres obtained by the electrospray process using a 20% PCL solution for a voltage of 11 kV and a pulse frequency of 60 Hz for various values of pulse duration from 2 to 8 ms. In this case it can be seen that for the pulse time values lower than 8 ms the diameter remains almost unchanged. Only at the pulse duration of 8 ms, a significant decrease in the diameter of the microspheres is noticeable.

An analysis of the influence of effective voltage (U_{eff}) on the diameter of the microspheres was carried out. It was determined whether for given pairs of variants f and τ, for which U_{eff} has the same value, the diameters show significant differences. U_{eff} values were determined for all cases on the basis of Eq. (1) and the results are shown in the graph in Fig. 10C. For a low value of the effective voltage, no differences are noticed between the two variants [20 Hz, 6 ms] and [60 Hz, 2 ms]. In the remaining cases, the mean diameters of the microspheres do not differ much from each other (about 2 µm), but these differences are statistically significant. As U_{eff} increases, the diameter of the microspheres decreases.

3.4. Influence of the used polymer/solvent on the structure of microspheres

Fig. 11. shows SEM pictures of microspheres made with solutions with different polymer/solvent combinations. The pictures also show the mean diameter of the microspheres along with the standard

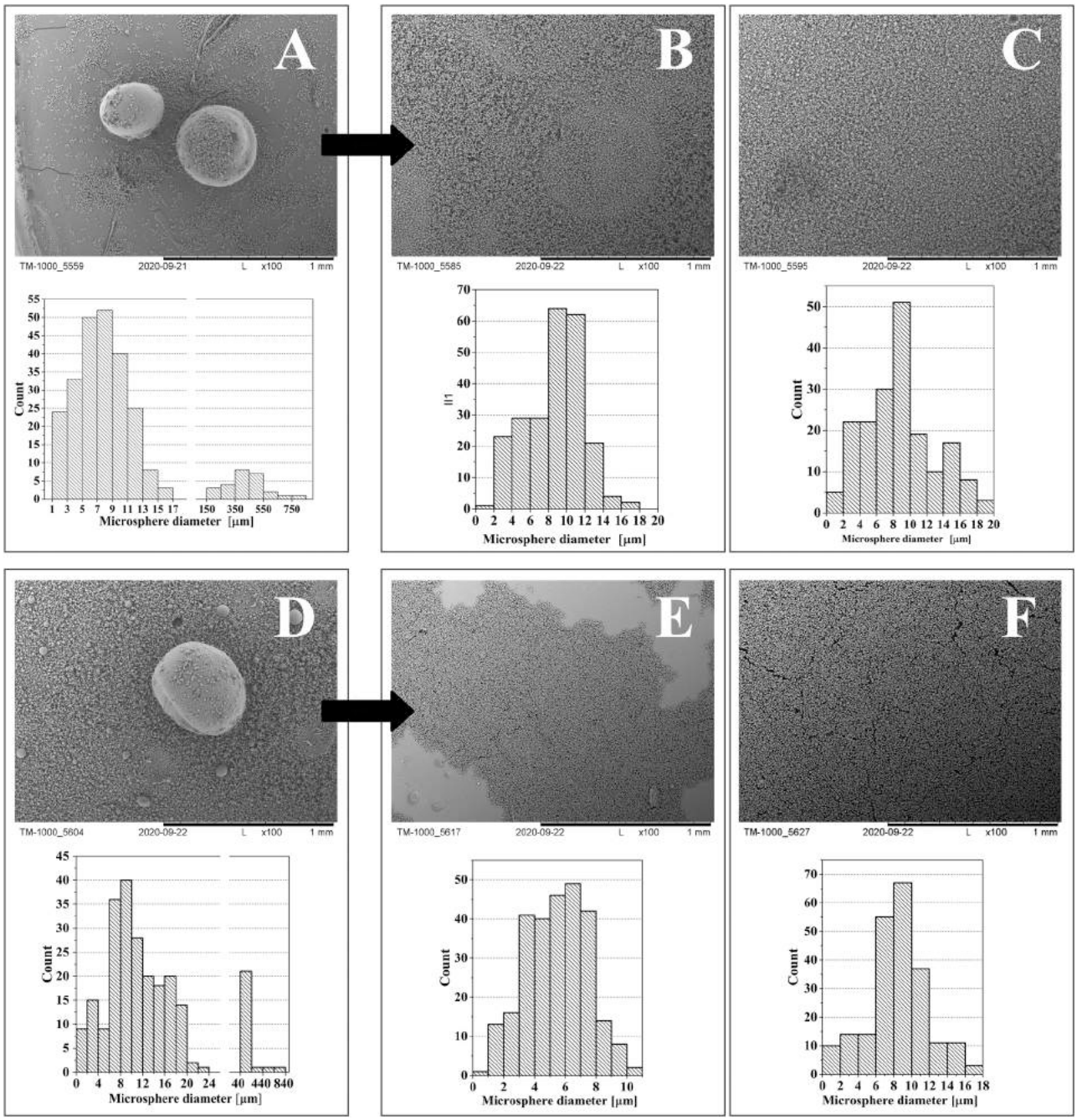

Fig. 7. Scanning electron microscope images of the PCL microspheres obtained with different PCL/DMF solutions under various electrical conditions: **(A)** 15%, DCV of 8 kV, **(B)** 15%, PV of 8 kV, 70 Hz, 8 ms, **(C)** 15%, PV of 8 kV, 50 Hz, 9 ms; **(D)** 18%, PV of 8 kV, 60 Hz, 6 ms, **(E)** 18%, PV of 11 kV, 60 Hz, 6 ms, and **(F)** 18%, PV of 8 kV, 80 Hz, 5 ms. Histograms showing the distribution of the measured microsphere diameters for a given sample were marked on the photos.

deviation.

The analysis of the SEM pictures presented in Fig. 11 leads to the clear observation that the selection of the polymer/solvent composition does have an impact on the structure of the microspheres obtained in the electrospray/phase inversion process while maintaining other process conditions. In the case of PCL, it can be seen that the microspheres obtained from the polymer solution in DMF are more spherical and their average diameter is larger, but this difference is not statistically significant. In the case of PES, the change of the solvent from DMF to NMP results in an improvement in the sphericality of the microspheres and a decrease in their mean diameter.

Based on the microscopic observation of PES microspheres, it was noticed that their surface morphology differed depending on whether DMF or NMP was used to dissolve the polymer. In the case of microspheres obtained from the PES/NMP solution, their surface seems to be more porous, uneven, and slightly reminiscent of an orange peel. A similar case is not observed for the PCL microspheres. In order to verify the validity of the above observations, the specific surface area of the microspheres was measured using BET nitrogen adsorption method. The results of the study are presented in Table 2.

The results of measurements of the specific surface of the microspheres confirm the observations made on the basis of SEM pictures. They additionally allow to determine measurably the difference in the surface morphology of the microspheres. In the case of PES microspheres, the specific surface area is several ten times larger than in the case of PCL. In addition, the use of NMP in the formation of PES

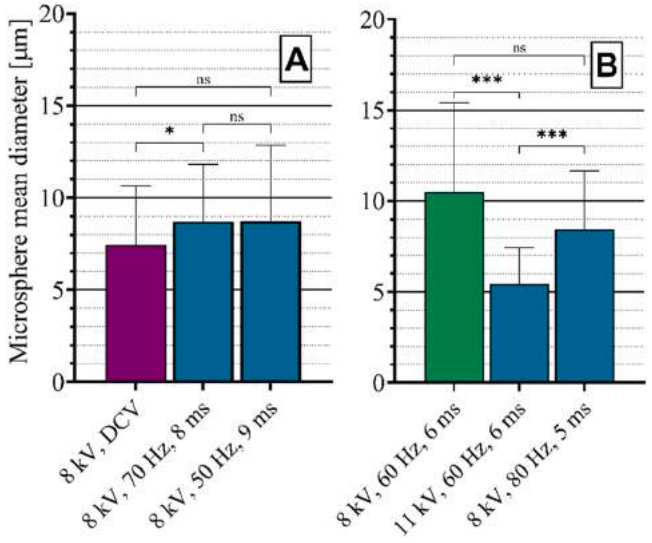

Fig. 8. The mean diameters of microspheres obtained from **(A)** the 15% PCL solution with DCV or PV, **(B)** the 18% PCL solution with PV of different parameters.

microspheres increases their specific surface almost threefold, which was also noticed in the microscopic pictures.

Fourier transform infrared spectroscopy (FTIR) and X-ray diffraction (XRD) tests were performed to check the influence of the use of different polymer/solvent compositions on the chemical structure and crystallinity of the obtained microspheres. Fig. SI1 (supporting information) presents the results.

The IR spectra shows that the chemical structure of the polymers (both PCL and PES) does not change after the microspheres production process, because in both cases the peaks appearing on the black curve (pure polymer) have their counterparts on the red (microspheres from a polymer solution in DMF) and blue curves (microspheres from a polymer solution in NMP) (Fig. SI1). However, there are some additional peaks present in the spectra. One of them is slender and occurs around 1662 – 1677 cm^{-1}, which corresponds to C═O stretching in the tertiary amide. These bonds are characteristic for the solvents used in the process (both DMF and NMP) and they are not present in the structure of any of the polymers (neither PCL nor PES). The second, double peak appears around 2880 – 2972 cm^{-1}. In the case of the PCL spectrum, it is derived from C–H stretching alkane. It appears to a small extent in the PES/DMF and PES/NMP spectra too, where it identifies the hydrocarbons present in the chemical structure of both solvents. Probably this stretch would also occur for PCL/DMF and PCL/NMP microsphere samples, however, the accumulation of alkane bonds in PCL overrides the ones in the solvents. The third peak is much wider. The IR spectrum shows a low intensity stretch at around 3426 – 3444 cm^{-1} corresponding to O–H, most likely for absorbed moisture or ethanol residues for all microspheres. Taking into account the above observations, it can be undoubtedly stated that the process of producing microspheres did not change the chemical structure of the polymers. However, there are some residual solvents in the samples, which should be removed by increasing the DMF (or NMP) leaching time with ethanol, additional rinsing after the end of the process with fresh portion of pure ethanol and more thorough drying.

The X-ray diffraction patterns of the PES microspheres have the same shape (Fig. SI1) and additionally it is the shape of a pure PES pattern [40]. Despite the method of producing microspheres, the amorphous nature of the PES remains intact. The case of PCL microspheres is similar – XRD diffraction patterns are the same for both types of material (after solution in DMF and NMP) and reveal the presence of significant crystallinity of PCL – the same as in the case of pure polymer [41]. Regardless of the method of producing microspheres, PCL shows a sharp peak at 2θ of 21° and a relatively low intensity peak at 23.5° corresponding to the (110) and (200) planes of the orthorhombic crystal structure [42]. The XRD results suggest that cristal nature of PCL does not change due to its dissolution in different solvents and subsequent preparation of the microspheres.

3.5. Rhodamine immobilization and release

Rhodamine was added to the microsphere-forming solution as well as to the precipitation bath and the electrospray was conducted. The microspheres obtained in this system were dried. A change in their color compared to pure microspheres was noticed – they were slightly pink (Fig. 4B). In order remove the rhodamine that was deposited on the surface of the microspheres due to the evaporation of residual ethanol from the bath solution, the microspheres were rinsed with the pure alcohol. The washed microspheres were placed in a fresh ethanol and the concentration of the solution was measured at specified time intervals and the charts showing the rhodamine release profiles from the microspheres (varying in the polymer/solvent combination) were plotted (Fig. 12 A-D).

Initial studies of marker (rhodamine) release over time from microspheres were carried out. In the case of microspheres produced from solutions of both polymers in DMF, a fairly rapid release of the marker is observed in the first 10 min of the experiment (Fig. 12A and C). In both of these cases, an initial burst of the marker occurs (above the equilibrium concentration), which is related to the rapid desorption of rhodamine from the outer surface of the microspheres. The burst release effect is not observed for the microspheres made of NMP polymer solutions (Fig. 12B and D). In both cases, the release of the marker occurs gradually, not exceeding the equilibrium concentration, although, most of the rhodamine is released in the first 30 min of the experiment. The above observations are consistent with the literature reports of other researchers, e.g. Berkland et al. [43]. They stated in their work that rhodamine, as a very hydrophilic substance, is mostly located towards the surface of the microspheres, which results in its relatively quick release, regardless of the size of microspheres.

In the case of PCL/DMF microspheres (Fig. 12A) the equilibrium state is reached after 30 min, while in the case of PES/DMF microspheres (Fig. 12C) this time is prolonged up to 240 min. These differences are probably caused by the difference in the surface structure of both types of microspheres – the surface of the PCL microspheres is relatively smooth, so both desorption of rhodamine molecules adsorbed on it and re-adsorption occur relatively quickly. On the other hand, the outer surface of the microspheres made of PES is more pleated and porous. Thus, in the first period of release, diffusion of marker molecules adsorbed on the surface occurs, followed by desorption of molecules inside the cavities or pores. For this reason, reaching the state of equilibrium takes more time. In both cases the equilibrium state is maintained after 72 h (4320 min).

Microspheres made of NMP polymer solutions have different profiles (Fig. 12B and D). In the case of PCL/NMP microspheres (Fig. 12B), an increase and then a decrease in the concentration of the marker are observed, which indicates that probably during the experiment the equilibrium concentration has not yet been achieved. The profile of rhodamine release from inside the PES/NMP microspheres is significantly different (Fig. 12D). After the initial release of rhodamine during the first 20 min, a gradual slowdown in release occurs, which lasts continuously until the end of the 6-hour test. During this time, rhodamine diffuses from the inside of the pores, which requires a longer time. Over time, the marker mass gains are smaller and smaller, but still visible. The equilibrium state has not been reached even after 72 h.

The estimated mass of rhodamine released after 72 h (expressed in the relation to the mass of the microspheres) is shown in Table 3. The obtained results confirm the differences in the surface structure of the microspheres, visible in the SEM photos (Fig. 11) and confirmed by tests of their specific surface (Table 2) – the greater the specific surface area,

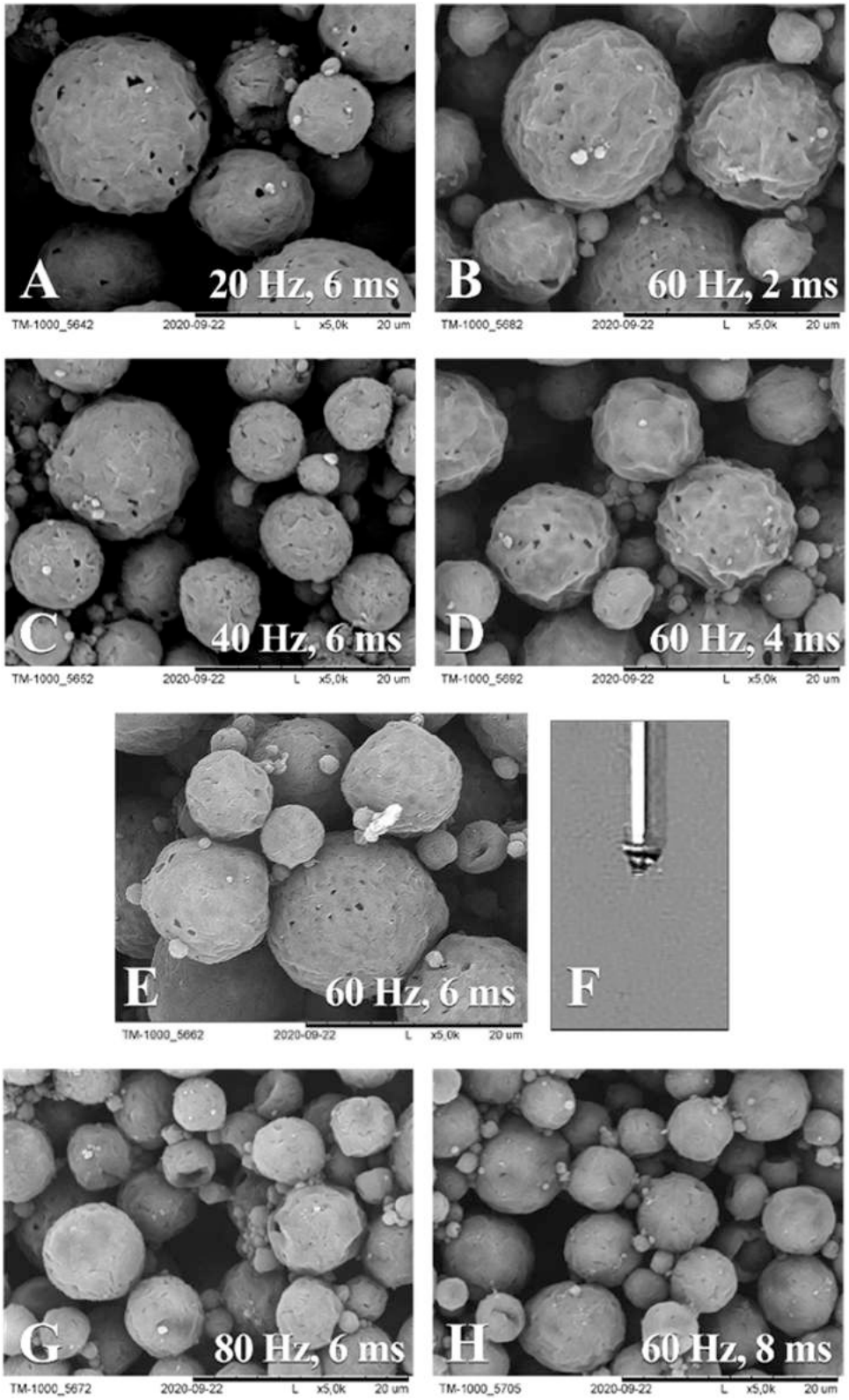

Fig. 9. Scanning electron microscope images of the PCL/DMF microspheres obtained with 20% polymer solution under different electrical conditions (f, τ) for PV of 11 kV: **(A)** 20 Hz, 6 ms; **(B)** 60 Hz, 2 ms; **(C)** 40 Hz, 6 ms; **(D)** 60 Hz, 4 ms; **(E)** 60 Hz, 6 ms; **(G)** 80 Hz, 6 ms; **(H)** 60 Hz, 8 ms; **(F)** a frame from the recording of the nozzle outlet showing the geometric shape of the liquid at the conditions [11 kV, 60 Hz, 6 ms].

the greater the mass of immobilized rhodamine.

3.6. Advantages of the proposed method

An attempt to combine the electrospray process and the use of a bath to collect polymer microspheres was undertaken by some researchers

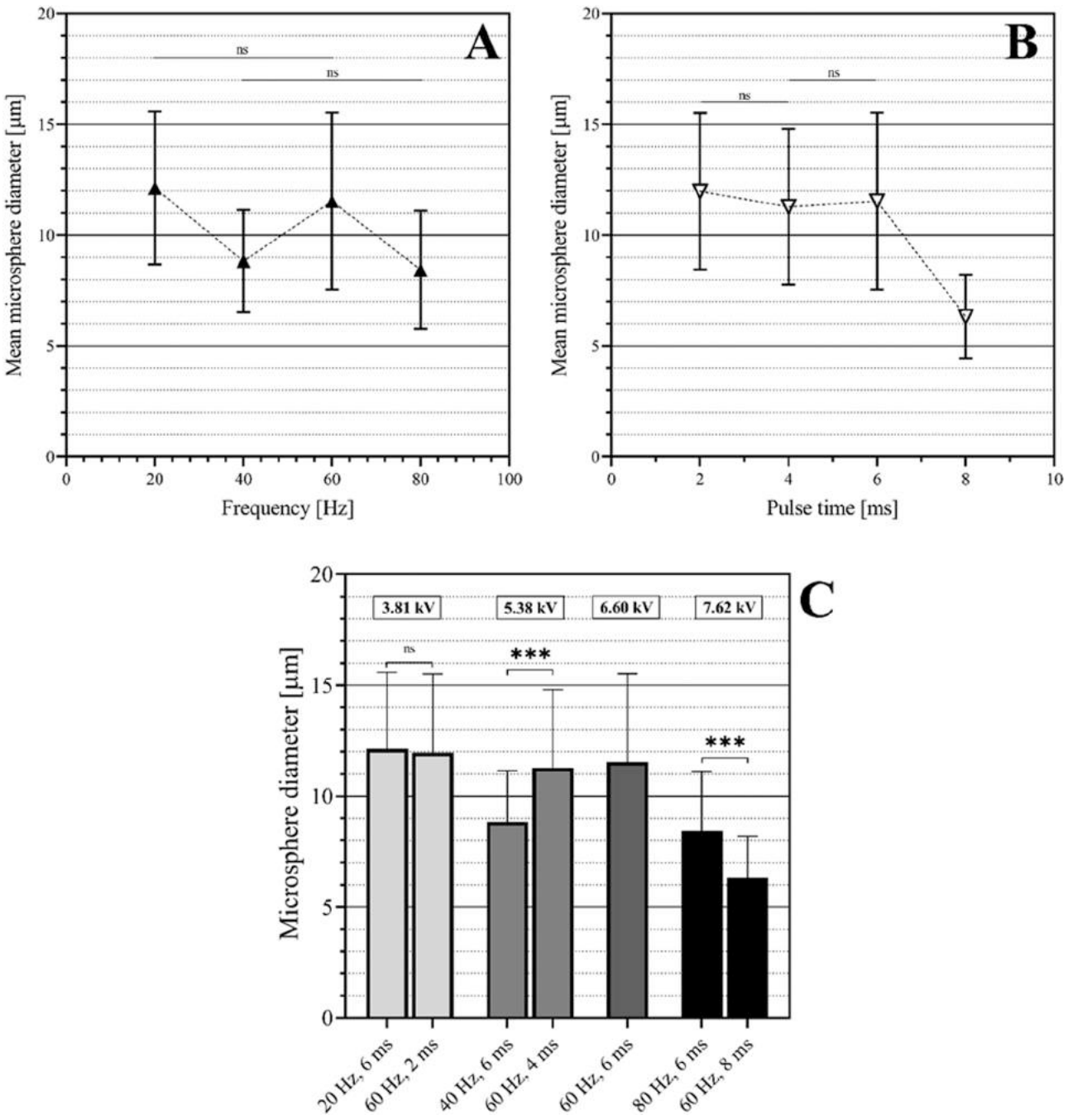

Fig. 10. The mean diameter of the microspheres obtained in the electrospray process from the 20% PCL/DMF solution with PV of 11 kV: **(A)** in the function of frequency of impulse application f for $\tau = 6$ ms; **(B)** in the function of the duration time of the voltage impulse τ for $f = 60$ Hz. **(C)** Influence of the change of effective voltage U_{eff} on the diameter of PCL/DMF microspheres electrosprayed with PV.

before. For instance, Malik et al. [44] manufactured microspheres from PLGA using the electrospray coupled with a novel thermally induced phase separation process with a liquid nitrogen collection bath. The particles had diameters of 16.77 – 122.91 µm, and the method proposed by them turned out to be chemical-free, sustainable and scalable. Another work combining electrospray with a gelation bath has been reported by Lee et al. *[45]*. They presented a coaxial tri-capillary electrostatic technique that can directly produce PLGA microspheres with multiple drug compounds incorporated in various layers. As a collector they used the ring immersed in a plastic dish containing a conductive mixture of olive oil and tributylphosphine. However, more than the method itself, they focused on controlling the thickness of the individual microsphere layers by changing the flow rate of the solution flowing through the nozzle.

Each of these methods described above uses a bath liquid that may cause difficulties to work with (liquid nitrogen, oil), whereas the authors of this work elaborated a method with ethanol as a non-solvent that is easily available and simple to operate. None of the methods is universal for many polymers, nor do they use pulsed voltage, which undoubtedly would increase the possibility of control over the obtained product by increasing the number of process parameters that can be adjusted.

The presented method has an easy and adaptable methodology and does not require any additional substances (apart from the polymer, its solvent and non-solvent) which could leave residues or change the structure of the polymer (e.g. crosslinking agents). The process is conducted in mild conditions such as ambient temperature and gentle

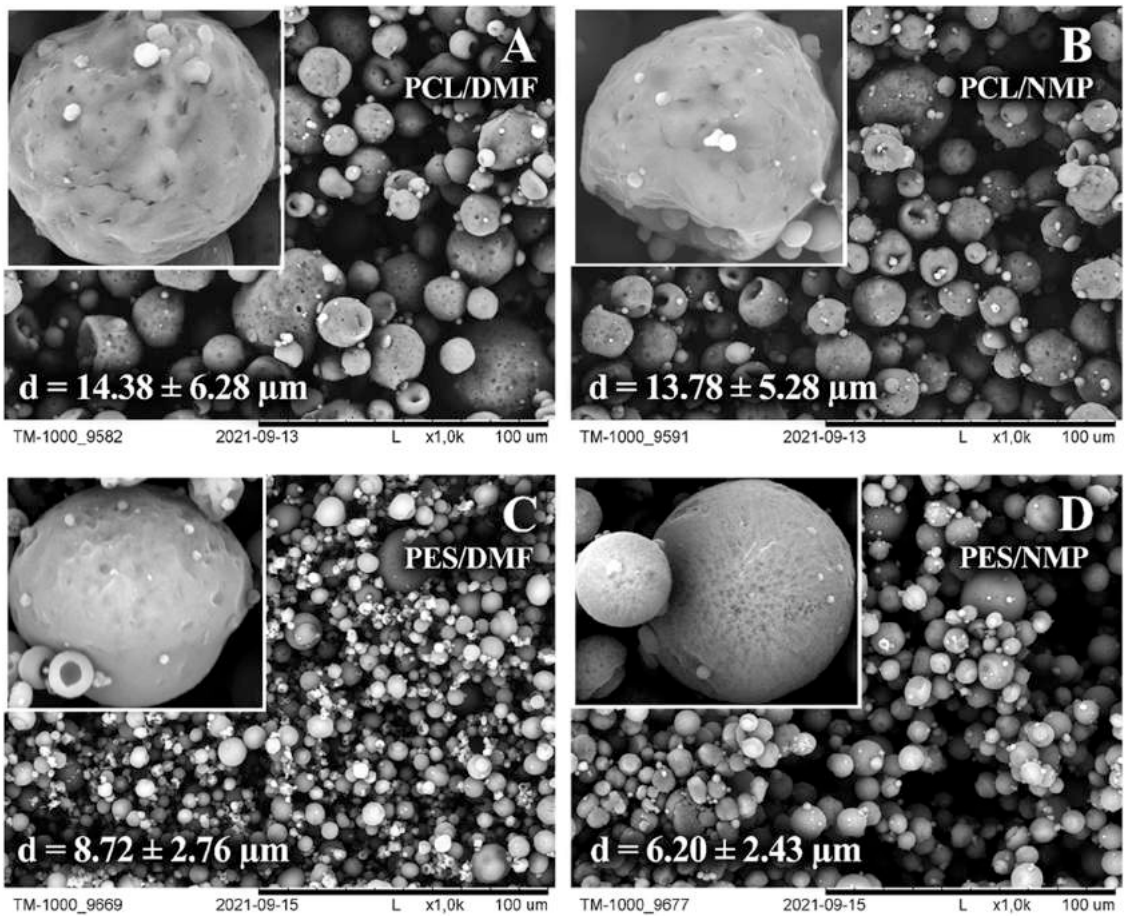

Fig. 11. Scanning electron microscope images of the microspheres obtained with 15% polymer solution with the microsphere average diameter d and standard deviation: **(A)** PCL in DMF [11 kV, 40 Hz, 4 ms], **(B)** PCL in NMP [11 kV, 40 Hz, 4 ms], **(C)** PES in DMF [8 kV, 60 Hz, 6 ms], **(D)** PES in NMP [8 kV, 60 Hz, 6 ms].

Table 2
Specific surface area of microspheres determined by BET nitrogen adsorption method.

Sample	Specific surface area [m^2/g]
PCL/NMP	0.607 ± 0.040
PCL/DMF	1.566 ± 0.044
PES/DMF	52.926 ± 0.260
PES/NMP	148.199 ± 1.189

stirring. Additionally, by conducting the experiments for many weeks, the authors of the study proved that there is an excellent reproducibility of the microspheres. A relatively large number of microspheres with a narrow diameter distribution of several micrometers is obtained. They do not form aggregates (neither in the bath nor after drying) and are simple to further process and use. The recovery of the product is easy and it can be directly applied afterwards. The advantages of the proposed method compared to the methods described in the literature are summarized in Table 4.

Polymer microspheres in the form of dried non-aggregated powder obtained according to the proposed method open up many possibilities for further use. In this work, it was proposed to use them as drug carriers. They could be dispersed in the polymer solution to form a suspension which can then be pressed through a nozzle in electrospinning or 3D bioprinting process to form novel drug delivery systems via extrusion-based techniques what would be their final use as planned by the authors of the work.

4. Conclusions

In the presented work, a method for manufacturing ready-to-use polymer microspheres was developed using combined pulsed voltage electrospray and wet phase inversion techniques. The method is simple and universal and it can be modified by using different polymers and solvents, and by changing the process parameters leading to the production of microspheres of various sizes and structures.

This work demonstrated the advantages of using a pulsed electric field instead of direct-current voltage. First of all, using of PV removes the unwanted extra fraction of large microspheres making the microspheres monodispersed. It stabilizes the liquid meniscus at the nozzle tip (keeping its geometric shape the same throughout the process). Finally, properly selected PV parameters (voltage U, pulse frequency f and pulse duration τ) result in obtaining the desired structures. The microspheres were made of two polymers (PCL and PES) dissolved in two solvents (DMF and NMP). It has been shown that the selection of the composition of the microsphere-forming solution has an impact on their size, homogeneity and specific surface area, but does not change their chemical or crystalline structure (compared to pure polymers).

As an example of the use of the microspheres, the ones with rhodamine for the controlled release of substances were presented. The marker-loaded microspheres were successfully produced and the differences in rhodamine release profiles resulting from the structure of the microspheres (especially specific surface area) were indicated.

The work described above has a very promising outcome as it provides support for our hypothesis that the combination of pulsed voltage electrospray and wet phase inversion techniques is a suitable method for the production of monodispersed ready-to-use polymer microspheres.

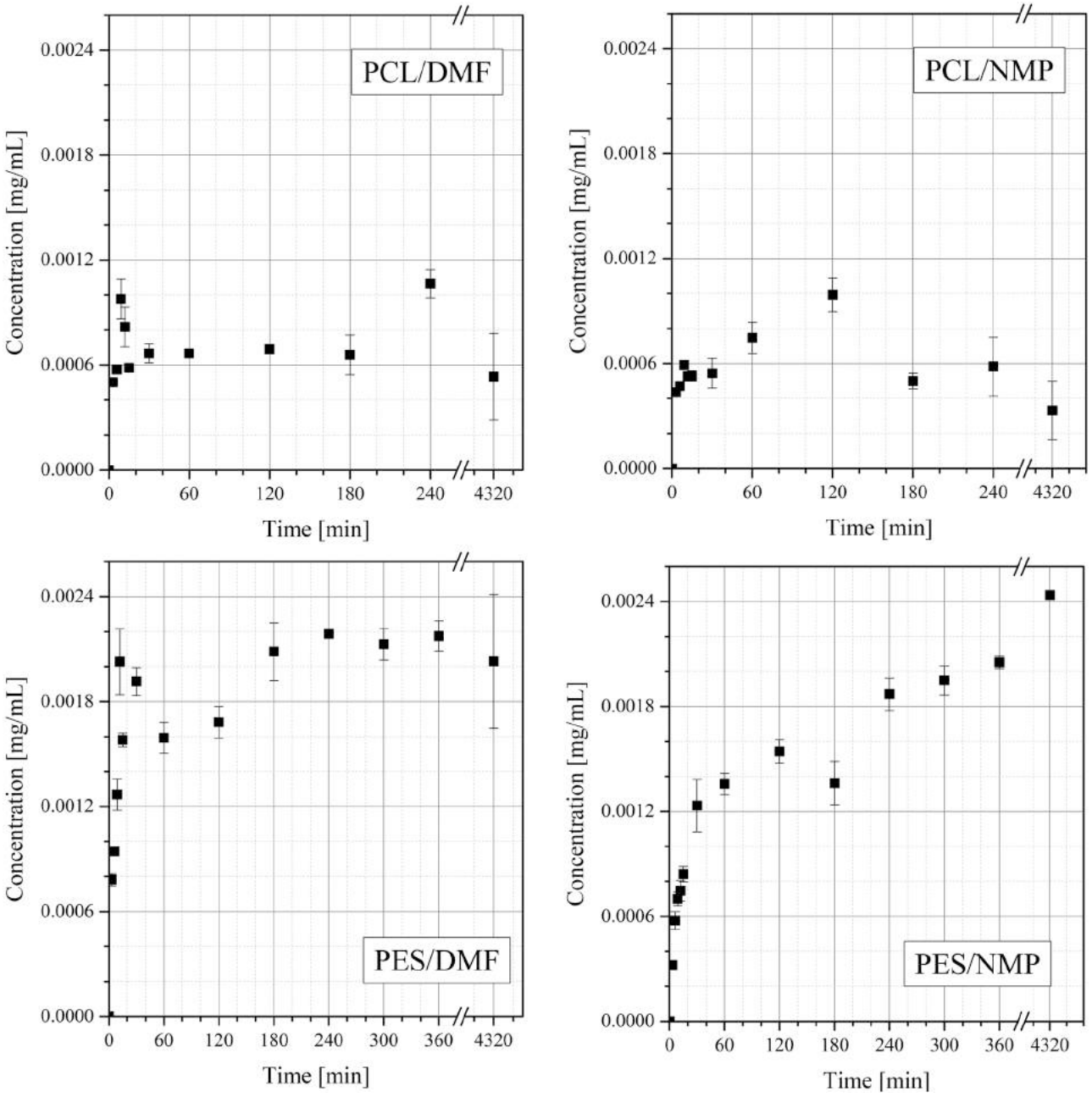

Fig. 12. Rhodamine release profile from the rinsed microspheres varying in the polymer/solvent combination: (A) PCL/DMF, (B) PCL/NMP, (C) PES/DMF, (D) PES/NMP.

Table 3
The mass of rhodamine released after 72 h from different microspheres.

Sample	Rhodamine mass [mg/g]
PCL/NMP	0.029 ± 0.014
PCL/DMF	0.043 ± 0.014
PES/DMF	0.143 ± 0.029
PES/NMP	0.171 ± 0.014

Such microspheres, for example, can be used as drug delivery systems but their application will certainly not be limited to biomedical engineering as it is easily transferable to other sectors.

CRediT authorship contribution statement

Adam Mirek: Conceptualization, Methodology, Formal analysis, Investigation, Validation, Data curation, Writing – original draft, **Marcin Grzeczkowicz:** Methodology, Software, Resources, Validation, **Cassandre Lamboux:** Methodology, Software, Resources, Formal analysis, **Syreina Sayegh:** Methodology, Investigation, Resources, **Mikhael Bechelany:** Conceptualization, Writing – review & editing, **Dorota Lewińska:** Conceptualization, Writing – review & editing, Supervision.

Declaration of Competing Interest

The authors declare the following financial interests/personal relationships which may be considered as potential competing interests:

Table 4
The advantages of the proposed method compared to the methods described in the literature.

Microsphere formation method with reference	Problem	Solution brought by the method described in the article
Electrospray droplet formation followed by the solvent evaporation (microspheres deposited on a grounded collector, usually aluminum plate)[34–37]	Microspheres forming the aggregates and layers. Using the microspheres as a dispersion in polymer solution for various extrusion-based techniques is very difficult or impossible.	Use of a different collector – a bath filled with a liquid in which polymer droplets suspended in non-miscible phase harden according to the sol–gel mechanism (precipitation).
Ultrasonic droplet formation followed by solvent extraction (microspheres deposited in the bath) [43]	Production of unwanted sphere sizes (satellite fraction). Nozzle clogging.	Use of a pulsed voltage method to form microdroplets with a narrow diameter distribution (monodisperse) by employing additional electrical process parameters which can be adjusted according to desired microsphere diameter.
Electrospray droplet formation followed by the solvent extraction (microspheres deposited in the bath) [31,44,45]	Collecting baths with various chemical compositions (oils, liquid nitrogen, salt solutions) difficult to operate. Non-universal methods strictly adapted to only one type of polymer. Use of additional substances which could leave residues or change the structure of the polymer (e.g. crosslinking agents).	Use of a common, pure solvent as a precipitation bath (e.g. ethanol). The uncomplicated system allows for quick modification of the composition of the microsphere forming solution as well as the non-solvent bath. Method of an easy and adaptable methodology and does not require any additional substances.

Other advantages of the proposed method:

- mild conditions (ambient temperature, gentle stirring),
- excellent reproducibility of the microspheres,
- the recovery of the product is easy and resulting microspheres are simple to be used in different extrusion-based techniques as a dispersion in polymer solution.

Adam Mirek reports financial support was provided by Nalecz Institute of Biocybernetics and Biomedical Engineering Polish Academy of Sciences. Adam Mirek reports financial support was provided by French Government. Adam Mirek reports was provided by National Centre for Research and Development.

Acknowledgements

This project was supported by European Social Fund [POWR.03.02.00–00-1028/17–00] as part of the POWER Och!Dok program. AM would like to thank Campus France for the funding through a French Government Scholarship.

Appendix A. Supporting information

Supplementary data associated with this article can be found in the online version at doi:10.1016/j.colsurfa.2022.129246.

References

[1] S. Raza, J. Zhang, M. Raza, X. Li, H. Wen, C. Liu, Biomass furfural-derived green polymer microspheres: synthesis and applications for the removal of environmental pollutants from wastewater, Microporous and Mesoporous Mater. 318 (11096) (2021).
[2] P.V. Antunes, A. Ramalho, E.V.P. Carrilho, Mechanical and wear behaviours of nano and microfilled polymeric composite: effect of filler fraction and size, Mater. Design 61 (2014) 50–60.
[3] M. Gokmen, F. Du Prez, Porous polymer particles - A comprehensive guide to synthesis, characterization, functionalization and applications, Progress in Polym. Sci. 37 (3) (2012) 365–405.
[4] K. Laeschke, Biocompatibility of microparticles into soft tissue fillers, Seminars in Cutaneous Med. Surg. 23 (4) (2004) 0–217.
[5] X. Tian, L. Zhang, H. Li, X. Zhang, Q. Wang, L. Jin, Q. Cao, Preparation of bio-oil-based polymer microspheres for adsorption Cu2+ and its adsorption behaviors, J. Dispersion Sci. Technol. 42 (7) (2021) 1021–1030.
[6] D.H. Kim, J.H. Jeong, H.-C. Woo, M.H. Kim, Synthesis of highly porous polymer microspheres with interconnected open pores for catalytic microreactors, Chem. Eng. J. 420 (2021), 127628.
[7] N.A. Liu, S. Zhao, Z. Yang, B. Liu, Patchy templated synthesis of macroporous colloidal hollow spheres and their application as catalytic microreactors, ACS Appl. Mater. & Interf. 11 (50) (2019) 47008–47014.
[8] H. Xia, G. Wan, F. Yang, J. Wang, Q. Bai, Preparation of monodisperse large-porous silica microspheres with polymer microspheres as the templates for protein separation, Mater. Lett. 180 (2016) 19–22.
[9] Y. Bai, F. Zhang, K. Xu, X. Wang, C. Wang, H. Zhang, P. Wang, Pickering emulsion strategy to control surface wettability of polymer microspheres for oil–water separation, Appl. Surf. Sci. 566 (2021), 150742.
[10] D. Kukkar, M. Kukkar, I. Kaur, J. Singh, L.M. Bharadwaj, Synthesis of poly (ϵ-caprolactone) microreactors from freeze-dried microspheres, Polym.-Plastics Technol. Eng. 51 (12) (2012) 1275–1281.
[11] N. Takasi, T. Toru, H. Toshiro, Novel microreactors for functional polymer beads, Chem. Eng. J. 101 (1–3) (2004) 23–29.
[12] P. Listewnik, M. Bechelany, M. Szczerska, Microsphere structure application for supercapacitor in situ temperature monitoring, Smart Mater. Struct. 30 (10LT01) (2021).
[13] C.Y. Wee, Z. Yang, E.S. Thian, Past, present and future development of microspheres for bone tissue regeneration: a review, Mater. Technol. 36 (6) (2021) 364–374.
[14] B. Lavine, N. Kaval, L. Oxenford, M. Kim, K. Dahal, N. Perera, R. Seitz, J. Moulton, R. Bunce, Synthesis and characterization of N-Isopropylacrylamide microspheres as pH sensors, Sensors 21 (6493) (2021).
[15] C.-Y. Lin, S.-J. Lin, Y.-C. Yang, D.-Y. Wang, H.-F. Cheng, M.-K. Yeh, Biodegradable polymeric microsphere-based vaccines and their applications in infectious diseases, Human Vaccines & Immunotherapeutics 3 (11) (2015) 650–656.
[16] V.D. Prajapati, G.K. Jani, J.R. Kapadia, Current knowledge on biodegradable microspheres in drug delivery, Expert Opinion on Drug Delivery 12 (4) (2015) 1–17.
[17] Y. Xia, D.W. Pack, Uniform biodegradable microparticle systems for controlled release, J. Controlled Release 82 (1) (2002) 137–147.
[18] P. Davoodi, W.C. Ng, W.C. Yan, M.P. Srinivasan, C.-H. Wang, Double-walled microparticles-embedded self-cross-linked, injectable, and antibacterial hydrogel for controlled and sustained release of chemotherapeutic agents, ACS Appl. Mater. Interfaces 8 (35) (2016) 22785–22800.
[19] S. Ravindra, K. Varaprasad, N. Narayana Reddy, K. Vimala, K. Mohana Raju, Biodegradable microspheres for controlled release of an antibiotic ciprofloxacin, J. Polym. Environ. 19 (2) (2011) 413–418.
[20] K.C. Scheiner, R.F. Maas-Bakker, M.J. van Steenbergen, S.P. Schwendeman, W. E. Hennink, R.J. Kok, Post-loading of proangiogenic growth factors in PLGA microspheres, European J. Pharmaceutics and Biopharmaceutics 158 (2021) 1–10.
[21] X. Dong, M.A. Tahir, L. Zhang, C.G. Schäfer, Gadolinium-containing polymer microspheres: a dual-functional theranostic agent for magnetic resonance imaging and cancer therapy, New J. Chem. 15 (2019).
[22] M. Kaur, S. Sharma, V. Sinha, Polymer based microspheres of aceclofenac as sustained release parenterals for prolonged anti-inflammatory effect, Mater. Sci. Eng.: C 72 (2017) 492–500.
[23] E. Gavini, A. Hegge, G. Rassu, V. Sanna, C. Testa, G. Pirisino, J. Karlsen, P. Giunchedi, Nasal administration of carbamazepine using chitosan microspheres: in vitro/in vivo studies, Intern. J. Pharmaceutics 307 (1) (2006) 9–15.
[24] V. Saez, J.R. Hernández, C. Peniche, Microspheres as delivery systems for controlled release of peptides and proteins, Biotecnología Aplicada 24 (2007) 108–116.
[25] A. Nicolini, L. Martinetti, S. Crespi, M. Maggioni, A. Sangiovanni, Transarterial chemoembolization with epirubicin-eluting beads versus transarterial embolization before liver transplantation for hepatocellular carcinoma, J. Vascular and Interventional Radiol. 21 (3) (2010) 327–332.
[26] K. Saralidze, M. Knetsch, C. van Hooy-Corstjens, L. Koole, Radio-opaque and surface-functionalized polymer microparticles: potentially safer biomaterials for different injection therapies, Biomacromolecules 7 (2006) 2991–2996.
[27] C. Berkland, M. King, A. Cox, K. Kim, D.W. Pack, Precise control of PLG microsphere size provides enhanced control of drug release rate,", J. Controlled Release 82 (1) (2002) 137–147.
[28] B. Kupikowska-Stobba, D. Lewińska, Polymer microcapsules and microbeads as cell carriers for in vivo biomedical applications, Biomater. Sci. 8 (2020) 1536–1574.
[29] H. Strathmann, K. Kock, Recent advances in the formation of phase inversion membranes made from amorphous or semi-crystalline polymers, J. Membr. Sci. 113 (2) (1996) 361–371.
[30] D. Poncelet, R.J. Neufeld, M.F.A. Goosen, B. Burgarski, V. Babak, Formation of microgel beads by electric dispersion of polymer solutions 45 (9) (1999) 2018–2023.

[31] Y. Shang, F. Ding, L. Xiao, H. Deng, X. Shi, Chitin-based fast responsive pH microspheres for controlled drug release, Carbohydrate Polym. 102 (2014) 413–418.
[32] D. Lewińska, S. Rosiński, A. Weryński, Influence of process conditions during impulsed electrostatic droplet formation on size distribution of hydrogel beads, Artificial Cells, Blood Substitutes, and Biotechnol. 32 (1) (2004) 41–53.
[33] U. Prüsse, L. Bilancetti, M. Bučko, B. Bugarski, J. Bukowski, P. Gemeiner, D. Lewińska, V. Manojlovic, B. Massart, C. Nastruzzi, V. Nedovic, D. Poncelet, S. Siebenhaar, L. Tobler, A. Tosi, A. Vikarto, Comparison of different technologies for alginate beads production,", Chemical Papers 62 (4) (2008) 364–374.
[34] L. Gasperini, D. Maniglio, C. Migliaresi, Microencapsulation of cells in alginate through an electrohydrodynamic process, J. Bioactive and Compatible Polym. 28 (5) (2013) 413–425.
[35] T. Ciach, Microencapsulation of drugs by electro-hydro-dynamic atomization, Intern. J. Pharmaceutics 324 (1) (2006) 51–55.
[36] A.Í.S. Morais, E.G. Vieira, S. Afewerki, R.B. Sousa, L.M.C. Honorio, A.N.C. O. Cambrussi, J.A. Santos, R.D.S. Bezerra, J.A.O. Furtini, E.C. Silva-Filho, T. J. Webster, A.O. Lobo, Fabrication of polymeric microparticles by electrospray: the impact of experimental parameters, J. Functional Biomater. 11 (4) (2020).
[37] Y. Tang, H. Zhao, J. Yao, Z. Zhu, D. Sun, M. Zhang, A doxorubicin and vincristine drug release system based on magnetic PLGA microspheres prepared by coaxial electrospray, J. Mater. Sci. 54 (13) (2019) 9689–9706.
[38] S. Yao, H. Liu, S. Yu, Y. Li, X. Wang, L. Wang, Drug-nanoencapsulated PLGA microspheres prepared by emulsion elec-trospray with controlled release behavior, Regenerative Biomater. 3 (5) (2016) 309–317.
[39] B. Kupikowska, D. Lewińska, K. Dudziński, J. Jankowska-Śliwińska, G. M., W. C. and A. Chwojnowski, Influence of changes in composition of the membrane-forming solution on the structure of alginate-polyethersulfone microcapsules, Biocybernetics and Biomed. Eng. 29 (3) (2009) 61–69.
[40] A. Benhalima, F. Hudon, F. Koulibaly, C. Tessier, J. Brisson, Polyethersulfone polymers and oligomers - morphology and crystallization, Canadian J. Chem. 90 (10) (2012) 880–890.
[41] A. Baji, S.C. Wong, T. Liu, T. Li, T.S. Srivatsan, Morphological and X-ray diffraction studies of crystalline hydroxyapatite reinforced polycaprolactone, J. Biomed. Mater. Res. Part B: Appl. Biomater. 81 (343) (2006).
[42] H. Bittiger, R. H. Marchessault and W. D. Niegisch, Crystal structure of poly-ε-caprolactone, Acta Crystallographica Section B, vol. B26, no. 1923, 1970.
[43] C. Berkland, M.J. Kipper, B. Narasimhan, K. Kim, D.W. Pack, Microsphere size, precipitation kinetics and drug distribution control drug release from biodegradable polyanhydride microspheres, J. Controlled Release 94 (2004) 129–141.
[44] S.A. Malik, W.H. Ng, J. Bowen, J. Tang, A. Gomez, A.J. Kenyon, R.M. (. Day, Electrospray synthesis and properties of hier-archically structured PLGA TIPS microspheres for use as controlled release technologies, J. Colloid and Interface Sci. 467 (2016) 220–229.

Supporting information

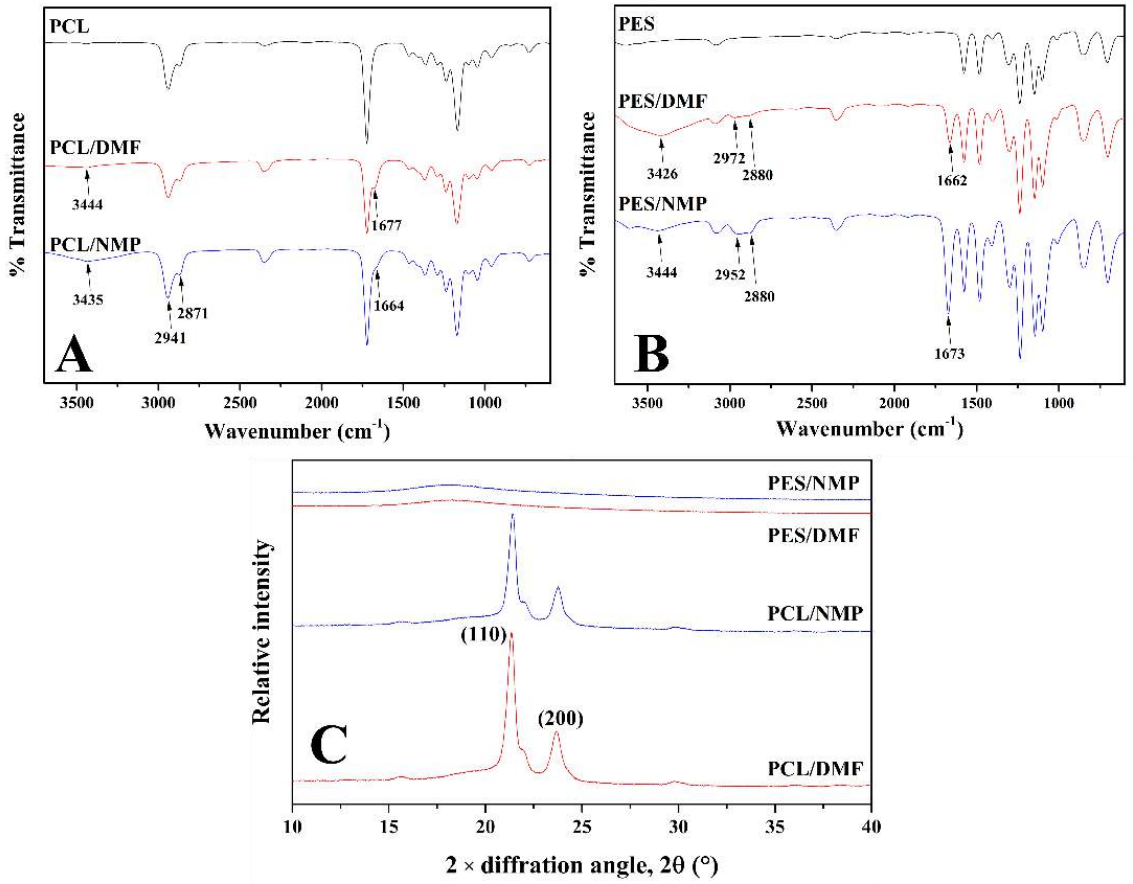

Figure SI1. **(A-B)** FTIR spectra of pure PCL and PES as well as the microspheres obtained from a polymer solution – in DMF (PCL/DMF and PES/DMF) and in NMP (PCL/NMP and PES/NMP). **(C)** XRD patterns of the microspheres.

PUBLICATION 3

Electrospun UV-cross-linked polyvinylpyrrolidone fibers modified with polycaprolactone/ polyethersulfone microspheres for drug delivery

Mirek, A., Grzeczkowicz, M., Belaid, H., Bartkowiak, A., Barranger, F., Abid, M., Wasyłeczko, M., Pogorielov, M., Bechelany, M., Lewińska, D.
Biomaterials Advances. 147, 213330 (2023).
DOI: 10.1016/j.bioadv.2023.213330

147 (2023) 213330

Contents lists available at ScienceDirect

Biomaterials Advances

journal homepage: www.journals.elsevier.com/materials-science-and-engineering-c

Electrospun UV-cross-linked polyvinylpyrrolidone fibers modified with polycaprolactone/polyethersulfone microspheres for drug delivery

Adam Mirek [a,b,*], Marcin Grzeczkowicz [a], Habib Belaid [b], Aleksandra Bartkowiak [a], Fanny Barranger [b], Mahmoud Abid [b], Monika Wasyłeczko [a], Maksym Pogorielov [c,d], Mikhael Bechelany [b], Dorota Lewińska [a]

[a] Nalecz Institute of Biocybernetics and Biomedical Engineering, Polish Academy of Sciences, 4 Ks. Trojdena St., 02-109 Warsaw, Poland
[b] Institut Européen des Membranes, IEM, UMR 5635, Univ Montpellier, CNRS, ENSCM Place Eugène Bataillon, 34095 Montpellier cedex 5, France
[c] Sumy State University, Medical Institute, 40018 Sumy, Ukraine
[d] NanoPrime, 32-900 Dębica, Poland

ARTICLE INFO

Keywords:
Electrospinning
Microspheres
Suspension
Drug delivery
UV-cross-linking

ABSTRACT

Electrospun fibers, often used as drug delivery systems, have two drawbacks – in the first stage of their action a sudden active substance burst release occurs and they have a relatively small capacity for a drug. In this work the fibers are modified by the addition of drug-loaded microspheres acting as micro-containers for the drug and increasing the total drug capacity of the system. Its release from such a structure is slowed down by placing the microspheres inside the fibers so they are covered with an outer layer of fiber-forming polymer. The work presents a new method (microsphere suspension electrospinning) of obtaining polyvinylpyrrolidone fibers cross-linked with UV light modified with polycaprolactone/polyethersulphone microspheres loaded with active substance – rhodamine 640 as a marker or ampicillin as a drug example. The influence of UV-cross-linking time and the microspheres addition on the degradation, mechanical strength and transport properties of fibrous mats was investigated. The mats were insoluble in water, in some cases mechanically stronger, their drug capacity was increased and the burst effect was eliminated. The antibacterial properties of ampicillin-loaded mats were confirmed. The product of proposed suspension electrospinning process has application potential as a drug delivery system.

1. Introduction

Electrospun fibrous mats have been studied since the beginning of 20th century in the context of their potential use as controlled drug delivery systems. What makes them a very good candidate for this purpose are their great specific surface area, high porosity and structure similar to the extracellular matrix [1].

For the production of nano- and micro-thin fibers from a polymer solution or melt, the electrospinning method is used [2]. Synthetic polymers such as aliphatic polyesters e.g. poly(glycolic acid) (PGA), poly(lactic acid) (PLA), their copolymer (PLGA) and polycaprolactone (PCL), as well as hydrophilic polymers – poly(ethylene glycol) (PEG), poly(vinyl alcohol) (PVA) or polyvinylpyrrolidone (PVP) – are commonly used in the electrospinning process [3]. They have much greater strength, repeatability and processing flexibility than the natural ones, they can also help to avoid immunogenicity and pathogen transmission [4]. Polymers present in drug delivery systems should be appropriately selected for the nature of the drug used in them. For example, hydrophilic polymers (e.g. PVA) will be suitable for delivering water-soluble substances [5], while on the other hand, the use of hydrophobic polymers (e.g. PCL) delays the release of the substance, thus prolonging the performance of the system [6]. Electrospun PVP fibers are especially interesting in the context of drug delivery as they can be loaded with both types of drugs. Domokos et al. used fast dissolving properties of PVP to design orally disintegrating fibrous mats containing carvedilol – a poorly soluble in water active substance, while other systems were not able to provide its adequate therapeutic dose [7]. On the other side, Maciejewska et al. used PVP fibers to design antibacterial surfaces by functionalizing them with lysozyme – a hydrophilic antimicrobial enzyme. The fibers were electrospun with the addition of

* Corresponding author at: Nalecz Institute of Biocybernetics and Biomedical Engineering, Polish Academy of Sciences, 4 Ks. Trojdena St., 02-109 Warsaw, Poland.
E-mail address: amirek@ibib.waw.pl (A. Mirek).

https://doi.org/10.1016/j.bioadv.2023.213330
Received 18 November 2022; Received in revised form 24 January 2023; Accepted 2 February 2023
Available online 9 February 2023

benzophenone and cross-linked with ultraviolet light to reduce the solubility of the PVP (active substance carrier) in water [8]. PES-based ultrafine fibers also have the potential to be used as a drug carrier in drug delivery [9], e.g. for wound dressings [10].

Despite all their advantages that make electrospun fibers potentially applicable as controlled drug delivery systems, they also have some limitation. Microparticles and fibers designed as carriers share a common drawback – burst effect, a sudden initial uncontrolled release of the drug [11–13]. Once the system is placed in the release medium, there is a great ejection of the drug before the release rate reaches a stable profile [14]. This significantly increases the concentration of the drug in the initial phase of delivery and reduces the effective lifetime of the system as the amount of total burst-released substance might reach up to 55 % of the total release [15]. Burst release may result in unpredictable and undesirable effects, such as pharmacological risks, ineffective treatment, and economic losses [1]. Due to the fact that burst release is quick and short, most mathematical models for substance release ignore it. A solution to the burst release problem should therefore be sought in the appropriate modification of the drug delivery system.

Another limitation of classic electrospun fibrous mats is the relatively small capacity of such a system for an active substance. The electrospinning process usually takes several hours and produces fibers with nanometric diameters. The resulting mats are characterized by low weight due to the low output of the process (0.01–0.1 g/h, [16]) and high porosity (up to 99.2 %, [17]). The amounts of drugs that could be encapsulated in such a system are small (up to 10 mg), and the fibrous mat becomes useful only for low-dose applications [18]. In order to increase the capacity of the system for the drug, it is proposed, for example, to scale-up the electrospinning process [18], increase the fiber diameter [19] or modify fibers by in situ formation of microspheres within electrospun mats [20].

Various modifications of the electrospinning are used and they aim to improve the fibrous mats by giving additional properties to the fibers and removing the above-mentioned flaws of classical technique. Post-processing modifications can be applied to the electrospun fibers [21], but the process itself can also be modified, for example, by changing the shape of the electrospinning spinneret, replacing a simple single nozzle with coaxial [6], multiaxial [22] or side-by-side ones [23]. The result of such action is fibers with a complex multilayer structure of the core/shell or Janus type. This changes their transport properties for immobilized substances (e.g. the shell can slow drug release), mitigates the drawbacks relative to burst release and allows the development of mats made of polymers of two different types: hydrophilic and hydrophobic, which also broadens the application potential [24]. For example, Mo et al. conducted a coaxial electrospinning process with biologically active oil as a core and PCL as a shell which allowed the drug to be released for three days [25], and Zhao et al. developed PCL/Zein core-shell fibers loaded with metronidazole and prolonged the drug dissolution time from 18 h to 72 h [26].

Another modification is the emulsion electrospinning process in which the drug solution disperses in the form of micelles in the polymer solution to form a stable emulsion [27]. The advantage of this method is the minimized contact of the bioactive substance with an organic solvent that could damage it. Moreover, it does not require the use of coaxial electrospinning nozzle to form multilayer structures. Basar et al. fabricated the fibrous mat by emulsion electrospinning of a PCL/gelatin (O/W) emulsion with ketoprofen dispersed in oil phase. Such a system eliminated drug burst release effect and allowed it to be sustainably released for up to 4 days [28]. Shibata et al. improved the solubility of poorly water-soluble probucol (PBC) by dispersing it in PVA fibers electrospun from O/W emulsion where PBC was dissolved in ethyl acetate and PVA in water. Such a system enabled controlled release of poorly water-soluble drugs [29].

Another particularly interesting drug delivery system manufacturing method would be the combination of the electrospinning process with the production of drug-loaded microspheres. Such a solution would link the advantages of both techniques, eliminating their disadvantages. The use of microspheres as micro-containers for the active substance would increase the total volume of the system, while the fibers would allow it to maintain its integral structure, eliminating the risk of sphere migration. Such solutions are currently being developed mostly for the oil/water separation systems, such as the one proposed by Gao et al. [30]. They simultaneously electrospun polyvinylidene fluoride (PVDF) and electrospray SiO_2/PVDF microspheres to obtain the hybrid structure described above. The system combined the flexibility of the fibers with the hydrophobicity of the microspheres, which increased the oil adsorption capacity. In a similar way potential fibrous wound dressing materials can be designed [31,32]. Li et al. [31] proposed a multi-layered fibrous mat made by spraying the silk fibroin (SF)/chitosan (CS) microparticles onto the polycaprolactone (PCL)-polyvinyl alcohol (PVA) fibers. The system was found to have high encapsulation rate of bovine serum albumin (BSA) and good antibacterial effect. Gungor-Ozkerim et al. [32] created a “sandwich system” in which an electrosprayed growth factor-loaded gelatin microspheres layer was placed between two layers of electrospun fibers (PCL/PLA and PCL/gelatin). This system remained stable for at least 2 months, prevented microsphere migration, and the bioactive nature of growth factor was maintained. Another “sandwich system” was proposed by Nagiah et al. [33]. The results of their study show that a composite system consisting of doxycycline hyclate-loaded poly (vinyl alcohol) microspheres sandwiched between poly (3-hydroxybutyric acid) electrospun fibers has an initial burst release despite the multi-layered system. It is noteworthy that each of the above methods assumes the formation of microspheres and fibers independently, with subsequent combination at the collector. This results in the entanglement of microspheres within the fiber network, forming mixed systems. The microspheres are not immobilized within the fiber structure, covered with an outer polymer layer. Such a structure could potentially be achieved through a microsphere suspension electrospinning, which is currently an under-explored method. The authors of the present study have identified a limited number of investigations that delve into the topic of the utilization of this technique for the production of potential drug delivery systems. Xu et al. [34] developed a biodegradable drug delivery system (electrospun poly (l-lactic acid) fiber mats loaded with chitosan microspheres) using a suspension electrospinning method. In vitro dual release showed short-lived release of bovine serum albumin, but long-lasting release of benzoins in all dual drug release systems. The diameters of both the microspheres and fibers were observed to range between 1 and 3 μm.

The aim of the presented work was to develop a new potential drug delivery system based on water-insoluble polyvinylpyrrolidone fibers modified with polycaprolactone (or polyethersulfone) microspheres manufactured using a suspension electrospinning process. A series of actions were undertaken to achieve the research objective. Firstly, it was decided to modify PVP fibers with microspheres of diameters 10–20 times greater than fiber diameters, used as drug carriers. The intention was to increase the capacity of the entire system for the active ingredient and to eliminate the burst effect that normally may occur when microspheres or electrospun fibers are used as individual drug systems. The microspheres used for modification were prepared by a method combining pulsed voltage electrospray and wet phase inversion techniques, as detailed in a previous study [35]. Subsequently, in order to stabilize the complex suspension electrospinning process, it was decided to supply the electric charge in a pulsed manner (pulsed voltage – PV). This unconventional method introduces two additional electric process parameters – the duration of electric pulses and their frequency, which significantly improves the ability to control the electrospinning process [36,37] and in consequence the properties of the obtained fibers. Finally, to improve the stability of the modified fibrous mats and prevent their dissolution in water, crosslinking of PVP with ultraviolet light using benzophenone as a photoinitiator was evaluated as a potential solution. In accordance with the established assumptions, such a novel modified electrospun drug delivery system would maintain its

therapeutic potential in an aqueous environment and release the drug in a controlled, prolonged manner which would improve its effectiveness. To fully understand the properties and capabilities of the proposed system, a comprehensive set of experiments were conducted, including assessments of degradation in water and ethanol, evaluations of mechanical characteristics, spectrophotometric studies of marker content and release, and examination of the antibacterial properties of the drug-loaded mats.

2. Materials and methods

2.1. Materials

Poly(vinyl pyrrolidone) (PVP, M_w = 1300 kDa, CAS Number: 9003-39-8) was purchased from Acros Organics (Belgium), polycaprolactone (PCL, M_w = 70 kDa, CAS Number: 24980–41–4) was purchased from Scientific Polymer Products (USA) and polyethersulfone (PES, M_w = 42 kDa, Ultrason E2020) from BASF (Germany). Dimethylformamide (DMF, Chempur, Poland, CAS Number: 68–12–2, ≥99 %) and *N*-methyl-2-pyrrolidone (NMP, Chempur, Poland, CAS Number: 872–50–4, ≥98 %) were used as solvents for the polymers (PCL and PES respectively). Ethanol (EtOH, Polmos, Poland, ≥95 %) was used as a solvent for PVP and a PCL/PES non-solvent to induce phase separation in a precipitation bath. Benzophenone (BP, Sigma Aldrich, CAS Number: 119-61-9, ≥99 %) was used as a fiber UV-cross-linking photoinitiator. Hanks' Balanced Salt solution (HBSS) was used as a medium for cross-linked PVP mat degradation tests. The ingredients were purchased from POCH (Poland): sodium chloride (NaCl, CAS Number: 7647-14-5, ≥99.5 %), potassium chloride (KCl, CAS Number: 7447-40-7, ≥99.5 %), sodium phosphate dibasic (Na_2HPO_4, CAS Number: 7558-79-4, ≥98 %), potassium phosphate monobasic (KH_2PO_4, CAS Number: 7778-77-0, ≥99.5 %), calcium chloride ($CaCl_2$, CAS Number: 10043-52-4, ≥96 %), magnesium sulfate heptahydrate ($MgSO_4{\cdot}7H_2O$, CAS Number: 10034-99-8, ≥99 %), sodium bicarbonate ($NaHCO_3$, CAS Number: 144–55-8, ≥99 %), glucose (CAS Number: 50–99-7, ≥99.5 %), phenol (CAS Number, 108-95-2, ≥99 %). Rhodamine 640 perchlorate (M_w = 591.05 Da, Exciton, USA, CAS Number: 72102–91–1) was used as a drug marker. Ampicillin sodium salt antibiotic (CAS Number: 69–52–3) was obtained from A&A Biotechnology (Poland). The non-pathogenic Gram positive *Staphylococcus aureus* and Gram negative *Escherichia coli* bacteria (K12 DSM 423, from DSMZ, Germany) were chosen as a model microorganism. The culture medium was a Tryptone Salt Broth (TSB, Sigma Aldrich). The chemicals were used without further purification. All solutions were prepared with MilliQ water (with a resistivity of 18.2 MΩ·cm; Millipore, USA).

2.2. Microsphere preparation

Microspheres were prepared using a method combining pulsed voltage electrospray and wet phase inversion techniques which was elaborated in our Laboratory [35]. The process setup scheme is shown in Fig. 1A. In this method, the polymer solution (PCL in DMF or PES in NMP) is pressed through a metal nozzle connected to a high pulsed voltage. At the nozzle outlet, electrospray process occurs and microdroplets are formed. Then, they are collected in a well-stirred precipitation bath filled with a non-solvent of the polymer. In this bath, wet phase inversion process takes place according to the Gibbs phase rule and solidified polymer microspheres are formed. The method can be modified by adding various substances (e.g. drug) to the polymer solution and bath and hence immobilizing them inside the microspheres.

The following polymer solutions were prepared to manufacture microspheres: 15 % PCL in DMF and 15 % PES in NMP. In order to prepare microspheres with an immobilized rhodamine or ampicillin, polymer solutions containing 0.57 mg/g (marker mass/polymer mass) of marker/ampicillin were used. The active substance was also added to the precipitation bath in the amount of 0.1 mg/mL. The values of the electrical parameters in the study were set as follows – electrical voltage U = 8 kV, pulse frequency f = 60 Hz, pulse duration τ = 6 ms. The polymer solution was delivered to the nozzle at a flow rate of 1.5 mL/h. After the formation of microspheres, the collecting bath content was transferred to a falcon and centrifuged in order to remove the excess ethanol off above the sedimented microspheres. Finally, they were dried at room temperature for several days to take the powder form ready for weighing and use in the next part of work. The temperature did not exceed 25 °C and a humidity – 40 % during whole procedure. The average diameters of the obtained microspheres were 14.38 ± 6.28 μm for PCL and 6.20 ± 2.43 μm for PES.

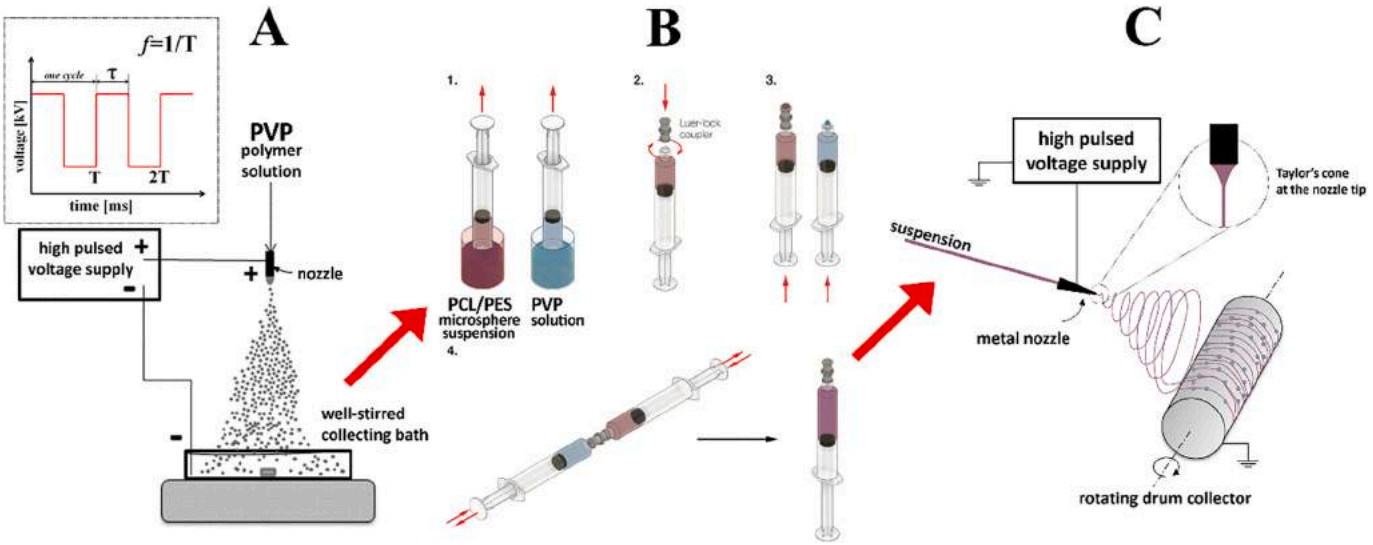

Fig. 1. The consecutive stages of the process of the manufacturing of polymer fibrous mats modified with microspheres. (A) Scheme of the process of microspheres production using the method developed previously by the authors [35]. (B) Scheme of mixing microspheres with polymer solution to obtain a suspension of microspheres by the syringe coupler method proposed by Allevi, Inc. [38], image used with permission from Allevi. (C) Scheme of the microsphere suspension electrospinning process on a drum collector.

2.3. Suspension electrospinning

The syringe coupler method (Fig. 1B) was used to prepare the suspension for electrospinning. 5.4 mL of the PVP solution in ethanol at the concentration of 18.5 % with the addition of benzophenone at the concentration of 3.75 % was placed in one syringe. 4.6 mL of the suspension of PCL or PES microspheres in the amounts of 50–300 mg in ethanol was placed in the other syringe. The syringes were connected using a syringe coupler and their contents mixed by moving the plungers back and forth approximately 40–50 times. In this way, a suspension of microspheres with a concentrations of 5–30 mg/mL in a PVP solution with a concentration of 10 % in ethanol with the addition of BP in an amount of 2 % was obtained.

The fibrous mats without the addition of microspheres were also electrospun for degradation tests and comparison purposes, using a PVP solution with a concentration of 10 % in ethanol with the addition of BP (2 %).

The electrospinning process was performed using a setup showed in the Fig. 1C. It is comprised of a custom-built high voltage pulse generator, an infusion pump with a syringe filled with microspheres/polymer suspension, a steel nozzle (external diameter of 0.9 mm), and a rotating grounded aluminum drum collector (diameter 47.5 mm, width 150 mm) placed 15 cm from the nozzle tip. The flow rate of the electrospun suspension was set as 0.6 mL/h. To avoid clogging the nozzle, the fibers were electrospun using pulsed voltage (PV) with electrical parameters – voltage U = 8 kV, pulse frequency f = 100 Hz, pulse duration τ = 8 ms. The geometric shapes of the suspension at the end of the nozzle were recorded. The resulting fibrous mats were being collected on a drum collector (rotation speed 120 min^{-1}) for 6 h each, the total volume of the electrospun solution was thus approximately 3.6 mL. After the process was completed, the polymer mats were cross-linked using ultraviolet light (365 nm). They were UV-exposed on each side for 5 min, 15 min and 60 min and marked 2 × 5 min, 2 × 15 min, and 2 × 60 min, respectively.

2.4. Characterization of the electrospun mats

The morphology of the polymer fibers with microspheres was examined using digital microscope (Keyence, VHX-7000) and SEM – the samples were coated with 10 nm thick gold layer for it. The microspheres in the mats were counted and their quantity *N* was determined as microspheres/mm^2. The diameters of 100–200 randomly selected fibers on a set of approximately 5–6 images for each condition were measured using the microscope software and their average values *d* were calculated. The statistical analysis of the obtained data was performed by determining the standard deviation from the mean value (*SD*) and the coefficient of variation (VC), which is represented as a percentage of the ratio of *SD* to the mean diameter (*d*).

The degradation of the UV-cross-linked fibrous mats was investigated. Samples 2 × 5 min, 2 × 15 min and 2 × 60 min of 5–6 mg weight were placed in 10 mL of HBSS solution each. The HBSS solution was prepared according to the method given in literature [39]. It was used because of its similar composition to blood plasma [40]. The degradation was carried out at 37 °C in a laboratory cradle with a rocking speed of 10 cycles per minute. The influence of degradation was assessed using scanning electron microscopy (SEM, Hitachi TM-1000) pictures of the mats made before the process, after 6 h and after 24 h. The diameters of 50 randomly selected fibers after degradation were measured and their average values were calculated. In addition, a long-term degradation test was performed – a 2 × 60 min mat sample was placed in ethanol for 2 months, and then analyzed by SEM.

The mechanical properties of the fibrous mats were tested using Zwick Roell ProLine tensile testing machine (Germany) with a solid fixture – tensile strength and elongation at break were measured. Mats were carefully peeled off from the aluminum collector surface and cut into 50 × 10 mm strips with the thickness about 0.3 mm. The speed of tensile testing was 0.2 mm/s. Five specimens were tested for each sample type. The mean values of mechanical parameters were determined as well as the statistical analysis of the obtained data was conducted, including the determination of the standard deviation (SD) and the coefficient of variation (VC) expressed as a percentage ratio of SD to the mean value. The measurement setup is shown in Fig. SI1 (supporting information). Microsoft Excel, OriginPro and GraphPad Prism software were used to perform all calculations and analyses as well as to plot the graphs.

2.5. Rhodamine immobilization in the mats

In order to check how the addition of microspheres increases the capacity of the system for the active substance compared to fibers without the addition, four types of electrospun fibrous mats with a marker (rhodamine) were made: without microspheres with the content of rhodamine in the electrospinning solution 0.0575 mg/mL, with rhodamine-loaded PCL microspheres at 10 mg/mL or 20 mg/mL and with rhodamine-loaded PES microspheres at 20 mg/mL. In each case, the microspheres which were used, were made by the technique described above, from a solution containing 0.1 mg/mL of rhodamine. They were distributed in an electrospinning solution with a rhodamine content of 0.0575 mg/mL. Two samples were taken from each mat and UV-cross-linked 2 × 5 min and 2 × 15 min. Then 4.4–6.7 mg of material were taken from each of them and placed in 2.40–3.65 mL of RO water, the volume of which was adjusted so that the ratio of mat weight to this volume remained the same in each case (5.5 mg/3 mL). Rhodamine was released from the mat samples for 4 h using a lab shaker to agitate the system. After this time, the rhodamine concentration in each of the solutions was determined using a spectrophometric method (light wavelength: 574 nm). The mean values of rhodamine concentration were determined based on three tests, the standard deviation (SD) and the coefficient of variation (VC) were determined as a part of statistical analysis.

2.6. Study of the rhodamine transport properties of the mats

For the study of rhodamine release profile, three types of mats were produced – with marker and no microspheres (PVP_Rod), with marker-loaded PCL microspheres (PVP_PCL/Rod) and with marker-loaded PES microspheres (PVP_PES/Rod). The amount of rhodamine was selected, and the mats were suitably prepared so that marker content in each mat (15 × 15 cm, fibers and microspheres) was ~0.6 mg. After the process was completed, the polymer mats were cross-linked using ultraviolet light for 2 × 5 min and 2 × 15 min. The kinetics of rhodamine release from fibrous mats was determined using a flow spectrophometric method (light wavelength: 574 nm). Two round samples with diameter of 14 mm and thickness 150–300 μm each and overall weight 5.0–6.5 mg were cut from each mat and placed together in a well-stirred glass container with 2.7–3.5 mL (V_0) of deionized water, the volume did not change during the experiment. Absorbance measurements were made every 2 min for the first 2 h, every 10 min for the next 1 h, every 30 min for the next 2 h, and after 6, 7 and 24 h after starting the experiment. The mean value of absorbance was determined based on a series of three experiments per case. The rhodamine release profiles were plotted on graphs. The transport properties of the tested mats towards rhodamine were investigated. They can be described with a linear function fitted to the plotted experimental points in the first stage of the substance release. The linear fitting in OriginPro software gave the equation of the line describing each case $y = \alpha x$, where α defines the slope of the line and thus the substance release rate.

The shape of the marker release curves from microsphere-loaded mats allows the use of a more complex Radcliff model [41] for the mathematical description of the release profile. According to Radcliff, mass transfer between two phases can be generally described by Eq. (1):

$$V_0\frac{dC}{dt} = -hA(C - C_S) \quad (1)$$

where: C (mg/mL) – the marker concentration in liquid outside the material (mats), C_S – concentration of the marker inside the material (mats) close to interphase boundary, A (cm^2) – interface surface area (total external surface area of the mats), V_0 (cm^3) – the volume of liquid outside the material (mats). The symbol h (cm/min) designated the mass transfer coefficient which describes the substance release rate in the first release period before equilibrium is reached.

Taking into account the specificity of the electrospun mats, it can be assumed that their entire volume is available for the marker, the marker does not reabsorb inside the material and initial marker concentration in solution is equal to 0, Eq. (1) can be supplemented with the mass conservation Eq. (2):

$$\frac{d(V_0C + V_CC_S)}{dt} = 0 \quad (2)$$

where V_c (cm^3) – the volume of fibers.

After solving Eq. (1) in this case, the change in the marker concentration in the surrounding solution is described by the Eq. (3) [42]:

$$C = C_{eq}\left(1 - e^{-hA\left(\frac{1}{V_0}+\frac{1}{V_C}\right)\bullet t}\right) \quad (3)$$

where: C_{eq} (mg/mL) – equilibrium marker concentration, t (min) – time (independent variable).

Mathematical modeling of the process of rhodamine release from fibrous mats containing microspheres was performed with OriginPro software. The curves were fitted to the data using the exponential fit with the *BoxLucas1* mathematical model available in the program library which is described by Eq. (4):

$$y = a \bullet \left(1 - e^{-bx}\right) \quad (4)$$

where: a, b – Origin model equation coefficients and x – independent variable.

After the comparison of the power exponents in Eqs. (3) and (4), the following relationship is obtained:

$$-hA\left(\frac{1}{V_0}+\frac{1}{V_c}\right) \bullet t = -b \bullet x \quad (5)$$

Finally, after solving the Eq. (5), assuming that $x = t$ (variable), the expression for the coefficient h is as follows:

$$h = \frac{b}{A\left(\frac{1}{V_0}+\frac{1}{V_c}\right)} \quad (6)$$

In order to determine the coefficient h, the values of b, A, V_0 and V_C must be determined.

Value of parameter b was generated by the *OriginPro* software using *BoxLucas1* mathematical model described by Eq. (4). An example of fitting the exponential model curve to the experimental results in the form of a graph with data generated by the software is shown in Fig. SI2A, while the geometric interpretation of model parameters a and b in Fig. SI2B (supporting information). The graphical interpretation of the h coefficient (associated with the parameter b) is the first derivative of the *BoxLucas1* function, while the value of the parameter a corresponds to the equilibrium concentration C_{eq} determined by the software. Interface surface area A was determined for each sample using nitrogen adsorption–desorption isotherms (BET analysis) at liquid nitrogen temperature using Micromeritics ASAP 2010 equipment (degassing conditions: 30 °C, 24 h). Solution volume V_0 is selected for each sample and varies from 2.7 to 3.5 mL. Sample volume V_c was estimated from the dimensions of the sample (cylinder of 14 mm in diameter and 0.2 mm in height on average) and its value equals approximately 0.031 cm^3. The standard deviation (SD) and the coefficient of variation (VC) for h values were determined as a part of statistical analysis.

2.7. Antibacterial activity of the electrospun mats loaded with ampicillin

For the antibacterial tests three types of fibrous mats were prepared – with no ampicillin, with ampicillin-loaded PCL microspheres and with ampicillin-loaded PES microspheres. Two types of mats were tested – cross-linked for 2 × 5 min and 2 × 15 min. The UV cross-linking provided sample sterilization too.

The antibacterial activity of ampicillin-loaded mats was examined against *Staphylococcus aureus* (*S. aureus*, Gram positive) and *Escherichia coli* (*E. coli*, Gram negative) bacteria. Fresh Tryptone Salt Broth (TSB) medium was inoculated by bacteria and incubated overnight at 37 °C in aerobic conditions. Bacterial cells were harvested by centrifugation and resuspended in a TSB when the stationary phase was reached. The bacterial suspension was then diluted to adjust the optical density at 620 nm (OD_{600}) to 0.75 ± 0.01 for *S. aureus* and 0.80 ± 0.01 for *E. coli*. Mueller-Hinton agar (GMH) plates were prepared by adding microbiological agar (15 g/L) to PBS medium; rectangular dishes were used. GMH agar plates were inoculated individually with 1 mL of *S. aureus* or *E. coli* suspension. Immediately after, the mat samples (10 × 10 mm) were put onto the plates to check their ability to prevent bacterial growth. Each sample contained approximately 0.003 mg of ampicillin. The plates were incubated at 37 °C in aerobic conditions overnight to allow the form a bacterial biofilm. To show inhibited bacterial growth (the clear zones), plates were pictured with a camera. The results of the study, which were obtained through three replicates of each test condition, were then quantified by measuring the diameter of the inhibition zone and calculating its area. The average values, along with standard deviations and coefficients of variation, are presented in a bar chart for ease of interpretation.

3. Results and discussion

3.1. Influence of UV-cross-linking on the fibrous mat degradation

The influence of the UV-cross-linking time of fibrous mats on their structure and properties was investigated. Fig. 2 shows SEM pictures of mats at successive stages of degradation in HBSS. Fig. 3 shows the change in fiber diameter during degradation.

The fibrous mat retains its structure regardless of the UV-cross-linking time (Fig. 2A, D, G), and the fiber diameters do not change ("0" bars in Fig. 3). The addition of BP and the UV-cross-linking process do not influence the smoothness of the fibers neither which was previously confirmed by Maciejewska et al. [8]. The mat UV-cross-linked for 2 × 5 min shows the phenomenon of formation of an outer layer ("skin") on the surface after 6 h (Fig. 2B) and 24 h of degradation (Fig. 2C). This "skin" is formed on both sides of the mat (Fig. 2J). Such a skin is not formed during the degradation of the UV-cross-linked mat 2 × 15 min and 2 × 60 min. In both of these cases, the fibers fuse with each other, creating irregular structures – in the case of the 2 × 15 min mat, this effect is visible after 24 h (Fig. 2F), and in the case of the 2 × 60 min mat also after 24 h (Fig. 2I) – marked in red circles.

UV-cross-linking of PVP fibers with benzophenone addition prevents their degradation not only in the aquatic environment. The mat UV-cross-linked for 2 × 60 min was placed in ethanol for 2 months. The degradation effect is different than in the case of the aqueous solution, there is no "skin". The fibers are highly swelled, the mat lost its original structure of individual, randomly arranged fibers, which stuck together, but did not completely degrade (Fig. 2K). This seems particularly relevant in view of the potential use of such fibers as a drug delivery system, because it opens the possibility of sterilizing the material using ethyl alcohol instead of, for example, UV radiation, which would alter the properties of the fibers through UV-cross-linking.

With the degradation time, the mean diameters of the UV-cross-

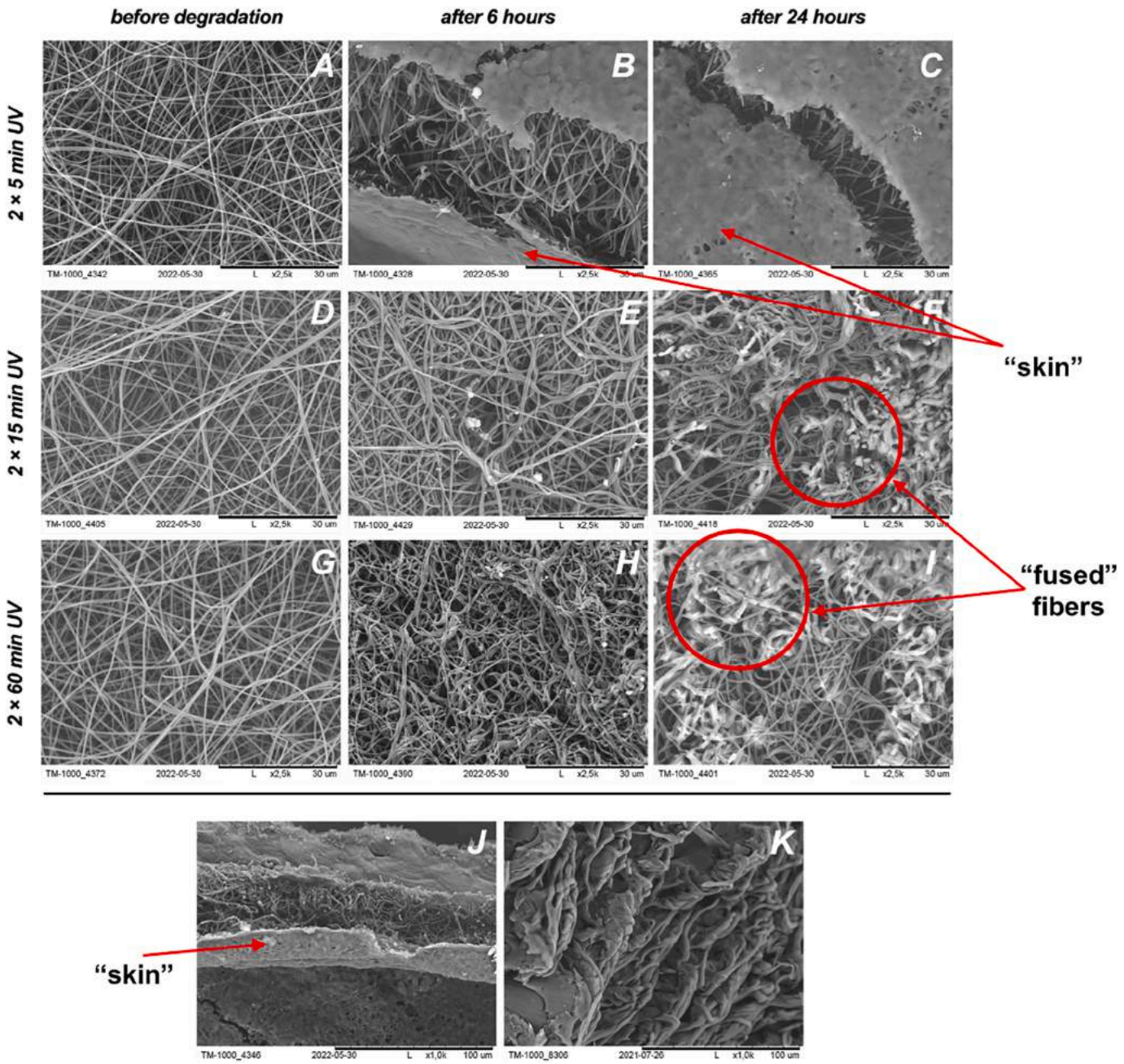

Fig. 2. Exemplary SEM pictures of the UV-cross-linked PVP fibers (without the addition of microspheres) at various stages of degradation in (A–J) HBSS or (K) ethanol. (A–C) cross-linking 2 × 5 min: (A) before degradation, (B) after 6 h of degradation; (C) after 24 h. (D–F) cross-linking 2 × 15 min: (D) before degradation, (E) after 6 h of degradation; (F) after 24 h. (G-I) cross-linking 2 × 60 min: (G) before degradation, (H) after 6 h of degradation; (I) after 24 h. (J) cross-linking 2 × 5 min after 24 h of degradation, side section. (K) cross-linking 2 × 60 min after 2 months of degradation in ethanol.

linked fibers for 2 × 5 min and 2 × 15 min increase from 0.5 to 0.7 μm, while UV-cross-linked fibers for 2 × 60 min do not change diameter. Furthermore, it can be observed that the uniformity of the fibers decreases, as evidenced by an increase in the coefficient of variation of diameter, which change from 13 % for non-cross-linked fibers up to 27 % for the cross-linked ones.

This effect is most likely due to the swelling of the fibers, which is more difficult in the case of a highly UV-cross-linked fibrous mat (2 × 60 min). This property of UV-cross-linked PVP fibers is not unexpected considering the fact that PVP is used, among others, to produce electrospun fibrous hydrogels capable of absorbing high levels of water or media uptake, spanning from 400 wt% to 1400 wt% [43].

The degradation process of the tested UV-cross-linked fibers can be divided into several stages. In the first stage, the slow swelling of the UV-cross-linked fibers leads to an increase in their diameters. In the second stage, the fibers begin to dissolve and lose their original structure (they join and fuse to form homogeneous structures on the surface, which may eventually take the form of a layer – "skin"). Such a layer, after drying, breaks, revealing non-degraded fibers inside (third stage).

The degradability of the UV-cross-linked PVP fibrous mats can be controlled by selecting the cross-linking time or the appropriate amount of benzophenone, as well as the thickness of the mat and the fiber diameters [44]. Such a system requires optimization with regard to its potential application.

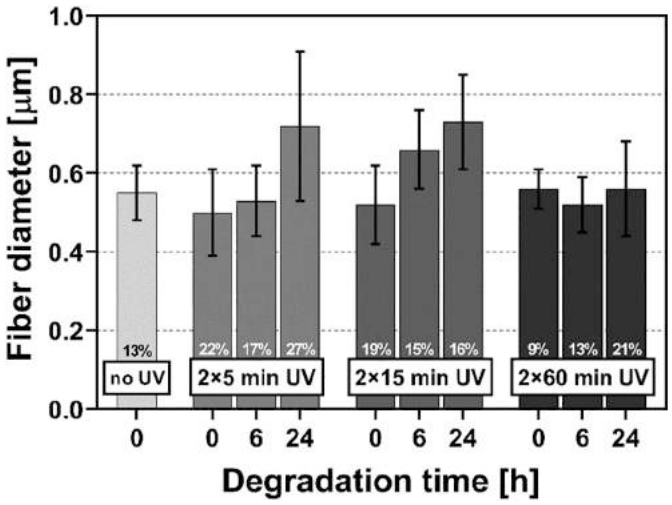

Fig. 3. Mean diameters of the UV-cross-linked PVP fibers (without the addition of microspheres) at various stages of degradation. The coefficient of variations of fiber mean diameter is indicated on each corresponding bar.

3.2. Microsphere suspension electrospinning feasibility

The feasibility of electrospinning of the PVP solution with PCL microspheres suspended was tested by checking their different contents in the initial suspension until a value was reached at which electrospinning did not proceed. The study was carried out only with PCL microspheres. Non-cross-linked mats were used in the research. Fig. 4 presents SEM pictures of fibers depending on the content of microspheres in the suspension Q [mg/mL] with the estimated content of microspheres in the mats N [mm^{-2}] and fiber mean diameter d [μm].

Electrospinning of a suspension of PCL microspheres in a PVP solution is possible, but there is a limitation in the amount of microspheres at which such a mixture is no longer electrospinnable. In the present work, it was determined as >20 mg of microspheres per 1 mL of solution. Below this value, for the microspheres contents of 5 mg/mL and 10 mg/mL, electrospinning is stable and the fibers with microspheres (Fig. 4A–B) are collected. For the microspheres content of 20 mg/mL, the resulting mat contains the most microspheres, according to predictions (Fig. 4C). The 30 mg/mL microspheres content turned out to be too high – fibers are not formed on the collector. Solvent evaporates too quickly, polymer clogs the nozzle in the case. It was therefore decided to conduct electrospinning with a microspheres content of 20 mg/mL because of the high content of microspheres in the mat and that potentially increases its volume, which is the main goal of our work.

The microspheres in the fibers are mostly centrally located and covered with a polymer (like in core/shell fiber type), as can be seen in the SEM photos in Fig. 4D–E, and confirmed by optical microscope studies, due to the fact that PVP fibers are transparent (Fig. 4F). This fiber structure (microspheres covered by the outer polymer layer) is desirable in drug delivery systems as it can limit the burst effect [22]. It was noticed that the amount of microspheres added did not affect the diameter of the fibers.

3.3. Mechanical properties

Mechanical properties of mats depending on the content of microspheres, their type and cross-linking time were investigated. The results in the form of graphs showing tensile strength and elongation at break are summarized in Fig. 5.

UV-cross-linking improves the mechanical strength of fibers without microspheres (red bars, Fig. 5) – tensile strength is increased from about 0.2 MPa to 0.25 MPa, while elongation at break from 10 % up to 25–35 % (depending on cross-linking time). Interestingly, the longer the cross-linking time, the lower the fiber strength for both types of fibers – those without the addition of microspheres and those containing PCL or PES microspheres. The values of the variation coefficients of the relevant parameters serve as an indication of the accuracy of the measurement method employed, and if they surpass 10–15 %, they can be understood as an indication of the inhomogeneity of the fibrous mats.

The phenomenon of improving the mechanical strength of PVP fibers UV-cross-linked with benzophenone was also noted by Maciejewska et al. [8] who explained it by the cross-linking mechanism. Benzophenone is a photoactive molecule which, after absorption of a UV photon with a wavelength of 250–365 nm, is excited and produces a ketyl

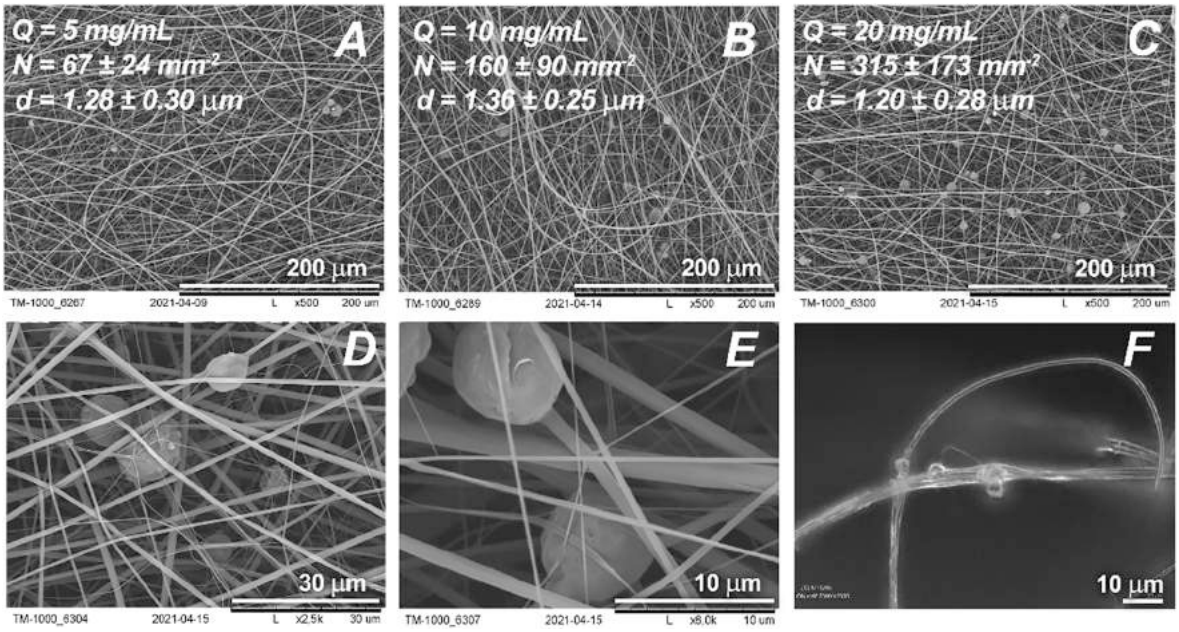

Fig. 4. (A–C) Exemplary SEM pictures (magnification 500×) of PCL microsphere-loaded PVP fibers depending on the content of microspheres in the suspension Q [mg/mL]: (A) 5 mg/mL, (B) 10 mg/mL, (C) 20 mg/mL. (D–E) Exemplary SEM pictures of fibers with PCL microspheres, magnification (D) 2500×, (E) 8000×. (F) Exemplary optical microscope picture of PVP fibers with PCL microspheres, magnification 2500×.

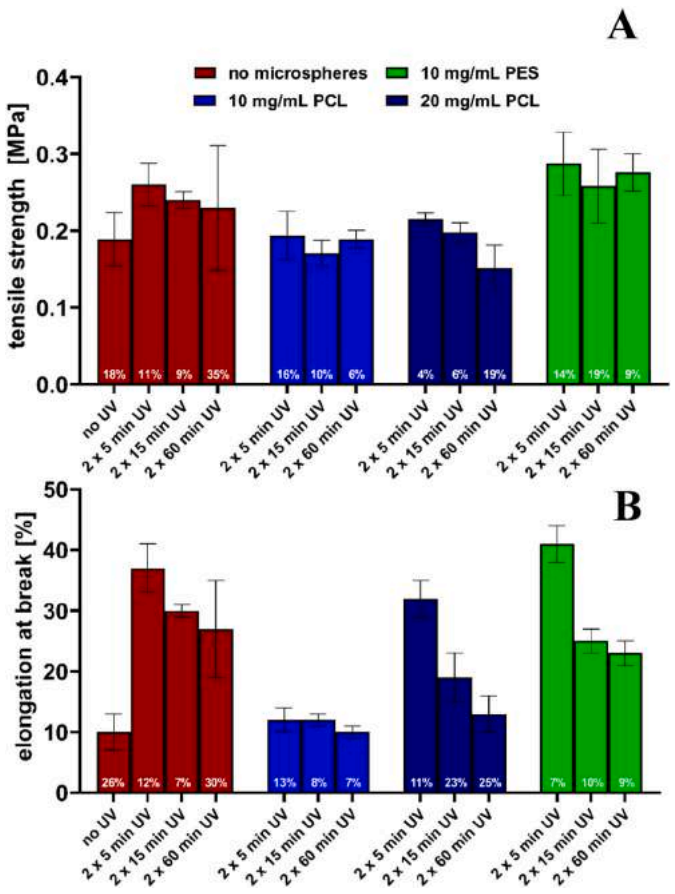

Fig. 5. Mechanical properties of UV-cross-linked microsphere-loaded PVP fibrous mats depending on the quantity and type of microspheres and cross-linking time: (A) tensile strength, (B) elongation at break. The coefficient of variations of mechanical parameters is indicated on each corresponding bar.

radical that affects the PVP molecule [45,46], see Fig. 6. The C—H bond in the CH_2 group adjacent to nitrogen is the weakest bond in lactams and N-alkylamides [47], therefore generation of a macroradical occurs on this group in PVP monomer. There are two potential sites for radical formation – one C atom in the lactam ring (4) and one C atom in the polymer chain (5) (Fig. 6). Abstraction of H atoms from the N adjacent carbon is achieved by the ketyl radicals. An aliphatic carbon-centered radical is formed (reaction (I) in Fig. 6) [45] as well as an alkyl radical which in the presence of oxygen is immediately oxidized to a peroxy radical transforming subsequently into pyrrolidone hydroperoxide (reaction (II) in Fig. 6) [46]. Ultimately, all the radicals that are generated recombine with each other to form a polymer net based on different cross-linking bonds (Fig. 6). The resulting covalent bonds increase the crowding of the molecules and shorten the distance between the atoms, thus tightening the polymer net. Such action makes the tensile strength and elongation at break of cross-linked fibers greater than that of non-cross-linked fibers. However, the longer the cross-linking time is, the more free radicals and more bonds in the polymer mesh are formed. Its elasticity decreases, and the more and more dense structure becomes prone to breaking.

The mechanical properties of fibrous mats change when the fibers are electrospun with the addition of microspheres. In the case of PCL microspheres, a decrease in their strength can be noticed compared to pure PVP fibers (blue bars, Fig. 5) – both for the content of microspheres of 10 mg/mL and 20 mg/mL, but the addition of a larger amount improves the mechanical properties, especially for a short cross-linking time (2 × 5 min). The addition of PES microspheres increases the mechanical strength of mats in relation to both pure PVP fibers and those with the addition of PCL – again especially for a short cross-linking time. A similar phenomenon of increasing the mechanical strength of fibers after adding microspheres was previously noted by Balzamo et al. [20].

Different properties of fibrous mats with the addition of PCL and PES may result from differences in the size of the microspheres. PES microspheres have more than twice smaller diameters than PCL ones (14.38 ± 6.28 μm for PCL and 6.20 ± 2.43 μm for PES) [35]. As a result, in the case of PCL microspheres in the fibrous net, there are more places where one microsphere is at the interface of two (or more) fibers, which obviously weakens the entire structure.

The microspheres are firmly attached to the fibers which can be observed in SEM pictures (Fig. 4E–F). During the strength tests and application of stress, the fibers elongate, change diameter, and align along the direction of the force while the microspheres maintain their shape and resist the tensile stress by holding the fibers. In addition, there is a high probability that during cross-linking with ultraviolet light, in the structure of microsphere-forming polymers free radicals may be formed too – both PCL and PES may undergo such a reaction [48,49]. These radicals can increase the strength of the polymer net by formation of the bonds between the fibers and the microspheres. This results in a higher stress required to rupture modified fibers.

Extending the cross-linking time of fibers makes them much less flexible (which is reflected in the elongation at break parameter, Fig. 5B), and thus much less mechanically resistant. There are no significant differences between the strength of UV-cross-linked fibers for 2 × 15 min and 2 × 60 min. Due to this, it was decided to reject the 2 × 60 min UV-cross-linked samples in the course of further research.

3.4. Rhodamine immobilization in the mats

In Fig. 7 a bar graph is presented showing the equilibrium concentration of rhodamine in solution after the release from PVP fibers UV-cross-linked for 2 × 5 and 2 × 15 min depending on the content of microspheres in the fibers and type of microspheres.

Fig. 7 shows that the addition of microspheres increases the drug capacity of the electrospun fibrous mat. Increased content of PCL microspheres from 10 mg/mL to 20 mg/mL increases the concentration of released rhodamine from about 0.0017 mg/mL to 0.0024 mg/mL for a 2 × 5 min sample. The addition of PES microspheres in the amount of 20 mg/mL does not cause the same increase in the capacity of the mat for the drug as the addition of PCL microspheres in this amount for the 2 × 5 min sample. This is due to the greater interface surface area of the PCL-microsphere-loaded fibers (10.20 ± 0.40 m^2/g) which is almost two times larger than the surface of PES-microsphere-loaded ones (5.17 ± 0.10 m^2/g), see Table 1. Fig. 7 also shows that the extended cross-linking time reduces the amount of rhodamine released from the microsphere-loaded fibers, confirming that UV radiation may have an effect on the marker content of the system. The process of UV-cross-linking with benzophenone resulted in the loss of the pink color of mats visible with the unaided eye, which was reflected in the determination of the amount of released rhodamine using the spectrophometric method.

In the current study, the diameters of the microspheres are significantly larger in comparison to the diameters of the fibers (up to 20 times), which serves as a contributing factor to the augmented capacity of the system for the active ingredient. Other systems, as previously documented in the literature, have employed microspheres with diameters that range from

1–3 μm [31,34], 36–39 μm [32] or 10–100 μm [33], however, none of the studies has evaluated the extent to which the total volume of the system has increased. The capacity of the proposed system for the active substance can be controlled by selecting the type, size and concentration of microspheres. The amount of the active substance should be selected depending on its specific therapeutic dose and individual needs.

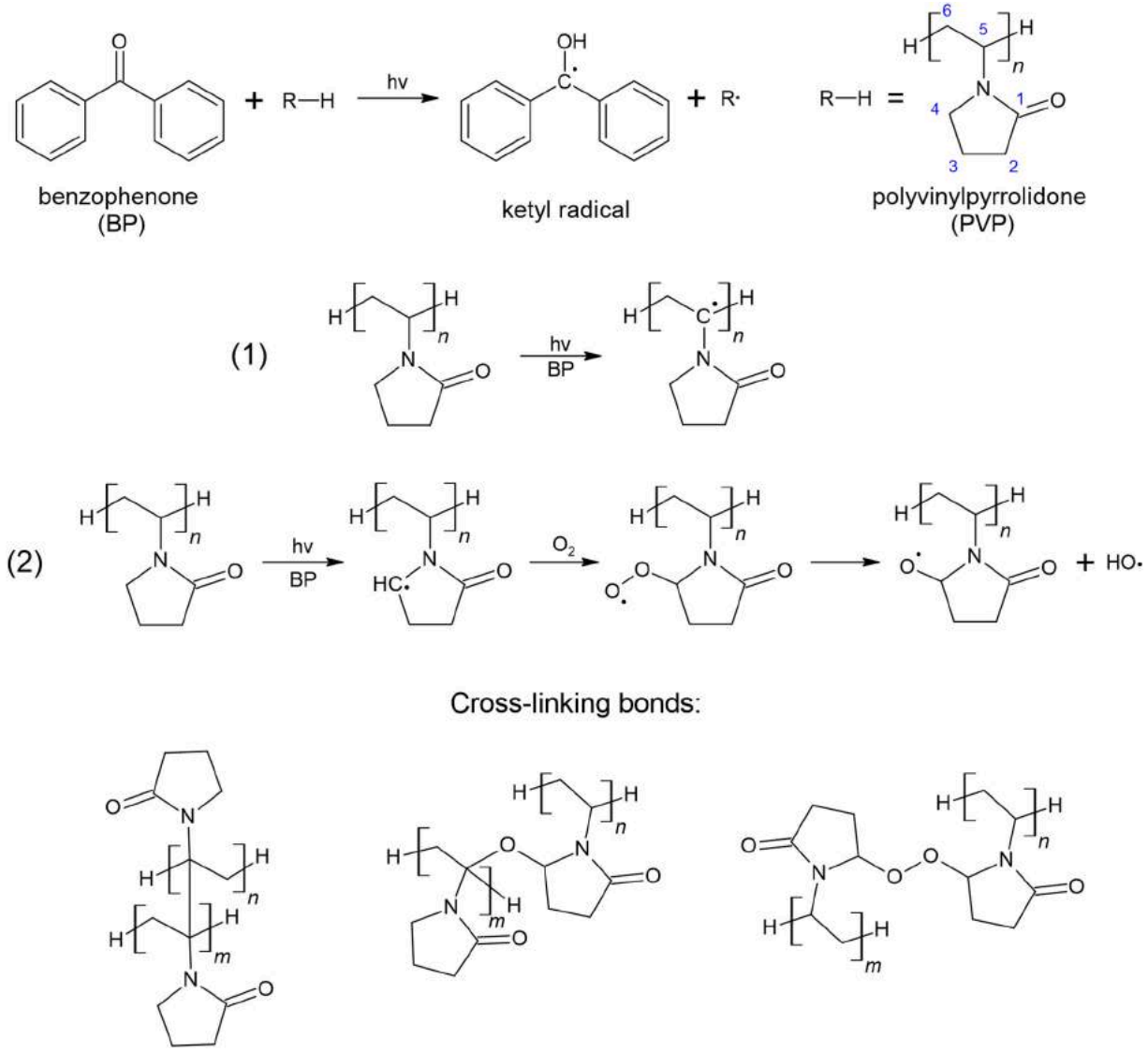

Fig. 6. Reaction mechanism of the formation of cross-linking bonds of PVP. Photocatalytic formation of free radicals and PVP hydroperoxide species [45,46].

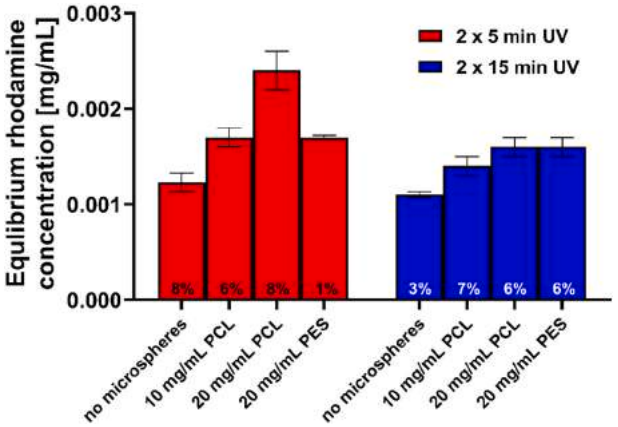

Fig. 7. Equilibrium rhodamine concentration after 4 h of release from UV-cross-linked PVP fibers with the addition of substance-loaded microspheres depending on the quantity and type of microspheres and cross-linking time. The coefficient of variations of equilibrium rhodamine concentration is indicated on each corresponding bar.

Table 1
Specific surface of microsphere-loaded fibers *A* and the transport coefficient *h* depending on the type of microspheres and the cross-linking time of the mats.

Sample	Coefficient of determination R^2 [−]	BET surface area *A* [m^2/g]	Transport coefficient $h \times 10^{-6}$ [cm/min] ± VC [%]
PVP_PCL/ Rod_2 × 5	0.9812	10.20 ± 0.40	2.32 ± 17 %
PVP_PCL/ Rod_2 × 15	0.9513	4.36 ± 0.19	6.43 ± 8 %
PVP_PES/ Rod_2 × 5	0.9367	5.17 ± 0.10	26.58 ± 11 %
PVP_PES/ Rod_2 × 15	0.9031	4.77 ± 0.09	5.69 ± 18 %

3.5. Kinetics of rhodamine release

The controlled substance release is an important ability of the fibrous mat from the point of view of its potential use as a drug delivery system. The next stage of research within the framework of the present work focuses on investigating rhodamine release profiles from the designed electrospun UV-cross-linked polyvinylpyrrolidone fibers modified with

polycaprolactone/polyethersulfone with a specific focus on the kinetics of the release process during the first stage. Fig. 8 contains the plots showing the rhodamine release profiles from different fibrous mats over the period of 24 h. The curves are divided into three groups differing in colors, red for samples of rhodamine-loaded PVP fibers without microspheres, blue for PCL/Rod-loaded fibers and green for PES/Rod-loaded ones. The bar plot in Fig. 8 the values of transport coefficient *h* determined with *OriginLab* software using Eq. (4).

For UV-cross-linked PVP electrospun fibers, the burst effect occurring at the beginning of the release process is clearly visible in the rhodamine release profiles of PVP_Rod mats without the addition of microspheres (Fig. 8A). It is characterized by a very rapid increase in the marker concentration above the equilibrium concentration reached later. For the 2 × 5 min UV-cross-linked fibers, the rhodamine concentration after burst release is about 0.33 mg/mL, and then it drops to 0.20 mg/mL in the equilibrium state. In the case of a 2 × 15 UV-cross-linked sample, this difference is smaller, and the mentioned concentrations are 0.14 mg/mL and 0.9 mg/mL, respectively. The decrease in this concentration is certainly not related to the adsorption of rhodamine in the measuring system, because appropriate tests were carried out before starting the experiments and such a problem was eliminated. This decrease may be the result of the cross-linking blocking the rapid release of substances from the fibers. In a highly cross-linked fibrous mat, the distances between the polymer chains are smaller according to the cross-linking mechanism described before. In such a case, the relatively large rhodamine molecule (591.06 g/mol) may have difficulty diffusing outward from the densely packed polymer net. The reduction of burst effect from cross-linked fibrous mats was also observed by Zhang et al. [50] who electrospun of polyvinyl alcohol/collagen fibers. They eliminated the burst effect of salicylic acid release after 4 h of UV-cross-linking.

Burst release occurs in the first 30 min of the experiment and the close-up of this period is shown in Fig. 8C. Fitting the model of the straight line to the experimental points allows one to obtain the value of the slopes, which explicitly determines the speed of the ongoing process. For fibers without microspheres cross-linked longer, the burst effect is lower, the slope of the line is more than twice as low (α = 0.649 for PVP_Rod_2 × 5 and α = 0.296 for PVP_Rod_2 × 15). The modification of the fibers by the addition of microspheres resulted in a slower release of

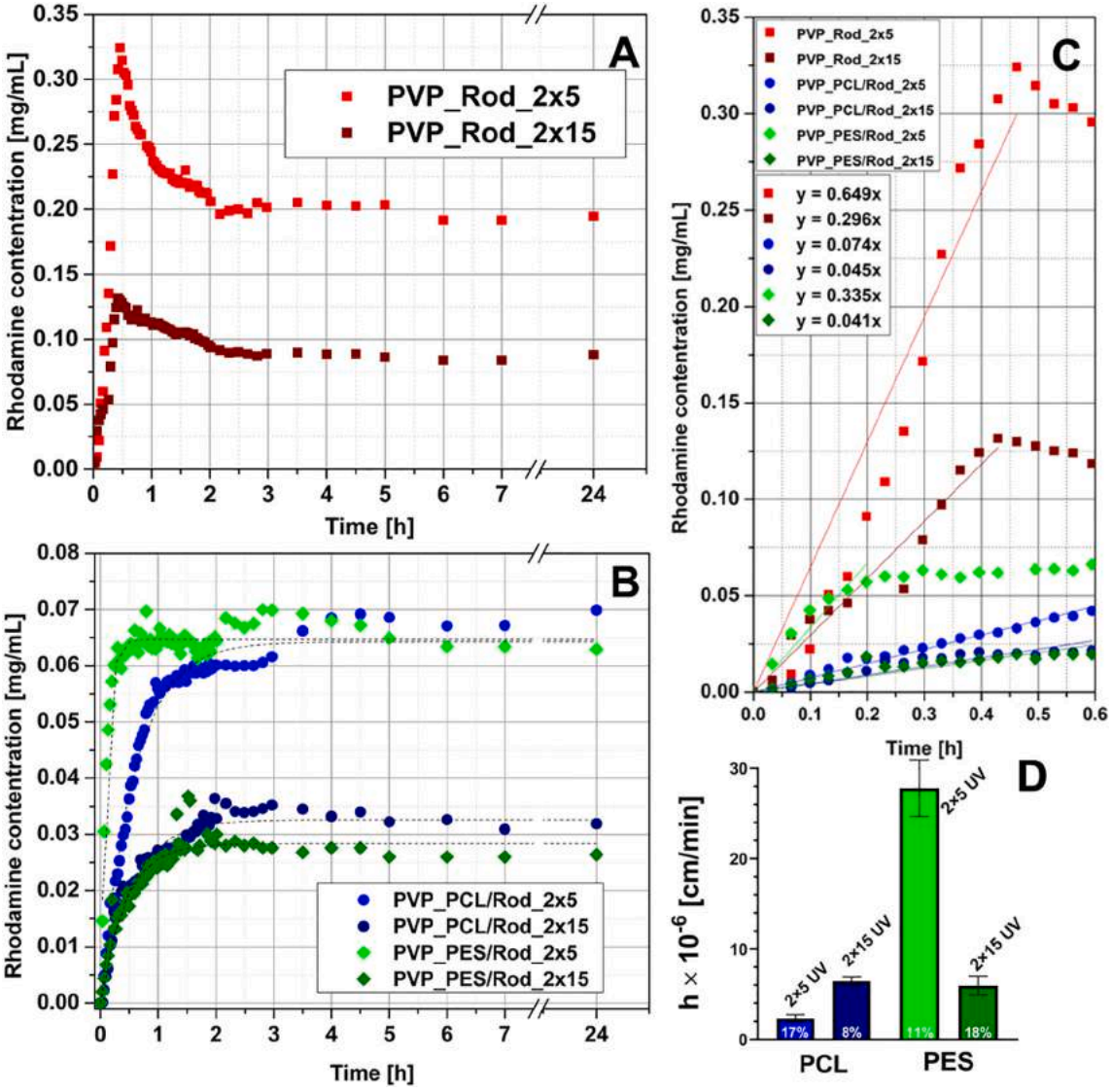

Fig. 8. Rhodamine release profiles from UV-cross-linked PVP fibrous mats. (A) Full release profile from fibers without microspheres – PVP_Rod (rhodamine encapsulated directly in the fibers). (B) Full release profile from fibers with the addition of rhodamine-loaded PCL (PVP_PCL/Rod) or PES (PVP_PES/Rod) microspheres with model curves fitted to experimental. (C) Close-up of the first release period of the first 30 min from all samples with linear model fit with the formula $y = \alpha x$, the equations of fitted functions are given in the graph. (D) The values of the transport coefficient *h* for UV-cross-linked PVP fibrous mats with the PCL or PES microspheres depending on the cross-linking time. The coefficient of variations of *h* are indicated on each corresponding bar as well as in Table 1.

the substance in the first period. The α coefficients for PCL-microsphere-loaded fibers (blue points in Fig. 8C) are an order of magnitude lower than those for mats without microspheres. In this case also a longer cross-linking time causes an almost two-fold decrease in the substance release rate (α = 0.074 for PVP_PCL/Rod_2 × 5 and α = 0.045 for PVP_PCL/Rod_2 × 15). A similar phenomenon is observed for fibers containing PES microspheres. Both for the cross-linking time of 2 × 5 min and 2 × 15 min, the slope coefficients of the straight line are lower than for analogous nonwovens without microspheres. On the other hand, increase of the cross-linking time causes an eightfold decrease in the release rate (α = 0.335 for PVP_PES/Rod_2 × 5 and α = 0.041 for PVP_PES/Rod_2 × 15).

No burst effect was observed in the rhodamine release profiles from mats with microspheres (Fig. 8B) – it was effectively eliminated by using fibers modified in the proposed manner. The release profiles of such microsphere-loaded fibers show that it proceeds in two steps in some cases. This may be due to the fact that the fibers swell slightly when submerged in water, which was previously observed as an increase in their diameter during degradation studies (Fig. 3). Moreover, the fiber/microsphere structure is specific. Rhodamine is not only enclosed in microspheres – at the stage of preparing the mixture for electrospinning (Fig. 1B) some of the rhodamine penetrates from the microspheres into the PVP solution. Thus, it is first released from the polymer shell covering the microsphere, and only later the substance enclosed inside the microspheres reaches the solution.

In previously reported studies [31–33], drug-loaded microspheres were incorporated into polymer fiber networks at different stages of the manufacturing process ("sandwich" system). Each of these systems was designed for different potential applications. Initial measurements of the concentration of the substance in solution were carried out only after 3 to 4 h, and, moreover, the authors did not take samples very often, which is necessary to accurately determine the kinetics of the release profile of the active substance.

Xu et al. [34] developed a biodegradable system for the delivery of two drugs by suspension electrospinning, in which the release of the active ingredient is based on a biodegradation process. The authors found that the burst effect was eliminated by coating the microspheres with an outer layer of a fibrous polymer, given that microsphere diameters were comparable to the fiber diameters. However, the results presented in the publication do not clearly indicate the elimination of the burst effect, as the authors included the results of measurements carried out only after 1 h, without thoroughly investigating the kinetics of the substance release during the first stage of the process.

On the other hand, S. Park et al. [51] showed that core/shell fibers with monolithic PCL coating, compared to PVP/PCL coated fibers, showed a reduced burst effect followed by prolonged sustained release of the drug substance. Da Silva et al. [52] found that monolithic PVA fibers showed burst release, while core-shell fibers composed of PLA and PVA were characterized by controlled albumin release. In the case of presented system – fibrous mats modified with PCL/PES microspheres with diameters up to 20 times larger than the fiber diameters – the burst effect does not occur either. It leads to supposition that it exhibit a structure similar to that observed in above studies – microspheres are covered with an outer PVP layer which delays the release of the substance. As such, the solution electrospinning technique employed in this study can be considered an alternative to more complex core/shell electrospinning systems, showcasing its potential as a competitive method in the field. However, further characterization of the structure of the fabricated systems would be necessary to confirm these conclusions.

Due to the absence of burst effect, the rhodamine release curves from mats with microspheres can be described by an exponential function (Eq. (4)). Relevant calculations were carried out, and an exemplary result is shown in Fig. SI2 (*Supporting Information*), the table with the results of the mathematical analysis is included. The values of the coefficients of determination R^2 for each sample are above 0.9 (Table 1), the fit is therefore very good. For each case, parameter *b* was determined from Eq. (4), and then using Eq. (6), the transport coefficient *h* was determined for each case. The results are shown in the Table 1 together with BET surface area and at the bar graph in Fig. 8D.

The value of the coefficient *h* obtained for the PVP/PES_Rod_2 × 5 min mats is the greatest (26.58×10^{-6} cm/min ± 11 %) and clearly exceeds the others by more than four times. For both samples UV-cross-linked for 2 × 15 min (PVP_PCL/Rod_2 × 15 and PVP_PES/Rod_2 × 15) the *h* values are similar (respectively, 6.43×10^{-6} cm/min ± 8 % and 5.69×10^{-6} cm/min ± 18 %). The PVP_PCL/Rod_2 × 5 sample differs from the others ($h = 2.32 \times 10^{-6}$ cm/min ± 17 %) which is due to the more than twice the interface surface area of this sample compared to the others (the value of this surface is in the denominator in the Eq. (6)). The explanation of such a large surface development in this specific case requires further research.

The applied method of mathematical description of substance release was previously proposed by Grzeczkowicz et al. [42] to model kinetics of the release of vitamin B12 from microcapsules using the transport coefficients *h*. For synthetic porous membranes, the value of *h* was three orders of magnitude greater than those observed in this work for UV-cross-linked microsphere-loaded fibers, although the materials tested in the cited work had a much greater thickness (182–272 μm) compared to the fibers and microspheres (1–15 μm). The release rate was mainly influenced by the porous structure of membranes which the UV-cross-linked PVP fibers do not have. A marked slowdown in the substance release is beneficial from the point of view of drug delivery systems, and it occurs even for a marker with a molecular weight twice as low (rhodamine: 591 g/mol, vitamin B12: 1355 g/mol). Besides, Grzeczkowicz et al. approximated the interface by the size of the total geometric area of all microspheres and no real specific surface area was used.

3.6. Antibacterial properties

UV-cross-linked microsphere-loaded fibrous PVP mats with enhanced capacity for active substance may be useful e.g. for wound dressing applications regarding the need to maintain sterility at the wound site. In that frame, we loaded such mats with ampicillin and performed an agar diffusion inhibitory growth test to characterize their antimicrobial activity. The tests were carried out with the sample 2 × 5 min and 2 × 15 min samples with drug-loaded PCL or PES microspheres. Each sample was deposited on the surface of nutrient agar plate previously inoculated with *E. coli* or *S. aureus* at a concentration of 10^8 CFU/mL and incubated for 24 h. Fig. 9 illustrates the results of the antibacterial properties study.

The studies presented in this work (Fig. 9) show that mats modified with both PCL and PES microspheres exhibit antibacterial activity, but it is much higher when exposed to *S. aureus* bacteria. Moreover, fibers with PCL microspheres have stronger bactericidal effect – a much larger clear zone is observed (Fig. 9B). On the other hand, prolonged crosslinking time results in a reduced clear zone, especially for fibers with PES microspheres. Both of these observations are consistent with the results of the research on the capacity of the systems for the active substance (Fig. 7). UV-treated PVP fibers without microspheres and without drug show no bactericidal activity, which confirms that no toxic substances are formed during UV-cross-linking and that the benzophenone used is also non-toxic. The bar chart in Fig. 9C presents the results of the inhibitory zone area measurements obtained from images of Petri dishes, in which the antibacterial properties of the modified mats were tested. The results are based on three replicate experiments and are presented with the mean values, standard deviation and coefficient of variation being depicted. The results of the antibacterial activity, as observed in the photos, are reflected in the chart. A trend can be identified, wherein an increase in the duration of cross-linking results in a decrease in the antibacterial activity of the mats. There is a slight difference in the activity between PCL and PES-loaded mats. However, the sample containing PES microspheres and cross-linked for 2 × 15 min (for both *E. coli* and *S. aureus*) deviates notably from the others. Further

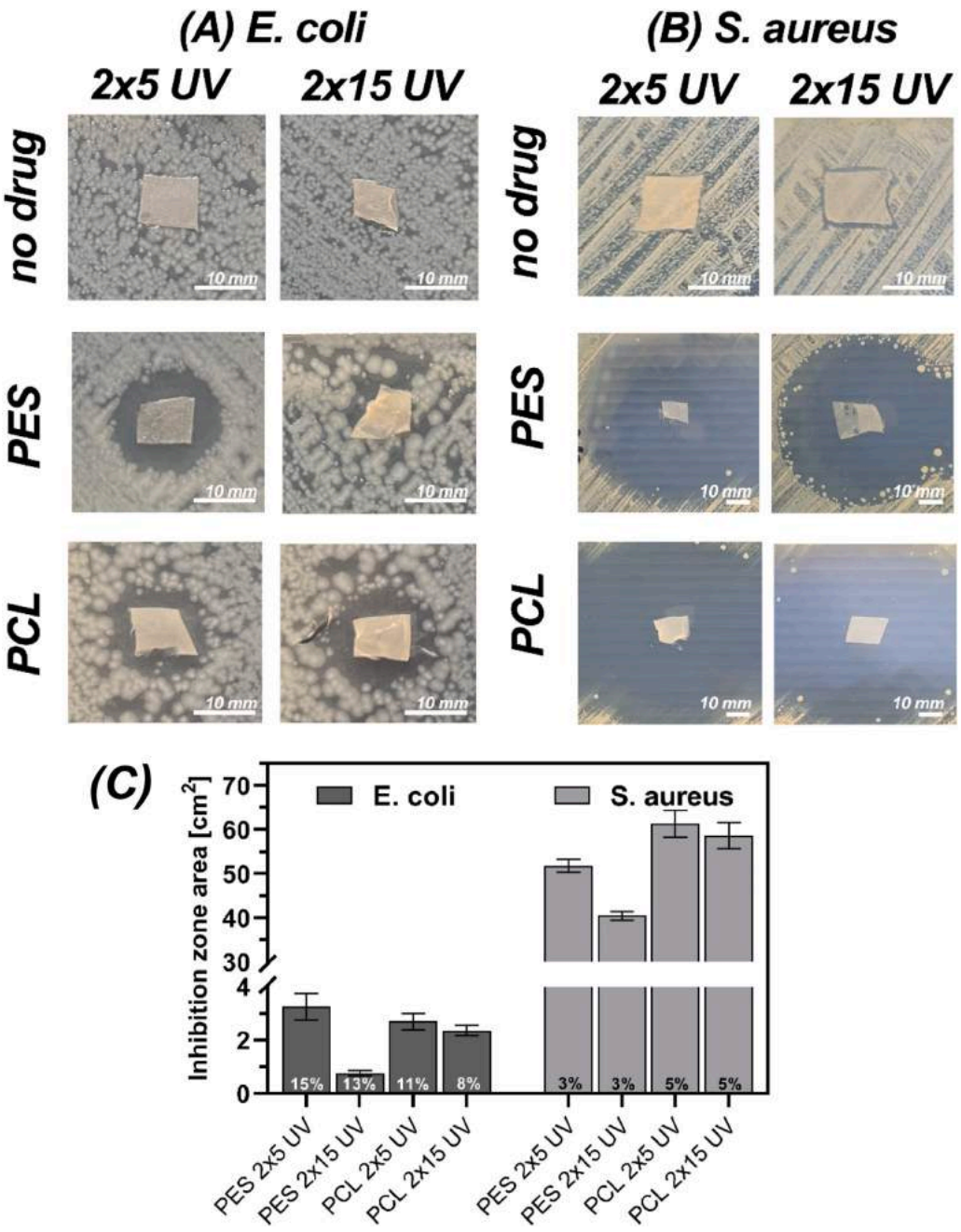

Fig. 9. Bacteriostatic tests of UV-cross-linked PVP fibrous mats with ampicillin-loaded microspheres on nutrient agar plates covered with (A) *E. coli* and (B) *S. aureus* biofilms after 24 h of material treatment. (C) Bar chart showing average inhibition zone areas [cm^2] based on images of Petri dishes from three test replicates. The coefficient of variations is indicated on each corresponding bar.

research is necessary to fully understand this phenomenon. Additionally, it can be noted that the zones of inhibited growth for *S. aureus* are significantly larger in comparison to those observed for *E. coli*.

Li et al. [31] report that the systems they developed (electrospun silk/PCL/PVA fibers with drug-filled silk/chitosan microspheres applied to their surface) showed excellent antimicrobial activity with 93.18 % and 97.15 % inhibition of *E. coli* and *S. aureus*, respectively, however, they used a different method to determine the antibacterial properties of fibrous mats. A similar test using nutrient agar plates coated with bacteria was conducted by Nagarajan et al. [53], who investigated the antibacterial properties of chemically crosslinked gelatin fibers loaded with chlorhexidine acetate. They obtained inhibition zone diameters of 2.7 ± 0.3 cm^2 for *E. coli* bacteria, similar to those obtained in presented study. They also tested Gram-positive bacteria, *Staphylococcus epidermidis* (the same genus as in this work) and they report an inhibition zone diameter of 2.7 ± 0.3 cm^2, 20 times less than in the case of ampicillin-loaded microsphere-modified fibrous mats, probably due to a stronger activity of ampicillin against the microorganisms. The reported bactericidal activity of this loaded electrospun mat is quite promising, as it demonstrated the ability to remove a significant number of colony-forming units within a small area, as determined by standardized contact tests (minimum 10^7 CFU of bacteria killed which corresponds to an area of 0.5 cm^2) [54]. The tests conducted evidenced that the integrity of the drug had not been affected during microsphere preparation and electrospinning process. Hence, the proposed fibrous mats could serve as controlled drug delivery systems.

4. Conclusions

All the assumed goals of the work have been achieved. The application of the microsphere suspension electrospinning method, incorporating the unconventional utilization of pulsed voltage, made it possible to manufacture electrospun PVP fibers modified with drug-loaded PCL (or PES) microspheres of a structure meeting a set of specific requirements. As expected, the addition of microspheres to electrospun fibers increases the capacity of the entire system for the drug and eliminates the undesirable burst effect. In addition, it was found that the amount and type of microspheres used in the electrospun mats notably affect their mechanical properties, increasing their strength, and upgrade the release profile of the active substance. As assumed, UV-crosslinking of modified electrospun mats (using benzophenone as photoinitiator) results in water- and ethanol-insoluble fibers, making them more flexible in terms of potential applications. It was also found that the time of UV-crosslinking remarkably impacts the properties of such mats, including degradation rate, mechanical strength and transport properties. Both electrospun mats with PCL and PES microspheres exhibit good antibacterial properties. The presented method of fiber mat manufacturing is highly versatile – allowing for a wide range of modifications to be made with respect to potential applications, such as the size and porosity of microspheres, the polymers used, the concentration of the cross-linking agent, and the duration of cross-linking, etc. Therefore, it can be concluded that the presented electrospun mat based on UV-crosslinked polyvinylpyrrolidone (PVP) fibers modified with polycaprolactone (PCL) or polyethersulfone (PES) microspheres demonstrates great potential as a drug delivery system.

CRediT authorship contribution statement

Adam Mirek: Conceptualization, Methodology, Formal analysis, Investigation, Data curation, Writing – original draft, Writing – review & editing, Visualization. **Marcin Grzeczkowicz:** Conceptualization, Methodology, Validation, Formal analysis, Writing – review & editing. **Habib Belaid:** Methodology, Investigation, Writing – review & editing, Visualization. **Aleksandra Bartkowiak:** Conceptualization, Validation, Writing – original draft, Writing – review & editing. **Fanny Barranger:** Investigation, Visualization. **Mahmoud Abid:** Investigation. **Monika Wasyłeczko:** Methodology, Investigation, Visualization. **Maksym Pogorielov:** Methodology, Validation, Resources. **Mikhael Bechelany:** Conceptualization, Methodology, Validation, Resources, Writing – review & editing. **Dorota Lewińska:** Conceptualization, Methodology, Validation, Resources, Writing – original draft, Writing – review & editing, Supervision.

Conflict of interest

All authors declare that they have no conflicts of interest.

Data availability

Data will be made available on request.

Acknowledgments

This project was supported by European Social Fund [POWR.03.02.00-00-1028/17-00] as part of the POWER Och!Dok program. AM would like to thank Campus France for the funding through a French Government Scholarship. Authors acknowledge the financial support of project H2020-MSCA-RISE-2017, “Novel 1D photonic metal oxide nanostructures for early stage cancer detection” (Project number: 778157).

Appendix A. Supplementary data

Supplementary data to this article can be found online at https://doi.org/10.1016/j.bioadv.2023.213330.

References

[1] C.A. Martínez-Pérez, Electrospinning: a promising technique for drug delivery systems, Rev. Adv. Mater. Sci. 59 (2020) 441–454.
[2] S.C. Kundu, N. Bhardwaj, Electrospinning: a fascinating fiber fabrication technique, Biotechnol. Adv. 28 (2010) 325–347.
[3] A. Memic, T. Abudula, H.S. Mohammed, K. Joshi Navare, T. Colombani, S. A. Bencherif, Latest progress in electrospun nanofibers for wound healing applications, ACS Appl. Bio Mater. 2 (3) (2019) 952–969.
[4] B. Guo, P.X. Ma, Synthetic biodegradable functional polymers for tissue engineering: a brief review, Sci. China Chem. 57 (2014) 490–500.
[5] M. Afrashi, D. Semnani, Z. Talebi, P. Dehghan, M. Maherolnaghsh, Comparing the drug loading and release of silica aerogel and PVA nano fibers, J. Non-Cryst. Solids 503–504 (2019) 186–193.
[6] Y. Liu, X. Chen, Y. Liu, Y. Gao, P. Liu, Electrospun coaxial fibers to optimize the release of poorly water-soluble drug, Polymers 14 (2022) 469.
[7] A. Domokos, A. Balogh, D. Denes, G. Nyerges, L. Zodi, B. Farkas, G. Marosi, Z. Nagy, Continuous manufacturing of orally dissolving webs containing a poorly soluble drug via electrospinning, Eur. J. Pharm. Sci. 124 (2018) 71–79.
[8] B.M. Maciejewska, J.K. Wychowaniec, M. Woźniak-Budych, Ł. Popenda, A. Warowicka, K. Golba, S. Jurga, UV cross-linked polyvinylpyrrolidone electrospun fibres as antibacterial surfaces, Sci. Technol. Adv. Mater. 20 (1) (2019) 979–991.
[9] Z. Wei, C. Xiong, Z. Liu, X. Wang, S. Long, J. Yang, Release characteristics and processing-structure-performance relationship of electro-spinning curcumin-loaded polyethersulfone based porous ultrafine fibers, J. Biomater. Sci. Polym. Ed. 29 (15) (2018) 1825–1838.
[10] Z. Wei, E. Liu, H. Li, Z. Wei, Z. Lv, Release characteristics of different diameter ultrafine fibers as antibacterial materials, J. Innov. Opt. Health Sci. 14 (2) (2021), 2041005.
[11] W. Chen, A. Palazzo, W.E. Hennink, R.J. Kok, Effect of particle size on drug loading and release kinetics of gefitinib-loaded PLGA microspheres, Mol. Pharm. 14 (2) (2017) 459–467.
[12] J. Yoo, Y.-Y. Won, Phenomenology of the initial burst release of drugs from PLGA microparticles, ACS Biomater. Sci. Eng. 6 (11) (2020) 6053–6062.
[13] J. Wu, Z. Zhang, J. Gu, W. Zhou, X. Liang, G. Zhou, C. Han, S. Xu, Y. Liu, Mechanism of a long-term controlled drug release system based on simple blended electrospun fibers, J. Control. Release 320 (2020) 337–346.
[14] X. Huang, C.S. Brazel, On the importance and mechanisms of burst release in matrix-controlled drug delivery systems, J. Control. Release 73 (2–3) (2001) 121–136.
[15] E.J. Torres-Martinez, J.M. Cornejo Bravo, A. Serrano Medina, G.L. Perez Gonzalez, L.J. Villarreal Gomez, A summary of electrospun nanofibers as drug delivery system: drugs loaded and biopolymers used as matrices, Curr. Drug Deliv. 15 (2018) 1360–1374.
[16] J. Xiong, Y. Liu, A. Li, L. Wei, L. Wang, X. Qin, J. Yu, Mass production of high-quality nanofibers via constructing pre-Taylor cones with high curvature on needleless electrospinning, Mater. Des. 197 (2021), 109247.
[17] J.M. Ameer, A.K. PR, N. Kasoju, Strategies to tune electrospun scaffold porosity for effective cell response in tissue engineering, J. Funct. Biomater. 10 (2019) 30.
[18] S. Omer, L. Forgach, R. Zelko, I. Sebe, Scale-up of electrospinning: market overview of products and devices for pharmaceutical and biomedical purposes, Pharmaceutics 13 (2021) 286.
[19] S.C. Chen, X.B. Huang, X.M. Cai, J. Lu, J. Yuan, J. Shen, The influence of fiber diameter on electrospun polu(lactic acid) on drug delivery, Fibers Polym. 13 (9) (2012) 1120–1125.
[20] G. Balzamo, X. Zhang, W.A. Bosbach, E. Mele, In-situ formation of polyvinylidene fluoride microspheres within polycaprolactone electrospun mats, Polymer 186 (2020), 122087.
[21] T. Kowalczyk, Functional micro- and nanofibers obtained by nonwoven post-modification, Polymers 12 (5) (2020) 1087.
[22] K. Ghosal, R. Augustine, A. Zaszczynska, M. Barman, A. Jain, A. Hasan, N. Kalarikkal, P. Sajkiewicz, S. Thomas, Novel drug delivery systems based on triaxial electrospinning based nanofibers, React. Funct. Polym. 163 (2021), 104895.
[23] J. Yang, K. Wang, D.-G. Yu, Y. Yang, S.W.A. Bligh, G.R. Williams, Electrospun Janus nanofibers loaded with a drug and inorganic nanoparticles as an effective antibacterial wound dressing, Mater. Sci. Eng. C 111 (2020), 110805.
[24] J. Wang, M. Windbergs, Controlled dual drug release by coaxial electrospun fibers – impact of the core fluid on drug encapsulation and release, Int. J. Pharm. 556 (2019) 363–371.
[25] A. Khan, K. Huang, M. Khalaji, F. Yu, X. Xie, T. Zhu, Y. Morsi, Z. Jinzhong, X. Mo, Multifunctional bioactive core-shell electrospun membrane capable to terminate inflammatory cycle and promote angiogenesis in diabetic wound, Bioact. Mater. 6 (9) (2021) 2783–2800.
[26] M. He, H. Jiang, R. Wang, Y. Xie, C. Zhao, Fabrication of metronidazole loaded polycaprolactone)/zein core/shell nanofiber membranes via coaxial electrospinning for guided tissue regeneration, J. Colloid Interface Sci. 490 (2016) 27–278.

[27] C. Zhang, F. Feng, H. Zhang, Emulsion electrospinning: fundamentals, food applications and prospects, Trends Food Sci. Technol. 80 (2018) 175–186.
[28] A.O. Basar, S. Castro, S. Torres-Giner, J.M. Lagaron, H. Turkoglu Sasmazel, Novel poly(ε-caprolactone)/gelatin wound dressings prepared by emulsion electrospinning with controlled release capacity of ketoprofen anti-inflammatory drug, Mater. Sci. Eng. C 81 (2017) 459–468.
[29] T. Shibata, N. Yoshimura, A. Kobayashi, T. Ito, K. Hara, K. Tahara, Emulsion-electrospun polyvinyl alcohol nanofibers as a solid dispersion system to improve solubility and control the release of probucol, a poorly water-soluble drug, J. Drug Deliv. Sci. Technol. 67 (2022), 102953.
[30] J. Gao, B. Li, L. Wang, X. Huang, H. Xue, Flexible membranes with a hierarchical nanofiber/microsphere structure for oil adsorption and oil/water separation, J. Ind. Eng. Chem. 68 (2018) 416–424.
[31] T.-T. Li, L. Sun, Y. Zhong, H.-K. Peng, H.-T. Ren, Y. Zhang, J.-H. Lin, C.-W. Lou, Silk fibroin/polycaprolactone-polyvinyl alcohol directional moisture transport composite film loaded with antibacterial drug-loading microspheres for wound dressing materials, Int. J. Biol. Macromol. 207 (2022) 580–591.
[32] P.S. Gungor-Ozkerim, T. Balkan, G.T. Kose, A.S. Sarac, F.N. Kok, Incorporation of growth factor loaded microspheres into polymeric electrospun nanofibers for tissue engineering applications, J. Biomed. Mater. Res. 102 (6) (2014) 1897–1908.
[33] N. Nagiah, G. Ramanathan, L. Sobhana, U.T. Sivagnanam, N.T. Srinivasan, Poly (vinyl alcohol) microspheres sandwiched poly (3-hydroxybutyric acid) electrospun fibrous scaffold for tissue engineering and drug delivery, Int. J. Polym. Mater. Polym. Biomater. 63 (11) (2014) 583–585.
[34] J. Xu, Y. Jiao, X. Shao, C. Zhou, C. Zhou, Controlled dual release of hydrophobic and hydrophilic drugs from electrospun poly(L-lactic acid) fiber mats loaded with chitosan microspheres, Mater. Lett. 65 (17) (2011) 2800–2803.
[35] A. Mirek, M. Grzeczkowicz, C. Lamboux, S. Sayegh, M. Bechelany, D. Lewińska, Formation of disaggregated polymer microspheres by a novel method combining pulsed voltage electrospray and wet phase inversion techniques, Colloids Surf. A Physicochem. Eng. Asp. 129246 (2022).
[36] A. Mirek, P. Korycka, M. Grzeczkowicz, D. Lewińska, Polymer fibers electrospun using pulsed voltage, Mater. Des. 108106 (2019).
[37] K. Li, Y. Wang, G. Xie, J. Kang, H. He, K. Wang, Y. Liu, Solution electrospinning with a pulsed electric field, J. Appl. Polym. Sci. 135 (15) (2017) 46130.
[38] Inc. Allevi, Allevi Protocols: Cell-Bioink Mixing: Syringe Coupler Method [Online]. Available:, Allevi, 13 July 2022 https://www.allevi3d.com/cell-bioink-mixing-syringe-coupler-method/. (Accessed 16 August 2022).
[39] W. Chrzanowski, E. Ali, A. Neel, D. Andrew, J. Campbell, Effect of surface treatment on the bioactivity of nickel - titanium, Acta Biomater. 4 (6) (2008) 1969–1984.
[40] A.W. Hansen, L.T. Fuhr, L.M. Antonini, D.J. Villarinho, C.E. Bruno Marino, C. de Fraga Malfatti, The electrochemical behavior of the NiTi alloy in different simulated body fluids, Mater. Res. 18 (1) (2015) 184–190.
[41] D.F. Radcliffe, J.D.S. Gaylor, Sorption kinetics in haemoperfusion columns. Part I. Estimation of mass-transfer parameters, Med. Biol. Eng. Comput. 19 (1981) 617–627.
[42] M. Grzeczkowicz, D. Lewińska, A method for investigation transport properties of partly biodegradable spherical membranes using vitamin B12 as the marker, Desalin. Water Treat. 128 (2018) 170–178.
[43] M. Contardi, D. Kossyvaki, P. Picone, M. Summa, X. Guo, J.A. Heredia-Guerrero, I. S. Bayer, Electrospun polyvinylpyrrolidone (PVP) hydrogels containing hydroxycinnamic acid derivatives as potential wound dressings, Chem. Eng. J. 409 (2021), 128144.
[44] P. Korycka, A. Mirek, K. Kramek-Romanowska, M. Grzeczkowicz, D. Lewińska, Effect of electrospinning process variables on the size of polymer fibers and bead-on-string structures established with a 23 factorial design, Beilstein J. Nanotechnol. 9 (2018) 2466–2478.
[45] S.K. Christense, M.C. Chiappelli, R.C. Hayward, Gelation of copolymers with pendent benzophenone photo-cross-linkers, Macromolecules 45 (2012) 5237–5246.
[46] X. Zhu, P. Lu, W. Chen, J. Dong, Studies of UV crosslinked poly(N-vinylpyrrolidone) hydrogels by FTIR, Raman and solid-state NMR spectroscopies, Polymer 51 (2010) 3054–3063.
[47] L. Tang, D. Sallet, J. Lemaire, Photochemistry of polyundecanamides. 1. Mechanisms of photooxidation at short and long wavelengths, Macromolecules 15 (5) (1982) 1432–1437.
[48] M. Przybysz-Romatowska, J. Haponiuk, K. Formela, Poly(ε-caprolactone)/poly (lactic acid) blends compatibilized by peroxide initiators: comparison of two strategies, Polymers 12 (1) (2020) 228.
[49] N.A. Alenazi, M.A. Hussein, K.A. Alamry, A.M. Asiri, Modified polyether-sulfone membrane: a mini review, Des. Monomers Polym. 20 (1) (2017) 532–546.
[50] X. Zhang, K. Tang, X. Zheng, Electrospinning and crosslinking of COL/PVA nanofiber-microsphere containing salicylic acid for drug delivery, J. Bionic Eng. 13 (2016) 143–149.
[51] S. Park, M. Kim, K. Choi, J. Kim, S. Choi, Influence of shell compositions of solution blown PVP/PCL core-shell fibers on drug release and cell growth, RSC Adv. 8 (57) (2018) 32470–32480.
[52] T.N. da Silva, R.P. Gonçalves, C.L. Rocha, B.S. Archanjo, C.A.G. Barboza, M.B. R. Pierre, F. Reynaud, P.H. de Souza Picciani, Controlling burst effect with PLA/PVA coaxial electrospun scaffolds loaded with BMP-2 for bone guided regeneration, Mater. Sci. Eng. C Mater. Biol. Appl. 97 (2019) 62–612.
[53] S. Nagarajan, L. Soussan, M. Bechelany, C. Teyssier, V. Cavaillès, C. Pochat-Bohatier, S. Balme, Novel biocompatible electrospun gelatin fiber mats with antibiotic drug delivery properties, J. Mater. Chem. B 4 (6) (2016) 1134–1141.
[54] R. Gläser, J. Harder, H. Lange, J. Bartels, E. Christophers, J. Schröder, Antimicrobial psoriasin (S100A7) protects human skin from Escherichia coli infection, Nat. Immunol. 6 (1) (2005) 57–64.

Supporting Information

Figure SI1. The mechanical properties measurement system setup.
The UV-cross-linked PVP fibrous mat sample is stretched vertically until it breaks.

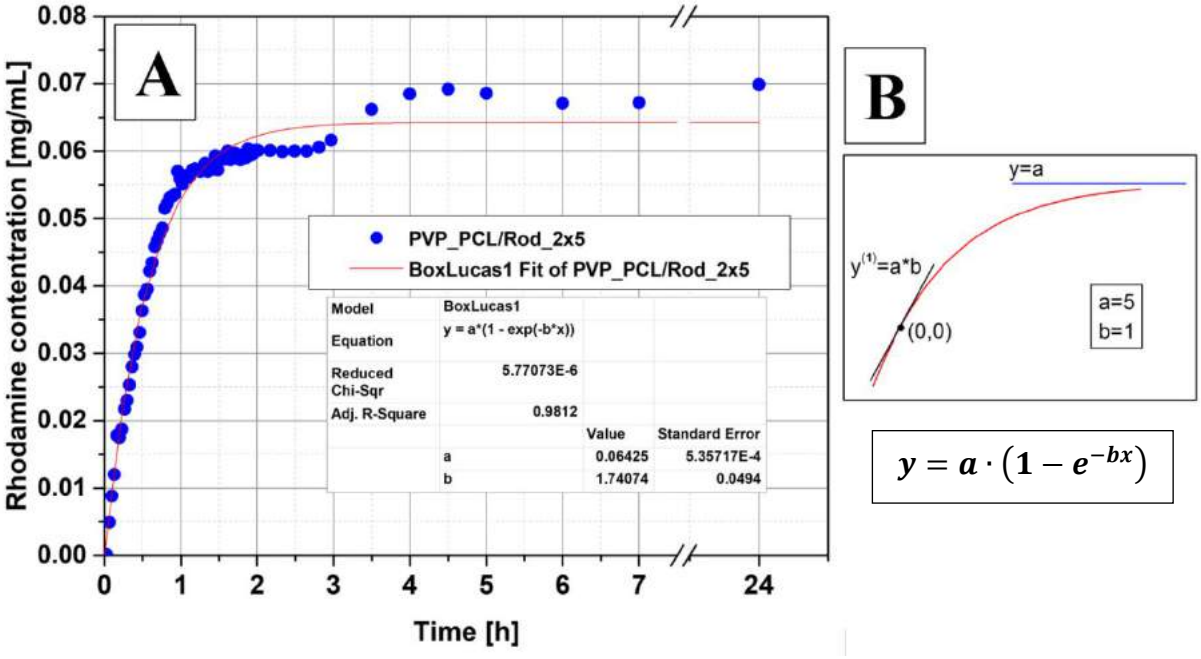

Figure SI2. Model curve (*BoxLucas1*, red) fitted to the experimental results (change in rhodamine concentration over time, blue points): (A) the result in the form of a graph and table from the *OriginPro* software, (B) geometric interpretation of the model parameters.

P U B L I C A T I O N 4

Development of a new 3D bioprinted antibiotic delivery system based on a cross-linked gelatin-alginate hydrogel

Mirek, A., Belaid, H., Barranger, F., Grzeczkowicz, M., Bouden, Y., Cavailles, V., Lewińska, D., Bechelany, M.

Journal of Materials Chemistry B. 10, 8862–8874 (2022).
DOI: 10.1039/d2tb01268e

featured in the Journal of Materials Chemistry B 2022 Most Popular Articles collection

Volume 10
Number 43
21 November 2022
Pages 8789–9012

Journal of Materials Chemistry B

Materials for biology and medicine

rsc.li/materials-b

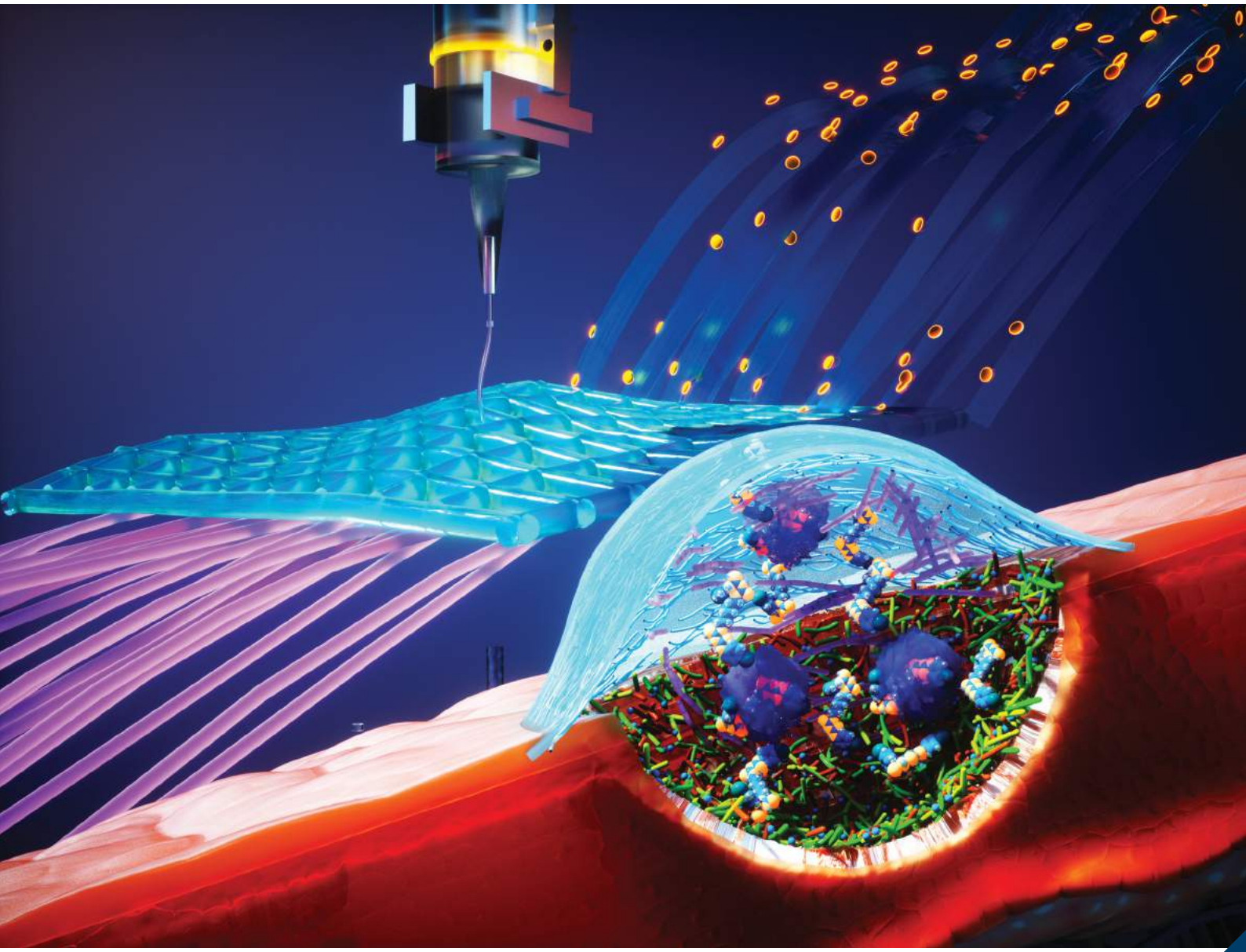

ISSN 2050-750X

ROYAL SOCIETY OF CHEMISTRY

PAPER
Mikhael Bechelany *et al.*
Development of a new 3D bioprinted antibiotic delivery system based on a cross-linked gelatin–alginate hydrogel

Indexed in Medline!

Journal of Materials Chemistry B

ROYAL SOCIETY OF CHEMISTRY

PAPER

View Article Online
View Journal | View Issue

Cite this: J. Mater. Chem. B, 2022, 10, 8862

Development of a new 3D bioprinted antibiotic delivery system based on a cross-linked gelatin–alginate hydrogel

Adam Mirek,[ab] Habib Belaid,[b] Fanny Barranger,[b] Marcin Grzeczkowicz,[a] Yasmine Bouden,[c] Vincent Cavaillès,[c] Dorota Lewińska[a] and Mikhael Bechelany *[b]

3D bioprinting uses bioink deposited directly on a collector to create any previously designed 3D model. One of the most common and the easiest to operate bioinks is gelatin–alginate hydrogel. The present study aimed to combine 3D bioprinting with different cross-linking techniques to develop a new stable and biodegradable gelatin–alginate hydrogel matrix for drug delivery applications. The matrix-building biopolymers were crosslinked by ionotropic gelation with Ca^{2+} ions, chemical crosslinking with GTA or a combination of the two crosslinkers at various concentrations. The influence of the crosslinking method on the hydrogel properties, stability and structure was examined using scanning electron and optical microscopy, differential scanning calorimetry and thermogravimetric analysis. Analyses included tests of hydrogel equilibrium swelling ratio and release of marker substance. Subsequently, biological properties of the matrices loaded with the antibiotic chlorhexidine were studied, including cytotoxicity on HaCAT cells and antibacterial activity on *Staphylococcus aureus* and *Escherichia coli* bacteria. The conducted study confirmed that the 3D bioprinted cross-linked drug-loaded alginate–gelatin hydrogel is a good and satisfying material for potential use as a drug delivery system.

Received 19th June 2022,
Accepted 5th August 2022

DOI: 10.1039/d2tb01268e

rsc.li/materials-b

1. Introduction

3D bioprinting has developed intensively since the beginning of 2010s and has gained significant interest in both medicine and pharmaceutics.[1] It is used for advanced tissue engineering,[2–5] drug delivery[6] and drug screening,[7] wound dressings,[8–10] and cancer research.[11] The most common 3D bioprinters use material jetting (noncontact bioprinting, generating picolitre droplets and firing at a frequency of thousands times per second),[12] vat polymerization (photohardening of bioresins)[13] or extrusion.[2,3,14] In this technique controlled volumes of liquid are delivered to predefined locations.[15] The material known as a bioink is deposited directly on a collector creating any previously designed 3D model. A wide variety of bio-artificial tissues has been printed including bone, cardiac, lung, pancreas, skin, and vascular tissues.[16] However, not only can bioink be loaded with living cells but also enriched with various bioactive substances. For instance, Jingjunjiao and co-workers bioprinted drug delivery systems based on chitosan-pectin hydrogel with lidocaine hydrochloride for wound dressings.[17]

Hydrogels seem to be the best bioinks, derived from both synthetic or natural polymers,[1] the latter being obtained from mammalian (collagen, gelatin, fibrin, elastin) or non-mammalian sources (agarose, alginate, chitosan).[18] They meet lots of requirements including good cell adhesion, expected biodegradation rate, non-cytotoxicity, suitable rheological properties (sufficiently viscous to be dispensed as a filament), fast gelation time and adequate strength and stiffness. One of the most common and the easiest to operate bioinks is gelatin–alginate hydrogel.[10,19–21] Its printing temperature (37 °C) makes it suitable for use with living cells and heat-sensitive substances such as drugs. It is solid in room temperature but the solidification process can be sped up by lowering the temperature of the collector.[21] Once the gelatin is dissolved in warm water, it is transformed into a hydrogel when cooled to room temperature as a result of forming weak hydrogen bond network. Moreover, gelatin addition into the alginate solution improves the viscosity and stiffness for extrusion.[19]

Depending on the composition, a hydrogel bioink can undergo various gelation processes. The biopolymer molecules can be assembled by non-covalent or covalent bonds.[1] A printable

[a] Nalecz Institute of Biocybernetics and Biomedical Engineering, Polish Academy of Sciences, 4 Ks. Trojdena St., 02-109 Warsaw, Poland
[b] Institut Européen des Membranes, IEM, UMR 5635, Univ Montpellier, CNRS, ENSCM Place Eugène Bataillon, 34095 Montpellier cedex 5, France. E-mail: mikhael.bechelany@umontpellier.fr; Fax: +33467149119; Tel: +33467149167
[c] IRCM, Institut de Recherche en Cancérologie de Montpellier, INSERM U1194, Université Montpellier, Montpellier F-34298, France

material can often be yielded thanks to weak binding forces between polymer chains (hydrogen-bonding, π-stacking and van der Waals forces). Another way to link polymer molecules is to use an ionic bond – *e.g.* for polysaccharides such as alginate, pectin and gellan gum that require bivalent cations (*e.g.* Ca^{2+}) to form intermolecular bonds between polymer chains. Non-covalent bonds are fast to form but due to their weakness and reversibility they cannot be used for long-acting systems or scaffolds. However, they can be a good starting point to create a 3D hydrogel model, which could then be subjected to post-processing action aimed at creating covalent bonds and thus strengthening the structure through photo or chemical cross-linking. For gelatin–alginate hydrogels, this can be achieved in two ways – ionotropic gelation creating links between anionic alginate chains (COO^- groups) by means of calcium cations (Ca^{2+}) or chemical crosslinking of gelatin chains with the use of glutaraldehyde (GTA). GTA undergoes a Schiff's base reaction with the amino groups of the amino acids present in gelatin. As a result –CO–NH– bonds are formed creating a sustainable network of gelatin–gelatin and gelatin–alginate chains.[22]

Alginate–gelatin hydrogel has been used in biomedical engineering for a long time, it is also widely used for the 3D printing of drug- and cell-loaded scaffolds.[10,19–21,23] Its printing temperature (37 °C) makes it suitable for use with living cells and mild to sensitive substances such as drugs. It is solid in room temperature but the solidification process can be sped up by lowering the temperature of a Petri dish where a printout is collected.[21] Once the gelatin is dissolved in warm water, it can transform into a hydrogel when is cooled to room temperature as a result of forming weak hydrogen bond network. Also, the addition of gelatin into alginate solution improves the viscosity and stiffness for extrusion.[19] Therefore, it is possible to print a 3D model quickly and easily and then strengthen it by crosslinking. In the context of novel drug delivery systems, it seems interesting that, by using different crosslinking techniques in different conditions, the degradation time of the printed hydrogel matrix could be controlled, and this can directly translate into the time of drug release. The highly cross-linked matrix-building biopolymer chains create a more compact structure, limiting swelling of hydrogel, and thus slowing down the substance release process. Moreover, the substance is released from such a material not only by diffusion, but also during the degradation or dissolution of the material – this phenomenon can be reduced by cross-linking, thus limiting the burst effect.[24,25]

Not only are hydrogels useful as drug delivery systems due to the cross-linking-based control over the substance release, but also because they can absorb wound exudates. This is a desirable feature of modern dressings due to the harmfulness of some enzymes present in such exudates which can delay the healing process by affecting cell proliferation and activity.[26] In addition, the high water content of hydrogel matrices used as wound dressing could ensure adequate hydration of the wound area, which can prevent desiccation and cell death, promote tissue regeneration and enhance epidermal migration.[27]

Based on these considerations, the present study aimed to combine 3D bioprinting technology with controlled release of chlorhexidine acetate in order to develop a novel stable biodegradable and antibacterial 3D bioprinted gelatin–alginate hydrogel matrix for potential wound dressing applications. Two different methods of cross-linking were used based on ionotropic gelation with Ca^{2+} ions or chemical crosslinking with GTA. Their influence on the gelatin–alginate matrices (GAMs) properties including equilibrium swelling ratio, drug release, cytocompatibility and antibacterial activity was examined using multiple techniques. The material developed in the work can be used as a new drug delivery system.

2. Materials and methods

Materials

Gelatin type B (CAS Number: 9000-70-8) from bovine skin (gel strength 225 g Bloom), sodium alginate (CAS Number: 9005-38-3), calcium chloride ($CaCl_2$, CAS Number: 10043-52-4, ≥97%), sodium chloride (NaCl, CAS Number: 7647-14-5, ≥99%), potassium chloride (KCl, CAS Number: 7447-40-7, ≥99%), potassium phosphate monobasic (KH_2PO_4, CAS Number: 7778-77-0, ≥99%), sodium phosphate dibasic (Na_2HPO_4, CAS Number: 7558-79-4, ≥99) and agar (CAS Number: 9002-18-0) were purchased from Sigma-Aldrich. Aqueous 25% glutaraldehyde (GTA) solution (CAS Number: 111-30-8) was purchased from Alfa Aesar. Glycine (CAS Number: 56-40-6) was purchased from Sigma-Aldrich and used as a neutralization agent for GTA. Rhodamine 640 perchlorate (CAS Number: 72102-91-1) was purchased from Exciton. Chlorhexidine acetate (CAS Number: 56-95-1) was obtained from Fluka Chemicals. The non-pathogenic Gram positive *Staphylococcus aureus* and Gram negative *Pseudomonas aeruginosa* (K12 DSM 423, from DSMZ, Germany) were chosen as a model microorganism. The culture medium was a Tryptone Salt Broth (TSB, Sigma Aldrich). The chemicals were used without further purification. Water at 18 MΩ was produced by MilliQ (Millipore).

Bioink preparation

The bioink used during 3D bioprinting was prepared, using the procedure described by Pan *et al.*[21] Sodium alginate (0.04 g mL^{-1}) was dissolved in reverse-osmosis water at a room temperature. Gelatin powder (0.2 g mL^{-1}) was added to the alginate solution and stirred at 40 °C for 2 hours. The matrices for *in vitro* release tests were prepared by adding rhodamine 640 (0.1 mg mL^{-1}) to pure water before the sodium alginate and it was stirred at a room temperature until rhodamine crystals were completely dissolved. The hydrogel matrices with drug for bioactivity studies were prepared using bioink loaded with chlorhexidine acetate (0.1 and 1 mg mL^{-1}) which was added to pure water before sodium alginate and completely dissolved (analogous to rhodamine). Each bioink was centrifuged for 2 minutes at 1500 rpm to remove air and carefully transferred to the bioprinting syringe. After preparation of the alginate–gelatin bioink and placing in the extrusion syringe, it can be stored in a fridge. Once it is set in the heating holder, bioink liquefies at 37 °C within 15–20 minutes, and then 3D model can be printed.

3D bioprinting of gelatin–alginate hydrogel matrices (GAMs) with rhodamine and drug

A model of matrices was designed using DesignSpark Mechanical 4.0 software as a cubic mesh (20 mm × 20 mm × 12 mm) made of 6 layers, each of height 0.2 mm; the grid size was set as 1 mm and line width as 0.2 mm (Fig. 1). The model was exported as an STL file, sliced by Repetier-Host/Slic3r software and converted into G-code. The gelatin–alginate matrices were manufactured using Allevi 2 3D bioprinter (Philadelphia, USA). The scheme of the experimental setup is shown in Fig. 1. The scheme of 3D bioprinting setup with a digital 3D mesh matrix design. The following settings were used: G30 nozzle with inner diameter of 0.164 mm, layer height of 0.2 mm, printing speed of 10 mm s^{-1}, temperature of the bioink in the syringe of 37 °C, temperature of the collector Petri dish of ~15 °C, and printing pressure of 380 kPa (55 psi). After printing, the samples were stored in a refrigerator (5 °C).

Cross-linking of the matrices

The obtained GAMs were treated using Ca^{2+} ions due to the cross-linking of alginate present in the structure and glutaraldehyde (GTA) due to the gelatin. In order to find the best cross-linking method for the hydrogel matrices produced, a series of experiments was carried out using various cross-linking methods. To provide calcium ions, the samples placed in the glass Petri dishes were sprayed with 2% or 5% solution on each side and left to cross-link for 10 minutes (method 1). Finally, the samples were dried by gently placing them on a tissue and touching them with the other piece of paper from the other side. For GTA cross-linking, the GAMs were treated with the method similar to the one by Zhang *et al.*[28] with use of the GTA aqueous solutions of concentrations 0.5%, 5% and 25%. The solution (20 mL) was placed in hermetic containers equipped with a plastic grate located about 5 mm above the surface of the solution. The GAMs were conditioned in GTA vapors for 24 h at 37 °C (method 2). After that, in order to remove and neutralize GTA residues, each sample was slightly rinsed with RO water, placed for 48 hours in PBS solution and then for next 24 hours in 20% glycine solution.

Table 1 List of prepared gelatin–alginate matrices with the cross-linking procedures

Sample	Cross-linking procedure
0_0_GAM	No cross-linking
0_0.5_GAM	0.5% GTA vapors
0_5_GAM	5% GTA vapors
0_25_GAM	25% GTA vapors
2_0_GAM	2% Ca^{2+} solution spraying
2_0.5_GAM	2% Ca^{2+} solution spraying + 0.5% GTA vapors
2_5_GAM	2% Ca^{2+} solution spraying + 5% GTA vapors
2_25_GAM	2% Ca^{2+} solution spraying + 25% GTA vapors
5_0_GAM	5% Ca^{2+} solution spraying
5_0.5_GAM	5% Ca^{2+} solution spraying + 0.5% GTA vapors
5_5_GAM	5% Ca^{2+} solution spraying + 5% GTA vapors
5_25_GAM	5% Ca^{2+} solution spraying + 25% GTA vapors

In the series of 12 experiments, the samples of matrices were cross-linked in different ways – using the first method, using the second method or using a combination of both methods. The obtained GAMs are summarized in Table 1 with a proper denotation for each of them (the first number corresponds to the concentration of calcium ions, the second number corresponds to the concentration of GTA in the solutions used for cross-linking). The GAMs for studies requiring anhydrous samples were frozen (8 h at −20 °C) and lyophilized (24 h at 12 Pa, −70 °C).

Characterization of the cross-linked GAMs

The morphology of the cross-linked and lyophilized GAMs was observed using scanning electron microscopy (SEM, HITACHI S4800), optical microscopy and fluorescent microscopy systems. The samples were covered with 10 nm layer of gold before observations with SEM.

Thermal properties

Differential scanning calorimetry (DSC) was used to investigate the thermal properties of GAMs. The thermal transition points and enthalpies (calculated as an area under the peak) of the differently cross-linked GAMs were analyzed using differential scanning calorimeter (DSC, TA Instruments 2920) equipped with a RCS90 cooling system. The samples were weighed (~2–3 mg)

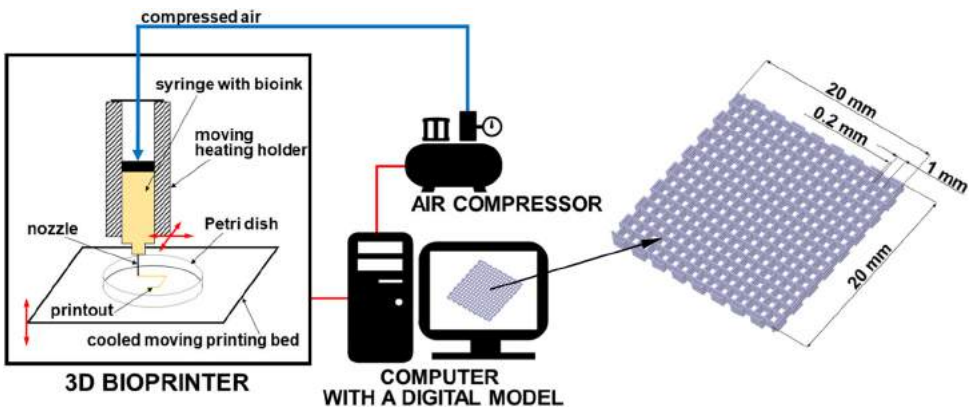

Fig. 1 The scheme of 3D bioprinting setup with a digital 3D mesh matrix design. To simplify the picture, only one syringe holder is shown in the diagram (the Allevi 2 3D bioprinter model has two holders that can be used simultaneously during one print).

in an aluminum TA pan and sealed. An empty sealed pan was used as a reference. The samples were cooled to −80 °C and then heated up to 200 °C with a heating rate of 20 °C min^{-1}. Moreover, the thermogravimetric analysis (TGA, TA Instruments TGA G500) was performed under oxygen flow of 60 mL min^{-1} to define the cross-linking influence on a thermal stability of matrices. The samples of ∼6–10 mg were heated up to 1000 °C at a heating rate of 10 °C min^{-1}.

Swelling of the matrices

The equilibrium swelling ratio (ESR) of cross-linked lyophilized GAMs in phosphate buffered saline (PBS) at 37 °C was determined using a gravimetric method.[29] Samples were weighed (∼15 mg) and placed in a tightly closed bottle with 10 ml of swelling medium (PBS). At the preset time intervals, the samples were withdrawn, surface water was gently removed with a tissue and the GAMs were immediately weighed and placed again in PBS. The experiments were continued until a constant weight was observed. The ESR was calculated using eqn (1):

$$\mathrm{ESR} = \frac{W_t - W_\mathrm{d}}{W_\mathrm{d}} \times 100\% \quad (1)$$

where W_t is the weight of GAM at a particular time (t) and W_d is the weight of dry GAM.

Three samples of the same hydrogel matrix were used to perform the experiment and count average ESR value.

Model drug molecule (rhodamine) release

The release profile of rhodamine 640 from GAMs was determined using a flow spectrophotometric method. Light wavelength: 574 nm. A sample of 5.0–7.5 mg was cut from each freeze-dried GAM and placed in a glass container with 2.0–3.5 mL of deionized water. The content of the container was stirred all the time. Measurements of absorbance of the solution were made every 2 minutes for the first 6 hours, every 30 minutes for the next 2 hours, and the last measurement was made after 9 hours. The volume of the tested liquid did not change during the process. Such a method was proposed by Grzeczkowicz *et al.*[30] On the basis of the obtained data, the profiles of rhodamine release from GAMs were plotted on graphs, and then the curves were fitted to them using the OriginPro software, using the linear and exponential fit with the *ExpDec1* function available in the program library. Selected samples were transferred with water to sealed tubes and their concentration was tested several times with a time interval of several weeks to check the long-term profile of rhodamine release from GAMs. All measeurements were repeated three times and the average value of absorbance for each sample was calculated.

Cell culture and cytotoxicity assays

HaCaT cells (immortalized human keratinocytes) were cultured using DMEM (Dulbecco's Modified Eagle Medium α) (Gibco 31331-028) media supplemented with 10% (v/v) fetal bovine serum (FBS) (Eurobio CVFSVF00-01). Cells were cultured at 37 °C in 5% CO_2 in a 10 cm diameter Petri dish and trypsinized using 0.05% Trypsin-EDTA (Gibco 25300-054). HaCat cells (10^4 cells per well) were seeded in 96 well plates and allowed to attach for 24 hours. After sterilization with 70% (w/v) ethanol for 30 min and UV irradiation for 1 h, the hydrogels were dried and added to the cell culture. The sterilized samples were added in the wells and incubated for 1, 4, 6 and 8 days. Cell viability was analyzed using MTT assay carried out by incubating 100 μL of 0.5 mg mL^{-1} of MTT solution on the cells for 3 h. Purple coloured formazan crystals were dissolved using 100 μL of dimethyl sulfoxide (DMSO, BDH Prolab 23486.297) and the absorbance was recorded at 560 nm using Multiskan plat reader (thermos, USA).

Antibacterial activity of the samples loaded with chlorhexidine acetate

The antibacterial activity of drug-loaded GAMs was examined against *Staphylococcus aureus* (*S. aureus*, Gram positive) and *Pseudomonas aeruginosa* (*P. aeruginosa*, Gram negative). These bacteria were selected because they are among the primary causes of delayed healing and infection in both acute and chronic wounds.[31] For the cultivation, bacteria aliquots frozen at −20 °C were used. Fresh Tryptone Salt Broth (TSB) medium was inoculated by bacteria and incubated overnight at 37 °C under constant rotation and in aerobic conditions. Once the stationary phase was reached, cells were harvested by centrifugation and resuspended in a TSB. The optical density at 620 nm (OD_{600}) of the bacterial suspension was then adjusted to 0.75 ± 0.01 for *S. aureus* and 0.80 ± 0.01 for *P. aeruginosa* by dilution.

For the antibacterial tests three samples were prepared – cross-linked with 2% Ca^{2+} and 0.5% GTA and neutralized with 20% glycine solution with the chlorhexidine acetate content: 0 mg mL^{-1}, 0.1 mg mL^{-1} and 1 mg mL^{-1}. The samples were sterilized by exposition to UVC light (10 min for each sample side). Mueller–Hinton agar (GMH) plates were prepared by adding microbiological agar (15 g·L^{-1}) to PBS medium; two rectangular dishes were used, each for one type of bacteria. GMH agar plates were inoculated individually with 1 mL of *S. aureus* or *P. aeruginosa* suspension. Immediately after, the samples of GAMs were put onto the inoculated GMH plates to characterize the ability of the materials to prevent bacterial growth around the samples. The plates were then incubated overnight at 37 °C in aerobic conditions to allow the formation of a bacterial biofilm. Plates were pictured to check the presence of clear zones (inhibited bacterial growth) around the samples and within the biofilm formed.

3. Results and discussion

3D bioprinting feasibility

A total of 12 different GAM were produced with different cross-linking methods (Table 1). When the hydrogel is extruded onto a cooled Petri dish at a temperature of about 10–15 °C, it solidifies quickly, allowing the printing of desired shapes. For example, freshly printed hydrogel matrix is shown in Fig. 2(A) – the digital model of the matrix was presented in the previous section (Fig. 1). The gelatin–alginate bioink shows good

printability with visible grid lines with its form so tight that it can be easily removed from the Petri dish, it has adequate mechanical integrity and maintains a shape. Fig. 2(B) presents GAM filled with rhodamine 640 – the addition of a marker does not affect bioink printability. The cross-linking process affects the macroscopic structure of hydrogel matrices. GAMs cross-linked with GTA vapors slightly shrunked and changed their color to yellow-orange (Fig. 2(C)) which is due to the establishment of aldimine bonds (CH═N) between the free amine groups of gelatin proteins and glutaraldehyde.[32–34] After processing, the GAMs become visibly harder and stronger but they do not lose their flexibility which improves the potential contact with wound and is beneficial for comfort of use.

During printing, each printed matrix layer solidified before the next layer was plotted on it, as illustrated by optical (Fig. 2(D)) and fluorescent (Fig. 2(E)) microscopy pictures. It is easy to see that the top layer (horizontal) covers the bottom layer (vertical). They do not fuse with each other. Unfortunately, not all matrices printed one after the other are identical. Despite the same model and printing parameters, the continuity of grid happens to be broken, which can be seen by comparing Fig. 2(F) and (G) (red circle). The reason for this may be over- or underliquefying (too little or too much hydrogel is supplied) or blocking the nozzle, which was also observed by Long *et al.*[17] with chitosan-pectin hydrogel. The structure of the matrix has been retained after printing, but the sizes of model elements (pores, grids) are not consistent with those designed in the computer model (Fig. 1). Adjusting the printing speed or greater control over the viscosity of the bioink (*e.g.* by changing the process and surrounding temperature) could solve those problems. The speed of the moving printing nozzle and the viscosity of the bioink are of great importance for ensuring the continuity of the printout.[1]

Effect of chemical cross-linking and lyophilization on the structure of GAMs

The surface morphology of 3D printed GAMs was examined using scanning electron microscopy (SEM). The SEM technique requires the samples to be dehydrated, so all of the matrices were lyophilized as described in the Materials and methods section. Analysis of SEM images (Fig. 3) and comparison with images from optical and fluorescent microscopes (Fig. 2(D)–(G)) showed a clear effect of freeze-drying on GAMs structure. Indeed, SEM showed matrices that are not clearly multi-layered (subsequent layers have fused together). In addition, the hydrogel surface appeared not smooth and depended on the crosslinking method (see smaller pictures provided in Fig. 3). The only smooth surface was the underside, which was deposited directly on the slide during printing as a first layer (Fig. 3(E)).

As shown in Fig. 3, GAMs that were not cross-linked retained a regular mesh structure, with slightly visible layers (Fig. 3(A)). The surface of the matrix cross-linked with calcium ions looked similar (Fig. 3(B) and (C)) *i.e.* rough, slightly porous, but uniform and compact. Cross-linking of GAMs with GTA caused significant changes in their structure. One modification is that subsequent layers of hydrogel fused with each other (Fig. 3(D) and (F)). Moreover, the holes in the matrix lose their rectangular shape and became rounded or disappeared, which is clearly visible especially in the case of matrices cross-linked with calcium ions and GTA vapors (Fig. 3(I) and (L)). Altogether, GTA vapor crosslinking impacted the uniformity and smoothness

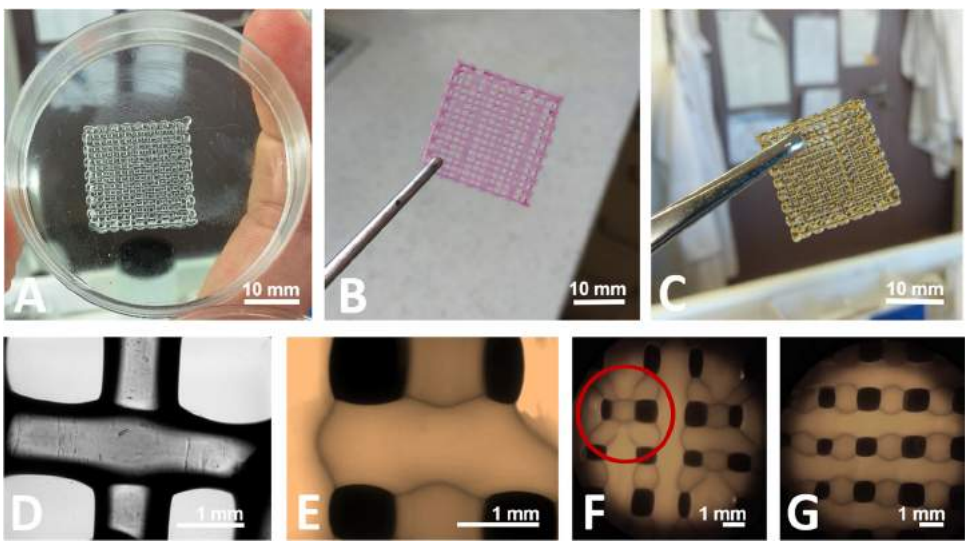

Fig. 2 3D bioprinted gelatin–alginate hydrogel (gelatin 0.2 g mL^{-1}, sodium alginate 0.04 g mL^{-1}) matrices before lyophilization – (A)–(C) phone camera pictures: (A) immediately after printing, bioink without additives, no cross-linking, (B) bioink with rhodamine, no cross-linking, (C) bioink without additives, after cross-linking with 2% Ca^{2+} and 25% GTA solutions; (D) optical microscopy picture, magnification 200×, bioink without additives, after cross-linking with 2% Ca^{2+} and 25% GTA solutions; (E) and (F) fluorescent microscopy pictures, bioink without additives, after cross-linking with 2% Ca^{2+} and 25% GTA solutions: (E) magnification 200×, (F) magnification 20×, (G) fluorescent microscopy picture, magnification 20×, bioink without additives, after cross-linking with 25% GTA solution.

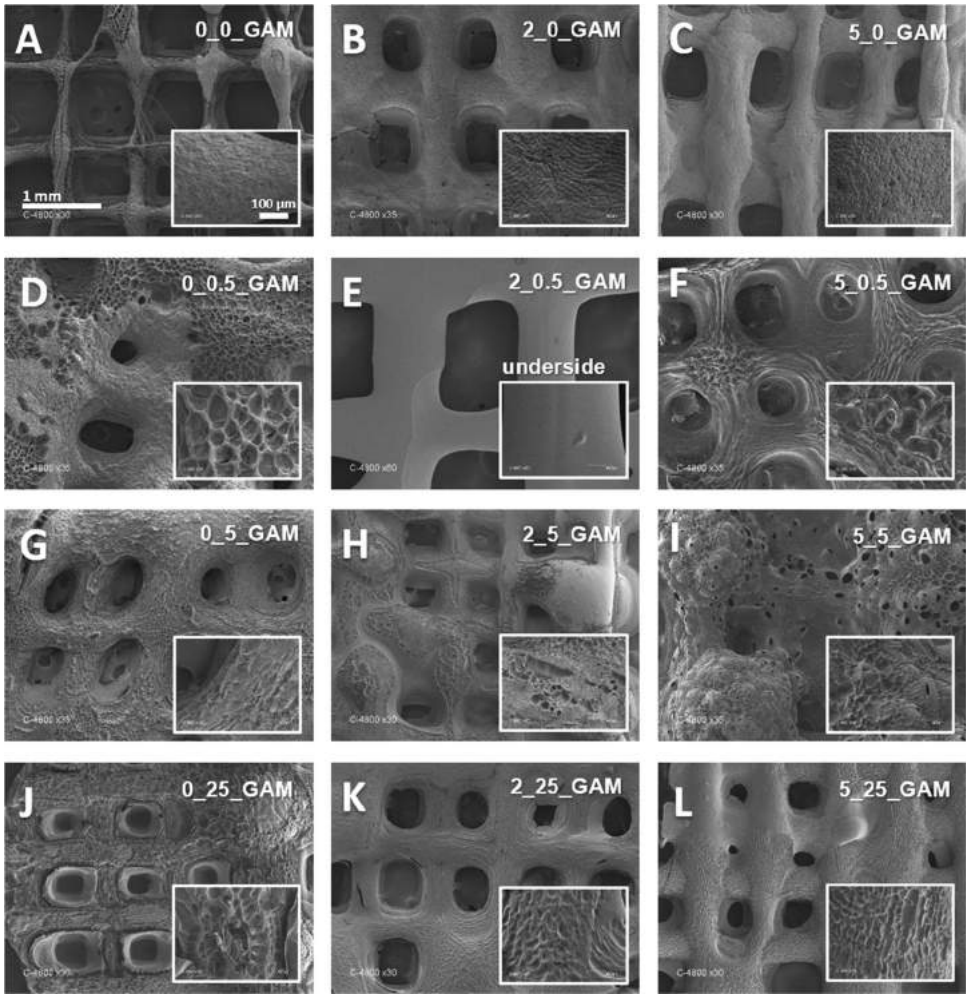

Fig. 3 SEM pictures of gelatin–alginate matrices cross-linked with agents of different concentration: (A) no crosslinking, (B) 2% Ca^{2+}, no GTA, (C) 5% Ca^{2+}, no GTA, (D) no Ca^{2+}, 0.5% GTA, (E) 2% Ca^{2+}, 0.5% GTA, (F) 5% Ca^{2+}, 0.5% GTA, (G) no Ca^{2+}, 5% GTA, (H) 2% Ca^{2+}, 5% GTA, (I) 5% Ca^{2+}, 5% GTA, (J) no Ca^{2+}, 25% GTA, (K) 2% Ca^{2+}, 25% GTA, (L) 5% Ca^{2+}, 25% GTA – magnification 30×; surface structures – magnification 300×.

of GAMs surfaces, which become porous with pores relatively big as compared to those of non-crosslinked matrices (Fig. 3(A)).

Fig. 4 shows the differential scanning calorimetry and thermogravimetric analysis curves of GAMs samples. Additionally,

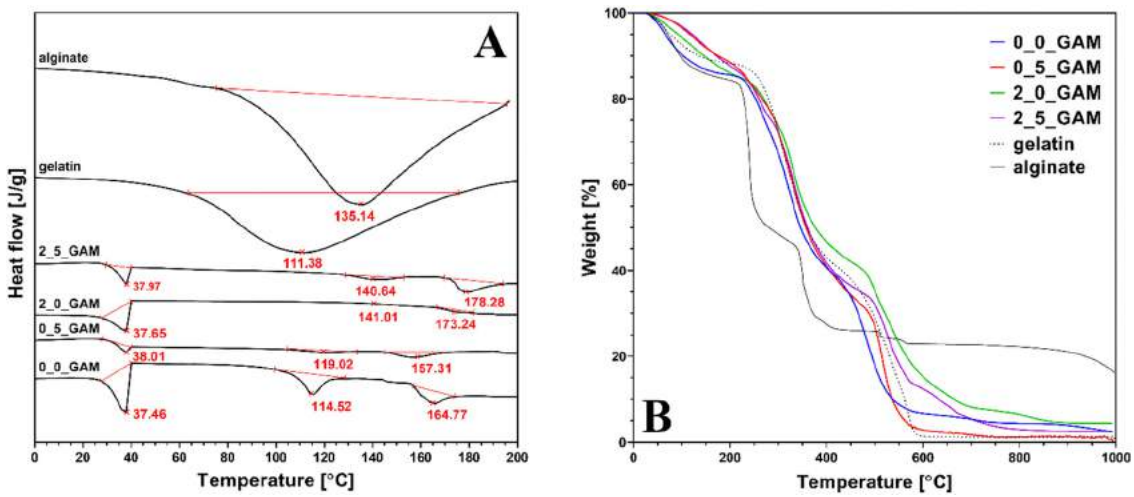

Fig. 4 (A) Differential scanning calorimetry and (B) thermogravimetric analysis of pure gelatin, sodium alginate and GAMs results.

the graphs were enriched with the curves for pure gel and sodium alginate as well as the temperatures of thermal transitions. Thermal transition enthalpies (ΔH_1 – gel–sol transition, ΔH_2 – glass transition, ΔH_3 – melting) with the total enthalpy change ΔH for pure gelatine, pure sodium alginate and the GAMs obtained from the DSC analysis are presented in Table 2. For sake of clarity of the data, it was decided to present only the ones for samples 0_0_GAM, 0_5_GAM, 2_0_GAM and 2_5_GAM, as there were no significant differences to the other samples or additional information that could be derived from an extended analysis.

For DSC research pure gelatin and sodium alginate showed wide endothermic peaks in the temperature range of 40–180 °C, with endothermic enthalpy change of 294.3 and 289.5 J g^{-1}, respectively, representing the dehydration of the polymers and changes in the structure of their chains.[35–37] The endothermic peaks observed in the GAMs hydrogel with reduced endothermic enthalpy of 7.31–46.11 J g^{-1} indicate that the formation of hydrogen bonds is correlated to a better organization of polymer chains and stronger bonding. It also suggests that the freeze-drying process successfully reduced the moisture content in the GAMs.

There are no low-temperature downward peaks situated around 0 °C due to the melting enthalpy of ice – all free and freezable water was removed as they are bound to the matrix less closely.[38] Although nonfreezable water itself is so strongly related to the polymer network that it does not show phase transition in calorimetric analysis, in the case of GAMs, its presence in the hydrogel is indirectly confirmed by the peaks seen in the graphs at around 37 °C. This is the temperature at which the alginate–gelatin hydrogel undergoes thermal transition. In the case of lyophilized GAMs, non-crystallized water acted as a plasticizer, increasing the mobility of the polymer chains and reducing the glass transition temperature, leading to the transformation of the hydrogel into sol. A similar phenomenon was described by Yoshida *et al.* for various polysaccharide hydrogels.[39] The differences that appear between differently crosslinked hydrogels result from the over-all hydrogen bonding ability (HBA) of the polymer. The only covalently cross-linked sample (0_5_GAM) shows the smallest peak due to the greatest reduction of said HBA. In the case of an ionotropically cross-linked sample (2_0_GAM), the cross-linking strength is lower, thus reducing HBA to a lesser extent. The under-curve area for the sample cross-linked with both methods (2_5_GAM) is between the peaks for the two samples described above, which may suggest that the two cross-linking methods do not always strengthen the polymer network simultaneously, but may be in opposition, *e.g.* by limited access to –COO– groups, needed in both Ca^{2+} ion cross-linking and GTA vapors covalent one, which also results from the work of Sun *et al.*[40]

The second peak appearing in the DSC plots can be attributed to the material's second glass transition temperature, T_g, caused by the helix-coil transition of gelatin and the release of bound water. With increasing temperature, alginate shows an increase in the overall hydrogen bonding ability due to the increased dissociation of the ions pairs, which was confirmed for other hydrophilic polymers.[35] The largest endothermic peak can be observed for the sample that was not cross-linked (0_0_GAM), so it can be concluded that in this case hydrogen bonds are involved in maintaining the triple helix structure. In other cases, cross-linked by any method, the peaks are barely marked on the DSC curve, which means that the structure is stabilized by stronger bonds than hydrogen ones – Ca^{2+} bridges and covalent –CO–NH– bonds from Schiff's base reaction. The reduction in the degree of unfolding of the triple helix structure of GTA vapor cross-linked gelatin compared to non-cross-linked gelatin was also demonstrated by Nagarajan *et al.*[41]

The third peak represents the melting temperature T_m of the material. Last endothermic peak in thermogram may be related to water tightly bonded through polar interactions with carboxylate. The presence of such bound water in polysaccharides has been reported by El-Houssiny *et al.*[42] and Sabater *et al.*[43] The highest peak was again observed for the non-cross-linked sample, which had the most unbound –COOH groups that could react with water molecules. The sample cross-linked only with GTA vapors (0_5_GAM) showed a smaller peak than the non-cross-linked one, suggesting that some of the carboxyl groups from alginate were used to cross-link the hydrogel with bonds between GTA-treated gelatin and alginate. The samples for which Ca^{2+} ions were used (2_0_GAM and 2_5_GAM) did not show any peak, indicating strong links between the alginate and gelatin chains as well as Ca^{2+} ions, which resulted in a high crosslinked network with few free reactive groups able to bind to water molecules.

The results of the TGA analysis presented in Fig. 4(B) confirm that the composition of the hydrogel did not change throughout the entire treatment. The first weight loss (10–15%) is observed between 100 and 200 °C. This decrease is related to the release of structural water and it is much slighter in cross-linked samples and occurs later than in the case of pure hydrogel components (sodium alginate and gelatin) or non-cross-linked samples. This confirms that in the case of cross-linked GAMs the bounded water is immobilized stronger. The second major weight loss observed between 200 and 400 °C shows the degradation of gelatin molecules. The third major weight loss observed from ~520 °C is due to the thermochemical decomposition of remaining organic content in the case of gelatin and GAMs. Although all GAMs samples degrade at much higher temperatures and in this matter the alginate content in the matrices does not affect their properties, it makes the GAMs leave more residue at the end of the analysis than pure gelatin. At the end of the TGA analysis, the difference between the amount of residual mass

Table 2 Thermal transition enthalpies (ΔH_1 – gel–sol transition, ΔH_2 – glass transition, ΔH_3 – melting) with the total enthalpy change ΔH for pure gelatine, pure sodium alginate and the GAMs

Sample	ΔH_1 [J g^{-1}]	ΔH_2 [J g^{-1}]	ΔH_3 [J g^{-1}]	ΔH [J g^{-1}]
Gel powder	—	294.3 ± 8.8	—	294.3 ± 8.8
Alg powder	—	—	289.5 ± 8.7	289.5 ± 8.7
0_0_GAM	17.7 ± 0.5	14.6 ± 0.4	13.9 ± 0.4	46.2 ± 1.4
0_5_GAM	3.0 ± 0.1	2.8 ± 0.1	8.1 ± 0.2	13.9 ± 0.4
2_0_GAM	5.5 ± 0.2	0.5 ± 0.1	1.3 ± 0.1	7.3 ± 0.2
2_5_GAM	3.6 ± 0.1	4.6 ± 0.1	8.4 ± 0.3	16.6 ± 0.5

after burning the gelatin (dashed line) and after burning the GAMs (colored lines) is about 3–4 percentage points. The only exception is the weight of the sample cross-linked only with GTA vapor (0_5_GAM, red line) which is equal to the weight of pure gelatin. This may suggest that cross-linked gelatin has a much greater effect on the thermal properties of the hydrogel than non-cross-linked sodium alginate. Likewise, the mass of the sample cross-linked only with calcium ions (2_0_GAM, blue line) at the end of the process is much greater than the mass of pure gelatin or the rest of the samples with a final mass value somewhere in between. This confirms the previous observation that the effects of hydrogel cross-linking with calcium ions and GTA vapors do not reinforce each other when they are used simultaneously, but are rather competitive.

Swelling of the matrices

Considering that the method used to cross-link the gelatin–alginate hydrogel has a large impact on its structure, it can be presumed that it will also affect its other properties. It is therefore important to properly select the concentrations of the cross-linking agents in order to obtain a desired material. A hydrogel suitable for drug delivery system for wound dressing (the purpose of this study) should be characterized by a high equilibrium swelling ratio because it directly affecets the hydrogel ability for absorbing the wound exudates which can contain possibly harmful substances.[26] The equilibrium swelling ratio (ESR) of GAMs is presented in Fig. 5.

Almost all lyophilized hydrogel matrices swelled rapidly and reached an equilibrium state after 40–60 min. The only exceptions were 2_0_GAM and 5_0_GAM samples cross-linked only with calcium ions. They did not reach equilibrium state before degradation, which occurred after 3 hours (for GAM cross-linked with the solution containing 2% Ca^{2+}) and after 4 hours (for the one cross-linked with the 5% Ca^{2+} solution) – this is visible as a sudden break in the curves due to missing data (sample decay). During the last measurement, the samples reached 980% and 1420% hydration, respectively. The samples degradation was caused by the displacement of calcium ions from the polymer network by monocations (Na^{+}) contained in the PBS solution. The greater stability was observed for the sample cross-linked with 5% Ca^{2+} and thus with more intermolecular bonds between alginate chains. Consequently, this sample absorbed more water being able to spend more time in the swelling medium.

For all other samples the equilibrium state was reached, although average equilibrium water content (EWC) values were slightly fluctuating. This value was the highest for samples 0_0.5_GAM, 0_5_GAM and 0_25_GAM cross-linked only with glutaraldehyde vapors – after 40 minutes, EWC for these samples reached approximately 400%, 380% and 325%, respectively. The matrices cross-linked by both methods (calcium ions and GTA vapors) showed reduced ability to absorb water. EWC for samples 2_0.5_GAM and 5_0.5_GAM were comparable and amounted to about 260–280%. Similarly, other samples can be combined into pairs – for the 2_5_GAM and 5_5_GAM samples, EWC was 200–240%, while for the 2_25_GAM and 5_25_GAM samples, it was the lowest and its value reached 180–200%. It can be easily noticed

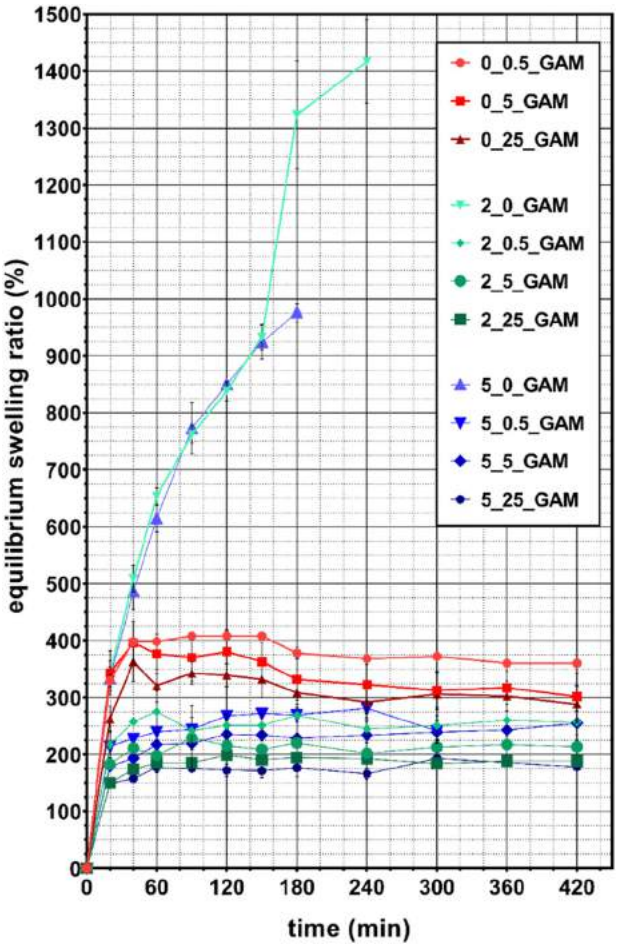

Fig. 5 Equilibrium swelling ratio of lyophilized GAMs depending on the cross-linking method and the concentrations of cross-linking agents. A chart uses points connected by line segments from left to right to demonstrate changes in value and to facilitate tracking of them.

that a higher concentration of GTA vapors results in lower hydrogel swelling capability. In addition, if this crosslinking agent is used together with calcium ions, then Ca^{2+} crosslinking has a negligible effect on matrix swelling properties. During the tests, it was also observed that after about 3 hours, the weight of samples cross-linked only with GTA vapors decreased due to their slow degradation (data not shown). This phenomenon does not occur for samples cross-linked by both methods (Ca^{2+} and GTA).

Rhodamine release from GAMs

The substance controlled release is an important ability of the hydrogel from the point of view of its potential use as a wound dressing. It is important that the release proceeds without a burst effect at the beginning and continues as long as possible. It is also useful to be able to control the release properties, for example by selecting the hydrogel cross-linking method. The marker dye rhodamine 640 was used due to its highly sensitive ability to absorb light at a wavelength of 574 nm. Moreover, the size of its molecule is comparable to the size of the chlorhexidine molecule, which was used in the study of the antibacterial

properties of GAMs (591 g mol^{-1} for Rod and 625 g mol^{-1} for CA), it may therefore mimic the release of this drug.

Fig. 6 and 7 show the rhodamine release profiles from hydrogel matrices over the period of 9 hours. The curves are divided into three groups differing in colors, red for samples cross-linked only with GTA vapors (with various concentrations ranging from 0.5–25%), green and blue for cross-link with GTA vapors and a 2% or 5% solution of Ca^{2+} ions, respectively.

In all three groups of samples mentioned, increasing the concentration of GTA vapors or calcium ions used for cross-linking causes a slower release rate of rhodamine. Additionally, for samples cross-linked with higher GTA concentrations, the lower concentrations of rhodamine are reached meaning that less rhodamine is released. The theoretical content of rhodamine in the matrices is the same. As shown in Fig. 6(A), the release of rhodamine is 10^{-4} mg mL^{-1} for the 5_25_GAM and 1.2×10^{-3} mg mL^{-1} for the 5_0_GAM. The hydrogel matrix 2_0.5_GAM, which was cross-linked by both methods, but under the mildest conditions, did not reach the equilibrium state even after 12 weeks (Fig. 6(B), green squares), unlike the other two matrices presented in the graph (0_0.5_GAM and 5_0.5_GAM). For the sample cross-linked only with 0.5% GTA vapors without Ca^{2+} (red circles), the equilibrium state is reached around week 5, for the sample cross-linked with 5% Ca^{2+} and 0.5% GTA vapors (blue triangles), the equilibrium state reached at the beginning of rhodamine release (burst release) is maintained until the week 12.

The shape of the rhodamine release profile from GAMs is of particular interest. In most cases, the release of rhodamine appears to be two-step. In order to better illustrate this phenomenon, curves were fitted to the experimental data, and the results are presented in Fig. 7. Since the matrices cross-linked with 2% and 5% of calcium ions showed similar properties, it was decided to further analyze the data only for samples cross-linked 2% of Ca^{2+}.

When a drug or model substance is released, it is possible to acquire a mathematical description of the relationship between release rate and time. Such a release profile can be usually described by a linear or an exponential function (zero- or first-order kinetics). The fit of an expotential curve to the experimental data of rhodamine releasing from GAMs is shown in Fig. 7(A). In general, this fit is good as indicated by the values of the coefficient of determination R^2_{exp1} which ranged from 0.8994 to 0.9892 (Table 3). However, this fit did not cover exactly all the experimental points, especially in the initial period of rhodamine release.

Therefore, the data was devided into two ranges in order to adjust the curve independently to the experimental points in each of them, as shown in Fig. 7(B). In the initial period of rhodamine release, a linear fit was applied. The values of the coefficient of determination R^2_{lin} for such a fit ranged from 0.9113 to 0.9908 (Table 3) and are higher than for the exponential fit covering all points. An exponential curve was fitted to the data following the linear range, however, in only two cases, the R^2_{exp2} was higher than 0.95 for this fit. In order to model the release of rhodamine from freeze-dried GAMs, a linear fit should be used in the initial release period and then an exponential fit for the resting data range.

It can therefore be concluded that the release of rhodamine from the freeze-dried GAMs initially follows zero-order kinetics.

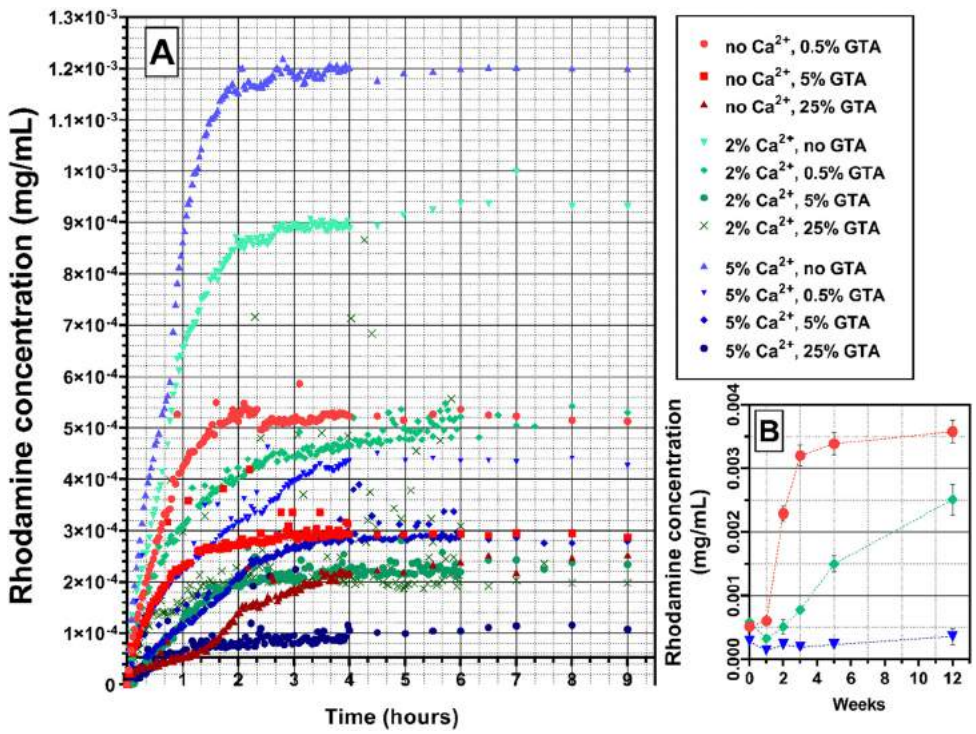

Fig. 6 Rhodamine 640 release profile from GAMs cross-linked with different methods: (A) initial release, 9 hours; (B) long-term release, selected samples, 12 weeks. A chart uses points connected by line segments from left to right to demonstrate changes in value and to facilitate tracking of them.

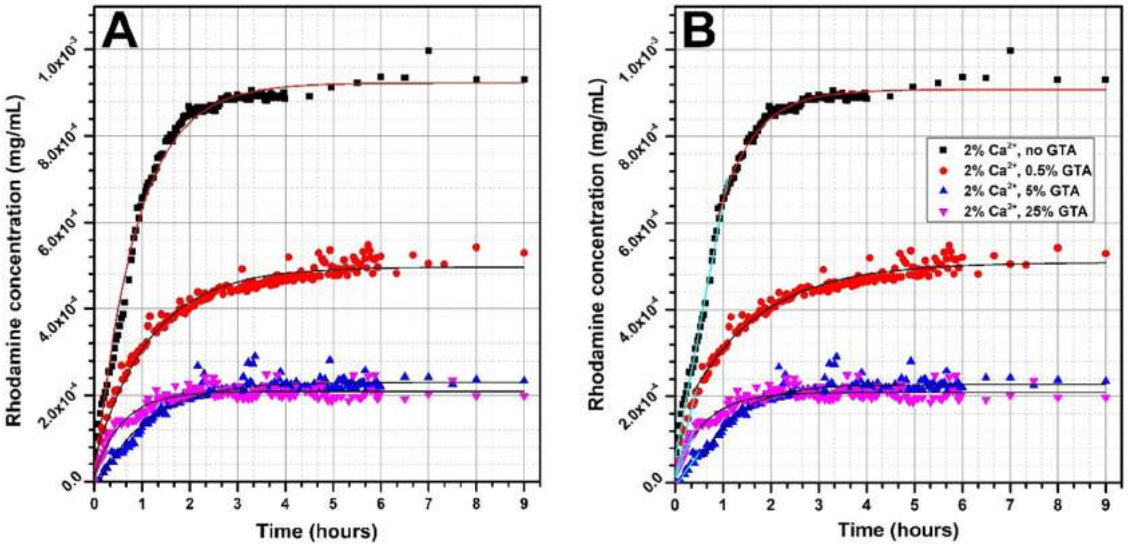

Fig. 7 Rhodamine 640 release profile from GAMs cross-linked with different methods with model fitted curves: (A) exponential fit for all the data, (B) linear fit for the initial period of releasing and exponential fit for the following data.

In this case, the release of the active substance is only a function of time, and the process proceeds at a constant rate regardless of the concentration of the agent. Comparing the time range in which the release takes place with zero-order kinetics (Table 3(B)) with the GAMs swelling over time graph (Fig. 5) leads to the observation that they correspond to the initial period of the fastest swelling of the matrices. When GAM is placed in the solution, the water is imbibed into the hydrogel structure dissolving the rhodamine. The active ingredient is first dissolved in the hydrating water and only then can be released into the solution. The constant release rate is due to the saturation of the hydrogel, because only the swollen matrix can be permeable to rhodamine, so its release rate depends on the swelling. Such behavior of active substance-releasing membranes according to zero-order kinetics after placing in a liquid has been previously described.[24,25] Once the full hydration is achieved, release of rhodamine from the hydrogel begins to follow first-order kinetics.[24] Systems that exhibit such a substance release mechanism are suitable for controlled sustained drug delivery because due to the zero-order kinetics in the initial subtance release period, the burst release effect is limited.[25]

Table 3 Coefficient of determination R^2 for the curves fitted to the data presented in Fig. 7

	A	B			
	Expotential fit	Linear fit		Expotential fit	
Sample	R^2_{exp1} [−]	Range [h]	R^2_{lin} [−]	Range [h]	R^2_{exp2} [−]
2% Ca^{2+}, no GTA	0.9892	0–1.10	0.9908	1.10–9.00	0.9674
2% Ca^{2+}, 0.5% GTA	0.9725	0–0.47	0.9466	0.47–9.00	0.9605
2% Ca^{2+}, 5% GTA	0.9419	0–0.50	0.9701	0.50–9.00	0.8776
2% Ca^{2+}, 25% GTA	0.8994	0–0.40	0.9113	0.40–9.00	0.6746

Cytotoxicity of GAMs

In order to validate the potential use of the 3D bioprinted gelatin–alginate hydrogel matrices for wound dressing application, we aimed to demonstrate its biocompatibility on human keratinocytes. The biocompatibility of the GAMs was analyzed after 1, 4, 6 and/or 8 days of culture using HaCat cells. As shown in Fig. 8(A), a clear cytotoxicity was observed upon increasing concentrations of GTA used for gelatin cross-link. This effect was strongly attenuated by glycine neutralization (Fig. 8(B)) and we measured a significant increase in cell proliferation between 1 and 8 days in the presence of neutralized GAMs thus demonstrating their cytocompatibility.

Antibacterial activity of chlorhexidine-loaded GAMs

Gelatin–alginate hydrogel matrices with antibiotic activity is useful for wound dressing applications regarding the need to maintain sterility at the wound site. In that frame, we loaded GAMs with different concentration of chlorhexidine acetate (CA) and characterized their antimicrobial activity using an agar diffusion inhibitory growth test. CA is a widely used well-known bisbiguanide compound with rapid bactericidal activity against both Gram-positive and Gram-negative organism.[44] It was used in our work due to its application in disinfection of the skin, as an additive to creams, toothpaste, deodorants, and antiperspirants as well as in pharmaceutical products.[45]

The antibacterial activity tests were carried out with the sample 2_0.5_GAM neutralized with a 20% glycine solution. Each sample was deposited on the surface of nutrient agar plate previously inoculated with *S. aureus* or *E. coli* at a concentration of 10^8 CFU mL^{-1} and incubated for 24 h. Fig. 9 illustrates the results of the anibacterial properties study.

In all cases, the concentration of CA was sufficient to suppress bacterial growth. The area of growth inhibition zones (clear zones) were visible around the materials for *S. aureus* and *E. coli*.

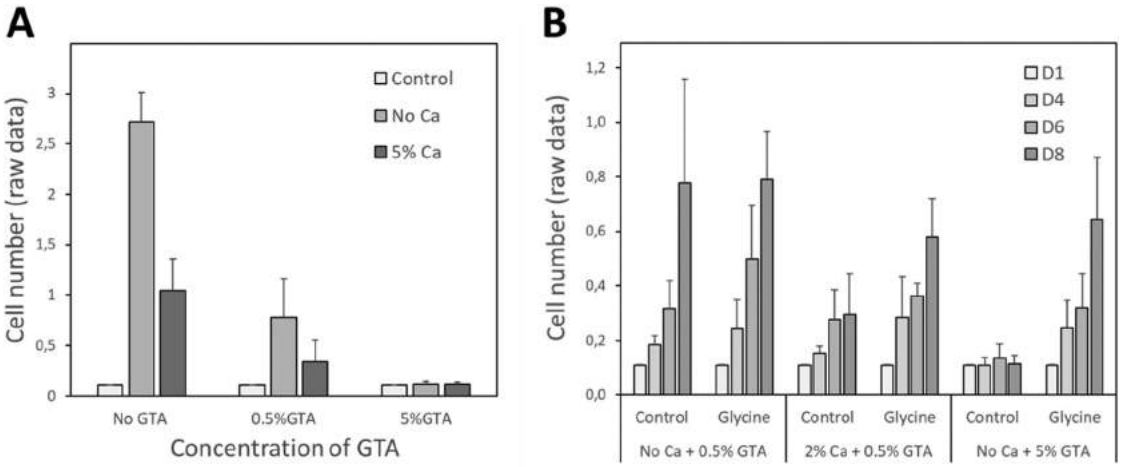

Fig. 8 Analysis of GAMs cytocompatibility using hFOB1.19 cells. (A) The cytotoxicity of GAMs cross-linked or not with 5% Ca^{2+} and 0.5% or 5% GTA tested at day 8 after seeding. (B) Effect of glycine neutralization on the cytotoxicity of GAMs cross-linking with or without 2% Ca^{2+} and 0.5% or 5% GTA analyzed. The analysis was performed 4, 6 and 8 days after cell seeding.

They were greater for material with a higher drug concentration. A tenfold increase in drug content (1 mg mL^{-1}, Fig. 9) resulted in a significant increase in the clear zone size. This observation was made only for drug-loaded GAMs, and not for the drug-free one, which means that there are no antibacterial glutaraldehyde residues in the material. This suggests that the GTA vapor concentration had been properly selected and the matrix had been neutralised. The antibacterial action of the material loaded with chlorhexidine was rapid (with a significant effect visible from 3 h of treatment) and persistent over at least 72 h. The antibacterial activity of the GAMs against the bacteria evidenced that the integrity of the drug had not been affected by the temperature or pressure during bioink preparation and 3D bioprinting. Hence, these types of GAMs are suitable materials for wound dressing applications to treat infected sites or to prevent infection.

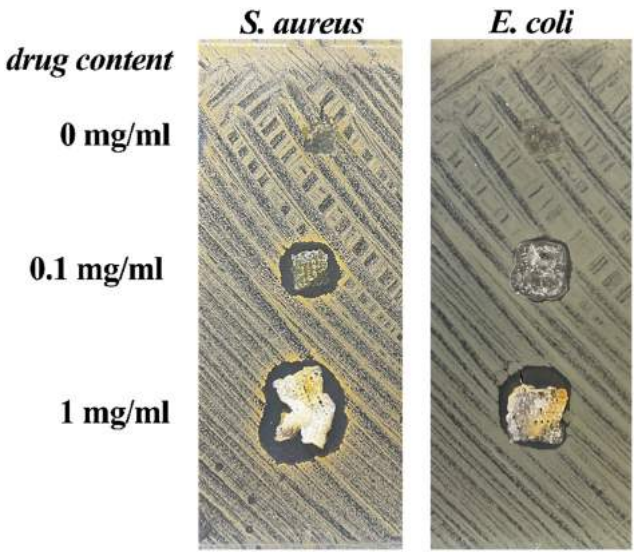

Fig. 9 Bacteriostatic tests of CA-loaded GAMs on nutrient agar plates covered with *S. aureus* and *E. coli* biofilms after 24 h of material treatment. GAMs cross-linked with 2% Ca^{2+} and 0.5% GTA, neutralized with glycine with no drug, 0.1 mg mL^{-1} CA or 1 mg mL^{-1} CA.

4. Conclusions

The gelatin–alginate bioink with the compunds concentrations of 0.2 g mL^{-1} and 0.04 g mL^{-1}, respectively, is a good and satisfying material for use in 3D bioprinting. Easy to prepare from the readily available substances, the hydrogel can be conveniently bioprinted in mild conditions. It represents an excellent basis for creating a novel stable biodegradable 3D bioprinted material for drug delivery purposes, potentially wound dressing applications. The gelatin–alginate hydrogels can be successfully cross-linked by exposure to calcium ions or glutaraldehyde vapors. The chosen method and concentrations of crosslinkers have an impact on the properties of the obtained materials including the structure of freeze-dried hydrogels and the morphology of their surface. The high equilibrium swelling ratio (ESR) and equilibrium water content (EWC) values of GAMs indicated their potential high effectiveness in absorbing wound exudates, a desirable feature of dressings. The study of rhodamine release showed that it can be described with a zero-order kinetics in the initial release period followed by a first-order kinetics release after 30–60 minutes, the burst release effect being limited. The data showed that the cross-linking method has an influence on the release rate.

In the present study, a compromise was made between physicochemical properties and cytotoxicity, leading to the selection of the combined method (ionotropic-covalent) with the lowest concentrations of cross-linking agents (2% Ca^{2+} and 0.5% GTA). The biocompatibility of the glycine-neutralized cross-linked GAMs and the antibacterial properties of chlorexidin-loaded hydrogels against both Gram positive and Gram negative bacteria were validated. The work presents coherently the 3D bioprinted cross-linked drug-loaded gelatin–alginate hydrogel

matrices and a detailed description of various properties important for a potential use as wound dressings. Such a material can be potentially applied in biomedical engineering, especially as controlled drug delivery systems.

Conflicts of interest

There are no conflicts to declare.

Acknowledgements

This project was supported by European Social Fund [POWR.03.02.00-00-1028/17-00] as part of the POWER Och!Dok program and partialy supported by ''Cancéropôle Grand Sud-Ouest'' through a project ''Emergence de projets 2021''. AM would like to thank Campus France for the funding through a French Government Scholarship. Authors acknowledge the financial support of project H2020-MSCA-RISE-2017, 'Novel 1D photonic metal oxide nanostructures for early stage cancer detection' (Project number: 778157).

References

1 L. Valot, J. Martinez, A. Mehdi and G. Subra, Chemical insights into bioinks for 3D printing, *Chem. Soc. Rev.*, 2019, **48**(15), 4049–4086.
2 K. Jakab, C. Norotte, F. Marga, K. Murphy, G. Vunjak-Novakovic and G. Forgacs, Tissue engineering by self-assembly and bioprinting of living cells, *Biofabrication*, 2010, **2**, 2001.
3 L. Moroni, J. de Wijnab and C. van Blitterswijka, 3D fiber-deposited scaffolds for tissue engineering: Influence of pores geometry and architecture on dynamic mechanical properties, *Biomaterials*, 2006, **27**(7), 974–985.
4 W. Long Ng, C. Kai Chua and Y.-F. Shen, Print me an organ! why we are not there yet, *Prog. Polym. Sci.*, 2019, **97**, 101145.
5 I. Matai, G. Kaur, A. Seyedsalehi, A. McClinton and C. T. Laurencin, Progress in 3D bioprinting technology for tissue/organ regenerative engineering, *Biomaterials*, 2019, **226**, 119536.
6 P. Shende and S. Agrawal, Integration of 3D printing with dosage forms: A new perspective for modern healthcare, *Biomed. Pharmacother.*, 2018, **107**, 146–154.
7 W. Peng, P. Datta, B. Ayan, V. Ozbolat, D. Sosnoski and I. T. Ozbolat, 3D bioprinting for drug discovery and development in pharmaceutics, *Acta Biomater.*, 2017, **57**, 26–46.
8 A. Rees, L. C. Powell, G. Chinga-Carrasco, D. T. Gethin, K. Syverud and K. E. Hill, 3D bioprinting of carboxymethylated-periodate oxidized nanocellulose constructs for wound dressing applications, *BioMed Res. Int.*, 2015, 1–7.
9 P. He, J. Zhao, J. Zhang, B. Li, Z. Gou, M. Gou and X. Li, Bioprinting of skin constructs for wound healing, *Burns Trauma*, 2018, **6**, 5.
10 B. Stubbe, A. Mignon, H. Declercq, S. van Vlierberghe and P. Dubruel, Development of gelatin–alginate hydrogels for burn wound treatment, *Macromol. Biosci.*, 2019, **19**(8), e1900123.
11 S. M. King, S. C. Presnell and D. G. Nguyen, Development of 3D bioprinted human breast cancer for *in vitro* drug screening, *Cancer Res.*, 2014, **74**(19), 2034.
12 X. Li, B. Liu, B. Pei, J. Chen, D. Zhou, J. Peng and T. Xu, Inkjet bioprinting of biomaterials, *Chem. Rev.*, 2020, **120**(19), 10793–10833.
13 W. L. Ng, J. M. Lee, M. Zhou, Y.-W. Chen, K.-X. A. Lee, W. Yeong and Y.-F. Shen, Vat polymerization-based bioprinting – process, materials, applications and regulatory challenges, *Biofabrication*, 2019, **12**(2), 022001.
14 T. Jiang, J. G. Munguia-Lopez, S. Flores-Torres, J. Kort-Mascort and J. M. Kinsella, Extrusion bioprinting of soft materials: An emerging technique for biological model fabrication, *Appl. Phys. Rev.*, 2019, **6**(1), 011310.
15 S. Murphy and A. Atala, 3D printing of tissues and organs, *Nat. Biotechnol.*, 2014, **32**(8), 773–785.
16 I. Ozbolat, W. Peng and V. Ozbolat, Application areas of 3D bioprinting, *Drug Discovery Today*, 2016, **21**(8), 1257–1271.
17 J. Long, A. E. Etxeberria, A. V. Nand, C. R. Bunt, S. Ray and A. Seyfoddin, A 3D printed chitosan-pectin hydrogel wound dressing for lidocaine hydrochloride delivery, *Mater. Sci. Eng., C*, 2019, **104**, 109873.
18 G. Poologasundarampillai and A. Nommeots-Nomm, *Materials for 3D printing in medicine, in 3D Printing in Medicine*, 2017, pp. 43–71.
19 B. Duan, L. A. Hockaday, K. H. Kang and J. T. Butcher, 3D Bioprinting of heterogeneous aortic valve conduits with alginate/gelatin hydrogels, *J. Biomed. Mater. Res., Part A*, 2012, **101A**(5), 1255–1264.
20 T. Gao, G. J. Gillispie, J. S. Copus, A. K. Pr, Y.-J. Seol and A. Atala, Optimization of gelatin–alginate composite bioink printability using rheological parameters: A systematic approach, *Biofabrication*, 2018, **10**(3), 034106.
21 T. Pan, W. Song, X. Cao and Y. Wang, 3D bioplotting of gelatin/alginate scaffolds for tissue engineering: Influence of crosslinking degree and pore architecture on physicochemical properties, *J. Mater. Sci. Technol.*, 2016, **32**(9), 889.
22 I. Migneault, C. Dartiguenave, M. J. Bertrand and K. C. Waldron, Glutaraldehyde: Behavior in aqueous solution, reaction with proteins, and application to enzyme crosslinking, *Biotechniques*, 2004, **37**(5), 790–802.
23 J. H. Y. Chung, S. Naficy, Z. Yue, R. Kapsa, A. Quigley, S. E. Moulton and G. G. Wallace, Bio-ink properties and printability for extrusion printing living cells, *Biomater. Sci.*, 2013, **1**(7), 763.
24 M.-L. Laracuente, M. H. Yu and K. J. McHugh, Zero-order drug delivery: State of the art and future prospects, *J. Controlled Release*, 2020, **327**, 834–856.
25 M. L. Bruschi, Mathematical models of drug release, *Strategies to Modify the Drug Release from Pharmaceutical Systems*, Woodhead Publishing, Cambridge, 2015, pp. 63–86.
26 J. S. Boateng, K. H. Matthews, H. N. E. Stevens and G. M. Eccleston, Wound healing dressings and drug delivery systems: A Review, *J. Pharm. Sci.*, 2008, **97**(8), 2892–2923.
27 D. Okan, K. Woo, E. A. Ayello and G. Sibbald, The role of moisture balance in wound healing, *Adv. Skin Wound Care*, 2007, **20**(1), 39–53.

28 Y. Zhang, J. Venugopal, Z. Huang, C. Lim and S. Ramakrishna, Crosslinking of the electrospun gelatin nanofibers, *Polymer*, 2006, **47**, 2911–2917.
29 J. R. Khurma, D. R. Rohindra and A. V. Nand, Synthesis and properties of hydrogels based on chitosan and poly(vinyl alcohol) crosslinked by genipin, *J. Macromol. Sci., Part A: Pure Appl. Chem.*, 2006, **43**, 749–758.
30 M. Grzeczkowicz and D. Lewińska, A method for investigating transport properties of partly biodegradable spherical membranes using vitamin B12 as the marker, *Desalin. Water Treat.*, 2018, **128**, 170–178.
31 P. Bowler, B. Buerden and D. Armstron, Wound microbiology and ssociated approaches to wound management, *Clin. Microbiol. Rev.*, 2001, **14**(2), 244–269.
32 O. Damnik, P. J. Dijkstra, M. Luyn, L. O. Damink, P. Dijkstra, M. J. A. Van Luyn, P. B. Van Wachem, P. Nieuwenhuis and J. Feijen, Glutaraldehyde as a crosslinking agent for collagen-based biomaterials, *J. Mater. Sci.: Mater. Med.*, 1995, **6**(8), 460–472.
33 Y. Z. Zhang, J. Venugopal, Z.-M. Huang, C. T. Lim and S. Ramakrishna, Crosslinking of the electrospun gelatin nanofibers, *Polymer*, 2006, **47**(8), 2911–2917.
34 T. Chaochai, Y. Imai, T. Furuike and H. Tamura, Preparation and properties of gelatin fibers fabricated by dry spinning, *Fibers*, 2016, **4**(4), 2.
35 Z. Ping, Q. Nguyen, S. Chen, J. Zhou and Y. Ding, States of water in different hydrophilic polymers—DSC and FTIR studies, *Polymer*, 2001, **42**(20), 8461–8467.
36 D. Chi-An, C. Yi-Fan and L. Ming-Wei, Thermal properties measurements of renatured gelatin using conventional and temperature modulated differential scanning calorimetry, *J. Appl. Polym. Sci.*, 2006, **99**(4), 1795–1801.
37 H. Hatakeyama and T. Hatakeyama, Interaction between water and hydrophilic polymers, *Thermochim. Acta*, 1998, **308**(1-2), 3–22.
38 M. U. Joardder, M. Mourshed and M. Hasan, Bound water measurement techniques, *State of bound water: Measurement and significance in food processing*, Springer International Publishing, NYC, 2019, pp. 47–82.
39 H. Yoshida, T. Hatakeyama and H. Hatakeyama, Effect of water on the main chain motion of polysaccharide hydrogels, *ACS Symp. Ser.*, 1992, **489**, 217–230.
40 J. Sun and H. Tan, Alginate-based biomaterials for regenerative medicine applications, *Materials*, 2013, **6**(4), 1285–1309.
41 S. Nagarajan, H. Belaid, C. Pochat-Bohatier, C. Teyssier, I. Iatsunskyi, E. Coy, S. Balme, D. Cornu, P. Miele, N. S. Kalkura, V. Cavailles and M. Bechelany, Besign of boron nitride/gelatin electrospun nanofibers for bone tissue engineering, *ACS Appl. Mater. Interfaces*, 2017, **9**, 33695–33706.
42 A. El-Houssiny, A. Ward, D. Mostafa, S. Abd-El-Messieh, K. Abdel-Nour, M. Darwish and W. Khalil, Drug-polymer interaction between glucosamine sulfate and alginate nanoparticles: FTIR, DSC and dielectric spectroscopy studies, *Adv. Nat. Sci.: Nanosci. Nanotechnol.*, 2016, **7**, 025014.
43 R. Sabater i Serra, J. Molina-Mateo, C. Torregrosa-Cabanilles, A. Andrio-Balado, J. M. Meseguer Duenas and A. Serrano-Aroca, Bio-nanocomposite hydrogel based on zinc alginate/graphene oxide: Morphology, structural confirmation, thermal behavior/degradation, and dielectric properties, *Polymers*, 2020, **12**(3), 702.
44 I. R. Sanchez, K. E. Nusbaum, S. F. Swaim, A. S. Hale, R. A. Henderson and J. A. Mcguire, Chlorhexidine diacetate and povidone-iodine cytotoxicity to canine embryonic fibroblasts and staphylococcus aureus, *Vet. Surg.*, 1988, **17**(4), 182–185.
45 T. Güthner, *Guanidine and Derivatives, in Ullman's Encyclopedia of Industrial Chemistry*, Wiley, 2007.

PUBLICATION 5

Gelatin methacrylate hydrogel with drug-loaded polymer microspheres as a new bioink for 3D bioprinting

Mirek, A., Belaid, H., Bartkowiak, A., Barranger, F., Salmeron, F., Kajdan, M., Grzeczkowicz, M., Cavaillès, V., Lewińska, D., Bechelany, M.
Biomaterials Advances. 150, 213436 (2023).
DOI: 10.1016/j.bioadv.2023.213436

Biomaterials Advances 150 (2023) 213436

Contents lists available at ScienceDirect

Biomaterials Advances

journal homepage: www.journals.elsevier.com/materials-science-and-engineering-c

Gelatin methacrylate hydrogel with drug-loaded polymer microspheres as a new bioink for 3D bioprinting

Adam Mirek [a,b], Habib Belaid [b], Aleksandra Bartkowiak [a], Fanny Barranger [b], Fanny Salmeron [c], Marilyn Kajdan [c], Marcin Grzeczkowicz [a], Vincent Cavaillès [c], Dorota Lewińska [a], Mikhael Bechelany [b,d,*]

[a] Nalecz Institute of Biocybernetics and Biomedical Engineering, Polish Academy of Sciences, 02-109 Warsaw, Poland
[b] Institut Européen des Membranes, IEM, UMR 5635, Univ Montpellier, CNRS, ENSCM Place Eugène Bataillon, 34095 Montpellier cedex 5, France
[c] IRCM, Institut de Recherche en Cancérologie de Montpellier, INSERM U1194, Université Montpellier, Montpellier F-34298, France
[d] Gulf University for Science and Technology, GUST, Kuwait

ARTICLE INFO

Keywords:
3D bioprinting
Bioink
Microspheres
Drug delivery
Gelatin methacrylate
Cross-linking

ABSTRACT

3D bioprinted hydrogel constructs are advanced systems of a great drug delivery application potential. One of the bioinks that has recently gained a lot of attention is gelatin methacrylate (GelMA) hydrogel exhibiting specific properties, including UV cross-linking possibility. The present study aimed to develop a new bioink composed of GelMA and gelatin modified by addition of polymer (polycaprolactone or polyethersulfone) microspheres serving as bioactive substance carriers. The prepared microspheres suspension in GelMA/gelatin bioink was successfully bioprinted and subjected to various tests, which showed that the addition of microspheres and their type affects the physicochemical properties of the printouts. The hydrogel stability and structure was examined using scanning electron and optical microscopy, its thermal properties with differential scanning calorimetry and thermogravimetric analysis and its biocompatibility on HaCaT cells using viability assay and electron microscopy. Analyses also included tests of hydrogel equilibrium swelling ratio and release of marker substance. Subsequently, the matrices were loaded with ampicillin and the antibiotic release was validated by monitoring the antibacterial activity on *Staphylococcus aureus* and *Escherichia coli*. It was concluded that GelMA/gelatin bioink is a good and satisfying material for potential medical use. Depending on the polymer used, the addition of microspheres improves its structure, thermal and drug delivery properties.

1. Introduction

3D bioprinting involves a variety of advanced manufacturing technologies to produce functional 3D tissues and organs layer by layer using bioink, which includes biological materials, additives and living cells [1–3]. Currently, 3D bioprinting technology, is widely used in the design and manufacture of drug delivery systems for therapeutic applications [4–6], tissue engineering and regenerative medicine to develop complex tissue structures that mimic native organs and tissues [7–10]. The advantages of using 3D bioprinting in the biomedical field are the development of patient-specific personalized designs, high precision and on-demand creation of complex structures in a short time [3].

As mentioned above, bioinks are the materials used in the preparation of processed (bioartificial) living tissues using 3D bioprinting technology. They can comprise only cells, but an extra carrier substance (a biocompatible synthetic or a natural polymer gel or a gel based on the combination of both), which surrounds the cells and acts as a 3D molecular scaffold, is often included. The bioinks used in 3D bioprinting technology should primarily be highly biocompatible and nontoxic, mechanically stable after printing, and should provide high resolution during printing, as well as printing temperatures below physiological temperatures [11–13]. Commonly used materials for 3D printing are: polymers, elastomers, ceramics and hydrogels. The most widely used synthetic polymers include: polycaprolactone (PCL), pluronic, polyvinylpyrrolidone (PVP) and polyethylene glycol (PEG). In turn, the most commonly used natural polymers are: gelatin, hyaluronic acid, collagen and matrigel [14].

Gelatin is a natural water soluble protein that comes from the partial hydrolysis of collagen. With its chemical structure and biological functions, it resembles collagen in the native extracellular matrix (ECM). For

* Corresponding author at: Gulf University for Science and Technology, GUST, Kuwait.
E-mail address: Mikhael.bechelany@umontpellier.fr (M. Bechelany).

https://doi.org/10.1016/j.bioadv.2023.213436
Received 12 December 2022; Received in revised form 12 April 2023; Accepted 17 April 2023
Available online 19 April 2023

this reason, it is considered an ideal material that can mimic the natural structure of the ECM. Gelatin is a biocompatible: non-toxic and non-immunogenic polymer and a biomimetic peptide with the ability to prevent cell apoptosis [15]. In addition, gelatin promotes cell proliferation and differentiation in a specific direction [16]. Among other things, these features and the adaptability of gelatin's rheological properties have determined its high popularity as a bioink for use in 3D bioprinting [17,18].

On the other hand, among the undoubted disadvantages of gelatin that pose an obstacle to the development of bioplastics for medical applications are its poor mechanical and thermal properties. For this reason, in order to obtain a material for use in tissue engineering, among other applications, gelatin is modified with methacrylic anhydride. Recently, gelatin methacrylate (GelMA)-based hydrogels have been widely used in tissue engineering [19]. Other applications of GelMA hydrogels include fundamental cell research, cell signaling, drug and gene delivery, and biosensing [18,20].

An interesting direction for modifying the properties of newly developed bioinks can be, for example, the addition of microspheres. Microspheres are spherical microparticles with diameters in the range of 1–1000 μm that can be loaded with hydrophilic and hydrophobic drugs or other bioactive components (e.g. DNA or proteins). They are usually made from biodegradable and biocompatible polymers, such as: cellulose, polyethersulfone, polycaprolactone, poly(lactic acid) and poly (glucolic acid). Drug release from microspheres occurs by degradation/erosion of the polymer matrix and simultaneous diffusion of the drug substance. Administration of medication via microparticulate systems is advantageous because microspheres can be tailored for desired release profiles and used for site-specific delivery of drugs and in some cases can even provide organ-targeted release [21,22].

A lot of attention is currently being paid to the development of new bioinks with improved performance properties and for increasingly broader applications, including drug delivery systems and tissue engineering. Our previous work [23] involved an attempt to develop a new bioink based on cross-linked gelatin-alginate hydrogel for potential use as an antibiotic delivery system. Over the past few years, there have been several papers proposing new microsphere-modified bioinks for use in 3D bioprinting [24–36]. Mirani et al. [29] used an alginate-gelatin methacryloyl (GelMA)-photoinitiator (PI) solution with suspended *all-trans retinoic acid (ATRA)*-loaded microspheres as the 3D bioprinting material. Three-dimensional porous hydrogel meshes loaded with ATRA-loaded polymer microspheres have been shown to be responsible for, among other things, prolonged ATRA release and induce apoptotic cell death in U-87 MG (malignant glioma). Chen et al. [30] successfully developed bioprinted multiscale composite scaffolds based on gelatin methacryloyl (GelMA)/chitosan microspheres as a modular bioink that mimicked the 3D integrated micro- and macroenvironment of the native nerve tissue very well. Among other things, the effect of these microspheres was shown to increase neurite growth and elongate PC12 cells. Sharma et al. in [31] presented the possibility of using guggulsterone-releasing microspheres contained in a new fibrin-based bioink to bioprint 3D tissues similar to those in the brain. Studies have shown that the addition of drug releasing microspheres to bioink improves cell survival and differentiation. In a subsequent study, Sharma et al. showed that the incorporation of microspheres in bioink enhanced the mechanical strength, lowered the degradation rate, and increased the elastic modulus of bioprinted [32]. In a recent paper [34], Kanungo et al. presented research on an attempt to develop a bioink composed of pectin and Pluronic® F-127 containing gelatin-coated pectin microspheres as vascularization-promoting agents for potential use in tissue bioengineering. When incorporated into bioink for scaffolding, the microspheres distributed evenly and did not display any negative effects on bioprintability. In addition Bonany et al. [36] introduced three types of microspheres with different mineral contents (gelatin, hydroxyapatite nanoparticle- containing gelatin; and calcium-deficient hydroxyapatite) into an alginate-based bioink. The results showed that the addition of microspheres generally improved the rheological properties of the ink, favored cell proliferation and positively affected osteogenic cell differentiation.

So far, the research presented in the literature is primarily concerned with attempts to develop special bioinks modified with drug-loaded microspheres, which act as microreservoirs with internal release of bioactive molecules which improve the survival and differentiation of living cells suspended in the bioink. Such bioinks are designed primarily for 3D bioprinting of tissue scaffolds. However, there is an acute shortage of research on the development of bioinks containing microspheres (microcarriers) to 3D bioprint constructs with external drug release – this kind of bioprintouts can be used as drug delivery systems or dressings for hard-to-heal wounds. In accordance with the assumptions of the presented research, placing microspheres in the 3D bioprinted matrices can guarantee a lot of benefits as follows: prolonged and controlled release of the immobilized substance, increased drug capacity of the entire system, elimination of burst effect and the direct action of drug in the diseased area. For these reasons, an attempt to develop such a bioink was the aim of this work.

The focus was on developing GelMA-gelatin-based bioink modified with two different types of microspheres made of polycaprolactone (PCL) or polyethersulfone (PES) for potential use in 3D bioprinting. These two types of microspheres were prepared as described in detail in our previous work [37]. The properties of the gelatin methacrylate-based bioink were enhanced by the addition of pure gelatin to combine the benefits of both substances. The studies of the printability of bioinks containing GelMA and gelatin in different ratios was conducted by Yin et al. [38], indicating such concentrations of ingredients in which smooth and uniform filaments were formed during bioprinting. The addition of gelatin increases the viscosity and stability of the bioink, as well as the flexibility of the 3D bioprinted model.

Presented research included evaluating the 3D bioprinting feasibility of a newly developed bioink modified with microspheres using an extrusion technique, characterizing the morphology of such 3D bioprinted matrices, assessing their thermal properties and degree of swelling, and evaluating their transport and antibacterial properties.

2. Materials and methods

2.1. Materials

Gelatin type B (CAS Number: 9000-70-8) from bovine skin (gel strength 225 g Bloom), methacrylic anhydride (CAS Number: 760-93-0, ≥94 %) sodium chloride (NaCl, CAS Number: 7647-14-5, ≥99 %), potassium chloride (KCl, CAS Number: 7447-40-7, ≥99 %), potassium phosphate monobasic (KH_2PO_4, CAS Number: 7778-77-0, ≥99 %), sodium phosphate dibasic (Na_2HPO_4, CAS Number: 7558-79-4, ≥99) and agar (CAS Number: 9002-18-0) were purchased from Sigma-Aldrich. Polycaprolactone (PCL, M_w = 70 kDa, CAS Number: 24980–41–4) was purchased from Scientific Polymer Products (USA) and polyethersulfone (PES, M_w = 42 kDa, Ultrason E2020) from BASF (Germany). Dimethylformamide (DMF, Chempur, Poland, CAS Number: 68–12–2, ≥99 %) and *N*-methyl-2-pyrrolidone (NMP, Chempur, Poland, CAS Number: 872–50–4, ≥98 %) were used as solvents for the polymers (PCL and PES respectively). Ethanol (EtOH, Polmos, Poland, ≥95 %) was used as a PCL/PES non-solvent to induce phase separation in a precipitation bath. Lithium phenyl-2,4,6-trimethylbenzoylphosphinate (LAP, Allevi, USA, CAS Number: 85073–19-4, ≥95 %) was used as a hydrogel UV-cross-linking photoinitiator. A drug marker rhodamine 640 perchlorate (M_w = 591.05 Da, CAS Number: 72102–91–1) was purchased from Exciton (USA). Ampicillin sodium salt antibiotic (CAS Number: 69–52–3) was obtained from A&A Biotechnology (Poland). The non-pathogenic Gram positive *Staphylococcus aureus* and Gram negative *Escherichia coli* bacteria (K12 DSM 423, from DSMZ, Germany) were chosen as model microorganisms. The culture medium was a Tryptone Salt Broth (TSB, Sigma Aldrich). The chemicals were used without further purification.

All solutions were prepared with MilliQ water (with a resistivity of 18.2 MΩ•cm; Millipore, USA).

2.2. Gelatin methacrylate synthesis

Gelatin methacrylate (GelMA) was prepared using a protocol first reported by Van Den Bulcke et al. [39] by reaction of gelatin with

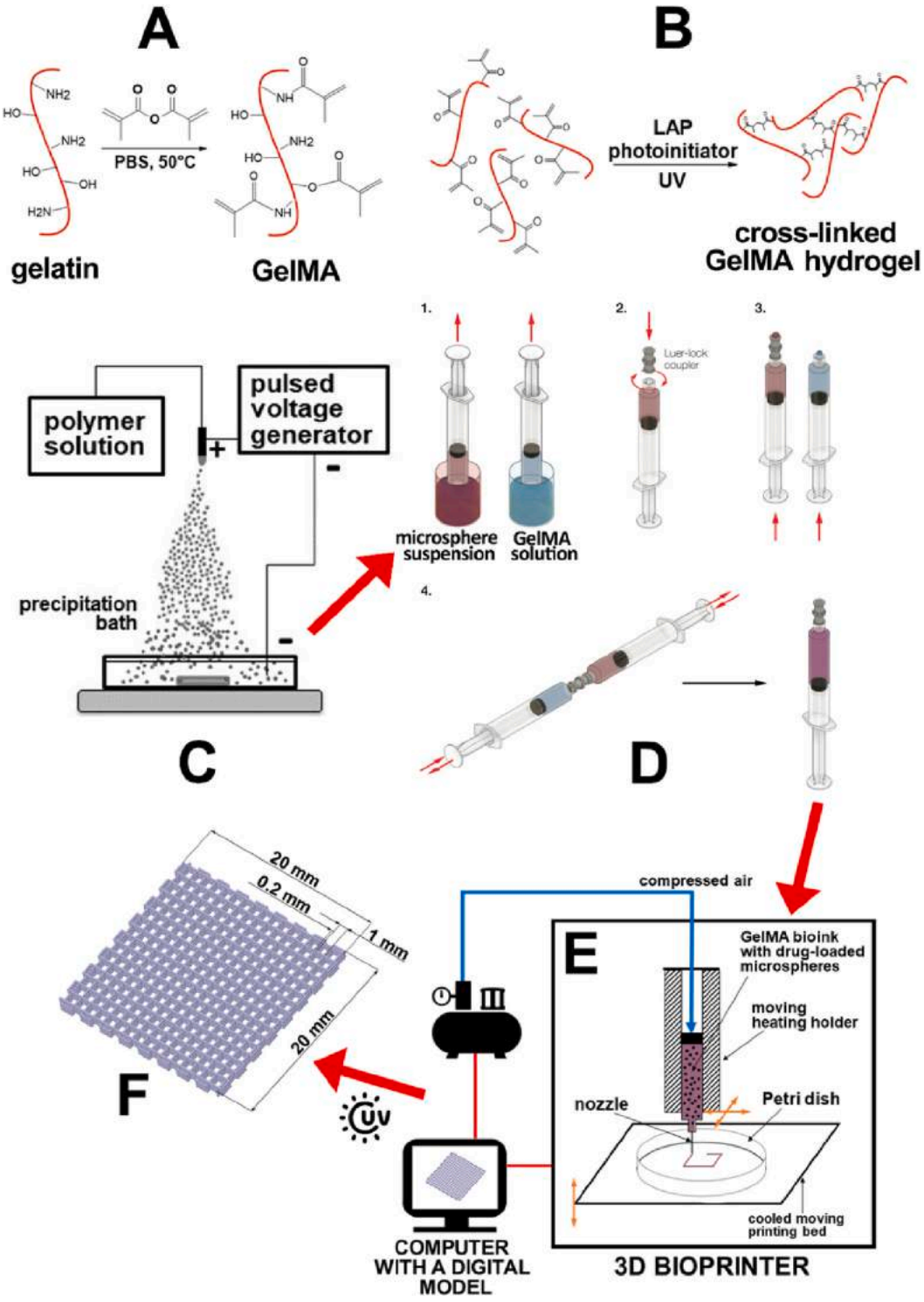

Fig. 1. Bioink preparation, 3D bioprinting and UV-cross-linking of microsphere-loaded GelMA/gelatin matrices. (A) Reaction of gelatin and methacrylic anhydride for gelatin methacrylate production. Protein chains are schematically marked with a red line, only amine and hydroxyl groups and their substitutions with methacryloyl groups are shown. (B) Simplified exemplary scheme of reactions during the UV-cross-linking of GelMA to form hydrogel networks – the free radical chain polymerization of the methacryloyl substitutions. (C) The microsphere production process scheme using the method combining electrospray and phase inversion developed previously by the authors [37]. (D) The syringe coupler method scheme proposed by Allevi, Inc. [40] (image used with permission from Allevi) for bioink preparation. Scheme presents mixing microspheres suspension with GelMA solution. (E) 3D bioprinting setup scheme. (F) A digital 3D mesh matrix model designed made using the DesignSpark Mechanical 4.0 software.

methacrylic anhydride (MA). In this reaction, the hydroxyl and amine groups of the amino acid residues are substituted with methacryloyl groups (Fig. 1A). A constant pH is important to maintain the reactivity of protein functional groups. Gelatin (5 g) was dissolved in phosphate buffer (PBS, pH = 7.4) at 50 °C. After 1 h MA (5 mL) was added gradually (0.5 mL/min) to the vigorously stirred solution. The reaction was run for at 50 °C and after 3 h it was quenched with 250 mL PBS (20 °C). The diluted reaction mixture was then dialyzed against deionized water through a dialysis tubing (12–14 kDa cutoff) for 7 days to remove potentially cytotoxic low-molecular-weight residues of MA. Dialysis water was changed every 24 h. The resulting solution was then freeze-dried (48 h at 12 Pa, −70 °C) leading to a white solid product – GelMA – which could be stored in a freezer.

2.3. Microsphere formation

A technology, the diagram of which is shown in Fig. 1C, combining pulsed voltage electrospray with wet phase inversion was used to prepare microspheres [37]. In this process developed in our group, the polymer solution is pumped through a metal nozzle attached to a high pulsed voltage. Microdroplets are created by the electrospray process at the nozzle outlet. Afterwards, they are collected in a well-agitated precipitation bath containing a polymer non-solvent. Based on the Gibbs phase rule, wet phase inversion occurs in this bath, resulting in the formation of hardened polymer microspheres. The procedure can be changed by incorporating different materials (such as drugs) into the polymer solution or bath to immobilize them inside the microspheres. The microspheres were prepared with a 15 % solution of PCL in DMF as well as a 15 % solution of PES in NMP. The electrical parameters in the study were set to the following values: electrical voltage $U = 8$ kV, pulse frequency $f = 60$ Hz, and pulse duration $\tau = 6$ ms and the polymer solution flow rate was 1.5 mL/h. Throughout the procedure, the temperature did not exceed 25 °C and the humidity was not >40 %. Microspheres with immobilized active substance were prepared from a polymer solution containing 0.57 mg/g (mass/polymer mass marker) of rhodamine or ampicillin and using a precipitation bath containing 0.1 mg/mL of the substance. Following microsphere formation, the bath suspension was transferred to a falcon and centrifuged to remove the excess ethanol. Then the microspheres were dried, weighed and suspended in distilled water for further use in the bioink preparation. The obtained microspheres had average diameters of 14.38 ± 6.28 μm for PCL and 6.20 ± 2.43 μm for PES.

2.4. Bioink preparation

The bioink presented in this work should be prepared just before it is used in the 3D bioprinting process. For this purpose, three preliminary mixtures were prepared and then combined into the final formulation. Mixture A was a solution of gelatin (10.8 g) in PBS (20 mL) – after 3 h of stirring at 40 °C a 35 % solution was obtained. Mixture B was a solution of GelMA (1.19 g) in PBS (7.31 mL) with the addition of LAP (50 mg). A photoinitiator was added to the PBS, stirred for 30 min at 60 °C, then GelMA was added and after stirring for 60 min at 60 °C a solution containing 14 % GelMA and 0.7 % LAP was obtained. Mixture C was a suspension of microspheres (PCL or PES, with or without bioactive ingredient) in PBS (or 0.1 mg/mL bioactive ingredient solution in PBS). Appropriate amount of microspheres was suspended in 2 mL of PBS resulting in formation of a suspension of desired microsphere concentration (e.g. 30 mg to get 5 mg/mL bioink suspension in the next step). Once all mixtures were ready, the syringe coupler method (Fig. 1D) was used to prepare the suspension for 3D bioprinting. A similar methodology was employed by Jeon et al., as evidenced in their work [41]. The mixtures were transferred to syringes: 1.9 mL of mixture A, 2.1 mL of mixture B and 2 mL of mixture C. First, the syringes A and C were linked with a syringe coupler, and the contents were mixed by moving the plungers back and forth 40–50 times. The resulting suspension of microspheres in gelatin solution was then placed in one of the syringes which was connected with a syringe coupler to the third syringe containing the mixture B. Again, the plungers were moved back and forth 40–50 times. In this manner, a suspension of microspheres with concentrations 5 mg/mL or 10 mg/mL in a 11 % gelatin and 5 % GelMA solution in PBS with a 0.25 % addition of LAP was obtained.

2.5. 3D bioprinting of GelMA/gelatin matrices

Once the bioink was ready, it was set in the heating holder of bioprinter (Fig. 1E) and then 3D model could be printed (Fig. 1F) forming hydrogel matrices cross-linked using UV light.

As a digital model of a bioprinting matrix, a cubic mesh (the grid size was set as 1 mm and line width as 0.2 mm) with dimensions of 20 mm × 20 mm × 12 mm made of 6 layers (0.2 mm in height each) was designed (Fig. 1F). The 3D model project was made in the DesignSpark Mechanical 4.0 software, exported as an STL file, sliced by Repetier-Host/Slic3r software and converted into G-code. The microsphere-loaded GelMA/gelatin matrices were printed using Allevi 2 3D bioprinter (Philadelphia, USA). Fig. 1E presents the scheme of the experimental setup. Bioprinting parameters were set as follows: temperature of the bioink in the syringe of 28 °C, temperature of the collector Petri dish of ~15 °C, printing pressure of 345 kPa (50 psi), printing speed of 10 mm/s, G30 nozzle (inner diameter of 0.164 mm), layer height of 0.2 mm.

The cross-linking of the bioprintout from the GelMA/gelatin bioink was carried out in two stages: first, the gelatin was thermally cross-linked directly on the collector, hydrogen bonds were formed, and then the initially hardened matrix was exposed to UV light, initiating GelMA cross-linking. During UV-curing of the GelMA/gelatin hydrogel in the presence of LAP, free radicals are generated from the photoinitiator. They initiate chain polymerization of methacryloyl substitutions and propagation between methacryloyl groups located on the same or different chains takes place (Fig. 1B). In the described research, samples of a freshly printed hydrogel matrix were placed in a chamber emitting ultraviolet light with a wavelength of 365 nm in a vertical position so that the entire sample was evenly illuminated. Two lengths of cross-linking time were tested: 5 min and 10 min.

Ten types of samples (without immobilized bioactive substance) differing in the content of microspheres in the bioink and cross-linking time were prepared in the manner described above. The obtained GelMA/gelatin matrices are summarized in Table 1 with a proper denotation for each of them (the first number corresponds to the microsphere content in the bioink, the second number – to the UV-cross-linking time expressed in minutes).

In addition, six types of samples for testing the transport properties of bioprinted matrices (microsphere content: 0 mg/mL or 5 mg/mL and cross-linking time 5 or 10 min) and four types of samples for testing antibacterial properties (microsphere content: 0 mg/mL or 5 mg/mL and cross-linking time 10 min) were prepared. The GelMA/gelatin matrices for studies requiring anhydrous samples were frozen (8 h at −20 °C) and lyophilized (24 h at 12 Pa, −70 °C).

Table 1
List of bioprinted GelMA/gelatin matrices differing in microsphere content and cross-linking time.

Sample	Details	
0_0	No microspheres	No UV-cross-linking
0_5	No microspheres	5 min of UV-cross-linking
0_10	No microspheres	10 min of UV-cross-linking
5_0_PCL	5 mg/mL PCL microspheres	No UV-cross-linking
10_0_PCL	10 mg/mL PCL microspheres	No UV-cross-linking
5_5_PCL	5 mg/mL PCL microspheres	5 min of UV-cross-linking
5_10_PCL	5 mg/mL PCL microspheres	10 min of UV-cross-linking
5_0_PES	5 mg/mL PES microspheres	No UV-cross-linking
5_5_PES	5 mg/mL PES microspheres	5 min of UV-cross-linking
5_10_PES	5 mg/mL PES microspheres	10 min of UV-cross-linking

2.6. Characterization of the cross-linked GelMA/gelatin matrices

The 3D bioprinting feasibility with proposed new bioink was assessed on the basis of observations made during the process, as well as based on printouts examined using digital microscope (Keyence, VHX-7000). After that, the samples were lyophilized and observed with scanning electron microscopy (SEM, HITACHI S4800) – the samples were coated with 10 nm thick gold layer for it.

Fourier Transform Infrared Spectroscopy (FTIR) was used to determine which functional groups are present in the analyzed sample and thus the influence of microsphere use as well as crosslinking on it. The FTIR spectra of GelMA/gelatin matrices was recorded using the NEXUS instrument equipped with and attenuated total reflection (ATR) accessory in the frequency range of 500–4000 cm^{-1} with an average of 64 scans at 2 cm^{-1} resolution.

Thermal properties of samples were investigated using differential scanning calorimetry (DSC) and thermogravimetric analysis (TGA). Differential scanning calorimeter (DSC, TA Instruments 2920) equipped with a RCS90 cooling system was used to determine the thermal transition points and enthalpies (calculated as an area under the peak) of the GelMA/gelatin matrices. The samples were weighed (~ 2–3 mg) in an aluminum TA pan and sealed, an empty sealed pan was used as a reference. The samples were cooled to −80 °C and then heated up to 200 °C with a heating rate of 20 °C/min. TA Instruments TGA G500 apparatus was used to perform the thermogravimetric analysis under oxygen flow of 60 mL/min to define the cross-linking influence on a thermal stability of matrices. The samples of ~3–12 mg were heated up to 1000 °C at a heating rate of 10 °C/min.

Samples for FTIR, DSC and TGA were frozen (8 h at −20 °C) and lyophilized (24 h at 12 Pa, −70 °C) before the analyses.

2.7. Cell culture and cytotoxicity assays

HaCaT cells (spontaneously transformed human keratinocytes) were cultured at 37 °C in 5 % CO_2 using DMEM (Dulbecco's Modified Eagle Medium α) media supplemented with 10 % (v/v) foetal bovine serum. HaCat cells (10^4 cells per well) were seeded in 96 well plates and allowed to attach for 24 h. After sterilization with UV irradiation for 1 h, the hydrogels were hydrated in culture medium for 24 h. The corresponding hydrogel eluates (25 mg/mL) was prepared and the culture medium of the HaCaT cells seeded in 96 well plates was replaced by 100 μL of the hydrogel eluate at various dilutions (up to 50-fold). After 24 h of incubation with the hydrogel eluates, cell viability was analyzed using MTT assay carried out as previously described [23] or with the CyQUANT® Cell Proliferation Assay Kit (Invitrogen, France) with a measurement of fluorescence at 520 nm on a Pherastar fluorimeter. Alternatively, HaCaT cells were also seeded directly onto the hydrated hydrogels (100 μL of cell suspension in 96 wells plate corresponding to 1.5×10^3 cells/well). After 16 h, the number of viable cells was determined by adding 11 μL of Alamar blue HS Cell Viability Reagent (Thermofisher, France) and fluorescence was measured 1 h later on a Pherastar fluorimeter (excitation 540 nm/emission 590 nm). Data ($n = 3$ to 18) were analyzed statistically using the Student *t*-test or the Mann-Whitney test.

2.8. Scanning electron microscopy analysis of cell-seeded matrices

HaCaT cells (1.2×10^6 cells/well in 12 wells plate) were seeded onto the different hydrogels previously hydrated and washed 3 times in cell culture medium. After 16 h of culture, the hydrogels were washed with PBS, fixed with 2.5 % glutaraldehyde in PHEM buffer (pH 7.2) for 1 h at room temperature and washed again in PHEM buffer. Fixed samples were dehydrated using a graded ethanol series (30–100 %), followed by 10 min in graded ethanol/hexamethyldisilazane (HMDS), and then HMDS alone. Subsequently, the samples were sputter coated with a 10 nm thick gold film and then examined under a scanning electron microscope (Hitachi S4000) using a lens detector with an acceleration voltage of 10 kV at calibrated magnifications.

2.9. Swelling properties of the cross-linked GelMA/gelatin matrices

3D bioprinted, crosslinked and lyophilized GelMA matrices were cut and weighted. Then, their equilibrium swelling ratio (ESR) in PBS at 37 °C was determined using a gravimetric method. Each sample (~ 60–150 mg, W_d) was placed in closed bottle with 10 mL of swelling medium (PBS). After predetermined immersion time intervals, they were retrieved and weighed (*Wt*) and placed again in PBS (surface water was gently removed with a tissue before measurements). The water ESC at time *t* was calculated according to the following equation:

$$ESR = \frac{W_t}{W_d} \bullet 100\% \quad (1)$$

where Wt is the sample weight at a particular time (t) and Wd is the weight of dried matrix.

The experiment was performed three times for different samples of each type of GelMA/gelatin matrix were used to perform and average ESR value as calculated.

2.10. Model drug molecule (rhodamine) release from the GelMA/gelatin matrices

The release profile of rhodamine 640 from GelMA/gelatin matrices was determined for six types of samples – with marker and no microspheres, with marker-loaded PCL microspheres and with marker-loaded PES microspheres, each group of samples UV-cross-linked for 5 or 10 min. Rhodamine 640 was used in the experiments because its concentration in the solution can be easily, quickly and accurately determined spectrophotometrically, which allows the transport properties of the system to be observed (including possible burst effect). A sample of 22.1–38.1 mg of each freeze-dried GelMA/gelatin matrix was placed in a glass container with 3.65–6.3 mL of deionized water (the amounts were selected so as to maintain a constant proportion between the weight of the sample and the volume of water ~1:6). The content of the container was stirred all the time and the total volume did not change during the experiment. A flow spectrophotometric method proposed before by Grzeczkowicz et al. [42] was used for the tests to determine rhodamine concentration (light wavelength of 574 nm used). Measurements of absorbance were made as follows: every 2 min for the first 2 h, every 10 min for the next 1 h, every 30 min for the next 2 h, after 6, 7 and 24 h. On the basis of the data, the rhodamine release profiles from GelMA/gelatin matrices were plotted on graphs. The transport properties of the tested matrices were described mathematically with a linear function fitted to the plotted experimental points of the initial 1 h of the substance release. A line describing each case ($y = ax$) was fitted in OriginPro software. The coefficient *a* defines the slope of the line and thus the substance release rate. In addition, a graph showing the concentration of rhodamine in solution after release in various samples for 24 h was plotted to check whether (and how) the addition of microspheres increases the amount of rhodamine released from the matrix compared to one without microspheres. The experiments were done three times, the average light absorbance (thus marker concentration) values were calculated.

2.11. Antibacterial activity of the GelMA/gelatin matrices with ampicillin-loaded microspheres

For the antibacterial tests four types of GelMA/gelatin matrices were prepared, all UV-cross-linked for 10 min – with no ampicillin, with ampicillin (no microspheres), with ampicillin-loaded PCL microspheres and with ampicillin-loaded PES microspheres. The sterilization was provided by the UV cross-linking. *Staphylococcus aureus* (*S. aureus*, Gram positive) and *Escherichia coli* (*E. coli*, Gram negative) bacteria were used

to examine the antibacterial activity of the samples. Microbiological agar (15 g·L^{-1}) was added to PBS to prepare Mueller-Hinton agar (GMH) plates. Two rectangular dishes– each for one type of bacteria – were inoculated individually with 1 mL of *S. aureus* or *E. coli* suspension. The optical density at 620 nm (OD600) of the bacterial suspension was then adjusted to 0.75 ± 0.01 for *S. aureus* and 0.80 ± 0.01 for *E. coli*. Immediately after the inoculation, the samples were put onto the dishes to check the ability of the drug-loaded matrices to prevent bacterial growth. The plates were then incubated overnight at 37 °C in aerobic conditions so the bacterial biofilm could be formed. The plates were pictured to show inhibited bacterial growth (the clear zones). The study outcomes were measured by quantifying the area of the inhibition zone through three replicates of each test condition, five measurements for each. Average area values were calculated and statistical significance of the measurements was determined using a one-way analysis of variance test (ANOVA) followed by a post-hoc Tukey HSD test. The results were presented in a bar chart, which included the average values and standard deviations, facilitating their comprehension.

3. Results and discussion

3.1. 3D bioprinting feasibility

The 3D bioprinting is multi-step process, and at each stage certain decisions must be made regarding its conditions affecting the final product – a hydrogel matrix. First, the composition of the bioink should be developed. On the basis of own experimental selection as well as the work of Yin et al. [38], it was decided to conduct research with bioink containing 5 % GelMA and 11 % gelatin. The bioink was modified by adding PCL or PES microspheres, selecting their content so that it is still printable. Then, a number of experiments were carried out to determine the optimal printing conditions to obtain GelMA/gelatin matrices compatible with the digital model. The obtained bioprintouts were analyzed using digital microscopy to characterize their macrostructure and microsphere distribution. The results in the form of images of matrices differing in the content and type of microspheres and UV-cross-linking time are shown in Fig. 2.

Addition of gelatin to the GelMA bioink eliminated the need for photochemical cross-linking during the bioprinting process (between each subsequent printed layer), which reduced the interruptions in printing caused by clogging of the nozzle with elements of unintentionally cross-linked bioink inside it. The concentrations of ingredients

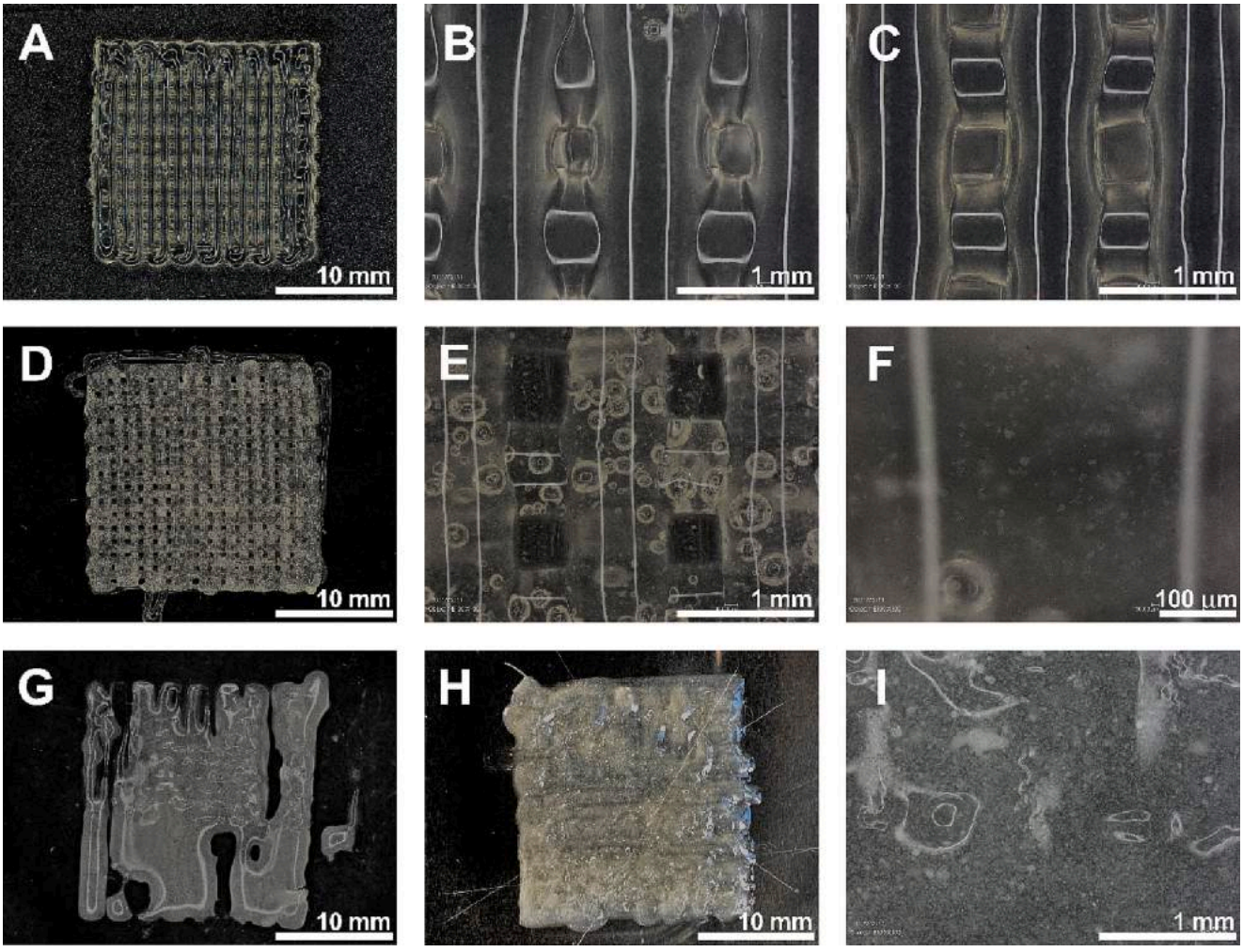

Fig. 2. 3D bioprinted GelMA hydrogel (5 % GelMA, 11 % gelatin) matrices before lyophilization pictures made with digital microscope. (A–B) Bioink without additives, matrix immediately after printing, no cross-linking, magnification (A) 20× and (B) 100×. (C) Bioink without additives, matrix UV-cross-linked for 10 min, magnification 200×. (D–F) Bioink with 5 mg/mL PCL microspheres, matrix UV-cross-linked for 10 min, magnification (D) 20×, (E) 100×, (F) 500×. (G) Bioink with 10 mg/mL PCL microspheres, unable to bioprint a model matrix, magnification 20×. (H–I) Bioink with 5 mg/mL PES microspheres, matrix UV-cross-linked for 10 min, magnification (D) 20×, (E) 100×.

that were chosen provided smooth and uniform filaments formed during 3D bioprinting.

In the case of the non-cross-linked GelMA/gelatin matrix (A), its structure coincides with the matrix designed using the computer model in Fig. 1F, but the sizes of the model elements (gaps, grids) are not the same. In the case of gaps, the size decreased (the gap size in the model is 1 mm, in the bioprinted matrix it is 0.3 mm) and for grids it increased (the grid width in the model is 0.2 mm, in the bioprinted matrix it is around 0.7 mm).

In addition, analysis of the images (B and C) suggests that there are no significant changes in the structure of the 3D printed matrix after the UV-cross-linking process. The only observable difference is a slight blurring of the structure of the non-cross-linked matrix (B) – the shrinkage effect of the non-cross-linked matrix is not observed in the cross-linked one.

The content of microspheres in the GelMa/gelatin matrix (5 mg/mL) leads to structures with slightly more "spilled" shapes (D). The obtained images of the macroscopic structure of the matrices also confirm the presence of PCL microspheres with diameters of about 10–14 μm evenly distributed in the 3D printed matrix structure (E and F). On the other hand, the content of microspheres in the bioink at the level of 10 mg/mL completely disabled the printing of the constructs (G). It can also be observed that numerous air bubbles were present in the structures of the 3D printed constructs (E) being a result of intense mixing the components with syringe coupler method during bioink preparation. Further bioink development is suggested to elaborate a method to remove the bubbles before printing.

In the case of GelMA/gelatin matrices modified with PES microspheres (H, I), the 3D bioprinting was possible. However, it was not possible to obtain a structure in accordance with the designed one (Fig. 1F). The 3D bioprinting conditions were identical as in the case of matrices without microspheres or with PCL microspheres. The presence of PES microspheres probably affects the rheological properties of the bioink used, which affects the 3D printed matrix. Another reason for obtaining such a 3D printed matrix can be attributed to the different thermal properties of the PES microspheres. Moreover, the fact that the structure is kept or not, is related to the interaction between PCL/PES and GelMA/gelatin. In the case of polycaprolactone (PCL), the intermolecular forces (hydrogen bonding or van der Waals forces) allow the matrix to keep the designed structure during printing enhancing the thermal cross-linking. It has been shown that three potential kinds of inter- and the intramolecular hydrogen bondings can occur in the PCL molecule between the CH2 and C═O groups [43]. In addition, there are also intermolecular dipole–dipole interactions (C═O···C═O) between PCL and GelMA/gelatin molecule [44]. All these interactions are weaker for polyethersulfone (PES) microspheres, because there is only one hydrogen bonding acceptor (—O—) in the polymer structure and no donors, the matrix structure is therefore not preserved. Due to this, the conditions for 3D bioprinting of PES-loaded GelMA/gelatin bioink and its composition should be selected individually. However, it was decided not to change them and use them in further research in order to be able to compare the obtained results without hindrance.

The 3D bioprinting process with GelMA/gelatin microsphere-loaded bioink can be influenced by many factors, the proper selection of which allows it to be carried out and lead to the expected product in the form of a hydrogel matrix. In addition to the already mentioned UV exposure time or the content of microspheres, others can be indicated: the degree of substitution during the reaction of gelatin with MA, bioink composition (gelatin – GelMA ratio), photoinitiator concentration, bioprinting parameters. The major parameters allow tuning of the physical properties of the GelMA hydrogels must be selected experimentally to be matched to the expected results.

3.2. Effect of UV-cross-linking and lyophilization on the structure of GelMA/gelatin matrices

The surface morphology, chemical structure and thermal properties of 3D bioprinted GelMA/gelatin matrices were examined using such techniques as SEM, FTIR, DSC and TGA. The samples were dehydrated in this part of research – all of the matrices were lyophilized as described in the Materials and methods section. Scanning electron microscopy pictures of different GelMA/gelatin matrices is presented in Fig. 3.

Based on the scanning electron microscopy (SEM) images (Fig. 3), the morphology of lyophilized non-cross-linked (A) and UV-cross-linked (B) GelMA/gelatin matrices, as well as the ones modified with PCL (C, D) and PES (E, F) microspheres was evaluated. Both analyses the one of images obtained by optical microscopy (Fig. 2) as well as the one of the SEM images (Fig. 3), indicate, first of all, a clear effect of the lyophilization process on the morphology of the GelMA/gelatin matrices studied. Their surfaces after the lyophilization process are highly corrugated and porous/wrinkled. Matrices (A–D) retained the structure of a regular grid after drying with visible layers. There are no significant differences in the morphology of UV-crosslinked and non-UV-crosslinked matrices (without the addition of microspheres) (Fig. 3 A and B). In contrast, modification of the 3D printed matrices with PCL microspheres leads to matrices with a significantly more compact and homogeneous structure (Fig. 3 C—D). The PCL microspheres probably acted as a filler that prevented the dried surface from creasing strongly, the shrinking hydrogel was retained on the microspheres in this case, in contrast to the matrices without microspheres, whose surface is severely wrinkled. Modification of the bioink with PES microspheres led to the formation of a completely different structure of the GelMA/gelatin matrix than in the other cases, which was already noticed in the analysis of samples by optical microscopy. In this case, the effect of cross-linking on the structure is noticeable – matrices exposed to UV light for 10 min are less porous.

Fourier transform infrared spectroscopy (FTIR) was performed to check the effectiveness of dialysis during GelMA synthesis as well as the influence of the addition of microspheres and UV-cross-linking on the chemical structure the GelMA/gelatin matrices. Fig. SI1 (supporting information) presents the results. The IR spectra of non-crosslinked GelMA/gelatin matrix without microspheres (0_0) show all characteristic chemical functional groups – the broad peak at 3291 cm^{-1} is attributed to the O—H and N—H stretching vibrations, two peaks between 2800 and 3100 cm^{-1} denoting C—H stretching of –CH2 and tertiary –CH groups present in both gelatin and methacryloyl functional groups, the backbone structure of gelatin is denoted by peaks at 1635 cm^{-1} (amide I, C═O stretching), 1543 cm^{-1} (amide II, N—H bending), 1236 cm^{-1} (amide III, C—N stretching). There are no strong peaks between 1690 and 1760 cm^{-1}, characteristic for methacrylate anhydride, indicating the carbonyl (C═O) group, which means that the post-reaction residues of this substance have been completely removed from GelMA. There are no peaks typical for microsphere-forming polymers in either spectrum – neither 1750–1735 cm^{-1} indicating C═O stretching in carboxylic esters (PCL) or 1350–1300 cm^{-1} indicating S═O stretching in sulfones (PES). There are also no new chemical bonds between GelMA, gelatin and microspheres. The addition of microspheres does not affect the chemical structure of the hydrogel.

The thermal properties of the UV-cross-linked GelMA/gelatin matrices with microspheres were determined by TGA and DSC (Fig. 4A and B). For reference purposes, an analysis of pure substances was also performed: gelatin, PCL and PES (see Table 2).

According to TGA (Fig. 4A), the first weight loss of pure gelatin (approx. 12–15 %) occurs in the temperature range 30 °C–160 °C and is attributed to the decrease in the content of structural water (bound to protein molecules by hydrogen bonds) and various volatile impurities. The largest weight loss in the range of 220 °C–600 °C by about 86 % results from the degradation of gelatin molecules. PCL shows only one weight loss (100 %) related to the decomposition of the polymer chain

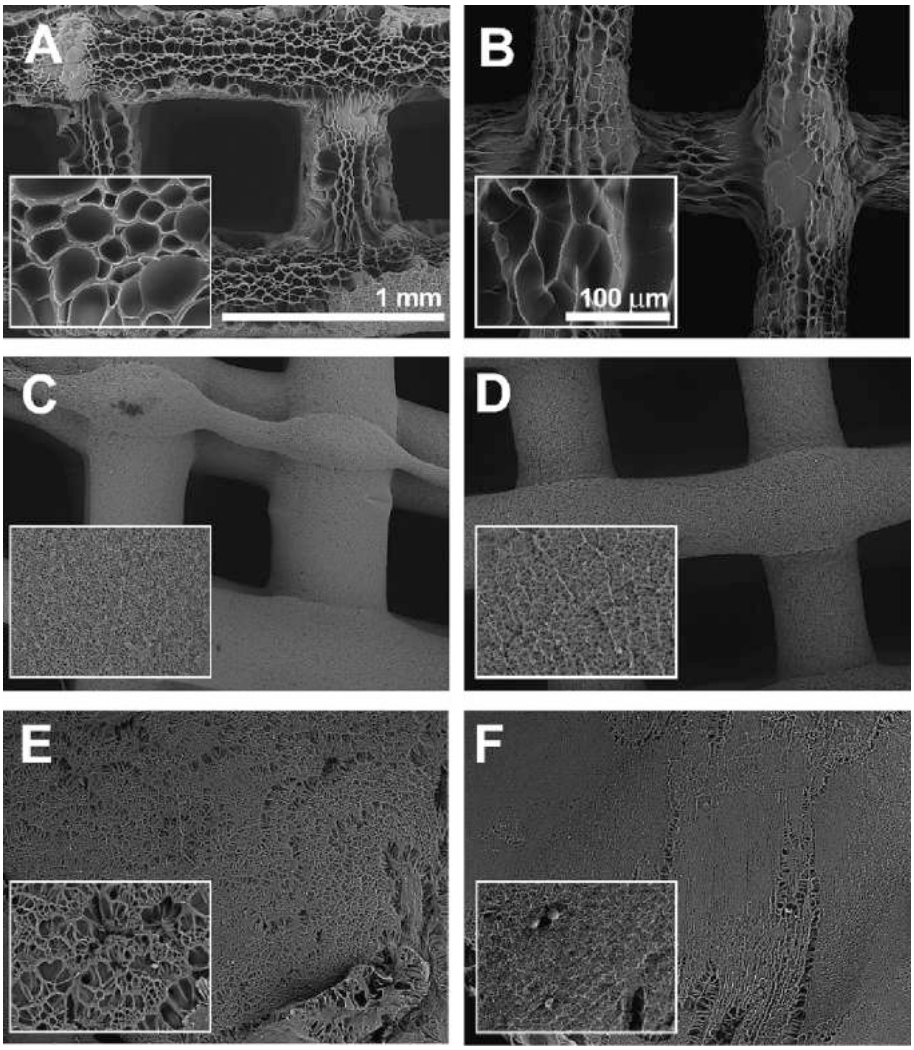

Fig. 3. SEM pictures of lyophilized GelMA/gelatin matrices: (A) no microspheres, no UV-cross-linking, (B) no microspheres, 10 min of UV-cross-linking, (C) 5 mg/mL PCL microspheres, no UV-cross-linking, (D) 5 mg/mL PCL microspheres, 10 min of UV-cross-linking, (E) 5 mg/mL PES microspheres, no UV-cross-linking, (F) 5 mg/mL PES microspheres, 10 min of UV-cross-linking – magnification 100×; close-up of surface structures – magnification 1000×.

from about 360 °C to 675 °C. For PES it is similar, one total weight loss over the temperature range of 420 °C to 730 °C. In the case of bioprinted matrices made of bioink containing GelMA and gelatin, there are three stages of mass loss in each case, and all four thermogravimetric curves have similar shapes, they are only slightly shifted relative to each other. The non-cross-linked GelMA/gelatin matrix without microspheres (0_0) loses mass for the first time in the temperature range of 30 °C–190 °C (15 % loss), i.e. at a temperature such as pure gelatin, it is analogously related to the loss of structural water. For 10 min UV-cross-linked samples (0_10, 5_10_PCL and 5_10_PES), the first weight loss (15 % loss) starts at a higher temperature (around 50 °C) because it is more difficult to remove water from the highly UV-cross-linked polymer network. The second stage of weight loss is also shifted in relation to pure gelatin, especially in terms of the decrease from 50 % to 5 % of weight – for hydrogel samples it occurs in the temperature range of 360 °C – 600 °C and is less mild. It results from GelMA content in bioink as well as the cross-linking, which causes the degradation of the polymer to occur at a higher temperature. The second stage of weight loss ends in the case of hydrogel at about 3–5 % mass, which is higher than for pure gelatin, confirms the presence of gelatin methacrylate in the sample. The third stage of mass loss does not occur in the case of pure gelatin, and for the hydrogel it runs in the range of 725 °C–825 °C and results from the degradation of GelMA. At the end of the analysis, all tested samples and pure gelatin show about 1.5 % residue. The content of microspheres in bioink is so small in relation to gelatin and GelMA (about 30 times less) that their percentage in the TGA chart is negligible. The assessed thermal stability of the dried GelMA/gelatin matrices suggests that they do not degrade at temperatures below 121 °C, which is particularly important for biomedical devices and products that are subjected to autoclaving sterilization at this temperature.

In DSC research pure gelatin showed wide endothermic peak in the temperature range of 25–170 °C, with endothermic enthalpy change of 294.3 J/g, which represents changes in the structure of polymer chains and the dehydration [45]. The DSC diagram corresponding to the PCL that it exhibits one endothermic peak (around 64 °C), which determines its melting point [46], while the curve for PES does not show any peak – it would appear at the melting point of the polymer (around 230 °C) [47], but it is outside the tested range important from the point of view of the biomedical hydrogel.

There are two endothermic peaks observed for each of GelMA/gelatin hydrogel samples. There is no peak corresponding to the melting enthalpy of ice at 0 °C, suggesting that the lyophilization of the samples was successful and no free or freezable water was left in the matrices [48]. The diagrams also do not exhibit any peak that would correspond to the phase transition of the hydrogel due to the presence of non-freezable water in it. Such a peak was observed by Mirek et al. [23] for

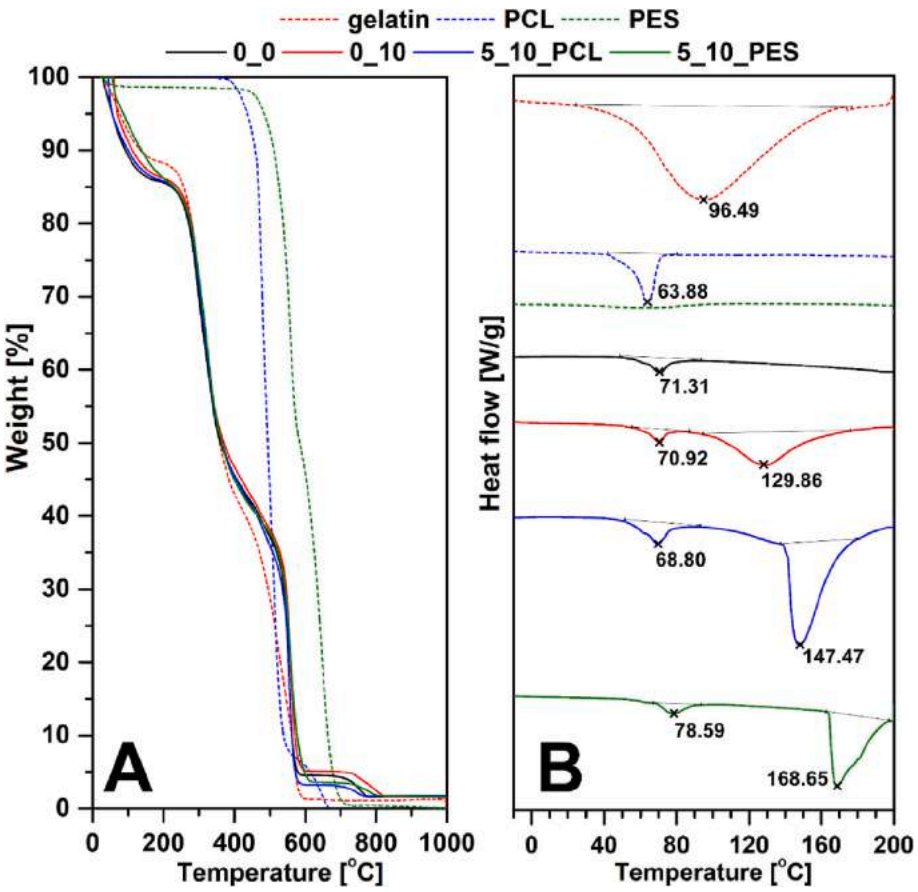

Fig. 4. Thermal properties of GelMA/gelatin matrices. Four samples were analyzed in each case: non-cross-linked matrix without microspheres (black) and 10 min cross-linked matrices without microspheres (red), with PCL (blue) or PES (green) microspheres. (A) Thermogravimetric analysis and (B) differential scanning calorimetry of pure gelatin, PCL and PES as well as GelMA/gelatin matrices.

Table 2
Thermal transition enthalpies (ΔH_1 – melting or helix-coil transition, ΔH_2 – melting) with the total enthalpy change ΔH for pure gelatin, pure PCL, pure PES and four types of lyophilized 3D bioprinted GelMA/gelatin matrices.

Sample	ΔH_1 [J/g]	ΔH_2 [J/g]	ΔH [J/g]
Gel powder	294.3 ± 8.8	–	294.3 ± 8.8
PCL polymer	32.0 ± 2.1	–	32.0 ± 2.1
PES polymer	8.0 ± 0.2	–	8.0 ± 0.2
0_0	11.8 ± 0.3	–	11.8 ± 0.3
0_10	7.7 ± 0.2	55.2 ± 3.1	62.872 ± 3.3
5_10_PCL	17.0 ± 1.1	195.2 ± 5.4	212.23 ± 6.5
5_10_PES	13.3 ± 0.8	46.5 ± 2.4	59.76 ± 3.2

gelatin-alginate hydrogel at about 37 °C and by Yoshida et al. [49] for hyaluronic acid, xanthan and pullulan hydrogels – the lack of non-freezable water in GelMA/gelatin hydrogel results from the lack of polysaccharides in the bioink. This beneficial phenomenon prevents changes in the structure of dried matrices at elevated temperature.

The first peak appearing in the DSC diagrams can be attributed to the release of bound water and the helix-coil transition of gelatin in the range of around 45–85 °C. At low temperatures, gelatin exhibits a high triple-helix level that decreases upon heating forming a random coil structure. Such a shift of the transition start towards higher temperatures in relation to pure gelatin (from 25 °C to 45 °C) results from the high content of GelMA in the sample. In GelMA, the triple-helix level is initially much lower than in the gelatin structure – intrachain hydrogen bonds in the gelatin's triple helix are reduces due to methacryloyation of free amino groups or hydroxyl groups, which leads to random coil level increase (helix level decrease) [39]. The enthalpy of the process is lower than for pure gelatin (7.7–17.0 J/g) due to the lower triple-helix level in GelMA/gelatin matrices. It is the highest for samples containing PCL microspheres (17.0 J/g), because of two overlapping effects – gelatin helix-coil transition and polymer phase transition (around 64 °C).

The second endothermic peak appears for the UV-cross-linked hydrogel samples and is related to the degradation of the material. This process is definitely more difficult in the case of a hydrogel which in its structure contains intrachains connected by methacrylic anhydride functional groups which reduces chain mobility [50]. In the case of GelMA/gelatin matrix without microspheres, the peak corresponding to the enthalpy of degradation (55.2 ± 3.1 J/g) ranges from 87 °C to 180 °C. The peak narrows and shifts towards higher temperatures (140 °C–190 °C for PCL, 160 °C–195 °C for PES), when polymer microspheres are added to the hydrogel, the process enthalpy increases significantly (195.2 ± 5.4 J/g) when PCL microspheres are used.

Differences in the thermal properties of the tested materials (ΔH change and different temperature values) could be related to several factors as follows: chemical interaction between polymers, homogeneity of microsphere dispersion, fraction of each polymer resulting from its obtaining method, porosity of microspheres, bioprintout structure, degree of cross-linking, etc. The explanation of the reasons for their properties requires further research. However, shift of the degradation temperature of bioprinted matrices towards higher values after adding microspheres to bioink is a beneficial effect from the point of view of the potential use of the proposed hydrogel for biomedical purposes due to the previously mentioned autoclaving temperature.

3.3. Biocompatibility of GelMA hydrogels with human keratinocytes

Using human keratinocytes (HaCat cells), the cytocompatibility of the 3D bioprinted gelatin-methacrylate hydrogel matrices was evaluated in order to validate their potential future use as wound dressings. The biocompatibility of the GelMA hydrogels (containing or not PCL or PES microspheres at a concentration of 5 mg/mL) was analyzed in an indirect contact test.

As shown in Fig. 5A, after 24 h of culture, a slight cytotoxicity was observed with the different hydrogel eluates at the highest concentrations (10 and 25 mg/mL), when tested using the MTT assay. At these concentrations, the GelMA hydrogels contain PCL or PES microspheres where significantly more cytocompatible than the control hydrogel without microspheres. No significant differences in cytocompatibility were observed between the three hydrogels when tested using the Cyquant dye, which relies on the direct measurement of fluorescence following its incorporation into DNA (Fig. 5B). These data suggest that the matrices were not cytotoxic in the experimental conditions tested. The proliferation of HaCaT cells in the presence of hydrogel eluates was also monitored and, as shown in Fig. 5C, a slight (around 2-fold) reduction of cell proliferation as compared to control cells grown in the culture medium was observed and again, the three hydrogels behaved similarly.

To determine that human keratinocytes were able to adhere on the different hydrogels, we first compared HaCaT cells viability when seeded either on the three different matrices or directly in the culture plate well. As shown in Fig. 6A, the use of the Alamar blue HS assay did not reveal a significant decrease in cell viability when cells were seeded onto the hydrogels. Finally, to validate these results, scanning electron microscopy analysis of HaCaT cells grown onto different hydrogels was performed. As shown in Fig. 6B, human keratinocytes adhered and exhibited normal morphology when seeded onto the different GelMA hydrogels. Although HaCaT cells have a very small cytoplasm and do not spread a lot, the highest magnification clearly showed cell surface invaginations and contacts with the different matrices. At the second magnification (scale bar 40 μm), PCL or PES microspheres are present at the surface of the corresponding hydrogels (white arrows). Altogether, these data confirm the in vitro cytocompatibility of the materials.

3.4. Swelling of the matrices

Swelling of the drug carrier is one of the mechanisms controlling the rate of the drug release process [51]. In addition, an insightful characterization of the degree of swelling of the matrices makes it possible to assess their suitability as drug delivery systems, as well as to predict their behavior under in vivo conditions.

Therefore, in the next stage of the study, the swelling degree of non-modified lyophilized GelMA/gelatin was evaluated as well as the swelling degree of the ones modified with PCL and PES microspheres previously subjected to UV-cross-linking (for 5 min and 10 min). Due to the potential use of such matrices as modified drug release systems, the swelling degree study was conducted for 8 h. Fig. 7 shows kinetic

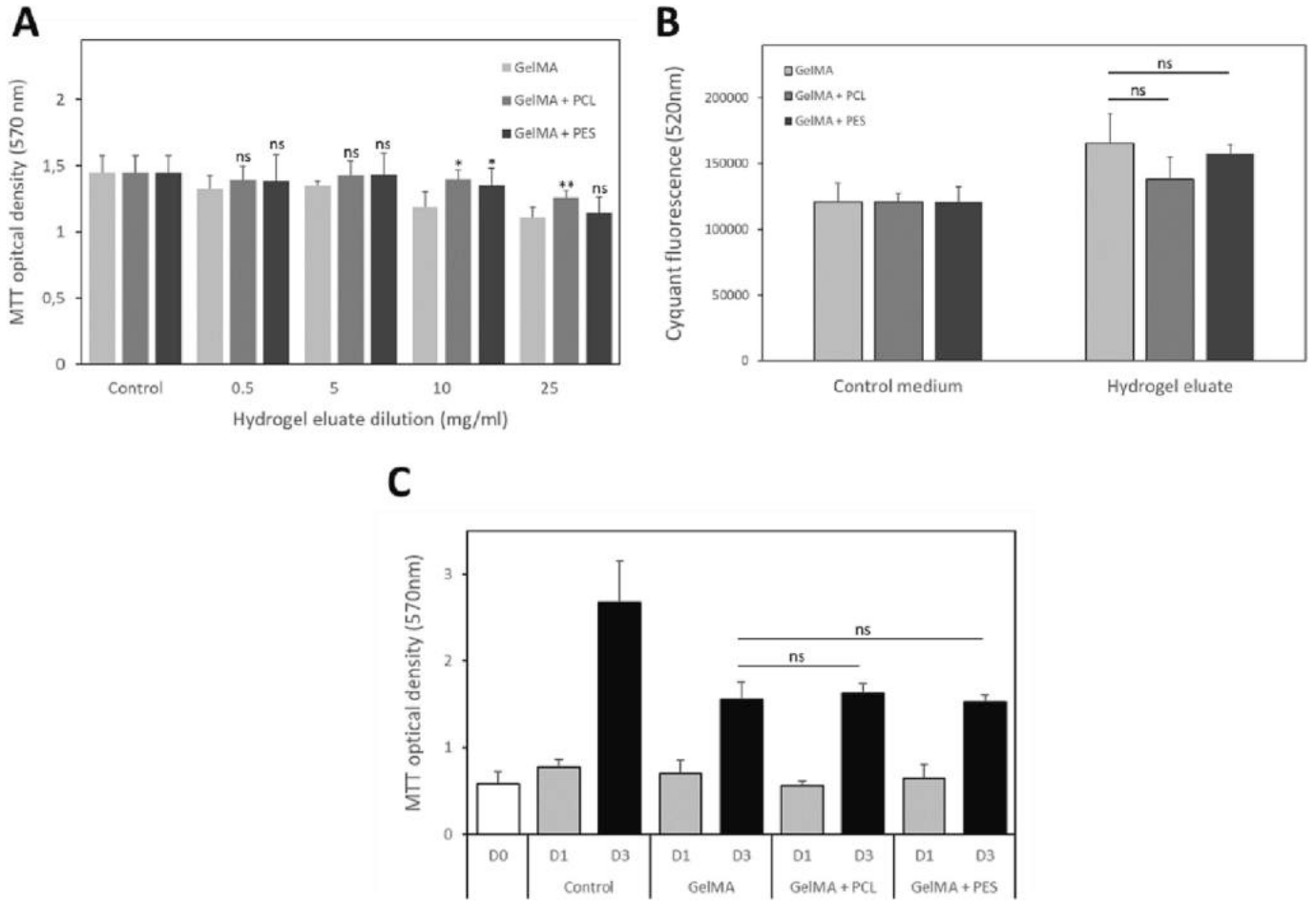

Fig. 5. Compatibility of GelMA hydrogels with human keratinocytes. A. Effect of various dilutions of GelMA, GelMA_PCL or GelMA_PES hydrogel eluates on HaCaT cell viability at 24 h of culture evaluated using the MTT assay. B. Effect of hydrogel eluate on HaCaT cell viability evaluated using the Cyquant assay. C. HaCaT cell proliferation evaluated at day 1 and 3 after seeding evaluated by the MTT assay. Statistical analysis was performed using the Student *t*-test or the Mann-Whitney test to compare GelMA with or without microspheres.

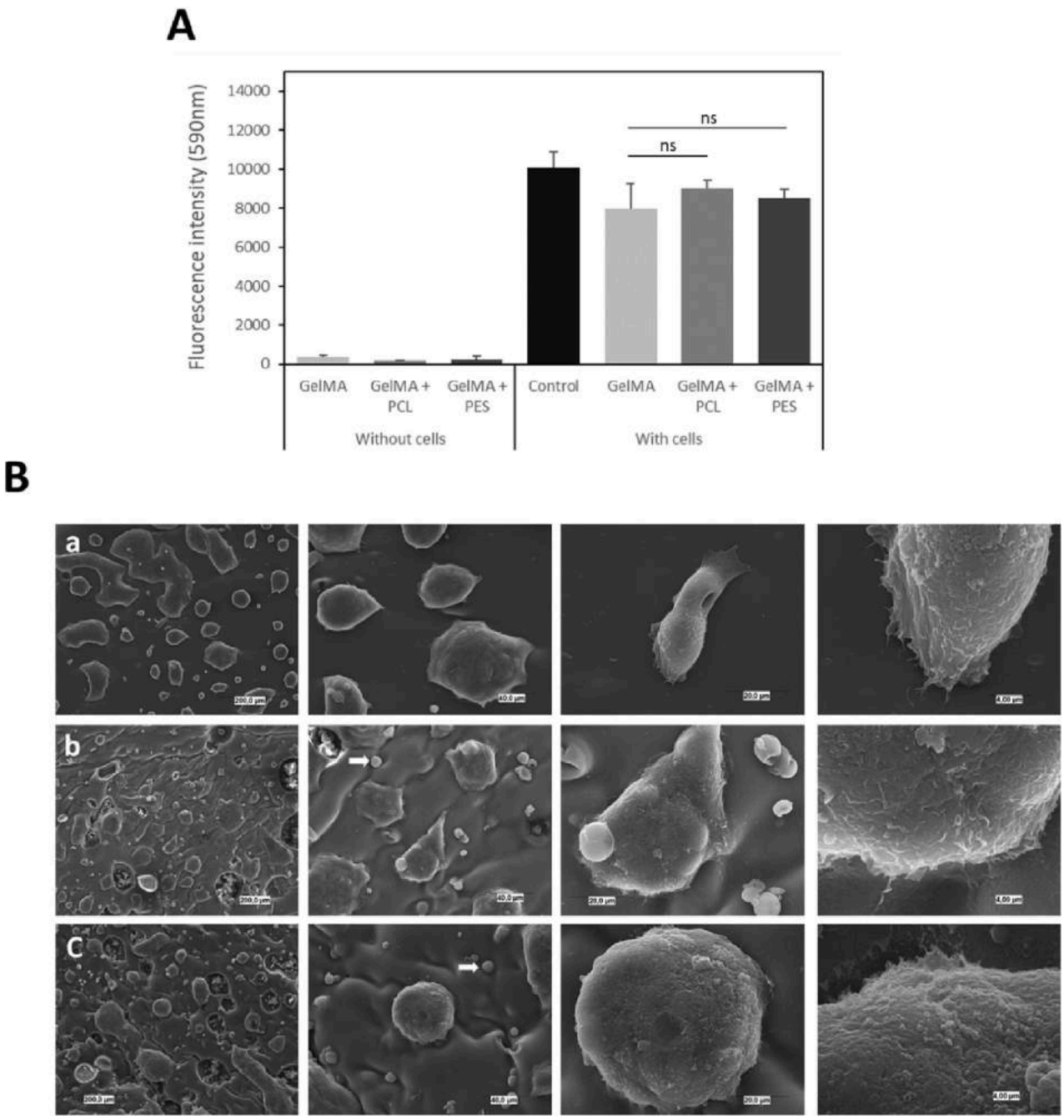

Fig. 6. Adhesion and viability of human keratinocytes grown onto the GelMA hydrogels. **A.** Viability of HaCaT cell grown during 16 h on the matrices. Cell viability was assessed using the Alamar blue assay. The fluorescence intensity corresponding to the same amount of cells seeded in a culture plate well (control) is provided for comparison. The level of fluorescence obtained on hydrogels without cell seeding is also shown. **B.** Scanning electron microscopy images showing HaCaT cells grown on the hydrogels (scale bar of 200, 40, 20 and 4 μm, as indicated). Images show pure GelMA hydrogel (a), with PCL (b) or with PES (c) microspheres. Statistical analysis was performed using the Mann-Whitney test to compare GelMA with or without microspheres.

swelling curves of the GelMA/gelatin matrices (Table 1) examined in PBS buffer.

As can be seen from Fig. 7, 3D bioprinted matrices without microspheres and those containing PCL microspheres reach equilibrium after about 1 h. The maximum hydration is about 125 % and 150 % for GelMA/gelatin matrices without microspheres and those containing PCL microspheres, respectively. Completely different effects are observed for GelMA/gelatin matrices modified with PES microspheres. They swell much faster reaching a maximum hydration of 550–600 % after about 1.5–2 h. Moreover, in the case of this system, a slight loss of weight during the test is also observed. We see the reason for these effects in the completely different morphology (before swelling) of the 3D printed matrices containing PES microspheres (Fig. 2, image H), which was discussed in the *3D bioprinting feasibility* section. In all likelihood, such a morphology results in easier solvent penetration and thus a very high degree of swelling of the 3D printed matrix modified with PES microspheres. In addition, analysis of Fig. 7 shows that the effect of UV-cross-linking time on the swelling of the 3D printed matrices tested is small for all materials tested. It should also be noted that non-cross-linked GelMA/gelatin matrices degraded immediately upon contact with water, confirming the necessity of UV-cross-linking of the matrices using the GelMA-based bioink we developed.

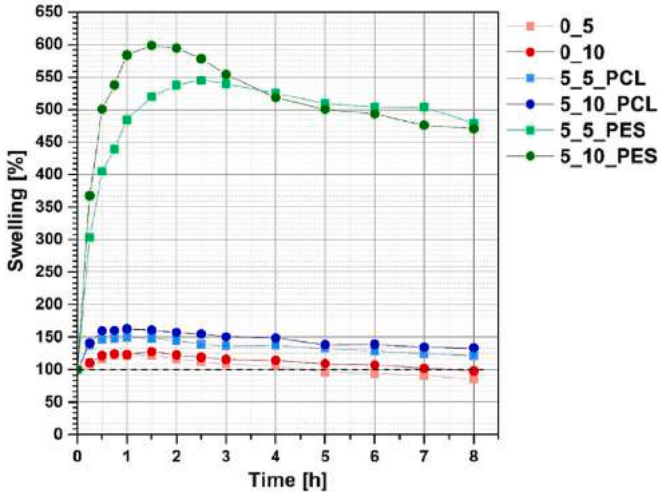

Fig. 7. Equilibrium swelling ratio of lyophilized GelMA/gelatin matrices depending on the microsphere content and cross-linking time. In order to facilitate tracking the experimental points, they are connected by line segments from left to right.

3.5. Rhodamine release from GelMA/gelatin matrices

One of the most important conditions that a 3D printed system with a potential use in biomedical engineering field must meet is its proper transport properties. This process should be as controllable as possible – it should run undisturbed (for example, without the burst effect at the beginning) and the appropriate selection of process conditions should lead to release of a defined amount of a substance at a certain rate. Hence, the GelMA/gelatin matrices have been tested in this regard using rhodamine as an active substance marker. The results in the form of release profile plots over the period of 7 h and a bar graph with its concentration after 24 h of releasing are shown in Fig. 8. The curves are divided into three groups differing in colors, red for GelMA/gelatin matrices without microspheres, blue and green for the matrices loaded with PCL or PES microspheres, respectively.

No burst effect (referring to very rapid initial increase in the marker concentration above the equilibrium concentration reached later) was observed in any of the examined cases, which is a very desirable property of drug delivery system. The curves describing the release of rhodamine from the matrices (Fig. 8A) are consistent with the curves for the equilibrium swelling ratio (Fig. 7). Such a phenomenon was noticed in one of our previous works [23], in which the release of rhodamine from 3D bioprinted gelatin-alginate matrices cross-linked with glutaraldehyde and calcium ions was described. Water is absorbed into the structure of a hydrogel matrix when it is immersed in the solution, dissolving the rhodamine. The marker will not be released into the solution until it has been dissolved in the hydrating water. The continuous release rate results from hydrogel saturation – the release rate is swelling dependent, because only the swollen matrix is permeable to rhodamine. This phenomenon limits the aforementioned burst effect and that the release in the first period follows the zero-order kinetics, so the process can be described mathematically by a linear equation. Such an approach to the problem of release of substances from swelling hydrogels has already been described [23,52,53].

Therefore, to determine the substance release rate from the matrices,

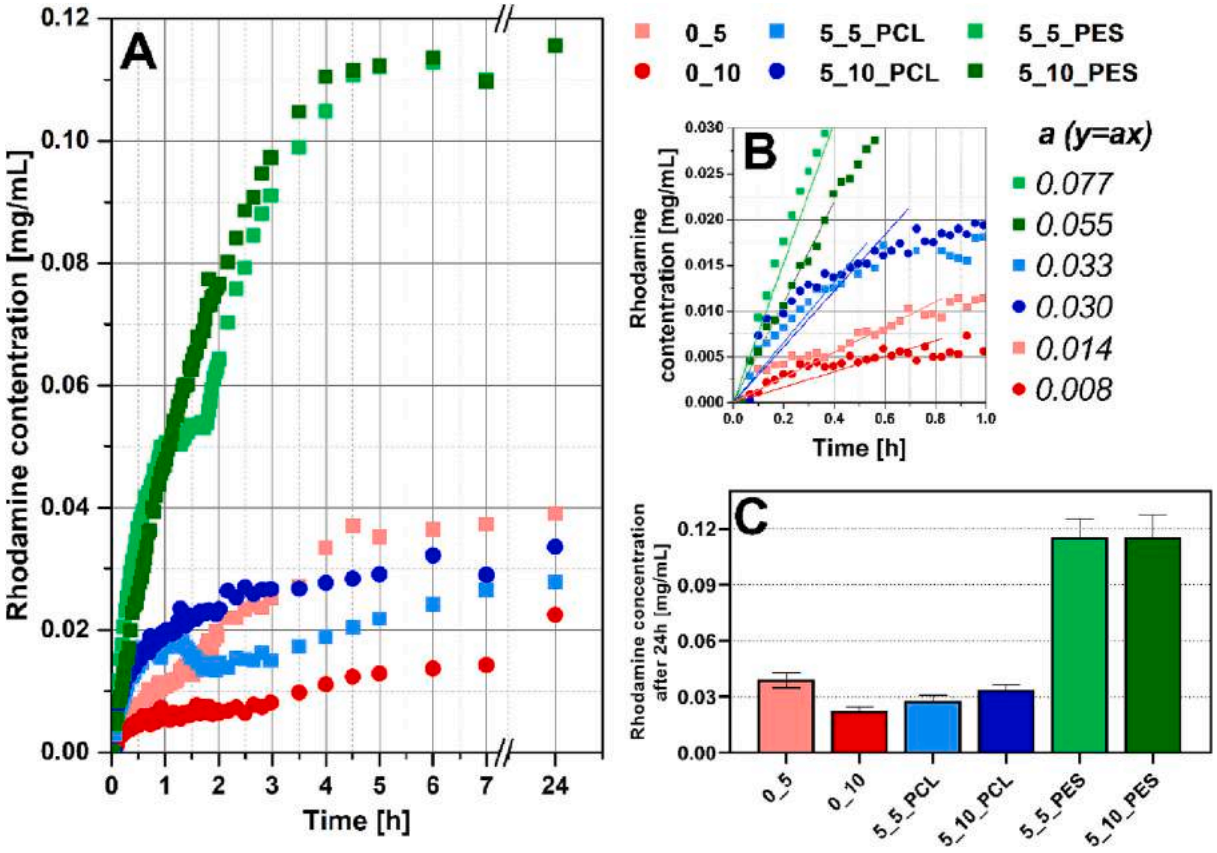

Fig. 8. Results of the studies of rhodamine release from GelMA/gelatin matrices depending on microsphere content and UV-cross-linking time. (A) Marker release profiles over the period of 24 h. (B) Close-up of the first release period (first 1 h) with linear model fit (formula $y = ax$), the values of a parameter are given in the list next to the graph. (C) Rhodamine concentration after 24 h of release from UV-cross-linked GelMA/gelatin matrices with the addition of substance-loaded microspheres depending on the microsphere type and cross-linking time.

a linear function was fitted to the points describing the change in rhodamine concentration in the initial period of the experiment (1 h), and its slope coefficient a was determined (Fig. 8B). The values of the coefficient of determination R^2 for all fits ranged from 0.9361 to 0.9960, they were therefore very good and the model is suitable for describing the experiment under study. The tested samples form three distinct groups that differ in the rate of rhodamine release. It is the fastest for matrices loaded with PES microspheres, then about two times slower for the ones with PCL microspheres, and the slowest for matrices without microspheres, 5–6 times slower than for those PES-loaded. Furthermore, it can be seen that the longer the cross-linking time, the slower the release process in each case.

The use of matrices loaded with PES microspheres clearly increases the amount of rhodamine released after 24 h compared to the other samples (Fig. 8C). The equilibrium concentration of rhodamine is reached only after 5 h in this case and it is about 0.11 mg/mL – 3 to 10 times higher than in other cases (matrices with PCL microspheres or no microspheres), where the equilibrium is not reached even after 24 h.

Some studies on the release of substances from hydrogel matrices modified with microspheres have already been conducted. Fahimipour et al. [26] investigated vascular endothelial growth factor (VEGF) release from biodegradable 3D tricalcium phosphate-based scaffolds containing VEGF-loaded PLGA microspheres. They showed that the release rate in the initial phase from the construct containing microspheres was slower than from the PLGA microspheres. However, they did not eliminate a burst effect by using microspheres in the 3D bioprinted construct, which was ensured by GelMA/gelatin matrices modified with PCL/PES microspheres proposed in presented work. Moreover, Chen et al. [30] were able to demonstrate that the use of gelatin methacryloyl (GelMA)/chitosan microspheres in the 3D bioprinted construct allows prolonged release of nerve growth factor (NGF) from the scaffolds over 9 h. However, they conducted the study with a less precise method (fluorescence microscopy) than spectrophotometric determination of the substance concentration and made only a few measurements, the first one after 0.5 h. Therefore, it cannot be said whether the burst effect was eliminated in their system. The use of spectrophotometry for determination of rhodamine concentration in our work allowed defining the exact release profile of the substance in the first stage, and these studies clearly showed that the burst effect was eliminated by using microsphere-loaded GelMA/gelatin matrices.

3.6. Antibacterial activity

Considering the potential use of microsphere-loaded 3D printed matrices, among others, as dressing materials in the last stage of the study we evaluated their ability to be loaded with an antibiotic in order to acquire antibacterial properties. An agar diffusion inhibition growth assay was performed to characterize the antimicrobial activity of the 3D bioprinted matrices selected for the study. The measurement of the antibacterial activity studies was conducted for four types of 3D printed matrices i.e. without ampicillin, with ampicillin, with ampicillin-loaded PCL microspheres and with ampicillin-loaded PES microspheres. The amount of microspheres in the tested matrices was 5 mg/mL of the bioink used in the 3D printing process. Tests were conducted only for materials cross-linked for 10 min with UV. Each sample was deposited on the surface of nutrient agar plate previously inoculated with 1 mL of *E. coli* or *S. aureus* bacteria suspension at a concentration of 10^8 CFU/mL and incubated for 24 h. Fig. 7. illustrates the results of antibacterial activity tests.

The study showed that all the drug-containing 3D printed matrices tested had antimicrobial activity, most potent against *S. aureus* bacteria (overlapping inhibition zones making them impossible to measure). A comparable phenomenon of varying antibiotic effectiveness depending on the bacterial type has been previously documented [23]. For *E. coli* bacteria matrices modified with PES microspheres show slightly higher antibacterial activity (as evidenced by a bit larger zone of growth inhibition – clear zones) than those modified with PCL microspheres which is confirmed by calculated areas of inhibition zones (Fig. 9E). These results correspond very well with the results of rhodamine release studies described in an earlier section (Fig. 8C). 3D printed matrices without drug and without microspheres showed no antibacterial activity, and the clear zone observed for sample A is the result of the very strong effect of the drug present in sample B against *S. aureus* bacteria (Fig. 9). The remarkable difference in the size of the inhibited growth zones for *S. aureus* compared to *E. coli* should be noted. The observed antibacterial activity of the matrices against the bacteria provides evidence that the drug integrity remained intact during both microsphere preparation and 3D bioprinting processes. As a result, the suggested 3D bioprinted matrices could potentially be used as controlled drug delivery systems.

4. Conclusions

A new bioink containing gelatin methacrylate, gelatin and LAP photoinitiator modified by the addition of either PCL or PES microspheres is a good material for application in 3D bioprinting using the extrusion technique. 3D bioprinted model can be cross-linked using UV light, creating a water-insoluble compact structure. The cross-linking time has almost no effect on the properties of the printed matrices. However, the obtained systems essentially differ depending on whether and what kind of microspheres was dispersed in the bioink.

The addition of PES microspheres to a bioink used for 3D bioprinting leads to a different structure of the printed matrix (than the one without microspheres or PCL-modified one) due to changes in thermal properties. The PES-modified matrices have a higher swelling degree. They are characterized by four times higher drug capacity than other tested systems and faster drug release with no burst effect. The other two systems (without microspheres and with PCL ones) are characterized by a lower drug capacity, nevertheless, the time of its release is longer which is beneficial for long-term therapies. Furthermore, the matrices with microspheres have higher degradation temperatures, which is beneficial in terms of the potential use of bioprinted hydrogels in biomedical engineering due to the autoclave sterilization process. All tested types of matrices are non-cytotoxic and can be loaded with antibiotic to acquire antibacterial properties against both Gram-positive and Gram-negative bacteria.

The new bioinks modified with microspheres presented in the work are a very good starting point for the design of various constructs with potential biomedical application, for example as controlled drug delivery systems or wound dressings.

Supplementary data to this article can be found online at https://doi.org/10.1016/j.bioadv.2023.213436.

CRediT authorship contribution statement

Adam Mirek: Conceptualization, Methodology, Formal analysis, Investigation, Validation, Data curation, Writing – original draft, Writing – review & editing. **Habib Belaid:** Methodology, Investigation, Data curation, Visualization, Writing – review & editing. **Aleksandra Bartkowiak:** Validation, Writing – original draft, Writing – review & editing. **Fanny Barranger:** Investigation, Visualization. **Fanny Salmeron:** Methodology, Investigation, Data curation, Visualization. **Marilyn Kajdan:** Methodology, Investigation, Data curation, Visualization. **Marcin Grzeczkowicz:** Methodology, Software, Resources, Validation. **Vincent Cavaillès:** Conceptualization, Methodology, Validation, Resources, Writing – review & editing. **Dorota Lewińska:** Methodology, Validation, Resources, Writing – original draft, Writing – review & editing. **Mikhael Bechelany:** Conceptualization, Methodology, Validation, Resources, Writing – review & editing, Funding acquisition, Supervision.

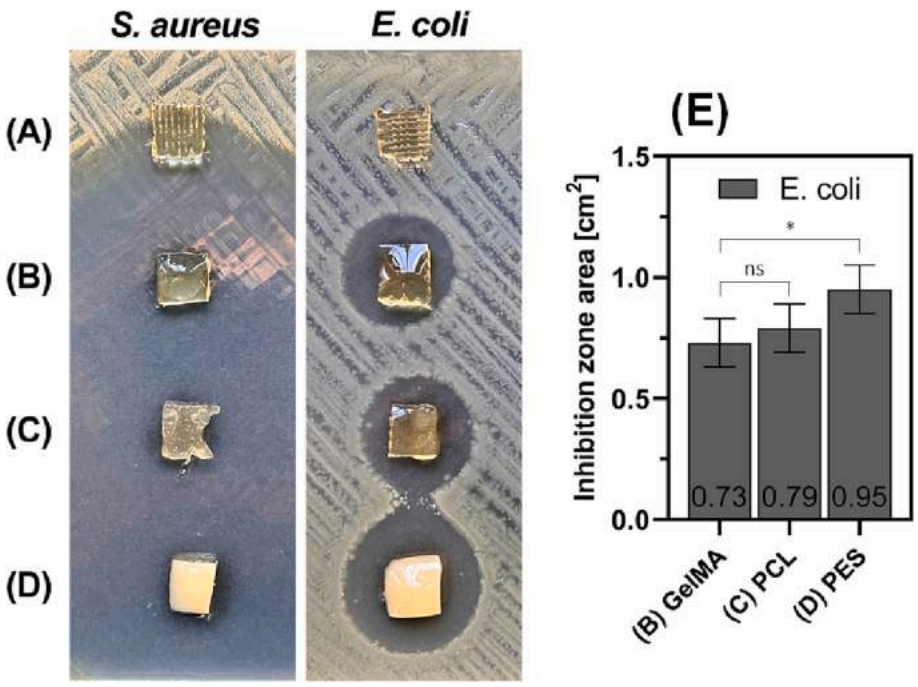

Fig. 9. Antibacterial activity of ampicillin-loaded GelMA/gelatin matrices depending on the microsphere content. Nutrient agar plates covered with *S. aureus* and *E. coli* biofilms after 24 h of material treatment. (A) Control matrices with no drug. (B) drug-loaded matrices without microspheres. (C–D) matrices with drug-loaded (C) PCL or (D) PES microspheres. (E) A graphical representation in the form of a bar chart illustrating the mean values of inhibition zone areas [cm^2] calculated using Petri dish images obtained from three independent test replicates for *E. coli*. Statistical analysis was performed using ANOVA followed by a post-hoc Tukey HSD test.

Declaration of competing interest

Authors declare no interest.

Data availability

Data will be made available on request.

Acknowledgements

The authors are grateful to Chantal Cazevieille (CoMET, Institut des Neurosciences Montpellier) for her technical assistance and for the interpretation of electron microscopy data. This project was supported by European Social Fund [POWR.03.02.00-00-1028/17-00] as part of the POWER Och!Dok program. AM would like to thank Campus France for the funding through a French Government Scholarship. Authors acknowledge the financial support of project H2020-MSCA-RISE-2017, "Novel 1D photonic metal oxide nanostructures for early stage cancer detection" (Project number: 778157).

References

[1] S. Beg, W.H. Almalki, A. Malik, M. Farhan, M. Aatif, Z. Rahman, N.K. Alruwaili, M. Alrobaian, M. Tarique, M. Rahman, 3D printing for drug delivery and biomedical applications, Drug Discov. Today 25 (2020) 1668–1681.

[2] A.C. Daly, M.E. Prendergast, A.J. Hughes, J.A. Burdick, Bioprinting for the biologist, Cell 184 (2021) 18–32.

[3] B. Tan, S. Gan, X. Wang, W. Liu, X. Li, Applications of 3D bioprinting in tissue engineering: advantages, deficiencies, improvements, and future perspectives, J. Mater. Chem. B 9 (2021) 5385–5413.

[4] G. Gao, M. Ahn, W.W. Cho, B.S. Kim, D.W. Cho, 3D printing of pharmaceutical application: drug screening and drug delivery, Pharmaceutics 13 (2021) 1373, https://doi.org/10.3390/pharmaceutics13091373.

[5] A.P. Tiwari, N.D. Thorat, S. Pricl, R.M. Patil, S. Rohiwal, H. Townley, Bioink: a 3D-bioprinting tool for anticancer drug discovery and cancer management, Drug Discov. Today 26 (2021) 1574–1590.

[6] C. Karavasili, G.K. Eleftheriadis, C. Gioumouxouzis, E.G. Andriotis, D.G. Fatouros, Mucosal drug delivery and 3D printing technologies: a focus on special patient populations, Adv. Drug Deliv. Rev. 176 (2021), 113858, https://doi.org/10.1016/j.addr.2021.113858.

[7] P. Jain, H. Kathuria, N. Dubey, Advances in 3D bioprinting of tissues/organs for regenerative medicine and in-vitro models, Biomaterials 287 (2022), 121639, https://doi.org/10.1016/j.biomaterials.2022.121639.

[8] G. Saini, N. Segaran, J.L. Mayer, A. Saini, H. Albadawi, R. Oklu, Applications of 3D bioprinting in tissue engineering and regenerative medicine, J. Clin. Med. 10 (2021) 4966, https://doi.org/10.3390/jcm10214966.

[9] Z. Wang, W. Kapadia, C. Li, F. Lin, R.F. Pereira, P.L. Granja, B. Sarmento, W. Cui, Tissue-specific engineering: 3D bioprinting in regenerative medicine, J. Control. Release 329 (2021) 237–256.

[10] Y.W. Ding, X.W. Zhang, C.H. Mi, X.Y. Qi, J. Zhou, D.X. Wei, Recent advances in hyaluronic acid-based hydrogels for 3D bioprinting in tissue engineering applications, Smart Mater. Med. 4 (2023) 59–68.

[11] D. Williams, P. Thayer, H. Martinez, E. Gatenholm, A. Khademhosseini, A perspective on the physical, mechanical and biological specifications of bioinks and the development of functional tissues in 3D bioprinting, Bioprinting 9 (2018) 19–36.

[12] L. Valot, J. Martinez, A. Mehdi, G. Subra, Chemical insights into bioinks for 3D printing chemical insights in bioinks for 3D printing, R. Soc. Chem. 48 (2019) 4049–4086.

[13] J. Gopinathan, I. Noh, Recent trends in bioinks for 3D printing, biomaterRes. 22 (2018), https://doi.org/10.1186/s40824-018-0122-1.

[14] S. Vanaei, M.S. Parizi, F. Salemizadehparizi, H.R. Vanaei, An overview on materials and techniques in 3D bioprinting toward biomedical application, Eng. Regen. 2 (2021) 1–18.

[15] R. Staros, A. Michalak, K. Rusinek, K. Mucha, Z. Pojda, R. Zagożdżon, Perspectives for 3D-bioprinting in modeling of tumor immune evasion, Cancers 14 (2022) 3126, https://doi.org/10.3390/cancers14133126.

[16] A.B. Bello, D. Kim, D. Kim, H. Park, S.H. Lee, Engineering and functionalization of gelatin biomaterials: from cell culture to medical applications, Tissue Eng. Part B Rev. 26 (2020) 164–180.

[17] G. Ying, N. Jiang, C. Yu, Y.S. Zhang, Three-dimensional bioprinting of gelatin methacryloyl (GelMA), Bio-Des. Manuf. 1 (2018) 215–224.

[18] R.L. Alexa, H. Iovu, J. Ghitman, A. Serafim, C. Stavarache, M.-M. Marin, R. Ianchis, 3D-printed gelatin methacryloyl-based scaffolds with potential application in tissue engineering, Polymers 13 (2021) 727, https://doi.org/10.3390/polym13050727.

[19] K. Yue, G. Trujillo-de Santiago, M. Alvarez, A. Tamayol, N. Annabi, A. Khademhosseini, Synthesis, properties, and biomedical applications of gelatin methacryloyl (GelMA) hydrogels, Biomaterials 73 (2015) 254–271.

[20] Y. Piao, H. You, T. Xu, H.-P. Bei, I.Z. Piwko, Y.Y. Kwan, X. Zhao, Biomedical applications of gelatin methacryloyl hydrogels, Eng. Regen. 2 (2021) 47–56.

[21] M. Lengyel, N. Kállai-Szabó, V. Antal, A.J. Laki, I. Antal, Microparticles, microspheres, and microcapsules for advanced drug delivery, Sci. Pharm. 87 (2019) 20, https://doi.org/10.3390/scipharm87030020.

[22] A.N. Yawalkar, M.A. Pawar, P.R. Vavia, Microspheres for targeted drug delivery - a review on recent applications, J. Drug Deliv. Sci. Technol. 75 (2022), 103659, https://doi.org/10.1016/j.jddst.2022.103659.

[23] A. Mirek, H. Belaid, F. Barranger, M. Grzeczkowicz, Y. Bouden, V. Cavaillès, D. Lewińska, M. Bechelany, Development of a new 3D bioprinted antibiotic delivery system based on a cross-linked gelatin-alginate hydrogel, J. Mater. Chem. B 10 (2022) 8862–8874.

[24] Y.J. Tan, X. Tan, W.Y. Yeong, S.B. Tor, Hybrid microscaffold-based 3D bioprinting of multi-cellular constructs with high compressive strength: a new biofabrication strategy, Sci. Rep. 6 (2016), https://doi.org/10.1038/srep39140.

[25] L.K. Narayanan, P. Huebner, M.B. Fisher, J.T. Spang, B. Starly, R.A. Shirwaiker, 3D-bioprinting of polylactic acid (PLA) nanofiber-alginate hydrogel bioink containing human adipose-derived stem cells, ACS Biomater. Sci. Eng. 2 (2016) 1732–1742.
[26] F. Fahimipour, M. Rasoulianboroujeni, E. Dashtimoghadam, K. Khoshroo, M. Tahriri, F. Bastami, D. Lobner, L. Tayebi, 3D printed TCP-based scaffold incorporating VEGF-loaded PLGA microspheres for craniofacial tissue engineering, Dent. Mater. 33 (2017) 1205–1216.
[27] H. Xu, J. Casillas, C. Xu, Effects of printing conditions on cell distribution within microspheres during inkjet-based bioprinting, AIP Adv. 9 (2019), 095055, https://doi.org/10.1063/1.5116371.
[28] D.L. Johnson, R.M. Ziemba, J.H. Shebesta, J.C. Lipscomb, Y. Wang, Y. Wu, K. D. O'Connell, M.G. Kaltchev, A. van Groningen, J. Chen, Design of pectin-based bioink containing bioactive agent-loaded microspheres for bioprinting, Biomed. Phys. Eng. Express 5 (2019), https://doi.org/10.1088/2057-1976/ab4dbc.
[29] B. Mirani, E. Pagan, S. Shojaei, J. Duchscherer, B.D. Toyota, S. Ghavami, M. Akbari, 3D bioprinted hydrogel mesh loaded with all-trans retinoic acid for treatment of glioblastoma, Eur. J. Pharmacol. 854 (2019) 201–212.
[30] J. Chen, D. Huang, L. Wang, J. Hou, H. Zhang, Y. Li, S. Zhong, Y. Wang, Y. Wu, W. Huang, 3D bioprinted multiscale composite scaffolds based on gelatin methacryloyl (GelMA)/chitosan microspheres as a modular bioink for enhancing 3D neurite outgrowth and elongation, J. Colloid Interface Sci. 574 (2020) 162–173.
[31] R. Sharma, I.P.M. Smits, L. de La Vega, C. Lee, S.M. Willerth, 3D bioprinting pluripotent stem cell derived neural tissues using a novel fibrin bioink containing drug releasing microspheres, Front. Bioeng. Biotechnol. 8 (2020), https://doi.org/10.3389/fbioe.2020.00057.
[32] R. Sharma, R. Kirsch, K.P. Valente, M.R. Perez, S.M. Willerth, Physical and mechanical characterization of fibrin-based bioprinted constructs containing drug-releasing microspheres for neural tissue engineering applications, Processes 9 (2021) 1205, https://doi.org/10.3390/pr9071205.
[33] R. Sharma, C. Benwood, S.M. Willerth, Drug-releasing microspheres for stem cell differentiation, Curr. Protoc. 1 (2021), https://doi.org/10.1002/cpz1.331.
[34] M. Kanungo, Y. Wang, N. Hutchinson, E. Kroll, A. DeBruine, S. Kumpaty, L. Ren, Y. Wu, X. Hua, W. Zhang, Development of gelatin-coated microspheres for novel bioink design, Polymers 13 (2021) 3339, https://doi.org/10.3390/polym13193339.
[35] L. de la Vega, L. Abelseth, R. Sharma, J. Triviño-Paredes, M. Restan, S.M. Willerth, 3D bioprinting human-induced pluripotent stem cells and drug-releasing microspheres to produce responsive neural tissues, Adv. Nanobiomed. Res. 1 (2021) 2000077, https://doi.org/10.1002/anbr.202000077.
[36] M. Bonany, L. del-Mazo-Barbara, M. Espanol, M.-P. Ginebra, Microsphere incorporation as a strategy to tune the biological performance of bioinks, J. Tissue Eng. 13 (2022), 204173142211198, https://doi.org/10.1177/20417314221119895.
[37] A. Mirek, M. Grzeczkowicz, C. Lamboux, S. Sayegh, M. Bechelany, D. Lewińska, Formation of disaggregated polymer microspheres by a novel method combining pulsed voltage electrospray and wet phase inversion techniques, Colloids Surf. A: Physicochem. Eng. Asp. 648 (2022), 129246, https://doi.org/10.1016/j.colsurfa.2022.129246.
[38] J. Yin, M. Yan, Y. Wang, J. Fu, H. Suo, 3D bioprinting of low-concentration cell-laden gelatin methacrylate (GelMA) bioinks with a two-step cross-linking strategy, ACS Appl. Mater. Interfaces 10 (2018) 6849–6857.
[39] A.I. van den Bulcke, B. Bogdanov, N. de Rooze, E.H. Schacht, M. Cornelissen, H. Berghmans, Structural and rheological properties of methacrylamide modified gelatin hydrogels, Biomacromolecules 1 (2000) 31–38.
[40] Allevi, Inc. n.d. Allevi Protocols: Cell-bioink Mixing: Syringe Coupler Method, Allevi, https://www.allevi3d.com/cell-bioink-mixing-syringe-coupler-method/, (accessed 16 August 2022).
[41] O. Jeon, Y.B. Lee, S.J. Lee, N. Guliyeva, J. Lee, E. Alsberg, Stem cell-laden hydrogel bioink for generation of high resolution and fidelity engineered tissues with complex geometries, Bioactive Materials 15 (2022) 185–193.
[42] M. Grzeczkowicz, D. Lewińska, A method for investigating transport properties of partly biodegradable spherical membranes using vitamin B12 as the marker, Desalin. Water Treat. 128 (2018) 170–178.
[43] C. Funaki, S. Yamamoto, H. Hoshina, Y. Ozaki, H. Sato, Three different kinds of weak C-H···O=C inter- and intramolecular interactions in poly(ε-caprolactone) studied by using terahertz spectroscopy, infrared spectroscopy and quantum chemical calculations, Polymer 137 (2018) 245–254.
[44] H. Lu, H. Shinzawa, S.G. Kazarian, Intermolecular interactions in the polymer blends under high-pressure CO2 studied using two-dimensional correlation analysis and two-dimensional disrelation mapping, Appl. Spectrosc. 75 (2021) 250–258.
[45] H. Hatakeyama, A.T. Hatakeyama, Interaction between water and hydrophilic polymers, Thermochim. Acta 308 (1998) 3–22.
[46] M. Rusu, M. Ursu, D. Rusu, Poly(vinyl chloride) and Poly(e-caprolactone) blends for medical use, J. Thermoplas. Compos. Mater. 19 (2006) 173–190.
[47] T. Tavangar, A. Hemmati, M. Karimi, F. Zokaee Ashtiani, Layer-by-layer assembly of graphene oxide (GO) on sulfonated polyethersulfone (SPES) substrate for effective dye removal, Polym. Bull. 76 (2019) 35–52.
[48] M.U. Joardder, M. Mourshed, M. Hasan Masud, Bound water measurement techniques, in: State of Bound Water: Measurement and Significance in Food Processing, Springer International Publishing, NYC, 2019, pp. 47–82.
[49] H. Yoshida, T. Hatakeyama, H. Hatakeyama, Effect of water on the main chain motion of polysaccharide hydrogels, in: W.G. Glasser, H. Hatakeyama (Eds.), Viscoelasticity of biomaterials, ACS Symposium Series, 489, ACS, Washington, 1992, pp. 218–230.
[50] S. Ramesh, M. Ramalingam, Aqueous-mediated synthesis and characterization of gelatin methacryloyl for biomedical applications, Biointerface Res. App.l Chem. 12 (2022) 6269–6279.
[51] M. Rizwan, R. Yahya, A. Hassan, M. Yar, A.D. Azzahari, V. Selvanathan, F. Sonsudin, C.N. Abouloula, pH sensitive hydrogels in drug delivery: brief history, properties, swelling, and release mechanism, material selection and applications, Polymers 9 (2017) 137, https://doi.org/10.3390/polym9040137.
[52] M.L. Laracuente, M.H. Yu, K.J. McHugh, Zero-order drug delivery: state of the art and future prospects, J. Control. Release 327 (2020) 834–856.
[53] M.L. Bruschi, Mathematical models of drug release, in: Strategies to Modify the Drug Release From Pharmaceutical Systems, Woodhead Publishing, Cambridge, UK, 2015, pp. 63–86.

SUPPORTING INFORMATION

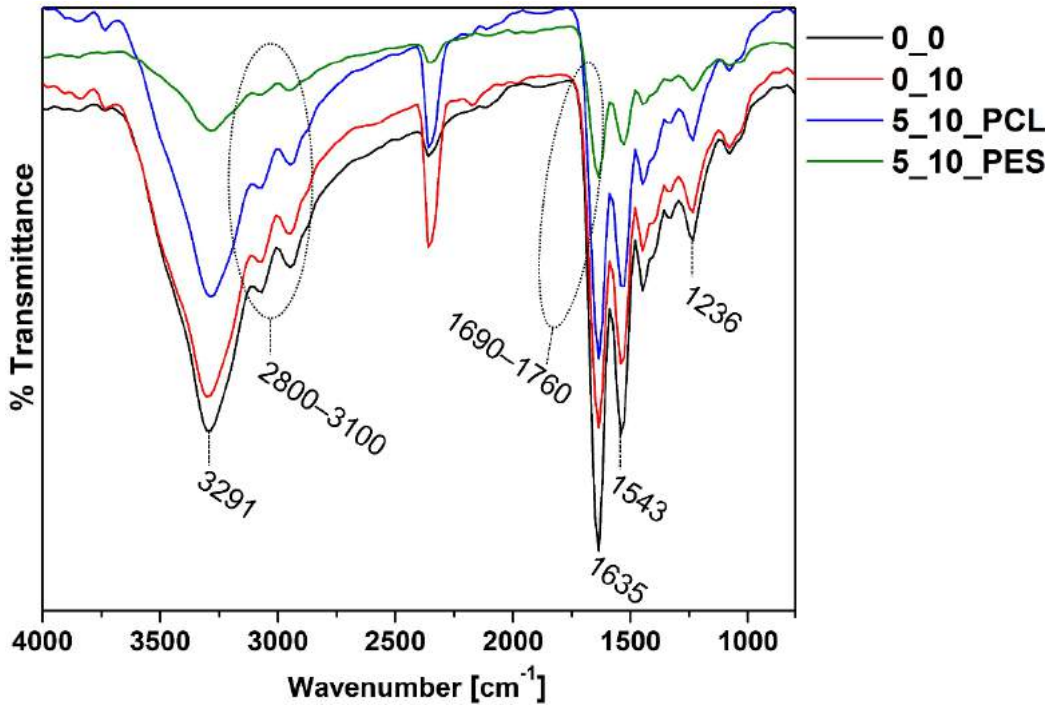

Figure SI1. FTIR spectra of GelMA/gelatin matrices.

A P P E N D I X I

DECLARATION OF AUTHORS' CONTRIBUTIONS

Dorota Lewińska, Ph.D., D.Sc.
Laboratory of Electrostatic Methods of Bioencapsulation
Nalecz Institute of Biocybernetics and Biomedical Engineering, Polish Academy of Sciences

As the Head of the Laboratory, I hereby declare the individual authors' contributions to following publications based on CRediT authorship contribution statement.

(1) Mirek, A., Korycka, P., Grzeczkowicz, M., Lewińska, D. Polymer fibers electrospun using pulsed voltage. *Materials and Design*. 183, 108106 (2019).

Adam Mirek: Conceptualization, Methodology, Formal analysis, Investigation, Validation, Data curation, Visualisation, Writing – original draft, Writing – review & editing. **Paulina Korycka:** Methodology, Formal analysis, Investigation, Validation, Data curation, Writing – original draft. **Marcin Grzeczkowicz:** Methodology, Software, Resources, Validation. **Dorota Lewińska:** Conceptualization, Writing – review & editing, Supervision.

---

(2) Mirek, A., Grzeczkowicz, M., Lamboux, C., Sayegh, S., Bechelany, M., Lewińska, D. Formation of disaggregated polymer microspheres by a novel method combining pulsed voltage electrospray and wet phase inversion techniques. Colloids and Surfaces A: Physicochemical and Engineering Aspects. 648, 129246 (2022).

Adam Mirek: Conceptualization, Methodology, Formal analysis, Investigation, Validation, Data curation, Writing – original draft. **Marcin Grzeczkowicz:** Methodology, Software, Resources, Validation. **Dorota Lewińska:** Conceptualization, Writing – review & editing, Supervision.

---

(3) Mirek, A., Grzeczkowicz, M., Belaid, H., Bartkowiak, A., Barranger, F., Abid, M., Wasyłeczko, M., Pogorielov, M., Bechelany, M., Lewińska, D. Electrospun UV-cross-linked polyvinylpyrrolidone fibers modified with polycaprolactone/polyethersulphone microspheres for drug delivery. Biomaterials Advances. 147, 213330 (2023).

Adam Mirek: Conceptualization, Methodology, Formal analysis, Investigation, Data curation, Writing – original draft, Writing – review & editing, Visualization. **Marcin Grzeczkowicz:** Conceptualization, Methodology, Validation, Formal analysis, Writing – review & editing. **Aleksandra Bartkowiak:** Conceptualization, Validation, Writing – original draft, Writing – review & editing. **Monika Wasyłeczko:** Methodology, Investigation, Visualization. **Dorota Lewińska:** Conceptualization, Methodology, Validation, Resources, Writing – original draft, Writing – review & editing, Supervision.

---

(4) Mirek, A., Belaid, H., Barranger, F., Grzeczkowicz, M., Bouden, Y., Cavailles, V., Lewińska, D., Bechelany, M. Development of a new 3D bioprinted antibiotic delivery system based on a cross-linked gelatin alginate hydrogel. Journal of Materials Chemistry B. 10, 8862–8874 (2022).

Adam Mirek: Conceptualization, Methodology, Formal analysis, Investigation, Data curation, Writing – original draft, Writing – review & editing, Visualization. **Marcin Grzeczkowicz:** Conceptualization, Methodology, Software, Resources, Validation; **Dorota Lewińska:** Methodology, Validation, Resources, Writing – original draft, Writing – review & editing, Supervision.

---

(5) Mirek, A., Belaid, H., Bartkowiak, A., Barranger, F., Grzeczkowicz, M., Lewińska, D., Bechelany, M. Gelatin methacrylate hydrogel with drug-loaded polymer microspheres as a new bioink for 3D bioprinting. Biomaterials Advances. 213436 (2023).

Adam Mirek: Conceptualization, Methodology, Formal analysis, Investigation, Validation, Data curation, Writing – original draft, Writing – review & editing. **Aleksandra Bartkowiak:** Validation, Writing – original draft, Writing – review & editing. **Marcin Grzeczkowicz:** Methodology, Software, Resources, Validation; **Dorota Lewińska:** Methodology, Validation, Resources, Writing – original draft, Writing – review & editing.

Dorota Lewińska

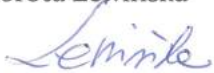

Mikhael Bechelany, Ph.D., D.Sc.
Design of Membrane Materials and Multifunctional Systems Department
Institut Européen des Membranes, Université de Montpellier

As the Head of the Department, I hereby declare the individual authors' contributions to following publications based on CRediT authorship contribution statement.

---

(2) Mirek, A., Grzeczkowicz, M., Lamboux, C., Sayegh, S., Bechelany, M., Lewińska, D. Formation of disaggregated polymer microspheres by a novel method combining pulsed voltage electrospray and wet phase inversion techniques. Colloids and Surfaces A: Physicochemical and Engineering Aspects. 648, 129246 (2022).

Cassandre Lamboux: Methodology, Software, Resources, Formal Analysis. **Syreina Sayegh:** Methodology, Investigation, Resources. **Mikhael Bechelany:** Conceptualization, Writing – review & editing.

---

(3) Mirek, A., Grzeczkowicz, M., Belaid, H., Bartkowiak, A., Barranger, F., Abid, M., Wasyłeczko, M., Pogorielov, M., Bechelany, M., Lewińska, D. Electrospun UV-cross-linked polyvinylpyrrolidone fibers modified with polycaprolactone/polyethersulphone microspheres for drug delivery. Biomaterials Advances. 147, 213330 (2023).

Habib Belaid: Methodology, Investigation, Writing – review & editing, Visualization. **Fanny Barranger:** Investigation, Visualization. **Mahmoud Abid:** Investigation. **Mikhael Bechelany:** Conceptualization, Methodology, Validation, Resources, Writing – review & editing.

---

(4) Mirek, A., Belaid, H., Barranger, F., Grzeczkowicz, M., Bouden, Y., Cavailles, V., Lewińska, D., Bechelany, M. Development of a new 3D bioprinted antibiotic delivery system based on a cross-linked gelatin alginate hydrogel. Journal of Materials Chemistry B. 10, 8862–8874 (2022).

Habib Belaid: Methodology, Investigation, Data Curation, Writing – review & editing. **Fanny Barranger:** Investigation, Visualization. **Mikhael Bechelany:** Conceptualization, Methodology, Validation, Resources, Writing – review & editing, Funding acquisition, Supervision.

---

(5) Mirek, A., Belaid, H., Bartkowiak, A., Barranger, F., Grzeczkowicz, M., Lewińska, D., Bechelany, M. Gelatin methacrylate hydrogel with drug-loaded polymer microspheres as a new bioink for 3D bioprinting. Biomaterials Advances. 213436 (2023).

Habib Belaid: Methodology, Investigation, Data Curation, Writing – review & editing. **Fanny Barranger:** Investigation, Visualization. **Mikhael Bechelany:** Conceptualization, Methodology, Validation, Resources, Writing – review & editing, Funding acquisition, Supervision.

Mikhael Bechelany

Vincent Cavaillès, Ph.D.
Department Institut de Recherche en Cancérologie de Montpellier
Université de Montpellier

As the Head of the Laboratory, I hereby declare the individual authors' contributions to following publications based on CRediT authorship contribution statement.

---

(4) Mirek, A., Belaid, H., Barranger, F., Grzeczkowicz, M., Bouden, Y., Cavaillès, V., Lewińska, D., Bechelany, M. Development of a new 3D bioprinted antibiotic delivery system based on a cross-linked gelatin alginate hydrogel. Journal of Materials Chemistry B. 10, 8862–8874 (2022).

Yasmine Bouden: Methodology, Investigation, Data Curation, Visualisation. **Vincent Cavaillès:** Conceptualization, Methodology, Validation, Resources, Writing – review & editing.

---

(5) Mirek, A., Belaid, H., Bartkowiak, A., Barranger, F., Salmeron, F., Kajdan, M., Grzeczkowicz, M., Cavailles, V., Lewińska, D., Bechelany, M. Gelatin methacrylate hydrogel with drug-loaded polymer microspheres as a new bioink for 3D bioprinting. Biomaterials Advances. 213436 (2023).

Fanny Samleron: Methodology, Investigation, Data Curation, Visualisation. **Marilyn Kajdan:** Methodology, Investigation, Data Curation, Visualisation. **Vincent Cavaillès:** Conceptualization, Methodology, Validation, Resources, Writing – review & editing.

Vincent Cavaillès

Maksym Pogorielov, Ph.D.
Sumy State University,
Medical Institute, Ukraine

I hereby declare my contribution to following publication based on CRediT authorship contribution statement.

(4) Mirek, A., Grzeczkowicz, M., Belaid, H., Bartkowiak, A., Barranger, F., Abid, M., Wasyłeczko, M., Pogorielov, M., Bechelany, M., Lewińska, D. Electrospun UV-cross-linked polyvinylpyrrolidone fibers modified with polycaprolactone/polyethersulphone microspheres for drug delivery. Biomaterials Advances. 147, 213330 (2023).

Maksym Pogorielov: Methodology, Validation, Resources.

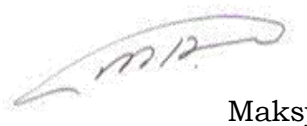

Maksym Pogorielov

A P P E N D I X I I

OTHER RESEARCH NOT INCLUDED IN THE THESIS

Korycka, P., **Mirek, A.**, Kramek-Romanowska, K., Grzeczkowicz, M., Lewińska, D. Effect of electrospinning process variables on the size of polymer fibers and bead-on-string structures established with a 2^3 factorial design. *Beilstein Journal of Nanotechnology*. 9, 2466–2478 (2018). DOI:10.3762/bjnano.9.231

Myakinin, A., Turlybekuly, A., Pogrebnjak, A., **Mirek, A.**, Bechelany, M., Liubchak, I., Oleshko, O., Husak, Y., Korniienko, V., Leśniak-Ziółkowska, K., Dogadkin, D., Banasiuk, R., Moskalenko, R., Pogorielov, M., Simka, W. In vitro evaluation of electrochemically bioactivated Ti6Al4V 3D porous scaffolds. *Materials Science and Engineering: C.* 121, 111870 (2021). DOI:10.1016/j.msec.2021.111870

Co-author of Polish **patent P-429649**, A method of producing a broad-porous biodegradable polymer membrane, 2021.

CONFERENCES

8th European Young Engineers Conference, oral presentation "Factorial design of the electrospun polymeric mat structures as a tool for selection of electrospinning process parameters", Warsaw, Poland, 2019.

10th IEEE International Conference on Nanomaterials: Applications & Properties, oral presentation "3D bioprinted cross-linked gelatin-alginate hydrogel matrices for biomedical purposes", Sumy, Ukraine, 2020.

22nd Polish Conference on Biocybernetics and Biomedical Engineering, oral presentation "How to create the electrospun polymeric mats of desired structure for biomedical applications?", Warsaw, Poland, 2021.

POWER Och!DOK Project Summer Schools, poster presentations, IBBE PAS, Warsaw, Poland, 2019, 2020 and 2021.

1st Polish Conference on Polymers in Medicine, poster presentation, Łódź, Poland, 2018.